THE UNIVERSITY *of* EDINBURGH

The role of membrane-associated guanylate kinases in somatosensory cortical development.

THE UNIVERSITY *of* EDINBURGH

Alex Crocker-Buqué

Presented for the degree of Doctor of Philosophy

The University of Edinburgh

2014

Declaration

This work was completed in the School of Biomedical sciences at the University of Edinburgh. The work in this thesis has not been submitted for any other degree or professional qualification. All work in this thesis was conducted by myself with the exception of the following figures;

Chapter 3 figure 1 panels A, B,D,E,G,H,
Chapter 3 figure 2 panels A,A',D,D',E,E',G,G'
Chapter 3 Figure 3 panels A,B,D,E,G,H,J,K,M,N
Sections in these figures were reacted with the help of Prof K.R. Duffy, who was visiting the Kind Laboratory while on Sabbatical.

Chapter 4 Figure 6
The histology and imaging required for this figures was the result completed in collaboration with Adrain Duszkiewicz a project student under my supervision in the lab.

Chapter 5 Figure 2 panels F,H
These panels were reacted and imaged by Dr. Anne Petrie, a previous PhD student in the lab.

Chapter 5 Figure 4

The histology in figure was conducting with two project students under my supervision in the lab, Laura Wagstaff and Victoria Hutchinson.

Alex Crocker-Buqué

May 2014

A note of thanks,

I would like to thank my primary supervisor Prof Peter Kind for accepting me on as a PhD candidate, and the members of my thesis committee Prof. David Wyllie and Dr John Mason.

To the past and present members of the Kind Lab who have always been available for help and support; Lasani Wijetunge, Sally Till, Viktoria Seidel, Aleks Domanski, Mel Chiang, lynsey Meikle, Tim O'leary, Aoife MacMahon, Mark Barnett and Anne Petrie.

I also wish to thank Trudi Gillespie, Vivian Allison, Grace Grant and Louise Dunn for all their technical help.

Finally I want to thank my family who were always there to provide a much-needed distraction.

To Jemma, for putting up with it all.

Abbreviations

(m)EPSC	(miniature) Excitatory postsynaptic current
$^{-/-}$	homozygous null geneotype
$^{-/y}$	hemizygous genotype
$^{+/-}$	heterozygous genotype
$^{+/+}$	wildtype genotype
µg	Micrograms
5HT1b	Serotonin 1b receptor
A	Auditory cortex
AKAP	A-kinase anchor proteins
AMPA receptor	α-amino-3-hydroxy-5-methyl-4-isoxazolepropionic acid
APV	((2R)-amino-5-phosphonovalieric acid
AS	Anterior snout
BDNF	Brain-derived neurotrophic factor
CA3	Cornu ammonis region 3
CamKII	Calcium/Calmodulin-dependent protein kinase
cAMP	Cyclic adenosine monophosphate
CL	Contra-lateral
CO-IP	Protein complex immunoprecipitation
CTX	Cortex
CTX-NR1	cortex specific GluN1 null mutant
DiI perchlorate	1,1'-dioctadecyl-3,3,3',3'-tetramethylindocarbocyanine
DLG	Disks large homolog 3
DNA	Deoxyribonucleic acid
ERK/MAPK	Extracellular signal-regulated kinases/Mitogen-activated protein kinase
FGF8	Fibroblast growth factor 8
Fl	Front limb
FMRP	Fragile X mental retardation protein
GABA	γ-Aminobutyric acid
GK	Guanlate kinase
IC	Internal capsule
IL	Ipse-lateral
ION	Infraorbital nerve
Ip	Intraperitoneal injection
Kg	Kilograms
LGE	lateral ganglionic eminence
LGN	lateral geniculate neucleus
LL	Lower lip
LTD	Long-term depression
LTP	Long-term potentiation
M	Molar
MAGUK	Membrane-associated guanylate kinase
MAOA	Monoamine oxidase
MASC	MAGUK-associated signalling complex

MBP	Myeline basic protein
MECP2	methyl CpG binding protein 2
Mg	Milligrams
mGluR5	metabotropic glutamate receptor 5
mls	millilitres
MUPP1	Multi-PDZ domain protein 1
NA	numerical aperture
NFH	Neurofilament 'heavy'
NFL	Neurofilament 'light'
NFM	Neurofilament 'medium'
NGF	Nerve growth factor
N_{ko}	number of knockout replicates
NMDA	*N*-methyl-D-aspartate
nNOS	neuronal nitric oxide synthase
NT4	Neurotrophi-4
N_{wt}	number of wildtype replicates
P	Postnatal day
PCPA	parachlorophenylalanine
PDZ	**P**SD95, **D**rosophilia disc tumor suppressor, **z**onula occludens-1 protein
PKArII beta	Protein Kinase A RII beta subunit
PLC-beta 1	Phospholipase C-beta 1
PMBSF	Posteromedial barrel subfield
POm	The posterior thalamic neucleus of the thalamus
ProSAP/Shank	Proline-rich synapse-associated protein/**SH**3 domain and **ank**yrin repeat containing protein
PSD	Post Synaptic Density
PSD93	Postsynaptic density 93
PSD-95	Postsynaptic density 95
PSD97	Postsynaptic density 97
RGC	radial glial cell
RIM1/2	Rab3 interacting molecule 1 /2
RNA	Ribonucleic acid
S1	The primary somatosensory cortex
SAP102	Synapse-associated protein 102
SERT	Serotonin reuptake transporter
SH3	SRC Homology 3
SOD1	Superoxide dismutase 1
SynGAP	Synaptic RasGTPase activating protein
T	Test statistic
T	Tongue
TARP	transmembrane GluA receptor regulatory proteins
TCA	Thalamocortical axon
TrkB	Tyrosine-related kinase B
Tukey HSD	Tukey Honestly Significant Difference test
V	Visual cortex
vAMP	Vesicle-associated membrane protein
Vc	The caudal nucleus
vGAT	Vesicular GABA transporter
vGlut	Vesicular glutamate transporter

Vi	The interpolar neucleus
Vo	The oral neucleus
Vp	The principle neucleus
VpM	The ventral-posterior nucleus of the thalamus
WT	Wild type

Contents

List of tables and figures

Chapter 1. Introduction

Chapter 2. Methods

Chapter 3. Characterisation of 3 Neurofilament subunits in the developing S1

Abstract

In order to process information, neurons must connect together to form a neuronal circuit. The formation of neuronal circuits is dependent on synaptic activity through glutamate receptors and downstream molecules within the post-synaptic density (PSD). The pathways downstream of glutamate receptors play an important role in maintaining appropriate synapses and forming neural circuits; mutations in genes that encode PSD proteins disrupt these pathways and are associated with many forms of intellectual disability in humans (Grant 2012). The development of neuronal circuits relies on two key developmental events; neurons must first send out axons locally and to disparate brain regions and then, neurons must form connections with the dendrites of target neurons.

The rodent trigeminal system is a neuronal circuit that processes somatosensory information from whiskers on the facepad via nuclei in the brainstem to the thalamus and ultimately the cerebral cortex. Brain regions that comprise the trigeminal system are organised in a manner that topographically recapitulates the whisker pattern; each whisker on the rodent facepad corresponds to a physiological and anatomical unit in the primary somatosensensory cortex (S1) called a *barrel*. This topographical organisation creates a pattern consisting of thalamocortical axons (TCA) clustered into distinct whisker-related bundles and layer IV spiny stellate cells which segregate around the outside of TCA bundles. Three different anatomical patterns can be identified within the mouse S1 by labelling the cell soma, axons or the extracellular matrix. This strict organisation makes the rodent S1 an excellent model for discerning the proteins involved in neural circuit formation, and by screening genetic mutants for S1 patterning defects the molecular pathway involved in setting up neuronal circuits can be elucidated. Furthermore an understanding of these

pathways may provide insight into how neuronal networks are disrupted in human intellectual disability.

In the first data chapter, the expression profile of three neurofilament subunits were characterised in order to develop a method of identifying anatomical defects in barrel morphology. The precise organisation of the rodent S1 can also be used as a method to identify the cellular localisation of neurofilament subunits *ex vivo*. Neurofilaments are polymers formed from three subunits identified by their relative molecular weight. By using the unique patterning of S1, each neurofilament subunit shows a unique spatial-temporal expression pattern in the somatosensory cortex. Two neurofilaments subunits; the medium and the heavy neurofilament subunits can be used to identify TCA which can be used as an indicator of anatomical defects in barrel patterning.

In chapter 4 neurofilament labelling was used in conjunction with other histological techniques to investigate S1 organisation in mice lacking synapse associated protein 102 (SAP102). SAP102 is a PSD scaffolding molecule that binds to both NMDA receptor subunits and SynGAP, a synaptic GTPase activating protein, furthermore it is associated with X-linked mental retardation in humans (Tarpey et al., 2004; Zanni et al., 2010). Mutant mice lacking functional NMDA receptors or PSD proteins such as SynGAP show defects in S1 pattern formation (Barnett et al., 2006; Iwasato et al., 2000; Wijetunge, Till, Gillingwater, Ingham, & Kind, 2008). *SAP102* null mutants (*SAP102*$^{-/y}$) have defects in synaptic plasticity and are slow to learn on behavioural tasks (Cuthbert et al., 2007), however it is unclear how the loss of SAP102 may disrupt neural networks. *SAP102*$^{-/y}$ were found to have a reduction in brain mass compared to wild-type littermates, but cortical thickness and patterning of S1 is unchanged. *SAP102*$^{-/y}$ have fewer TCA reaching the cortex compared to littermates; furthermore *SAP102*$^{-/y}$ mutants have layer specific defects in the density of dendritic spines.

These data suggest that in the absence of SAP102 connectivity in the S1 is altered by layer specific changes in synapses number and fewer axons innervating cortical layer IV.

In the final experimental chapter (chapter 5) the combined role of SAP102 and Postsynaptic density protein 95 (PSD95) in S1 patterning was investigated. SAP102 and PSD95 are the main members of the membrane-associated guanylate kinase (MAGUK) family expressed during early cortical development. These proteins share a similar protein structure, perform similar functions at the synapse (Elias & Nicoll, 2007) and have been shown to compensate for each other *in vitro* (Elias, Elias, Apostolides, Kriegstein, & Nicoll, 2008). Genetic mutants lacking both SAP102 and PSD95 are not viable and do not survive beyond birth (Cuthbert et al., 2007; Petrie, 2008). Therefore in order to investigate the combined role of these proteins a novel approach was developed that utilises X-inactivation to produce mosaic animals containing cells that lack both proteins. The distribution of cells containing the same X-chromosome was investigated and found to be evenly distributed throughout the cortex, demonstrating that this method could be used to investigate allosomal genes. In mosaic animals where approximately half the cells only lack PSD95 and the remaining cells lack both SAP102 and PSD95, double knockout cells are viable and are equally represented in S1. These double knockout cells contribute to normally barrel formation which suggests that SAP102 and PSD95 are not required for barrel formation.

Chapter 1

Introduction

1.1. Overview

In order to process information neurons must connect together to form a neuronal circuit. These neuronal circuits require precise connectivity both within and between different brain areas. The site of neuronal connections is the synapse and therefore the formation of appropriate synapses is integral to neural connectivity and the development of neuronal circuits. Mutations in a number of genes that encode synaptic proteins have been associated with psychiatric or neurological disorders in humans, collectively these disorders are referred to as synaptopathies (Grant 2012). Synaptopathies are hypothesised to be the result of inaccurate or inappropriate synapses forming between neurons, this disrupts neuronal circuits and results in intellectual disability.

The adult mammalian brain is a compartmentalised and heterogeneous structure and contains specialised areas which perform particular tasks, for example neurons involved in the planning of motor tasks are clustered together in a separate location to those that process visual information. Different brain areas correspond to specific aspects of information processes, therefore the organisation of the brain provide a representation or a *map* of the information being processed. The gross organisation of the brain is laid out in a *coarse map* which can be identified by cytoarchitectural differences between brain areas, within these coarse maps are *fine maps* which correspond to the spatial or functional features of a stimulus. Different developmental mechanisms are required to set up course and fine maps; coarse map development is mostly dictated by transcription factors whereas fine maps rely on the precise innervation of axons from other brain regions and forming appropriate synapses with neurons in those brain regions. Therefore fine map formation can serve as a model for the formation of appropriate synapses and the development of neuronal circuits.

This thesis uses the rodent trigeminal system as a model system to investigate the role of synaptic proteins in the development of cortical maps. This introductory chapter is divided into four topics, first an overview of cortical maps will be discussed, focusing on their development. Then rodent trigeminal system will be introduced, which will serve as the model system. Following this synaptogenesis and the formation of dendritic spines will be discussed. The final section will provide an overview of the Membrane Associated Guanylate kinases (MAGUKs), the role of these synaptic proteins is the focus of this thesis.

1.2. Cortical maps

1.2.1. Coarse cortical maps

As previously mentioned the cortex is segregated into separate areas that have distinct functional roles. These areas can be readily identified by differences in cytoarchitecture. The broad arrangement of coarse cortical maps is determined by the expression of transcription factors (reviewed in Rakic, Ayoub, Breunig, & Dominguez, 2009) which determine the fate of neurons during early stages of development. Genetic manipulation of transcription factors such as FGF8 or EMX2 results in the displacement of cortical areas (Fukuchi-Shimogori & Grove, 2001; Hamasaki, Leingärtner, Ringstedt, & O'Leary, 2004).

1.2.2. Fine cortical maps

Fine maps are best exemplified in brain regions that receive sensory information from the periphery. Fine cortical maps are categorised by either the features or the position of a particular stimulus and are called feature and topographical maps respectively. Examples of feature maps can be seen in the visual cortex where clusters of

cells will selectively respond to the orientation or movement direction of a visual stimulus. Topographical maps identify the position of a sensory stimulus on the surface of the sensory organ, e.g. the position of light hitting the retina (retinotopic map), or the location of tactile stimuli hitting the skin (somatotopic map). In the visual cortex cells cluster depending on the eye that receives the visual stimulation, some cells respond to stimuli from only one eye whereas other cells have a bias towards the contra- or ipsi-lateral eye, this is referred to as ocular dominance and is another example of a topographical map. Another aspect of fine maps is the *receptive field* of a cell; this is the position on the receptive surface where a stimulus will evoke a response from the cell. For example the receptive field of a neuron in the somatosensory cortex will be the area on an animal's skin, or a neuron in the auditory cortex may have a receptive field that corresponds to a position on the basal membrane of the cochlea.

1.2.3. The development of fine cortical map

One of the most salient examples of a fine map is the organisation of the retina which is topographically recapitulated in the superior colliculus. The distance between the somata of two cells in the retina is proportional to the distance between their axonal terminations in the superior colliculus. This precise organisation is the result of gradients of receptors (Ephs) and the corresponding surface bound ligand (Ephrins) expressed along the medio-lateral/anterior-posterior axis of the superior colliculus and the nasal-temporal/dorsal-ventral axis of the retina (Hindges et al. 2002; Cheng et al. 1995; reviewed in Triplett & Feldheim 2012). These surface molecules provide the spatial cues required for axons to reach their corresponding targets.

Whilst the retinotopic organisation of the superior colliculus is a prime example of surface molecules directing fine map organisation, there are many other surface molecules

that play a role in the development of synaptic specificity as well as synapse structure and function (reviewed in Benson et al. 2001). The vast number of such molecules suggest that some axonal terminals and dendrites may have a specified molecular signature that identifies their required targets, and that this mechanism may be involved in the development of other fine maps.

It has long been hypothesised that correlated neuronal activity is instrumental in the formation and maintenance of new synapses and is therefore a key requirement in setting up cortical circuitry (Hebb, 1949). For example, in the retina co-ordinated spontaneous activity propagates across the retina; this activity is referred to as retinal waves. Retinal waves can be observed during topographic map formation but before the eyes open, demonstrating that this activity is not evoked by a sensory stimuli (Meister, Wong, Baylor, & Shatz, 1991; Penn, 1998; Shatz, 1996; Shatz & Stryker, 1988; Rachel O L Wong, 1999). Retinal waves are thought to determine the eye-specific segregation of retinal projections to the dorsal lateral geniculate nucleus (dLGN), as manipulations that alter retinal waves disrupt the eye-specific organisation of dLGN (reviewed in Feller 2009, but see Chalupa 2009 for alternative view). Recently *in vivo* calcium imaging experiments have identified networks of spontaneous activity in the developing visual system that are dependent on retinal waves (Ackman, Burbridge, & Crair, 2012; M. Feller, 2012; Siegel, Heimel, Peters, & Lohmann, 2012). Retinal waves and corresponding network activity in other areas of the visual system carry spatial and temporal information about the organisation of the retina and are therefore well-placed to play a role in retinotopic map formation. The development of topographic maps will be further discussed in section 1.3.3, which focuses specifically on the topographical maps of the rodent primary sensory cortex (S1).

1.2.4. Sensory induced activity

The influence of sensory-induced activity in cortical map formation has been extensively studied, mostly in the visual system where sensory experience can be easily manipulated. Experiments conducted in a variety of animal models have demonstrated that sensory experience is not required for cortical maps to form. For example orientation selective maps are formed before kittens receive visual stimuli (Crair et al., 1998); primates reared in the dark still form ocular dominance columns (Horton & Hocking, 1996); and direction and orientation specific neurons are present in the mouse visual cortex before the eyes have opened (Rochefort et al., 2011).

Whilst the development of fine maps in the visual does not require visual experience, there is clear evidence that sensory induced activity can act to modify and maintain fine maps (reviewed in Espinosa & Stryker 2012). For example, exposing kittens to only one orientation of visual stimulus increases the number of cells that specifically respond to that orientation, however some cell still respond to a novel angle (Sengpiel, Stawinski, & Bonhoeffer, 1999). Furthermore depriving one eye of visual stimulation (monocular deprivation) in a cat reduces the area dedicate to processing information from the deprived eye (Hubel, Wiesel, & LeVay, 1977; LeVay, Wiesel, & Hubel, 1980). The presence of cells that respond to an orientation that has not been view before (Sengpiel et al., 1999) or a visual area corresponding to a deprived eye (Hubel et al. 1977) demonstrate that stimulus driven activity can modify fine maps, but is not necessary for their formation. This is known as playing a *selective* role, and is in contrast to an *instructive* role, where activity is required for the formation or modification of a neuronal network. The third way activity can influence the development of fine maps is via a *permissive* role were a minimum level of activity is required to develop a neuronal network but increased activity beyond this threshold has no further effect on the network.

These deprivation paradigms only elicit effects within a particular time frame called a *critical period*. The critical period describes the time during brain development when sensory experience can affect neuronal structure or function (Erzurumlu & Gaspar, 2012; Hensch, 2004). This is demonstrated in cats where monocular deprivation after the first 8 postnatal weeks did not affect orientation map formation (LeVay et al., 1980). Critical periods can vary in onset and duration, depending on the sensory system, the manipulation being enforced or the species being studied (reviewed in Levelt & Hübener 2012). The role experience plays in shaping S1 patterning will be addressed in section 1.3.5, on lesion induced plasticity.

1.3. The rodent trigeminal system

Rodents rely heavily on tactile sensation to explore their environment. The primary sensory organs for receiving somatosensory information in rodents are the large whiskers or vibrissae on the facepad. The vibrissae move rhythmically and when deflected can determine the location and texture of objects (reviewed in Kleinfeld & Deschênes 2011). Regions in the periphery that receive somatosensory information are organised in topographical maps in the brainstem, thalamus and cortex (reviewed in Fox 2008). Peripheral areas that are highly sensitive to somatosensory input are disproportionally represented in the brain, for example approximately 70% of the mouse primary somatosensory cortex is dedicated to receiving information from the facial vibrissae alone (Lee & Erzurumlu, 2005).

1.3.1.i. Vibrissae to brainstem

Each large whisker follicle on the rodent facepad is innervated by a unique branch of the infraorbital nerves (ION). The ION enters the brainstem on the ipsilateral side to the whisker corresponding follicles. There are four nuclei in the brainstem that receive the fifth (V) cranial nerve; the principle nucleus (Vp), the oral nucleus (Vo), the interpolar nucleus (Vi) and the caudal nucleus (Vc). Of these brainstem nuclei three (Vp, Vi and Vc) show a whisker-related topographical patterning when reacted for cytochrome oxidase or nissl stained, this pattern in the brainstem is referred to as *barrelettes* (Ma, 1991). Of all these brainstem nuclei, Vp receives the most innervation and is the main relay station *en route* to the thalamus, however Vi also projects to some thalamic nuclei.

1.3.1.ii. Brainstem to Thalamus

Neurons in the brainstem project their axons to thalamic nuclei on the contralateral hemisphere of the brain. Axons from the Vp innervate the ventral-posterior nucleus of the thalamus (VpM), whereas projections from the Vi target the ventro-lateral VpM and the posterior thalamic nuclei (POm). Although both POm and VpM represent input from the vibrissae, the VpM is the main target for somatosensory processing and can respond to single whisker stimulation at a higher temporal (Diamond, Armstrong-James, & Ebner, 1992) and spatial resolution (Chiaia, Fish, Bauer, Bennett-Clarke, & Rhoades, 1992) than the POm. This demonstrates that the main lemniscal axon responding to tactile stimuli in the rodent is from the Vp in the brain stem to the VpM in the thalamus.

1.3.1.iii. Thalamus to cortex

Neurons from both the POm and VpM project to the cortex, however projections from POm and VpM neurons form a complimentary pattern in cortical layer IV (see anatomical organisation of S1 patterning; Koralek et al. 1988; Wimmer et al. 2010). Axons from VpM cells branch extensively in layer IV and to a lesser extent in layer VI (Bernardo & Woolsey, 1987), these axons make up the main lemniscal pathway, therefore in following chapters this group of axons are referred to as thalamocortical axons (TCA). Axons from the PoM also project to a different subset of cells to VpM projections (see section 1.3.2 on S1 patterning). The trajectory taken by TCA from both the PoM and VpM are guided to their destination by a multitude of factors including guidepost cells, attractant or repellent cues, intermediate targets and axonal fasciculation (reviewed in Molnár et al. 2012).

1.3.2. Anatomical organisation of S1 patterning

TCA innervating the rodent S1 maintains the toprographical representation of vibrissae on the facepad. Furthermore there is a direct relationship between a single whisker on the face and a given functional unit in S1 so that when a whisker is manipulated experimentally, neurons will fire in the corresponding functional unit. In the cortex these functional units can be visualised by labelling thalamocortical axons, the region between functional units called septa and cells of layer IV that segregate around the outside of thalamocortical axons. The term *barrel* is used to describe a single whisker-related unit, however this is imprecise, here I will distinguish between the segregation of layer IV cells calling it a *barrel* pattern, TCA bundles calling them thalamocortical axon *patches* and inter-barrel regions labelling them a *septal* pattern. As previously mentioned projections from the VpM and POm both project to cortical layer IV, however projections from the VpM form the main innervations to layer IV and are restricted to individual functional units in a TCA *patch* pattern. Axons from the POm project to layer IV and are restricted to septae.

The formation of S1 patterning occurs in the first postnatal week in rodents and provides a model to study postnatal cortical development. Thalamocortical axons segregate into vibrissae-related patches by P3 (Lee, Iwasato, Itohara, & Erzurumlu, 2005; Rebsam, Seif, & Gaspar, 2002), between P4 and P6 cells in layer IV of the cortex segregate around the outside of these patches. Between P4 and P14 layer IV cells selectively elaborate their dendrites towards the centre of the barrel, forming synapses with TCA (Espinosa, Wheeler, Tsien, & Luo, 2009). For the purpose of labelling in this thesis the cell dense ring of cells is called the barrel *wall* and the cell sparse barrel centre is called the *hollow* (see **Fig. 2**).

Figure 1. Anatomical organisation of S1

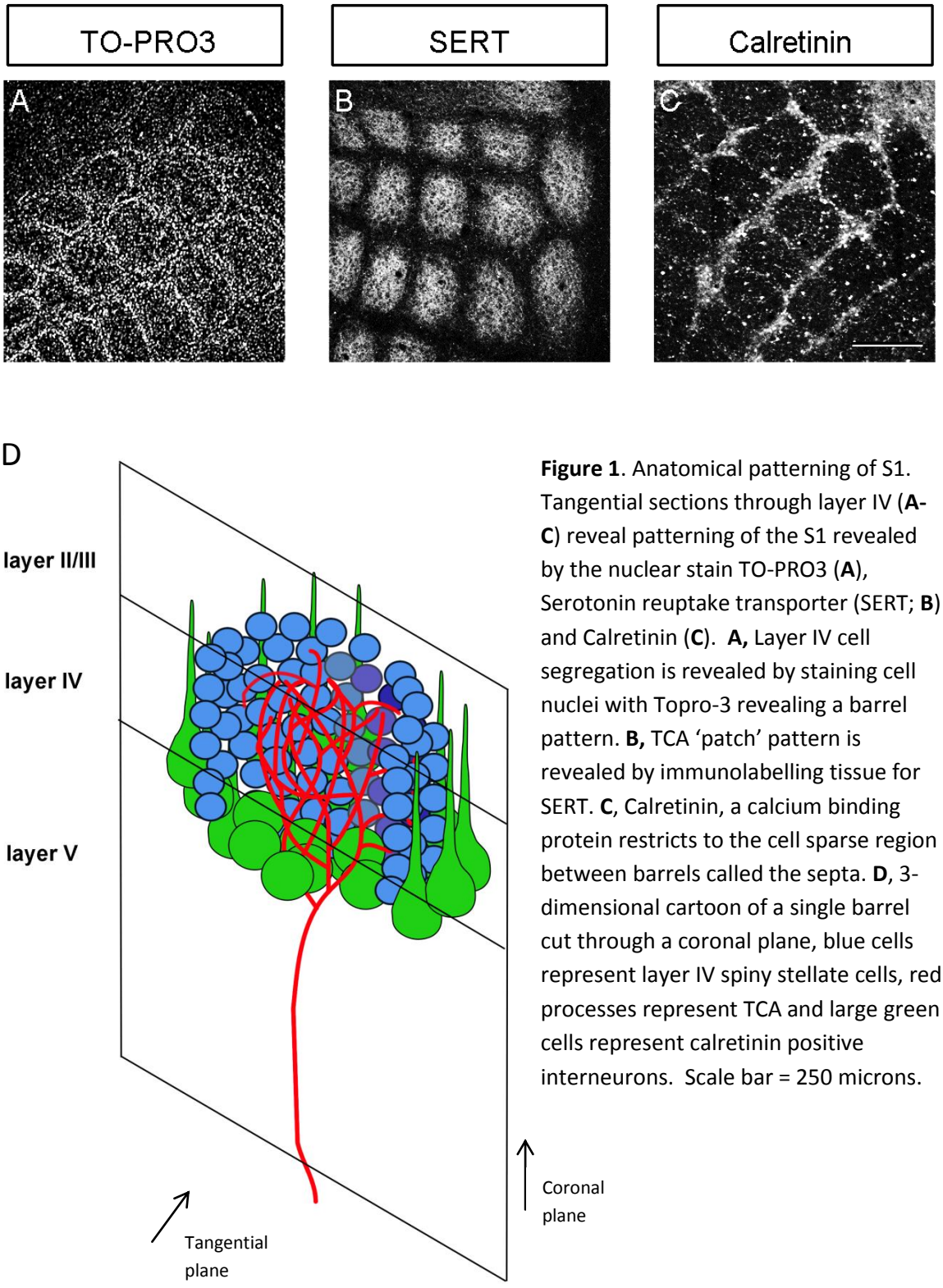

Figure 1. Anatomical patterning of S1. Tangential sections through layer IV (**A-C**) reveal patterning of the S1 revealed by the nuclear stain TO-PRO3 (**A**), Serotonin reuptake transporter (SERT; **B**) and Calretinin (**C**). **A,** Layer IV cell segregation is revealed by staining cell nuclei with Topro-3 revealing a barrel pattern. **B,** TCA 'patch' pattern is revealed by immunolabelling tissue for SERT. **C**, Calretinin, a calcium binding protein restricts to the cell sparse region between barrels called the septa. **D**, 3-dimensional cartoon of a single barrel cut through a coronal plane, blue cells represent layer IV spiny stellate cells, red processes represent TCA and large green cells represent calretinin positive interneurons. Scale bar = 250 microns.

Figure 2. Anatomical organisation of a single barrel

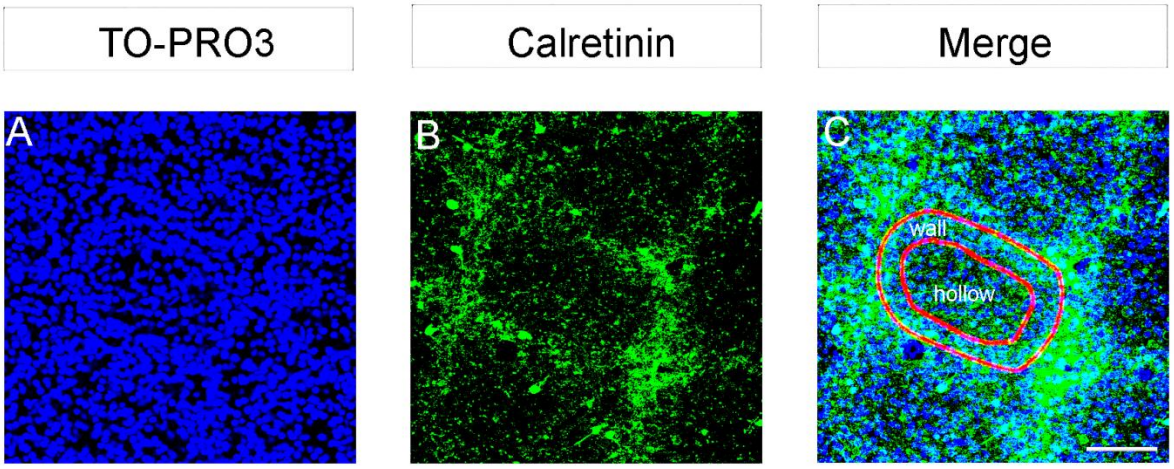

Figure 2. Anatomical organisation of a single barrel. Tangential section through layer IV of S1 labelled for TO-PRO3 reveals the barrel pattern (**A**), and calretinin which labels the barrel septa (**B**). For the purpose of barrel quantification this thesis will distinguish between the cell dense region labelled the barrel *wall* and the cell sparse region called the barrel *hollow* (**C**)**.** Scale bare = 250 µm

1.3.3. Development of Thalamocortical axon patterning in the cortex

Shortly after leaving the thalamus, TCAs lose their near neighbour relationships (Senft & Woolsey 1991), and the orientation of S1 is shifted 180 degrees relative to the thalamus, therefore TCA must receive some organisational cues before segregating into whisker-related patches. This organisational cue is thought to be provided by a dorsal-ventral gradient of Ephs in the VpM and medio-lateral gradient of ephrins in S1 (Dufour et al., 2003). In support of this hypothesis the size of individual barrels is distorted in mutants lacking EphrinA (Dufour et al., 2003; Triplett & Feldheim, 2012; Vanderhaeghen et al., 2000). In the mouse S1, Ephrin A5 is expressed until P3 however it is unclear in which cortical layer TCA segregate into a vibrissae-related pattern. Radial bands of TCA have been seen coursing straight through layer V in a pre-arranged pattern before the formation of S1 patterning (Agmon et al. 1993, **Fig. 3A**), suggesting that TCAs arrange into a whisker-related

pattern in layer V. However labelling axons for SERT (serotonin reuptake transporter) suggests TCA are arranged in a uniformed manner in the cortical plate at P1 and elaborate laterally across the cortex before restricting axon back into individual functional units (Rebsam et al., 2002). This is supported by axon tracing experiments where two lipophilic dyes were placed next to each other in the cortex at different developmental ages and the distance between labelled VpM cell bodies was measured; dye placed at P0 labelled cell bodies further apart than those placed at older ages, demonstrating that at young ages TCA innervated a larger cortical regions (Agmon et al. 1995). Furthermore, single axon reconstructions in adults find that some TCA do not project straight through layer V in a radial manner, instead axons project at an angle spanning the width of multiple barrels before reaching layer IV (Catalano et al. 1996; Rebsam et al. 2002, **Fig. 3B**).

Recently a role for subplate neurons has been identified in the formation of S1 patterning. Subplate neurons are a transient population of cells that form synapses with TCA and layer IV cells during early development (reviewed in Kanold & Luhmann 2010). Ablation of subplate neurons at P0 affects spontaneous activity in S1 and disrupts the formation of cytochrome oxidase-labelled barrel pattern (Tolner, Sheikh, Yukin, & Kanold, 2012). Therefore subplate neurons may provide early positioning cues to TCA before they have reached cortical layer IV.

Figure 3. TCA organisation

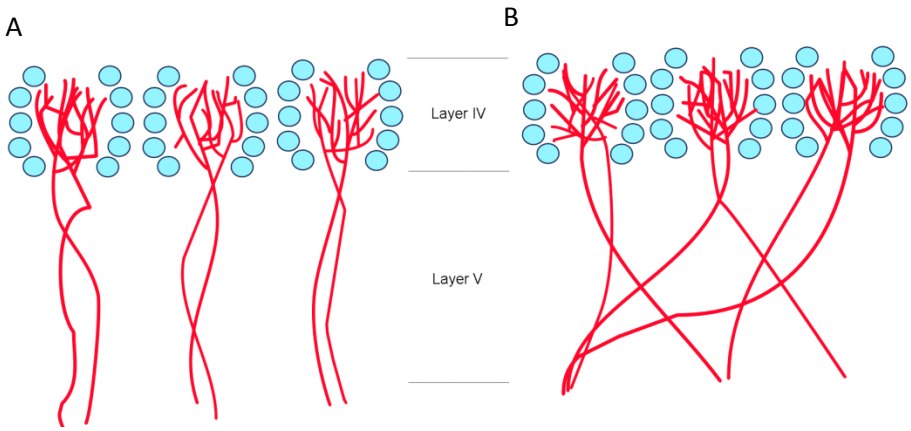

Figure 3. Two possible theories of TCA organisation. Schmatic represents a coronal section through the cortex with TCA in red lines and cells comprising the layer IV barrel pattern shown using blue circles. In layer IV TCA elabourate within a barrel forming a TCA 'patch' within the cell-sparse barrel 'hollow'. TCA may take a direct route through layer V, maintaining the same lateral position (**A**) as suggested by Agmon et al. 1995. Alternatively TCA may project laterally across layer V as they find their layer IV targets (**B**; Catalano et al. 1996, Rebsam et al. 2002).

1.3.4. Mechanisms of Barrel formation

Once TCA segregate into whisker related patches, cells in layer IV segregate around the outside of TCA patches to create a barrel pattern. Although the mechanisms by which layer IV cells segregate is not known, insight into this mechanism can be gained by studying the structure of the S1 pattern. The first event to occur in the developing S1 is the invasion of thalamocortical axons, which project to layer IV and branch to form tight bundles. Shortly after TCA branching, layer IV cells segregate around the outside of thalamocortical axons patches and orientate their dendrites towards TCA to form synapses with them. The ratio between cells on the outside of thalamocortical axons patches and inside them is small; for every 3 cells on the cells dense region, there are 1-2 cells in the centre, however this ratio is sufficient for a pattern to be readily discernible by the human eye. The septa are a cell sparse region between barrels, which contain a number of cell adhesion molecules, such as tenascin C (Steindler et al., 1995), neurocan (Watanabe et al., 1995) and

lectins (Cooper & Steindler, 1986). The septal region can also be identified by labelling with the calcium binding protein calretinin (Melvin & Dyck, 2003); calretinin labels a subpopulation of large interneurons present at the layer IV/V boundary, and the processes of these cells are restricted to the septal region. Several theories provide an explanation of how layer IV cells transition from being uniformly distributed at birth to segregating into whisker related barrels at around P4-5; these include passive displacement, cell migration and selective cell adhesion (Barnett, Watson, & Kind, 2006).

1.3.4.i. Passive cell displacement

Individual barrels appear to consist of a ring of cells that have been displaced to an outer diameter. This is due to the barrel containing a normal cell density in the centre, a cell sparse ring followed by a cell dense ring. The centre of the barrel is dense with neuropil, not only the extensive TCA branches in this region, but also dendritic elaboration of layer IV cells that extend their dendrites towards TCAs, this elaboration could push cells out of the barrel centre (see **Fig. 4**). This mechanism is able to explain the 3 different cell densities within a single barrel; cells initially located in the peripheral portion of the TCA patch would be pushed out to form the cell dense region whereas cells in the centre of the barrel would not move because they are being pushed in from all directions. The elaboration of TCA occurs around the time of barrel formation (Lee et al., 2005; Rebsam et al., 2002), however a number of mutants have been identified where TCA elaborate normally and barrels still fail to form (Hannan et al., 2001; Narboux-Nême et al., 2012) demonstrating that TCA elaboration alone is insufficient to form barrels. Layer IV dendrites begin to elaborate around P3 and show an orientation preference at P6 (Espinosa et al., 2009), asymmetric elaboration towards the centre of TCA may provide the dense neuropil required to displace layer IV cell bodies into a barrel pattern, however some mutants which

have fewer orientated dendrites still form a normal barrel pattern (Takuji Iwasato et al., 2008) suggesting that dendritic orientation is not the only mechanism responsible for forming barrels.

Figure 4. Barrel formation by passive cell displacement

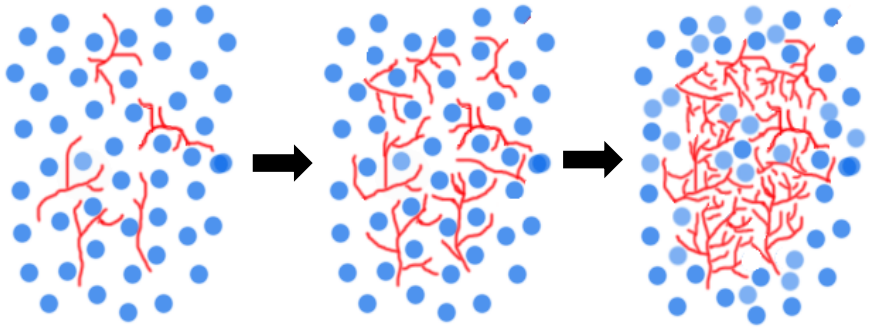

Figure 4. Passive cell displacement model of barrel formation. Thalamocortical axon (red) elaboration occurs at approximately the same time as barrels form. Thalamocortical elaboration may displace cell soma (blue circles) towards the outside of the barrel creating a ring of cells, with a few cells in the centre of the barrel which have been pushed on all sides. This mechanism is able to explain the 3 different cell densities seen in a single barrel.

1.3.4.ii Cell migration

Incoming TCA may express repulsive cues that cause layer IV cell bodies to disperse to form a barrel pattern, however this causes a problem because dendrites from the same layer IV cells would then need to orientate towards TCA. This could be resolved with either multiple attractant and repulsive cues or a single cue that has different effects on the soma and dendrites of a layer IV cells. Layer IV cells do not completely orientate towards TCA until P14 providing temporal separation between the two developmental events, therefore

TCA could initially be repulsive, then attractant to layer IV cells. A cell migration mechanism could work in conjunction with extra cellular molecules expressed in the septa acting as a boundary which prevents layer IV cells migrating outside of the S1, however there is no experimental evidence to support this mechanism.

1.3.4.iii Cell Adhesion

During the first postnatal week cortical area expands significantly and differential cell adhesion could result in the different cell densities seen in S1. Tenascin C is an extracellular protein that is expressed during early neural development, in the rodent S1 tenascin C is downregulated and is restricted to the septal despite being uniformly distributed throughout the rest of layer IV (Mitrovic, Dörries, & Schachner, 1994). Tenascin C can prevent fibronectin-mediated cell adhesion and neurite outgrowth (Probstmeier & Pesheva, 1999) therefore a down-regulation of tenacin C during barrel formation would allow cells to migrate away from the TCA patches concurrent with cortical expansion. Furthermore application of GluN antagonists prevents this down regulation of tenascin C and prevents barrels from forming (Mitrovic, Mohajeri, & Schachner, 1996), providing a potential mechanism by which GluN activation would affect S1 patterning. Contrary to this hypothesis tenascin C knockout animals still form a normal barrel pattern, however there are other cell adhesion molecules downregulated in TCA patch region that are still expressed in the tenascin C null mutant and these may also affect cell adhesion within S1; demonstrating that there may be redundant mechanisms working to ensure the development of the whisker-related topographic maps (Steindler et al., 1995).

1.3.5. Lesion induced plasticity

In section 1.2.4 we saw how fine maps can be modified by sensory experience, and the development of the rodent S1 is also influence by the periphery. This is demonstrated by mice with additional whiskers on the facepad also containing extra barrels in S1 (Welker & Van der Loos, 1986). Furthermore, lesioning individual whisker follicles early in development can also affect the formation of S1 patterning (reviewed in Erzurumlu & Gaspar 2012). For example, cauterising a row of whiskers will prevent the corresponding row of layer IV cells segregating into barrels, instead these cells will orientate their dendrites towards neighbouring unaffected rows (Harris & Woolsey 1979). This structural re-organisation only occurs within a specific critical period; if whiskers are removed after P5 no anatomical changes will occur (Woolsey & Wann 1976; Harris & Woolsey 1979). Application of the NMDA receptor antagonist (2R)-amino-5-phosphonovaleric acid (APV) prevents the alteration in anatomical structure following whisker follicle ablation, demonstrating that this re-arrangement is dependent on glutamate neurotransmission (Schlagger, Fox, & O'Leary, 1993).

The critical period for lesion induced alteration in S1 architecture ends shortly after TCA have segregated (Rebsam et al., 2002), it is therefore possible that the same mechanism is responsible for both the normal development of S1 patterning and re-arrangement of the cytoarchitecture following follicle lesion. Mutant mice lacking the monoamine oxidase enzyme do not form TCA patches; however this phenotype can be rescued by reducing serotonin, either by reducing the expression of 5HT1b receptors or the application of the tryptophan hydrocylase parachlorophrenylalanine (PCPA; Rebsam et al. 2005). The rescue of S1 patterning in *MAOA* knockout animals by reducing serotonin release can be delayed by up to six days, yet the critical period for lesion induced plasticity

is unaltered in these animals (Rebsam et al., 2005), demonstrating that S1 reorganisation following whisker ablation and barrel formation were induced by separate mechanisms.

It is important to note that the experiments described above should not be taken as evidence of sensory experience shaping S1 patterning. These experiments involved whisker cauterisation, which damages the follicle and results in several cellular processes including degeneration of the ION that induces transneuronal cell death in VpM of the thalamus (Erzurumlu & Gaspar, 2012). Furthermore, barrel formation is maintained in ION sectioned animals by application of neurotrophic factors such as brain derived neurotrophic factor or nerve growth factor (Baldi et al., 2000). Trimming whiskers from birth is a less invasive method of sensory deprivation and this has no effect on the cytoarchitecture of the S1 (Simons & Land, 1987), suggesting that it is not experience that shapes S1 patterning but a process that requires intact whisker follicles, and supports the notion that spontaneous activity is sufficient to drive barrel formation. Finally following Row C follicle ablation, the layer 4 cells form a cell dense wall around the fused Row C TCAs suggesting that spontaneous release of glutamate from the spared TCA axons may be sufficient to signal barrel formation (Van der Loos & Woolsey 1973).

Whilst whisker trimming does not affect the organisation of S1, it does affect the receptive field of cells in layer IV; cells in barrels corresponding to deprived whisker lose their selectivity to individual whisker stimulation (Fox, 1992; Simons & Land, 1987). Trimming whiskers can also affect anatomical aspect of S1 that are not reflected in the overall barrel pattern; barrels corresponding to deprived whiskers contained TCA with fewer branch points (Wimmer, Broser, Kuner, & Bruno, 2010) and layer IV cells in those barrels had a larger dendritic span and increased spine density (Lee, Chen, Chuang, & Wang, 2009). Once whiskers have regrown TCA density returns to normal levels regardless

of the age of the animal when deprived, therefore this aspect of experience dependent development does not display a critical period (Wimmer, Broser, et al., 2010).

1.3.6. Molecular pathway of barrel formation

Although it is unclear how layer IV cells segregate, the molecular pathway involved in S1 patterning can be investigated by screening mutants for S1 defects (Erzurumlu & Kind, 2001). Using this method a number of pre- and post-synaptic proteins have been identified which are involved in barrel formation.

1.3.6.i Pre-synaptic mechanisms of barrel formation

There are two lines of evidence that demonstrate that the formation of barrels is dependent on a presynaptic signal from TCA. Firstly a number of mutants lacking pre-synaptic proteins fail to form a barrel pattern and secondly, no mutant has been identified in which cells in layer IV segregate in the absence of TCA segregation. Genetic deletion of the enzyme monoamine oxidase A (MAOA), which is responsible for the breakdown of serotonin released from TCAs, disrupts both barrel formation and TCA segregation (Cases et al., 1996). Genetic mutants lacking the serotonin reuptake transporter (*SERT*) also have deficits in S1 patterning in a similar fashion to the *MAOA* mutant (Salichon et al., 2001). Lack of S1 patterning in these mutants was due to excessive serotonin via its effect on the 5-hydroxytryptamine 1b receptors (5HT1b receptor), as genetic deletion of *5HT1b* in either monoamine oxidase A (*MAOA*) or serotonin reuptake transporter (*SERT*) null mutants results in normal TCA patch patterning (Rebsam et al., 2002), and barrel formation (Salichon et al., 2001). Furthermore reducing presynaptic vesicle release also affects barrel formation. Deletion of presynaptic active zone organiser rab3 interacting molecule 1 and 2

(RIM1 and RIM2), which controls synaptic vesicle release, reduce glutamate neurotransmitter release to approximately 30% of normal levels (Kaeser et al., 2011). Thalamus-specific deletion of RIM1 and RIM2 prevented the formation of barrels, but did not affect TCA segregation; in contrast cortex specific deletion of RIM genes did not have an effect on S1 patterning, either TCA or cellular segregation (Narboux-Nême et al., 2012), strongly suggesting that barrel formation relies on presynaptic signalling.

1.3.6.ii Post-synaptic mechanism

Whilst the formation of a barrel pattern in layer IV relies on a pre-synaptic signal from TCA, there are a number of post-synaptic receptors and signalling proteins that are also required. Glutamate is the main excitatory neurotransmitter in the brain and a number of attempts have been made to pharmacologically block activity or glutamate binding in the developing S1 with mixed results (Chiaia et al. 1992; Schlagger et al. 1993; but see Mitrovic et al. 1996; reviewed in Erzurumlu & P C Kind 2001). However, cortex specific deletion of GluN1 (CTX-NR1), the obligatory subunit of NMDA receptors, prevents the formation of barrels (Datwani et al. 2002; Iwasato et al. 2000) indicating a role for NMDA receptor signalling in S1 patterning. While TCA form whisker-related patches in *CTX-NR1* null mutants the TCA patches are smaller and poorly defined (Datwani et al. 2002; Iwasato et al. 2000); furthermore individual TCAs do not restrict to a single barrel (Lee et al., 2005). These findings suggest that a post-synaptic mechanism via NMDA receptors are required to fine tune the precision of TCAs, whereas the crude pattern is driven by a different mechanism. Metobotrophic glutamate receptor 5 (mGluR5) is a G-protein-coupled glutamate receptor that is expressed post-synaptically in layer IV of S1 (Wijetunge, Till, Gillingwater, Ingham, & Kind, 2008). Genetic deletion of *mGluR5* prevents the formation of barrels and partially disrupts TCA segregation. In these mutants TCAs are segregated into

rows however individual whisker patches do not develop (Hannan et al., 2001; Wijetunge et al., 2008).

S1 patterning relies on pre-synaptic vesicle release and post-synaptic activation of glutamate receptors, but what is the downstream intracellular target for glutamate receptors? PLC-Beta1 is a g protein-coupled phosphodiesterase required for mGluR5 induced inositol phosphate hydrolysis, and PLC-Beta1 null mutant also fail to form barrels (Hannan et al. 2001). However, unlike mGluR5, PLC-Beta1 mutants show normal TCA patch patterning; this suggests that the loss of mGluR5 affects TCA via a PLC-Beta1 independent mechanism (Hannan et al., 2001; Wijetunge et al., 2008). Protein Kinase A is a heterodimer formed of two catalytic components and two regulatory components. A screening of all viable subunit deletions revealed PKARII β subunit as required for barrel formation (Watson et al., 2006); this subunit is localised to the post-synaptic density via its binding with MAGUKs (Membrane associated guanylate kinase; see section 1.5) and A kinase anchoring proteins (AKAP; Colledge et al. 2000). Association of PKARII β with the PSD-95 is calcium dependant (Watson et al., 2006) and therefore could be activated either by the intracellular release of calcium via mGluR5/PLC-beta1 or NMDA receptor activity (Kind & Neumann 2001).

Finally two small G protein regulators have been identified that when genetically mutated cause defects in S1 patterning. In mutants lacking SynGAP, a Synaptic GTPase activating protein both the TCA patch pattern and the barrel pattern fails to form (Barnet et al. 2006). Mutants lacking Neurofibromin, another cortical Ras GTPase, also fail to form a barrel pattern (Lush, Ma, & Parada, 2005), providing further evidence that small G protein regulation plays a role in barrel formation. The downstream target for GTPases is the ERK/MAPK pathway, which has been implicated in NMDA receptor mediated intracellular signalling (Komiyama et al., 2002), synaptic plasticity (Sweatt, 2001) and visual cortex

development (Di Cristo et al., 2001). Many of the post-synaptic proteins required for barrel development have been shown to activate the ERK/MAPK pathway (mGluR5; Gallagher et al. 2004, GluN; Zhu et al. 2002, SynGAP; Chen et al. 1998; Kim et al. 2003, PKA; Cancedda et al. 2003), and this pathway has been proposed as an integrator of multiple intracellular signals (Adams & Sweatt 2002), suggesting that ERK/MAPK may be the downstream target required for barrel formation. The role of SynGAP and its regulation of the ERK/MAPK pathway in synapse maturation are discussed in section 1.5.7.

SynGAP binds to the NMDA receptor via the MAGUK associated signalling complex (MASC, Husi et al. 2000, see section 1.4.1). Included in this complex are many of the post-synaptic proteins that can affect patterning of the S1 such as NMDA receptors, mGluR5, PKArII β, PLC β1 and SynGAP (Husi et al., 2000). MAGUK scaffold a number of post-synaptic proteins required for barrel formation close to the synaptic membrane, therefore the deletion of MAGUK proteins may also affect barrel formation (see section 1.3.6.ii on the post-synaptic proteins required for barrel formation).

1.4. The synapse and dendritic spines

In the previous section we saw how fine maps and specifically barrel formation relies on the release of neurotransmitters and a number of specialised proteins in both the pre and post-synaptic neuron. This next section will take a closer look at the myriad of proteins located in the post-synaptic neuron and identify some of the signalling complex involved in synaptic transmission.

1.4.1. The post-synaptic density

The post-synaptic density (PSD) is an electron dense region on the post-synaptic membrane at excitatory synapses. 3 dimensional reconstructions of electron microscopy images demonstrate the size and morphology of the PSD can vary between synapses. PSDs can be circular, annular or split in two, and can be between 200 and 500nm wide and 30-60 nm thick (Okabe 2007; Harris et al. 1992). The circular shape of large PSDs is thought to be the first stage of a synapse growing too large as a result of repeated synaptic activation causing it to split into two separate synapses (Hering & Sheng, 2001).

Large scale immunoblotting and mass spectrometry experiments have been undertaken to identify the components of the PSD (Collins et al. 2006; Grant et al. 2005; Husi et al. 2000). Over 1000 proteins within the PSD have been identified and validated (Collins et al., 2006). Three complexes have been identified within the PSD and are classified by their association with different glutamate receptor subtypes, the AMPA receptor complex (Collins et al., 2006), the metabotropic glutamate receptor complex (Farr et al., 2004) and the MAGUK Associated Signalling complex (MASC; Grant et al. 2005) which associates with NMDA receptors. The largest of these complexes is the MASC, which contains 186 proteins (Grant et al. 2005). Many behavioural and cognitive defects are

caused by mutations in MASC components (Pocklington, Cumiskey, Armstrong, & Grant, 2006), suggesting that the MASC is key to cognitive function (Grant 2012). Furthermore we have already seen how mutants lacking MASC components have defects in S1 patterning, such as SynGAP and GluN1, it is therefore likely that disruption of the MASC not only causes behavioural and cognitive deficits in humans but also affects fine map formation.

1.4.2. Synaptogenesis

The formation of the presynaptic active zone is thought to be the first component of a functional synapse and clusters of active zone components including vesicle-associated membrane protein (vAMP), synapse vesicle 2, synapsin 1 alpha, and calcium channel alpha 1a can be visualised *in vitro* before pre-synaptic vesicles are released (Ahmari, Buchanan, & Smith, 2000). Furthermore, active zones can form in the absence of the post-synaptic cell (Prokop, Landgraf, Rushton, Broadie, & Bate, 1996) and in non-neuronal cells when only neuroligin is expressed (Scheiffele, Fan, Choih, Fetter, & Serafini, 2000).

Interactions between small surface molecules such as the Ephs and their receptor the Ephrins are thought to initiate synaptogenesis. Binding of EphrinB to the EphB receptor recruits synaptic proteins such as NMDA receptors, CAMKII on the postsynaptic neuron (Dalva et al. 2000; reviewed in Xu & Henkemeyer 2012). In addition the expression of trans-synaptic cell adhesion molecules such as Neuroligin1 in the presence of the MAGUK PSD95 can trigger the formation of excitatory synapses (Chih, Engelman, & Scheiffele, 2005; Cline, 2005). This suggests that cell adhesion molecules can help recruit post-synaptic proteins to help form the PSD.

1.4.3. Dendritic spines

This next section will introduce dendritic spines as an anatomical structure which houses the PSD in mature, excitatory synapses in the cortex; as such dendritic spines provide an anatomical readout for the maturity and number of excitatory synapses.

Although synapses can form on the dendritic shaft, the majority of excitatory synapses are formed on dendritic spines (Harris et al. 1992). Dendritic spines are small (0.5-2 microns in length) protrusions located on the dendrites of excitatory neurons of the cortex. They are closely associated with a number of presynaptic markers like synaptophysin (Fischer, Kaech, Knutti, & Matus, 1998) and FM dye (Star, Kwiatkowski, & Murthy, 2002) and co-localise with postsynaptic markers like PSD-95 (Jaworski et al., 2009), demonstrating they correspond to functional synapses. The density of dendritic spines can vary between cell types and brain regions, however many dendrites show a similar distribution of spines along a dendritic shaft with few spines located proximal to the soma, then the number of dendritic spines rapidly increases, reaching a plateau in the middle of the dendrite, and fewer spines seen at the distal end (Nimchinsky, Sabatini, & Svoboda, 2002).

1.4.3.i. Dendritic spine morphology

Dendritic spines can vary widely in shape and there have been a number of attempts to classify their morphology (Hering & Sheng 2001; Peters & Kaiserman-Abramof 1970). These are usually qualitative classifications, so for the purpose of this chapter a simple classification has been adopted; long thin spines are termed *filopodium*, spines with a distinctive neck and bulbous head are *mushroom*-shaped, spines with a large head but no discernible neck are called stubby and bifurcated spines are termed *cup*-shaped (Hering and

Sheng 2001, **Fig. 5**). Dendritic spine morphology has been shown to relate to the functional output of an individual synapse, the size of the spine head positively correlates with the size of the PSD (see section 1.4.1, Harris & Stevens 1989), the number of postsynaptic receptors (Nusser et al., 1998) and the size of presynaptic pool of vesicles (Schikorski & Stevens 1997). These functional correlates of large dendritic spines imply spine with larger 'heads' are associated with strong, stable synapses. The morphology of individual dendritic spine also has functional consequences to the synapses, by affecting calcium dynamics (Korkotian & Segal, 2000).

Dendritic spines are highly dynamic structures and can change morphology, extend or retract over tens of minutes in response to synaptic activity, sensory experience and learning (Harms & Dunaevsky, 2007; Yuste & Bonhoeffer, 2001). Dendritic spines turnover is particularly high during development (Ziv & Smith, 1996), whereas spines dynamics in adults occur over a much longer time scale (Trachtenberg et al., 2002). There are a number of molecules that affect dendritic spine morphology (reviewed in Ethell & Pasquale 2005) these act on actin (Jaworski et al., 2009) or microtubules (J. Gu, Firestein, & Zheng, 2008) to change the cytoskeletal composition of dendritic spines. These findings demonstrate how synaptic activity can alter spine morphology which in turn increases synaptic strength by preventing the diffusion of intracellular calcium.

Dendritic spines are of particular interest because a number of human diseases are associated with alteration in density or morphology of dendritic spines including schizophrenia, intellectual disabilities including, fragile X, Rett and Down's syndromes (reviewed in Fiala et al. 2002). A number of mutants lacking synaptic proteins have alterations in the density of dendritic spines; these include NMDA receptor subunits (Ultanir et al., 2007), PSD95 (Vickers et al., 2006) SynGAP (Vazquez, Chen, Sokolova,

Knuesel, & Kennedy, 2004), ProSAP/Shank (Sala et al., 2001; Schmeisser et al., 2012) and FMRP (Galvez & Greenough, 2005; Grossman, Elisseou, McKinney, & Greenough, 2006; Nimchinsky, Oberlander, & Svoboda, 2001; Till et al., 2012).

Figure 5. Dendritic spine morphology

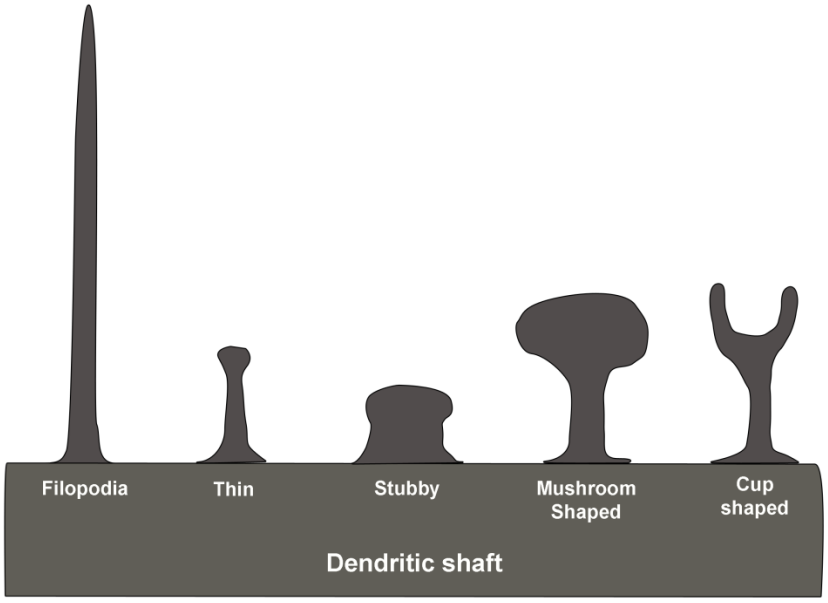

Figure 5. Classifications of dendritic spines morphology as described by from Hering and Sheng 2001. Whilst the development of dendritic spines is not completely understood, spines with a larger 'head' (*Mushroom* and *Cup* shaped) are thought to correspond to more mature synapses.

1.4.3.ii. Development of dendritic spines

Over the course of development there is a reduction in the number of filopodial spines, these are replaced with *mushroom* type spines (Papa, Bundman, Greenberger, & Segal, 1995; Ziv & Smith, 1996), this is thought to accommodate the increased PSD associated with mature, stable synapses (Harris et al. 1992). Some have suggested that filopodia develop into mature dendritic spines (Dailey & Smith, 1996). Whilst it was initially thought that there were too few filopodia to precede all mushroom shaped spines (Papa et al. 1995), live imaging has demonstrated that filopodia have a significantly shorter lifespan

compared to other types of dendritic spine (Dailey and Smith 1996). Therefore the accumulation of transient filopodia over time would be sufficient for each filopodia to precede *mushroom* type dendritic spines (Dailey and Smith 1996). Others have adapted this theory to create a more complex role for filopodia; 3 dimensional reconstructions of dendritic spines during development using serial section electron microscopy reveal a large number of shaft synapses (Fiala et al. 1998). A model was proposed whereby motile filopodia would identify nearby axons, adhere to them and retract back towards the dendritic, dragging the newly-acquired axons with it to form a shaft synapses before more mature spines develop (Fiala et al. 1998). This model explains why some cells that do not form dendritic spines, contain filopodia during development (Linke et al. 1994; Wong et al. 1992). Furthermore dendritic spines still form in the absence of axonal contract; as demonstrated in mutant mice lacking the G-protein-activated, inwardly rectifying K+ channel (Girk2), these animals lack granule cells which provide the main axonal contact to Purkinje cells, yet in the Girk2 mutants Purkinje cells still form dendritic spines (O'Brien & Unwin, 2006; Sotelo, 1990).

The formation of dendritic spines in the absence of presynaptic terminals suggests that dendritic spines are intrinsic properties of cells rather than a response to presynaptic stimulus. It is possible that these models are not mutually exclusive, for example the dendritic spines found in the Grik2 mutants could be the filopodial precursors described by Fiala et al. 1998. Filopodial spines precede the formation of both synapses and the formation of the presynaptic active zone, suggesting that dendritic spines play some role in initialising synaptogenesis (Knott, Holtmaat, Wilbrecht, Welker, & Svoboda, 2006; Nägerl, Köstinger, Anderson, Martin, & Bonhoeffer, 2007).

1.4.4. Thalamocortical synapse maturation

The maturation and maintenance of synapses is a key component of any cortical network, in this next section the development and maturation of thalamocortical synapses are discussed. Synaptic plasticity refers to the ability of a synapse to alter the response to a given stimulus, this is an important mechanism in determining which synapses are relevant to the cortical circuit and which are redundant. There are a number of physiological mechanisms that mediate synaptic plasticity in the neocortex (reviewed in Feldman 2009) however thalamocortical synapses are glutamatergic therefore this section will only focus on glutamate mediated synaptic maturation.

The development of the thalamocortical slice preparation has been used to investigate electrophysiological properties of thalamocortical synapses. This preparation maintains the connections between the thalamus and cortex allowing TCA to be stimulated in the thalamus whilst recording responses from cells in the cortex (Agmon et al. 1993; Lee et al. 2005, see 2.2.2 in methods chapter). During the first two postnatal weeks a number of developmental events occur at thalamocortical synapses including an increase in AMPA receptor mediated currents, a decrease in the number of silent synapses and a change in NMDA receptor subunit composition (reviewed in Wu et al. 2011). The development of inhibitory circuits also plays a key role in synaptic development but is outside the scope of this introduction (Daw, Scott, & Isaac, 2007).

1.4.4.i. AMPA and NMDA receptors

Although both NMDA and AMPA receptors bind glutamate the two receptors fulfil different roles at the synapse. At low membrane potential NMDA receptors are blocked by magnesium ions, if the membrane potential is sufficiently depolarised in the presence of glutamate (via AMPA receptor activation) the magnesium ion is removed from the pore of NMDA receptors, allowing the channel to open and calcium ions to enter the post-synaptic neuron. This allows the NMDA receptors to act as a molecular mechanism for detecting repeated glutamate release over a brief time course.

The blockade of NMDA receptors at low membrane potential can be utilised to infer the ratio of NMDA and AMPA receptors expressed by a neuron. This can be achieved by maintaining different membrane potentials of a cell in voltage clamp and recording the miniature excitatory postsynaptic current (mESPC; the change in membrane potential caused by the probabilistic release of glutamate in the absence of stimulation) the contribution of NMDA and AMPA receptors can be calculated. Alternatively mEPSC can be recorded in the presence of pharmacological compounds which will specifically block either AMPA or NMDA receptors. Towards the end of the first postnatal week in rats the ratio between NMDA to AMPA receptors mediated EPSC decreases at thalamocortical synapses (Crair & Malenka, 1995), suggesting an increase in the AMPA receptor component at these synapses. This is supported by biochemical analysis which demonstrates an increase in AMPA receptors in the PSD from P7 onwards (Watson et al., 2006). It is important to note that the kainate receptor is also expressed at thalamocortical synapses during the first postnatal week, however the kainate component is reduced in an activity dependant manner at the end of the first postnatal week, it has been suggested that kainate receptors are replaced by AMPA receptors as they do not co-localise with each other (Kidd & Isaac 1999).

Synapses can alter their long-term response to a stimulus via an activity dependant mechanism called long term potentiation (LTP), this will increase synaptic strength whereas long term depression (LTD) will attenuate it, both mechanisms can be artificially elicited using a variety of protocols. NMDA dependent LTP can be elicited in thalamocortical synapses in the first postnatal week (Barth & Malenka 2001; Crair & Malenka 1995) and whilst there are an number of mechanism that could elicit LTP, one likely explanation at thalamocortical synapses is the increase in AMPA receptor insertion (Daw et al. 2007; Crair & Malenka 1995).

In early development (P2-5) many TCA synapses are functionally silent; that is they contain NMDA but not AMPA receptors, therefore a synapse void of AMPA receptors will be 'silent' at resting membrane potential (Isaac et al. 1997). The conversion of silent to functional synapses is achieved by recruiting AMPA receptors to the surface membrane by LTP (Isaac 2003; Isaac et al. 1997; Shepherd & Huganir 2007; reviewed in Malinow 2003). Like alterations to cortical maps, alterations to synaptic strength can only occur in a limited time window or critical period. LTP can be observed in TCA synapses between P3 and P7, but not past P8 (Crair & Malenka 1995). The critical period for inducing LTD is more fluid with robust LTD observed at P4-5 but only a few cells showing modest LTD at P10-12 (Feldman, Nicoll, Malenka, & Isaac, 1998).

1.4.4.ii. NMDA receptor subunit expression

NMDA receptors are heterotetramers composed of two obligatory GluN1 subunit and a combination of 2 GluN2A-D or GluN3A subunits (Wenthold et al '03), however in the cortex NMDA receptors are mostly composed of GluN1 with either GluN2A or GluN2B (Sheng et al. 1994). The expression of NMDA receptor subunit also changes in the first postnatal weeks; GluN2B subunits are the predominant subunit expressed perinatally and

then at P6-8 these are replaced with GluN2A subunits (Petralia et al. 2005; Sheng et al. 1994; Sans et al. 2003). This is demonstrated by application of Ifenprodil, a selective GluN2B antagonist, which reduces a greater proportion of the NMDA receptor mediated EPSCs in the first postnatal week than in later development (Barth & Malenka, 2001). NMDA receptor subunits have different decay dynamics; GluN2A subunits having faster opening and closing kinetics compared to NR2B subunits, therefore the switch from GluN2B to GluN2A subunits reduces the latency of evoked spikes which would decrease the window for co-incidence detection (Daw, Bannister, & Isaac, 2006). Some have suggested that this switch in subunit expression may be related to the end of the synaptic plasticity critical period (Barth & Malenka, 2001). However, while blocking GLuN2B with the selective antagonist ifenprodil prevents thalamocortical LTP, mutant mice lacking GluN2A closure of the critical period for synaptic plasticity was unchanged (Lu et al. 2001), suggesting that the developmentally regulated change in NMDA receptor composition is not responsible for the end of the critical period for synaptic plasticity although the presence of GluN2B is required for LTP.

Coinciding with the end of the S1 critical period for LTP is a switch in the distribution of NMDA /AMPA receptors expressed at synapses. Therefore it is possible that the decrease in the number of silent synapses is responsible for the closure of the synaptic plasticity critical period. In support of this hypothesis, mutant mice lacking fragile X mental retardation proteins display a delay in critical period plasticity and an increase in the number of silent synapses (Harlow et al. 2010).

1.5. Membrane associated guanylate kinases

Membrane associated guanylate kinases (MAGUKs) are key components of the MASC and act as scaffolding molecules binding proteins close to the cell membrane (Hering and Sheng 2001). This section will focus on four post-synaptic MAGUKs; SAP97, PSD93, SAP102 and PSD95, the so-called disks large homolog (DLG) MAGUKs because of their structural similarity to the Drosophila Discs-Large tumor suppressor protein (Cho, Hunt & Kennedy 1992) , and in humans these genes are called *DLG1-4*.

Figure 6. DLG-style MAGUK structure

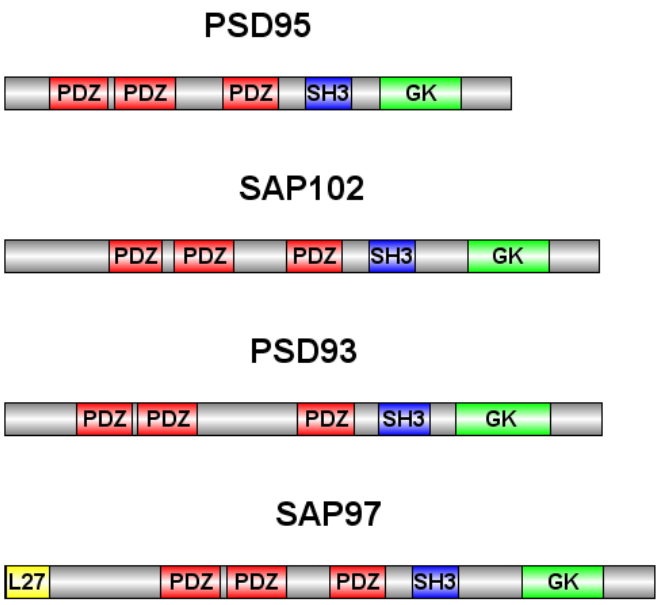

Figure 6. Diagram of DLG-style MAGUKs. DLG-style MAGUK all share 3 PDZ, a SH3 and a GK binding domains. Drosophila melanogaster have only one DLG style MAGUK; Dlg whereas there are four DLG paralogues found in mammals; PSD-93,PSD-95,SAP102 and SAP97 (Ryan and Grant 2009). Adapted from Kim and Sheng 2001.

1.5.1. The role of DLG MAGUKs

DLG-style MAGUKs share a similar protein structure (Kim & Sheng 2004) and each protein contains 3 PDZ (**P**ost synaptic density 95, **D**rosophila disc large tumor suppressor, **Z**onula occludens-1) domains, a SH3 and a GK binding domain (**Fig. 4**). These protein binding domains create multiple protein-protein interactions within the PSD, MAGUKs create intracellular signalling microdomains by tethering synaptic signalling molecules close to the surface membrane (Kim & Sheng 2004). The complexes formed by MAGUK are of interest because disruption of these complexes have been implicated in over 100 neurological and psychiatric disorders (Grant 2012). As well as acting as the physical link between NMDA receptors and intracellular signalling molecules, MAGUKs play a key role in glutamate receptor trafficking (Elias & Nicoll 2007) and synaptogenesis (Montgomery, Zamorano, & Garner, 2004). The loss of MAGUKs affects synaptic plasticity and performance on learning and memory tasks (Carlisle, Fink, Grant, & O'Dell, 2008; Cuthbert et al., 2007; Migaud et al., 1998).

Multiple DLG-style MAGUKs are a recent addition to the genome, with protostomes containing only one DLG gene (Emes et al., 2008). Comparative genomics and proteomics of the MASC between species reveal the evolutionary path of the synapse; species that diverged from mammals more recently share more MASC components (Emes et al., 2008). Recently different DLG-MAGUK mutations have been found to cause differential learning defects in mice suggesting that different MAGUK are involved in different cognitive processes (Nithianantharajah et al., 2012). In the next section we will take a detailed look at some of the phenotypic differences observed between MAGUK mutants. The different synaptic functions between DLG MAGUKs has led some to conclude that different MASC composition accounts for synaptic complexity between species and that synaptic diversity

in higher order animals may be the result of increased MASC composition diversity at individual synapses (Ryan & Grant 2009; Emes et al. 2008).

1.5.2. MAGUK mutant phenotypes

Four separate mutant mouse lines have been created that lacking each of the DLG MAGUKs and mutants lacking either *SAP102*, *PSD95*, or *PSD93* are viable (Carlisle et al., 2008; Cuthbert et al., 2007; Migaud et al., 1998). Mutants lacking *SAP97* have cranio-facial abnormalities that cause feeding problems and die perinatally (Caruana & Bernstein, 2001). All MAGUK mutants have defects in electrophysiological properties, but there are subtle phenotypic differences between these mutants.

Slice preparations from adult *SAP102* and *PSD93* null mutants show basal synaptic transmission is normal (Carlisle et al., 2008; Cuthbert et al., 2007). However, in mutant mice lacking *PSD95* some groups have found altered AMPA to NMDA receptor ratios (Béïque et al. 2006; Carlisle et al. 2008; but see Migaud et al. 1998). In neurons cultured from *SAP97* knockout animals basal transmission was also normal but AMPA and NMDA receptor EPSCs were both increased in immature neurons (Howard, Elias, Elias, Swat, & Nicoll, 2010). While it is difficult to make comparisons between slice preparation and the cell cultures, these data suggest that the loss of different MAGUKs does not have the same effect on basal synaptic transmission.

The loss of MAGUK also has differential effects on synaptic plasticity paradigms. Mutants lacking *PSD95* display enhanced LTP under a variety of protocols (Carlisle et al., 2008; Migaud et al., 1998) but *SAP102* mutants only exhibit increased LTP using a low frequency stimulation protocol. Furthermore, the enhanced LTP observed in *SAP102* mutants is dependent on ERK activity and phosphorylated ERK is increased (Cuthbert et al.,

2007) demonstrating a specific defect in ERK signalling in *SAP102* mutants that is not found in animals lacking *PSD95* (Cuthbert et al., 2007; Opazo, Watabe, Grant, & O'Dell, 2003). By contrast in *PSD93* knockout animals spike-time dependent plasticity is disrupted, paired pulse facilitation is significantly increased and LTP is reduced (Carlisle et al., 2008).

Although the four DLG MAGUKS share a similar structure, the variety of electrophysiological phenotypes associated with the loss of different MAGUKs demonstrate that MAGUKs play different functional roles in synaptic transmission and plasticity. In mutants lacking *SAP102*, *PSD93* and *PSD95* these electrophysiological phenotypes also manifest in different behavioural defects on learning and memory tasks (Nithianantharajah et al., 2012). These findings supports the hypothesis that different MAGUKs perform separate roles at the synapse and can account for synaptic diversity in higher order animals (Ryan & Grant 2009; Emes et al. 2008).

1.5.3. SAP102 and PSD95 during S1 development

SAP102 and to a lesser extent PSD95 are the only two MAGUKs expressed during early S1 development (Sans et al. 2000; Barnett, Watson, Vitalis, et al. 2006; Wijetunge et al. 2008). They are also two of the few post-synaptic proteins that are upregulated during synapse formation and early cortical development (Petralia et al. 2005) suggesting that they play a key role at this developmental time point. Although the onset of expression for SAP102 and PSD95 is similar, the two proteins differ in their peak expression. In the rat hippocampus, SAP102 reaches peak expression at P10 whereas PSD-95 expression is still increasing at P35 (Sans et al. 2000), in S1 SAP102 expression gradually increases over the first postnatal week whereas PSD95 rapidly increases around P14 (Watson et al., 2006). This temporal expression in homogenates is mirrored in immunogold-labelled electron microscopy with SAP102 found at synapses in the first postnatal week and fewer gold

particles found at synapses after P10, whereas PSD95 increases in the later stages of development, (Sans et al. 2000; Petralia et al. 2005). While both SAP102 and PSD95 are found in dendritic spines (Sans et al. 2003; Sans et al. 2000) , there are some differences in subcellular localisation; with SAP102 also found in cell bodies, dendrites (Sans et al., 2005) and axons (El-Husseini et al., 2000). Synapses double-labelled for both SAP102 and PSD95 were found throughout development, however the number of double-labelled synapses was never more than 30%, suggesting that both proteins are not required at all synapses (Sans et al. 2000). SAP102 is also located further from the PSD and, in culture, has a larger mobile fraction than PSD95 (Zheng et al. 2010), which provides further evidence for different functional roles for SAP102 and PSD95 at the synapse.

1.5.4. The role of SAP102 and PSD95 in synaptogenesis

As a principle component of excitatory synapses, MAGUKs are hypothesised to play a role in synaptogenesis (Montgomery et al. 2004; Elias & Nicoll 2007; Chih et al. 2005). SAP102 and PSD95 are well-placed for this role because of their binding to glutamate receptors, expression during synaptogenesis, and trafficking of NMDA and AMPA receptors (Chen et al. 2011; Müller et al. 1996; Schnell et al. 2002; Waites et al. 2009; Sans et al. 2003). Immunogold labelled electron microscopy reveals SAP102 is also expressed at synapses with mature PSDs at P2, a time point when few mature synapses are seen, this suggests that SAP102 may be a key component in synaptogenesis (Sans et al. 2003). PSD95 is one of the synaptic proteins that cluster as a result of EphrinB/EphB binding (Dalva et al., 2000) and in the presence of Neuroligin can trigger the formation of excitatory synapses (Chih et al., 2005; Cline, 2005). Furthermore, clusters of mobile complexes that include MAGUKs and other scaffolding molecules have been shown to develop into functional

synapses (Gerrow et al., 2006), demonstrating that MAGUKs not only contribute to the structural organisation of the PSD, they also traffic receptors and are a principle component of synaptogenesis.

1.5.5. SAP102 and PSD95 in AMPA receptor trafficking

Unlike SAP97, SAP102 and PSD95 do not bind directly to AMPA receptor subunits (Leonard, Davare, Horne, Garner, & Hell, 1998) instead they are hypothesised to bind AMPA receptors via transmembrane AMPA receptors regulatory proteins (TARPs; Elias and Nicoll 2007). PSD95 binds AMPA receptors via its interaction with the TARP stargazin (Schnell et al., 2002) and disrupting the binding of stargazin to the PDZ domain of PSD95 decreases AMPA receptors EPSCs (Chen et al., 2000), although SAP102 does not associate with stargazin *in vivo* (Dakoji, Tomita, Karimzadegan, Nicoll, & Bredt, 2003). Both SAP102 and PSD95 are capable of trafficking AMPA receptors to the surface membrane, this is evident from overexpression or knockdown experiments that increase or decrease AMPA receptors EPSCs respectively. Knockdown or overexpression of PSD95 affects AMPA receptor EPSCs in adult animals (Elias et al. 2006) and during synapses maturation (Elias et al. 2008), however the effects of SAP102 overexpression or knockdown on AMPA receptor EPSCs only occur during the first postnatal week (Elias et al. 2008). Furthermore knockdown of SAP102 results in a decreased amplitude and frequency of AMPA receptor mEPSCs (Elias et al. 2006) whereas knockdown of PSD95 only decreases the frequency of events. Providing further evidence that SAP102 and PSD95 have slightly different functions at the synapse.

1.5.6. SAP102 and PSD 95 in NMDA receptor expression and trafficking

The peak temporal expression of SAP102 and PSD95 mirrors the expression of GluN2B and GluN2A subunits respectively; GluN2B gradually increases in the first postnatal week but by P14 GluN2A is the primary subunit expressed (Sans et al. 2000). Although both SAP102 and PSD95 can bind both GluN2A and GluN2B subunits, complex immunoprecipitation (CO-IP) experiments have demonstrated a preferential binding of SAP102 to GluN2B and PSD95 to GluN2A (Sans et al. 2000), possibly due to an additional N-terminal binding site (Chen et al. 2011). Complimentary expression and preferential binding between these MAGUKs and GluN2 subunits suggests that MAGUK may mediate the switch in NMDA receptor subunit composition which is a key stage in thalamocortical synapse maturation (see section 1.4.4). The developmental switch in expression between SAP102/GluN2B and PSD95/GluN2A has also been demonstrated both in the S1 (Barnett et al. 2006) and in the visual cortex (Shi, Aamodt, & Constantine-Paton, 1997; Yoshii, Sheng, & Constantine-paton, 2003). However SAP102 is still found at synapses in adult animals (Sans et al. 2000), and in the adult hippocampus there was no preferential interaction between MAGUKs and either NMDA receptor subunit (Al-Hallaq, Conrads, Veenstra, & Wenthold, 2007).

Evidence from overexpression studies suggests a more complex interaction between specific MAGUKs and NMDA receptor subunits. As previously mentioned the contribution of NMDA receptor subunits can be determined by different decay dynamics and SAP102 overexpression had no effect on NMDA receptor EPSC decay dynamics at either P6-8 or P15-17 however PSD95 overexpression through development did significantly reduce decay time of NMDA receptor EPSCs (Elias et al ’08), suggesting that PSD95 overexpression causes more NMDA receptors containing GluN2A subunits to be

inserted into the membrane. These findings suggest that not only can SAP102 traffic both GluN2A and GluN2B subunits at both time points, but PSD95 overexpression is capable of inducing a premature developmental switch in NMDA receptor subunit expression.

1.5.7. SynGAP and ERK/MAPK pathway in synapse maturation

SynGAP is a Synaptic GTPase-activating protein, it is localised to the synapse (Husi et al. 2000) and binds to MAGUKs via the PDZ binding domain (Kim et al. 1998) although not all splice variants of SynGAP contain the PSD binding domain required for MAGUK binding (Li et al., 2001). As a regulator the small GTPases Ras and Rap SynGAP can influence the ERK/MAPK pathway, which is involved in a number of neural developmental mechanisms including critical period plasticity, synaptic plasticity, and receptor trafficking (Di Cristo et al. 2001; Adams & Sweatt 2002; Gu & Stornetta 2007; Thomas & Huganir 2004). Intellectual disability has been associated with defects in the regulation of small GTPases (Hamdan et al. 2011; reviewed in Valnegri et al. 2012). The ERK/MAPK pathway can also affect the cytoskeleton, synaptogenesis, cortical development, local translation and spatial learning (Ho et al. 2001; Adams & Sweatt 2002; Di Cristo et al. 2001; Bozon et al. 2003; Boda et al. 2010), demonstrating that this pathway maybe involved in a number of neurodevelopmental events.

Phosphorylated SynGAP is bound in a complex with Multi-PDZ domain protein 1 (MUPP1; another PDZ containing scaffolding molecule) and Calcium/Calmodulin-dependent protein kinase (CamKII), this complex is disrupted by GluN activation causing calcium to enter the PSD and dephosphorylate SynGAP (Krapivinsky et al. 2004; Chen et al. 1998). Dephosphorylation of SynGAP increases its GAP activity, inactivating RAP, which decreases p38 MAPK activity (Krapivinsky et al. 2004) and prevents the removal of AMPA receptors from the surface membrane (Zhu et al., 2002). SynGAP also negatively regulates p42 MAPK

which reduces the synaptic delivery of AMPA receptor to the cell surface (Komiyama et al., 2002; Zhu et al., 2002), this way SynGAP can serve as both a positive and negative regulator of synaptic strength via its effect on AMPA receptor trafficking. Furthermore a number of SynGAP isoforms have been identified all of which contain the GAP domain required to regulate small GTPases (Li et al. 2001) and overexpression of different isoforms can either attenuate or increase synaptic strength (McMahon et al., 2012).

1.6. Summary and aims

Fine maps, like all neuronal circuits, require precise connectivity both between and within distinct brain regions. Both the formation and maintenance of fine maps requires activity dependent mechanism as well as a number of pre and post-synaptic proteins, however the precise intracellular signalling pathway involved in setting up fine maps is unclear. The rodent trigeminal system is an example of a fine map that can be clearly identified by its distinct anatomical patterning and therefore can be readily used as an anatomical model for normal neural connectivity.

MAGUKs are a major constituent of the PSD, by linking NMDA receptors to downstream signalling targets they are hypothesised to play a role in synaptogenesis, receptor trafficking, synapse maturation and dendritic spine formation. Furthermore genetic deletion of MAGUKs or MASC components results in intellectual disability in humans (Zanni et al. 2010; Tarpey et al. 2004; Grant 2012). Whilst MAGUKs share the same protein binding domains, mutant mice lacking different MAGUKs do not display the same electrophysiological phenotype (Carlisle et al., 2008; Cuthbert et al., 2007; Howard et al., 2010; Migaud et al., 1998). As post-synaptic scaffolding molecules MAGUKs bind NMDA receptors to downstream intracellular targets such as SynGAP (Sans et al. 2000; Kim et al. 1998). SynGAP can regulate small G proteins and can therefore affect the ERK/MAPK pathway which is a major intracellular signalling mechanism known to affect a variety of developmental and synaptic processes (Di Cristo et al. 2001; Adams & Sweatt 2002; Gu & Stornetta 2007). Deletion of *GluN1* and *SynGAP* result in defects in synaptic plasticity, cortical map formation and dendritic spine abnormalities (Barnett, Watson, Vitalis, et al. 2006; Datwani et al. 2002; Iwasato et al. 2000; Komiyama et al. 2002). Therefore disrupting

the NMDA receptor-MAGUK-SynGAP pathway may affect a number of key developmental mechanisms including synaptogenesis, neuronal connectivity, and fine map formation.

1.6.1. Thesis aims

Chapter 3- Characterisation of 3 neurofilament subunits in the developing S1

In this chapter the expression profile of 3 neurofilament subunits in the developing S1 was characterised in the hope of finding a suitable marker for TCA. The developmental expression of neurofilament subunits revealed a number of interesting avenues of research and results are discussed in terms of the organisation of sensory maps, thalamocortical axon development, neurofilament composition and the influence of experience on patterning in the S1.

Chapter 4-The role of SAP102 is the developing mouse S1

This chapter focuses on the developmental characterisation of mutant mice lacking SAP102 through post-natal development and use techniques developed in chapter 3 to label TCA. This chapter tests 4 specific hypotheses:

1. Mutant animals lacking SAP102 have normal neuroanatomical development.
2. Map formation and S1 patterning are unaffected by the loss of SAP102.
3. The number and morphology of TCA are not affected by the loss of SAP102.
4. Dendritic spine density is unaffected by the loss of SAP102 in the S1.

The results of this chapter are discussed in terms of SAP102 function and the deficits in cortical connectivity that arise in the absence of SAP102.

Chapter 5- The combined role of SAP102 and PSD95 in S1 patterning

This chapter focuses on the combined role of SAP102 and PSD95 in the patterning of the S1. Animals lacking both *SAP102* and *PSD95* do not survive and a strategy was designed using X-inactivation to identify the contribution of double knockout cells to barrel formation in a mosaic environment. The aims of this chapter were two fold, firstly evaluating the strategy used to identify double knockout cells and secondly to investigate double SAP102 and PSD95 knockout cells in the developing S1. This chapter focuses on 4 specific aims;

1. Are cells containing either the maternal or paternal X-chromosome evenly distributed throughout the cortex in female mice?
2. Do MAGUK genotypes affect the distribution of X-inactivation in females?
3. Do double *SAP102*/*PSD95* knockout cells survive?
4. Do these double knockout cells contribute to barrel cortex development?

Chapter 2

Methods

2.1 Animals

2.1.1 Transgenic animals

SAP102 and PSD95 mutants were generated in Prof Seth Grant's laboratory (Cuthbert et al. 2007; Migaud et al. 1998). SAP102 mutants were created by incorporating a vector containing a neomycin cassette which caused a frameshift between exons 1 and 9 deleting the majority of the PDZ binding domains (Cuthbert et al., 2007). Polymerase chain reaction (PCR) was used to identify the genotype of these mutants using one forward primer (GGT CTC TGA TGA AGC AGT GAT TTT T) located upstream of the cassette integration site and 2 reverse primers (TGA TGA CCC ATA GAC AGT AGG ATC A) in the wild type sequence deleted by the mutation and (CTA AAG CGC ATG CTC CAG AC) located in the neomycin cassette. Amplification was conducted by 33 cycles of 30s at 94^{o}C, 30s at 56^{o}C and 60s at 72^{o}C, this produced a wild type 215 bp product and a 535bp band corresponding to the knockout allele.

PSD95 mutants were created by introducing a stop codon at the 3rd PDZ binding domain producing a truncated protein which is not localised to the synapse (Migaud et al. 1998). To identify the wild type allele primers were designed against a sequence in the 3rd PDZ domain using forward primers (AAC CAA GGC GGA TCG TGA TCC A) and reverse primers (TCT CTT TGG TGG GCA GTG) to produce a 220bp band. To identify the knockout allele forward (CAT TCG ACC ACC AAG CGA AAG ATC) and reverse (CAG GGA GCG GGG ACG GAT GA) primers were designed against the neomycin cassette which produced a 2 kb band. The amplification for these primers was for 30 cycles of 30s at 93^{o}C, 60s at 55^{o}C and 60s at 72^{o}C.

2.1.1. Background strain of mice used

Mice used for the characterisation of SAP102 (chapter 4) were backcrossed onto a C57Bl/6JOla line over a minimum of 5 generations. Mice used for the characterisation of NF subunits were also maintained on this background. Due to the complex breeding paradigm involved in generating SAP102/PSD95 double mutants (chapter 5), these mice were on a highly mixed background which mostly consisted of C57/Bl6JOla, with small contributions of DBA-2 and Bl6/129.

2.1.3. Whisker trims

To access the impact of sensory deprivation on neurofilament expression, whiskers were trimmed using an electric razor on one side of the rodent facepad from birth every day for 8 days. Trimming whiskers does not require anaesthetic and is a less invasive technique that whisker plucking, however the rate of regrowth is faster and there are different physiological and anatomical results produced by either plucking or trimming whiskers (see introduction 1.3.5).

2.2 Tissue preparation and histology

2.2.1 Perfusions

Mice were anaesthetized with sodium pentobarbital (Euthanol 200mg/kg, ip) prior to transcardial perfusion with PBS followed by approximately 10mls 4% paraformaldehyde in 0.1 M phosphate buffer for animals aged P7 and older, approximately 5ml of fixative and PBS were used for younger animals. Brains were removed from the skull, post-fixed in 4% paraformaldehyde for a minimum of 12 hours at 4^{o}C.

Figure 2.1. Preparation of coronal sections

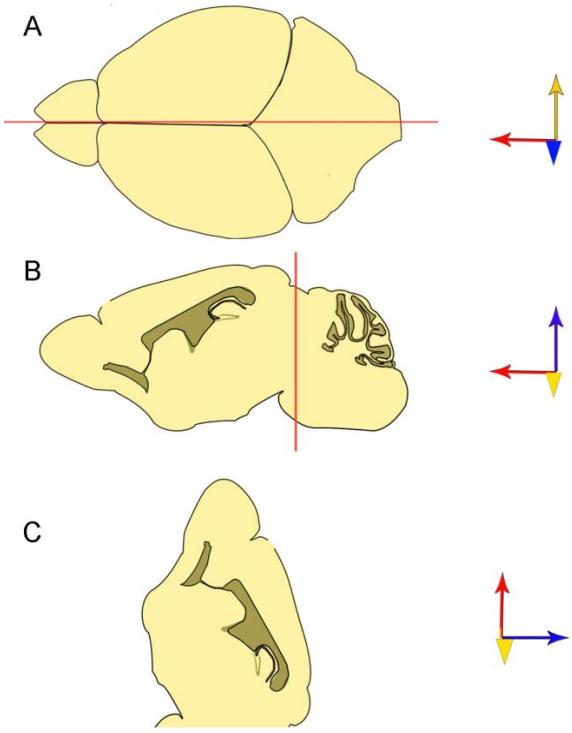

Figure 2.1. Preparation of coronal sections. Postfixed brains were bisected down the midline as demonstrated by the red line in **A**. The cerebral cortex was then removed with a razor blade (red line in **B)** and mounted vertically on the cutting stage (**C**). The three arrows provide an orientation to the tissue; yellow points towards the medio-lateral plane, red; anterior and blue; dorsal.

2.2.2 Histology

For all immunohistochemistry brains were cryoprotected in a 30% sucrose in phosphate buffered saline (w/v) overnight. Three different planes of section were collected:

1) Coronal sections were obtained by bisecting the brain along the mid-line, removing the cerebellum and mounting the hemisphere vertically on the freezing stage (**Fig. 1**).

2) To investigate TCA in the internal capsule, thalamus and cortex, pseudo-coronal sections which maintain the TCA tract were cut at a 55^{o} angle as described by Lee et al. (2005) (**Fig.2**).

3) To visualise the layer IV patterning of the S1, flattened tangential sections were cut (**Fig. 3**). Two separate methods were employed to achieve this plane of section;

flattened neocortical sections maintain the proportions of the neocortical sheet, but can slightly distort primary sensory areas, this method was used to investigate the arealisation of the neocortex (**Fig.3C**). Flattened S1 sections do not cause any distortion to the S1 region therefore this method was used for confocal images and cell counts (**Fig. 3D**).

All tissue sectioned for immunohistochemistry was cut at a thickness of 48 microns using a microtome with a freezing stage. Tissue reacted using the golgi-cox method was cut on a vibrotome at a thickness of 80 microns. Tissue sectioned for DiI labelling was also cut on a vibrotome but at a thickness of 250 microns for single axon tracing using the TCA preparation and 100 micron thickness using a "neocortical flat" preparation for bulk labelling of TCA.

Figure 2. Preparation of TCA sections

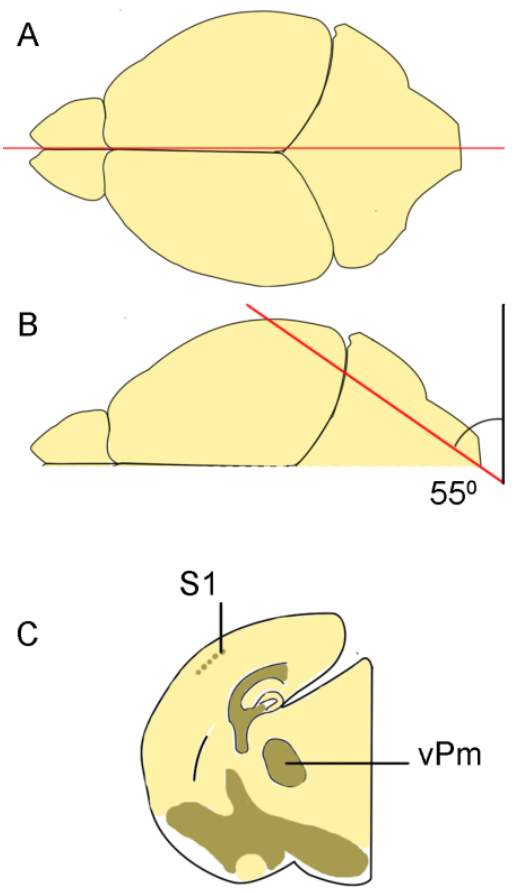

Figure 2. Preparation of TCA sections which preserve the corrections between the thalamus and the cortex. Post-fixed sections are bisected along the mid-line as shown by the red line in **A.** The hemisphere is then cut along a 55^{o} angle across the cerebellum and posterior cortex (red line **B**), the brain is then mounted with the flat edge made by the red line of **B** secured to the stage. The brain is then cut at an angle parallel to the red line of **B** starting at the anterior tip. Sections cut parallel to the red line of **B** provides a psudo-coronal section (C) which contains both the thalamic neuclei (vPm) and the primary somatosensory cortex (S1). The orientation of each figure is provided; yellow points towards the lateral plane, red; anterior, and blue; dorsal.

2.2.2.i Flattened neocortical section

Flattened neocortical sections were cut to investigate the size of the neocortical sheet, the relative size of sensory areas and positioning of cortical regions. To achieve this plane of section post fixed brains were bisected down the midline and the thalamus, cerebellum and striatum were removed with forceps (**Fig. 3**). The neocortical sheet was then flattened between two glass slides using capillary tubes with a diameter of 1.5mm as spacers. These sections were submerged in 4% PFA for a further 12 hours at which point the solution was removed and replaced with 30% sucrose, for a minimum of 12 hours to cryoprotect the tissue.

2.2.2.ii Flattened S1 section

To reveal patterns in the primary S1 post-fixed brains were bisected and thalamus, cerebellum and striatum were removed as described above (**Fig. 3**). A blade was used to remove the olfactory bulb and piriform cortex then the hippocampus and pieces of internal capsule were removed until the cortex was flat. The tissue was then submerged in 30% sucrose solution for 12 hours.

Figure 3. Preparation of tangential flattened sections

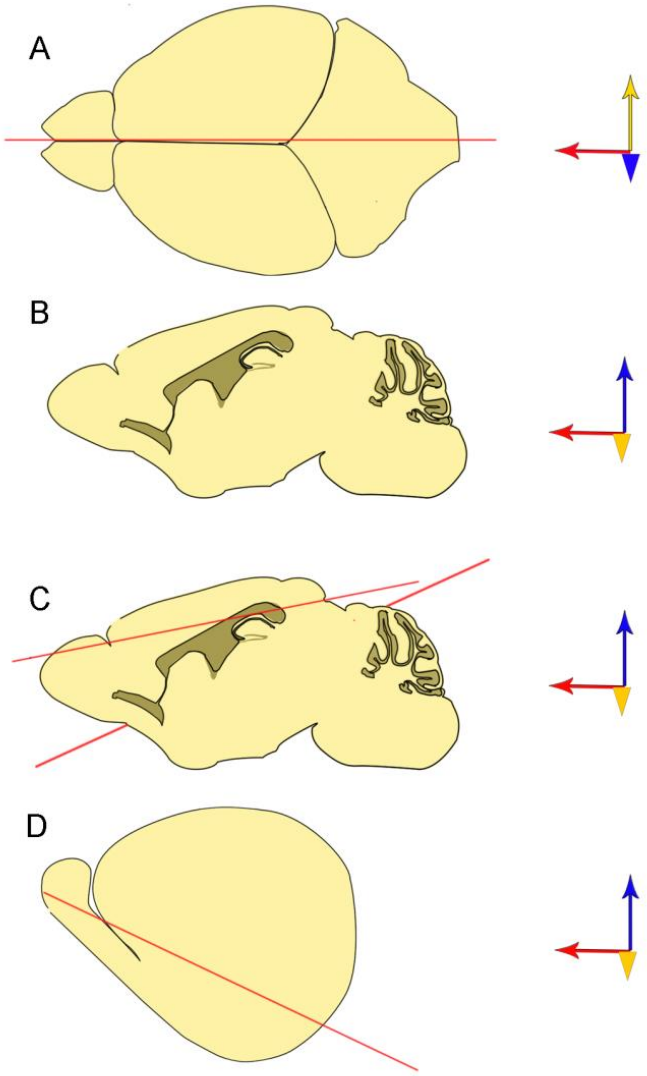

Figure 3. Preparation of tangential flattened sections. The brain is bisected along the midline (**A**), using a pair of forceps the cerebellum, thalamus and striatum are removed (**C**) leaving only the cortical sheet. Sections prepared using the *neocortex* flat are then flattened between glass slides. For sections prepared using the S1 *flat* method the piriform cortex is also removed as shown by the red line in **D**. Pieces of the hippocampus, striatum and thalamus are then removed using forceps so that the cortex lies flat. Orientation cues are provided by the coloured arrows in each diagram; yellow points towards the lateral plane, red; anterior, and blue; dorsal.

2.2.3. Golgi-Cox staining

Free-floating sections containing PMBSF were reacted in 4% osmium solution for 30 minutes. Sections were then washed 3 times in PB and left in 3.5% potassium dichromate solution overnight. Sections were then mounted onto glass slides approximately 7mm from

the right-hand edge, covered with another slide and held together with electrical tape. Slides were then immersed in silver nitrate until dendritic arborisations were visible. Sections were then washed and mounted onto 2.5% chrome alumn charged slides. Sections were then dehydrated in an alcohol series and dewaxed in 2 xylene washes. Finally slides were coverslipped in DPx (BDH *Poole*, Dorset).

Dendrites were reconstructed using Neurolucida (MBF Bioscience, Williston, VT, USA). The number of dendritic spines was quantified using an oil immersion x100 objective attached to a camera lucivid (MBF Bioscience, Williston, VT, USA).

2.2.4. Immunohistochemistry

Sections reacted using 3,3'-diaminobenzidine tetrahydrochloride (DAB) were first free-floated in a bath of PBS with hydrogen peroxide (1:500) for 20 minutes to reduce the influence of endogenous peroxidases on our reaction product. These sections were then washed with PBS and all tissue reacted for immunohistochemistry was incubated in primary antibody overnight at room temperature. The details of primary antibodies used are listed in **table 1**.

Sections were then washed 3 times with PBS, and using the same media and triton concentration as the primary antibody incubation step, a biotinylated secondary antibody (1:250, Vector Labs, Burlington, CA) was added to the media. If sections were reacted with 2 primary antibodies a fluorescent secondary raised against the host of one of the primary antibodies was added to the secondary solution (Alexa fluor; invitrogen, Carlsbad, CA, USA). Sections were then left free floating at room temperature for 90 minutes in secondary antibody before being washed 3 times in PBS. Sections labelled with fluorescent probes

were then incubated in streptavidin conjugated Alexa Fluor (1:250; Invitrogen, Carlsbad, CA, USA), these were then washed 3 times in PBS and incubated in TO-PRO3 (1:1000; Invitrogen, Carlsbad, CA, USA) for 20 minutes. Sections were then mounted onto glass slides, and coverslipped with Vectashield mounting medium (Vector Labs, Burlingame, CA). For DAB reacted sections after incubation with biotinylated secondary, sections were washed 3 times in PBS and placed for 90 minutes into PBS with peroxidase-conjugated biotin and avidin (PK-6100; Vector Labs, Burlingame, CA). Labelling was revealed by turnover of the chromogen substrate 3,3'-diaminobenzidine tetrahydrochloride in PBS. Reacted sections were mounted onto glass slides and allowed to dry before they were dehydrated in ethanol, cleared in xylene, and then coverslipped with DPX (BDH Labs, Poole, England).

Table 1. Details of primary antibodies used

Antibody	Reference	Company	Concentration	Media	Triton concentration
Neurofilament light (NFL)	MAB1615	Millipore, Billerica, MA, USA	1:1k	1	0.10%
Neurofilament medium (NFM)	ab7794	Abcam, Cambridge, MA, USA	1:3k	1	0.10%
Neurofilament heavy (NFH)	AB5539	Millipore, Billerica, MA, USA	1:5k	1	1%
ctip2	ab18465	Abcam, Cambridge, MA, USA	1:250	1	1%
Serotonin reuptake transporter (SERT)	PC177L	Milliipore, Billerica, MA, USA	1:2k	2	2%
Calretinin	7699/3H	Swant, Switzerland	1:2k	1	1%
β-galactosidase (β-gal)	A-11132	Life technologies, Paisley, UK	1:500	1	1%
myelin basic protein (MBP)	clone 12	AbD/Serotec, Oxford, UK	1:400	1	0.10%

Table 1. Details of antibodies used. Media refers to the solution in which the tissue was reacted. 1=PBS with 1:500 normal goat serum, 2= Dulbecco's Modified Eagle Medium with 5% heat inactivated goat serum

2.3 Imaging and quantification

2.3.1 Imaging

Tissue reacted for with 3,3'-diaminobenzidine tetrahydrochloride (DAB) were imaged with a compound microscope (DMLB; Leica, Wetzlar, Germany) fitted with a high-resolution digital camera (DFC480; Leica, Wetzlar, Germany). Confocal images for cell counts and calretinin septal area were imaged on a confocal microscopy (Leica TCS-NT) using an oil immersion x20 lens. High power confocal images were taken at Nyquist sampling rate with x63 Apochromat objective (NA 1.4, oil immersion) and were deconvolved using Huygens software (Scientific Volume Imaging, Hilversum, Netherlands). Images were arranged into figures with Photoshop CS3 (Adobe, San Jose, CA) and imageJ (NIH, Maryland USA).

2.3.2. Mass measurements

Body mass was taken after injection with anaesthetic prior to perfusion. As animals were then sacrificed, comparisons between ages were conducted on separate litters. Brains were postfixed for 24 hours and patted dry with tissue before being weighed. Tissue that was clearly damaged was not included in this analysis.

2.3.3. Cortical measurements

2.3.3.i Cortical laminar measurements

48µm Coronal sections through the PMBSF were cut and every 3rd section was collected and reacted for calretinin. Calretinin is a calcium binding protein that specifically labels interneurons in the barrel septa and defines the layer IV/V boundary (Melvin & Dyck 2003). Cortical thickness was measured in three different sections equidistant along the

anterior posterior axis but still within S1. The different positions were defined by the anatomy of the hippocampus; in the anterior section the dentate gyrus of the hippocampus was just emerging (**Fig. 4A**), the middle section the cell body layer of CA3 is perpendicular to the midline (**Fig. 4B**) and in the posterior section CA3 had curled round the cortex (**Fig. 4C**). In each section three measurements were taken, the total cortical thickness, the distance from white matter to layer IV and from layer IV to pial surface.

Figure 4. Cortical thickness measurements

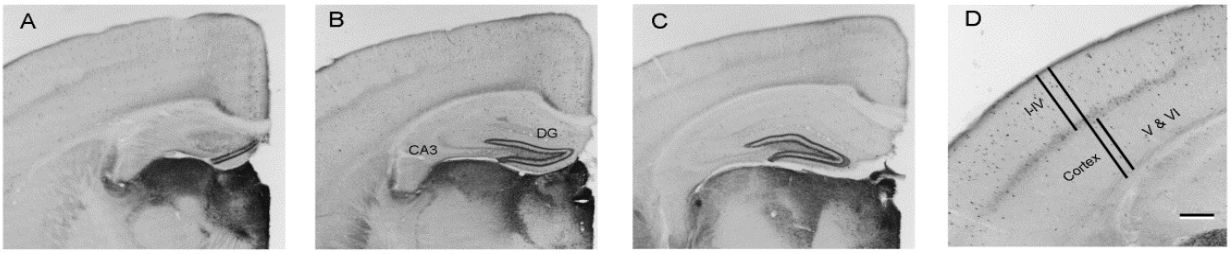

Figure 4. Measurements of cortical thickness. Serial coronal sections were reacted for calretinin, three sections along the anterior-posterior axis were selected to measure lamination and total cortical thickness. The positioning of each section was determined by the morphology of the hippocampus; in the most anterior section the dentate gyrus was only just visible but other hippocampal structures could not be discerned (**A**). The middle section (**B**) contains a clear dentate gyrus (DG) and CA3 is perpendicular to the midline. The most posterior section was identified where CA3 begins to curve round the cortex but the septal pattern of the S1 can still be seen (**C**). Three measurements through the PMBSF were taken for each section; the total length of the cortex, the length of layers I-IV and the length

2.3.3.ii Cortical area measurements

In order to compare cortical areas in SAP102$^{-/y}$ and SAP102$^{+/y}$ littermates one cerebral hemisphere was by flattened using the *flattened neocortex* method described in **Fig. 3** and

sectioned in the tangential plane. Serial 48µm sections were reacted for Serotonin reuptake transporter (SERT). SERT is located on TCA and projections from the raphe, SERT positive correspond to cortical areas that receive thalamic input. The sections that contain PMBSF were imaged using a 1.6x objective and the area of neocortex was measured as shown in **Fig. 5B**. PMBSF and individual TCA patch measurements taken using x5 images, the area of PMBSF was defined as the area surrounding barrel in row A-C in arcs 1-4 and in rows D and E in arcs 1-8 (as shown in **Fig. 5C**), the total area of these barrels was traced and measured in mm^2. The individual TCA patch size was obtained by tracing the individual SERT positive area corresponding to barrels in rows B and C in arcs 1-3, the sum of these areas was recorded for each animal. The positioning of the PMBSF was defined by the ratio between the distance from barrel C2 to the most anterior point of the neocortical sheet (**Fig. 5a** line **T**) and the distance from barrel C2 to the most rostral point (line **R**). The length of neocortex was also measured and defined as the distance from the most anterior point to the most caudal point (line C). All measurements of cortical area were conducted using imageJ (NIH, Maryland, USA).

Figure 5. Position and area measurements of cortical regions

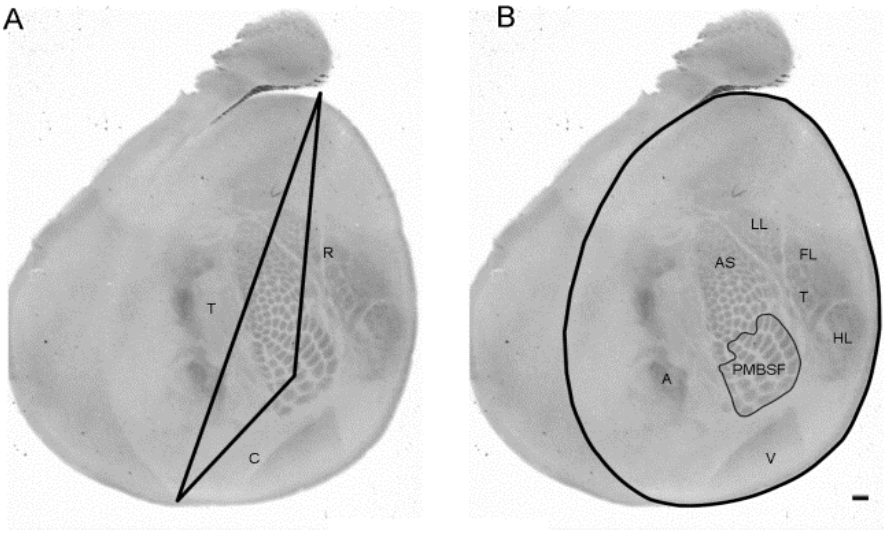

C

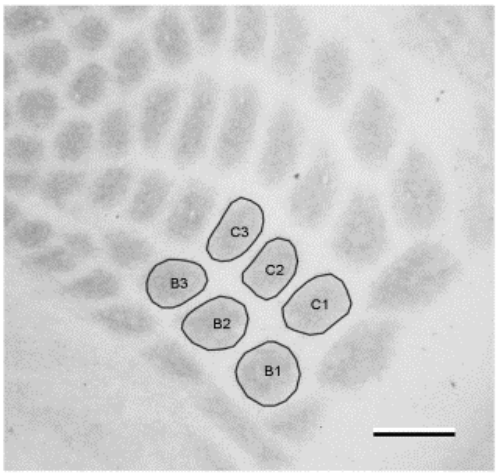

Figure 5. Positioning and area measurements from SERT labelled flattened tangential sections. Position of S1 was calculated using three measurements (**A**); the total distance (T) between the anterior and posterior points, the rostral distance (R) from the anterior pole to barrel C2, and the caudal distance (C) from barrel C2 to the most posterior point. Area measurements of the neocortex and posterior medial barrel subfield are shown in **B**, other cortical areas can also be identified; A; primary Auditory cortex, V; primary visual cortex, AS; anterior snout, LL; lower lip, FL; front limb, T; tongue, HL; hind limb. Individual thalamocortical 'patches' are identified at x5 magnification (**C**), the total area of 6 individual TCA patches were quantified, these corresponded to barrels B1-3 and C1-3. Scale bar 250µm

2.3.3.iii Septal area measurements

In order to measure the septal area sections were flattened using the *S1 flattening* technique and reacted for calretinin. Sections containing the PMBSF were imaged on a confocal microscope using an oil immersion x20 objective (Leica, Wetzlar, Germany). A stack of images taken through barrel C3 was obtained for all sections that contained PMBSF, if barrel C3 could not be identified then the section was removed from analysis. As previously mentioned, Calretinin labels the layer IV/V boundary as well as the septal area between barrels, therefore the laminar position would affect the area labelled by calretinin (at the layer IV/V boundary calretinin labelling is uniform). A single optical section was selected 54 microns above the uniform calretinin distribution to be measured; this ensures equal comparisons were made between animals. The area of calretinin positive processes and cells was measured using imageJ (NIH; Maryland, USA).

2.3.4. NFM positive axon analysis

A stack of confocal images were taken of sections reacted for calretinin, TO-PRO3 and the medium neurofilament subunit (NFM), five adjacent sections were selected from the middle of the stack. A region of interest 100 microns by 30 microns was placed either in layer IV septa, layer IV TCA, layer V septa or layer V TCA. Region of interest positioning was determined using calretinin labelling which restricts to the septal area and the layer IV/V boundary, and the cell density as determined by TO-PRO3 staining. In order for an axon to be quantified it must be

possible to trace the same axon across the 30 micron width of the region of interest (yellow box **Fig. 6D**). Axons were marked using the cell counter plugin for imageJ (NIH; Maryland, USA). For each animal the number of crossing axons in each area was quantified in two sections and mean was calculated.

Figure 6. Quantification of NFM- positive neurites

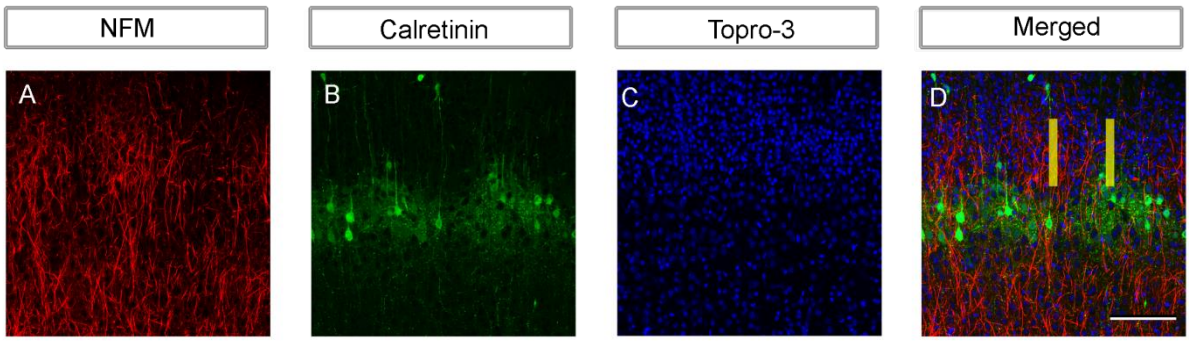

Figure 6. Placement of regions of interest for crossing neurite analysis. Coronal section were reacted for NFM (**A**), calretinin (**B**), and TO-PRO3 (**C**). Images were taken at x20 magnification and four regions of interest were placed; two in layer IV as determined by the cell dense TO-PRO3 stain and two in layer V. Using the calretinin label as a guide regions of interest were either placed in the TCA patch regions or the septal area (**D**). Scale bar 125µm.

2.3.5. Fluorescent Intensity analysis

Coronal sections through the PMBSF were reacted for TO-PRO3 and either myelin basic protein (MBP) or medium neurofilament subunit (NFM) and a stack of confocal images were taken at x10 magnification through the cortex. Confocal settings were calibrated to ensure no part of the image was saturated, 8bit images were converted to 32bit float and the series of optical sections were combined to produce a maximum projections, this projection was then converted back into an 8bit image. This ensured that no part of the

digital image was saturated and kept the relative intensity within the image constant. All animals used for this analysis were sacrificed, reacted and imaged together, this was to control for any degradation of the fluorescent signal. Images were also taken of the fasciculus retroflexus, a major fibre tract that runs through each coronal section that is heavily labelled for both NFM and MBP, this acts as a positive control to determine a maximum intensity value in each section. A region of interest was specified in layers II/III, IV and V as determined by the TO-PRO3 counterstain, each region of interest was placed within a single barrel because the septal region contains fewer TCA (**Fig. 7C**). One region of interest was placed in the pia to determine the background fluorescent, and one in the fasciculus retroflexus to identify the fluorescent maximum. The background fluorescent (pial measurement) was subtracted from the other intensity measurements and for each section the intensity level for each cortical layer was normalised to the maximum level in the fasciculus retroflexus. Two sections were analysed from each animal and a mean of these numbers was taken.

Figure 7. Fluorescence intensity of MBP staining

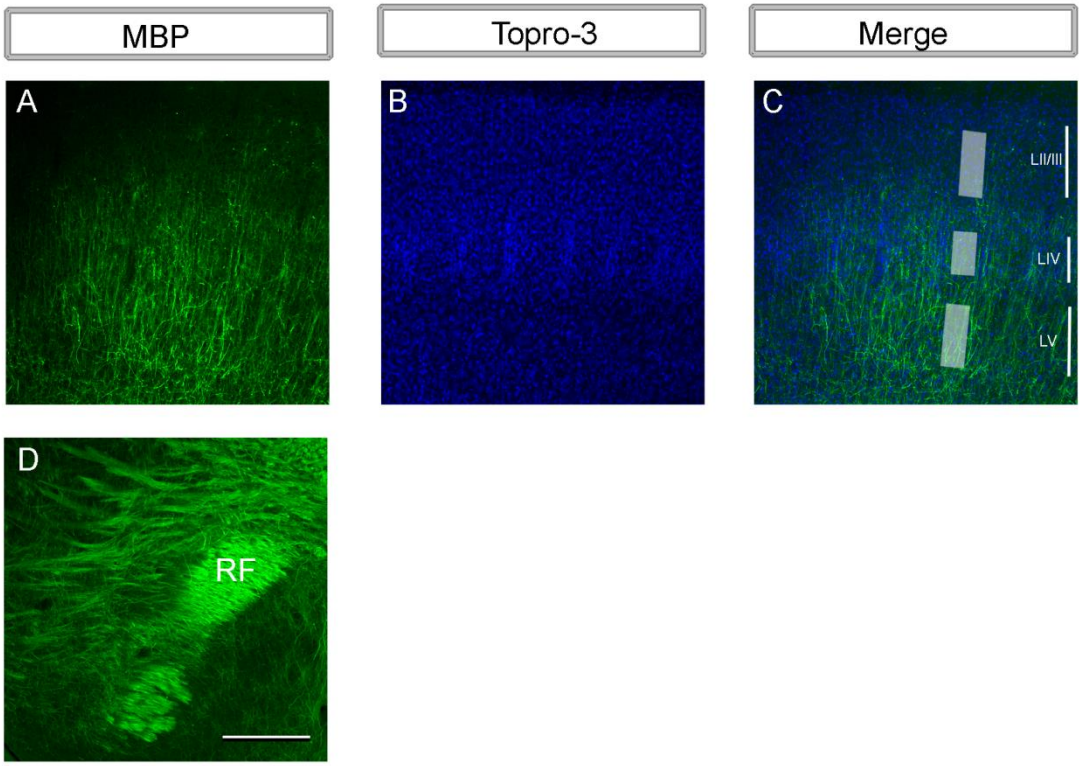

Figure 7. Quantification of MBP staining. Coronal sections were reacted for MBP (**A,D**) and TO-PRO3 (**B**) and imaged at x10 magnification. Regions of interest were identified in each cortical layer to measure fluorescence intensity (**C**) regions of interest were also place in the fasciculus retroflexus to provide a maximum value to act as a positive control within each section (**D**). Scale bar = 250 µm.

2.3.6. TCA tracing

Small pieces of 1,1'-dioctadecyl-3,3,3'3'-tetramethylindocarbocyanine perchlorate (DiI) paper were placed in the VpM of vibrotome sections cut using the TCA slice preparation as described above. Sections were left at 4^{o}C in the dark for approximately 4 weeks. Sections were checked every few days to determine the progress of the DiI transport. When DiI was visible in the cortex, sections were counterstained for Topro-3,

mounted in soft set vectorshield in a perfusion open and closed (POC) chamber on an inverted Zeiss scanning confocal microscope. This set up allowed the section to be imaged without being fully mounted which would have distorted the thick (250µm) section. Sections were imaged using a x20 objective, sampling every 3 microns. Axons were reconstructed from z-stack using Neuronstudio (Wearne et al. 2005).

Figure 8. Single axon reconstruction using DiI

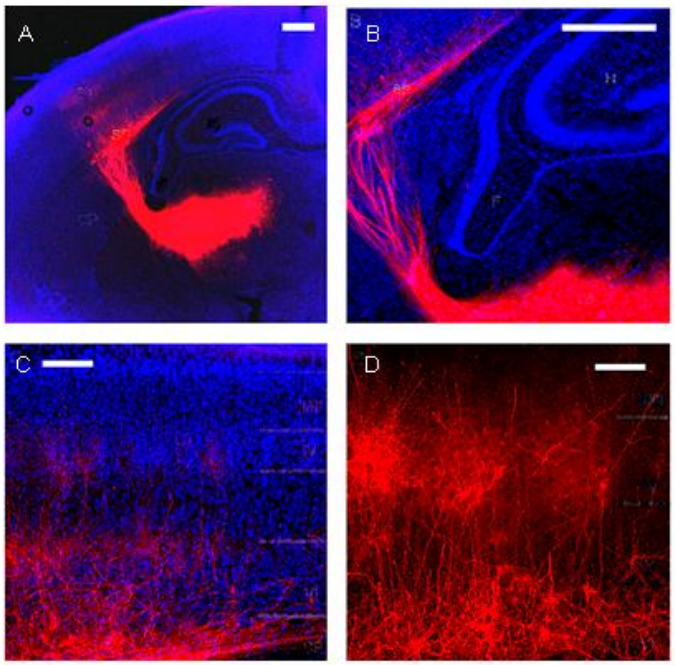

Figure 8. Single axon TCA tracing in the cortex by placing DiI in the vPn. 250µm thick TCA sections (**Figure 2**) were cut on a vibrotome and a single DiI crystal placed in the thalamus, sections were then left free floating in the dark for 4 weeks, then reacted for TO-PRO3 (blue counter stain). Confocal stacks through S1 were taken and individual axons were reconstructed using Neuronstudio. Scale Bar **A,B** = 400µm, **C** = 200µm, **D** = 100µm.

2.3.7. DiI TCA axon analysis

Bulk labelling of TCA is not possible using the TCA slice preparation as some of the axons between the thalamus and cortex will be cut. Instead the cortex was removed using the 'neocortical flattening' method and DiI crystals placed in the white matter tract. Sections

were flattened between glass slides for one week at room temperature to allow the DiI to transport to layer IV. The cortex was then sectioned into 100µm tangential sections using a vibrotome and counterstained with TO-PRO3. A stack of confocal images through the PMBSF were imaged using a x20 objective. A series of 5 consecutive images from the middle of the confocal stack were included in the analysis in a similar fashion to the neurofilament crossing analysis. Regions of interest were placed in the centre of the TCA patch and the septal region, and the number of DiI labelled axons crossing these regions of interest was quantified.

Figure 9. Bulk TCA labelling with DiI

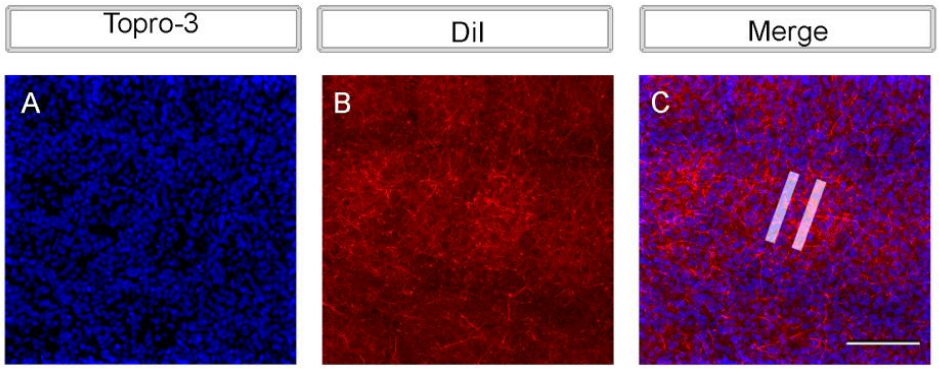

Figure 9. Bulk DiI labelling of TCA. Post-fixed was prepared using the "neocortex flat" method (figure 3**A-C**) and a DiI crystal placed in the internal capsule before flattening the tissue between glass slides. After the DiI had transported the tissue was sectioned on a vibrotome and reacted for TO-PRO3 (**A**), regions of interest (pink boxes **C**) were placed in the septal or TCA patch (**C**) and the number of DiI positive axons (**B**) that crossed the regions of interest were counted. Scale Bar 125µm.

2.3.8. Statistical analysis

All statistical analysis was conducting in R, data was first assessed for normality using a Shapiro-Wilk test and plotting a histogram of the data. In two sample tests, the data was also assessed for homogeneity of variance using a F-test, if the variance was significantly different Welch's correction was applied to the "Student" T-test (identified as a 'T' for the test statistic). If a dataset failed the Shaprio-Wilk test for normality, a Wilcoxon signed-rank test was conducted (identified as a 'W' for the test statistic). For multiple sample datasets, Analysis of Variance (ANOVA) was conducted with a Tukey post-hoc test.

Pseudo-replication, where the number of replicates is artificially increased by using the number of cells as the number of replicates when a comparison is to be made between animals is a prevalent problem in neuroscientific literature (Lazic 2010). All statistical analysis the number of replicates (n) was taken to be the number of animals analysed. When multiple measurements were made per animal (for example in dendritic spine density where 3 cells were counted per animal), a mean for each animal was taken.

2.4 Quantification of cellular segregation in layer IV cells

Cellular segregation of layer IV cells in the S1 (the barrel pattern) can serve as an indicator of normal postnatal cortical development (See introduction 1.3.0). By screening genetic mutants for S1 defects, a number of proteins have been identified that are integral for the formation of this pattern, these include PKA (Watson et al. 2006), SynGAP (Barnet et al., 2006), cortex-specific GluN1 (Iwasato et al. 2000; Datwani et al. 2002), and mGluR5 (Wijetunge et al., 2008). In an attempt to identify mutants lacking a barrel pattern a technique has been published to quantify the segregation of layer IV cells (Watson et al. 2006; Wijetunge et al. 2008; Till et al. 2012). However some mutants have been identified that might have subtle defects in the barrel cortex, and an attempt was made to evaluate the current quantification method and explore some possible alternative techniques. This section will introduce the problem of quantifying barrel formation, document some of the alternative methods and discuss the limitation of each technique. The terms used in this section to describe the anatomy of S1 are defined in 1.3.2. on the anatomical organisation of S1 (1.3.2.).

2.4.1 Difficulties in quantifying barrel segregation

There are typically 34 barrels that make up the mouse PMBSF, these can be visualised at low power when cell bodies, or nuclei are labelled. In order to quantify the segregation of cells in layer IV, x20 confocal images are required, at this magnification one barrel in the 3rd arc will fully occupy the field of view, more barrels can fit in high-numbered arcs however these can be difficult to identify. If a stack of confocal sections are imaged the area would 'bleach' and prevent adjacent barrels from being imaged, this limits the

number of barrels that can be imaged in a section. Although the segregation of layer IV cells is visible at low power, the segregation in a single optical section at x20 is difficult to visualise. When quantified, the ratio of cells in a barrel *wall* to the barrel *hollow* from a single confocal section can be as low as 1:1.2, however this low segregation ratio is sufficient to identify a barrel pattern by eye. In previous analysis of mutants, barrel cortex phenotypes were clear; in mutants lacking *SynGAP* (Barnett et al. 2006), cortex-specific *GluN1* (Iwasato et al. 2000) or *PKARIIß* (Watson et al. 2006) layer IV cells fail to form a barrel pattern. Analysis of *mGluR5* heterozygous animals show a reduction in barrel segregation compared to wild type animals but not as severe as mutants lacking both copies of *mGluR5* (Wijetunge et al. 2008), *FMR1* knockout animals at P7 show a slight reduction in barrel segregation (Till et al. 2012). Furthermore some mutants appear to have alterations in barrel cortex that might not affect the cellular segregation of layer IV cells, for example, it has been suggested that *SAP102* mutants have thicker barrel walls (Petrie, 2008). The published method of characterising barrel phenotypes was designed to identify clear differences in cellular segregation, therefore an evaluation of the current method and comparison with alternative quantification methods was undertaken.

Figure 10. Montage of confocal images through a single barrel

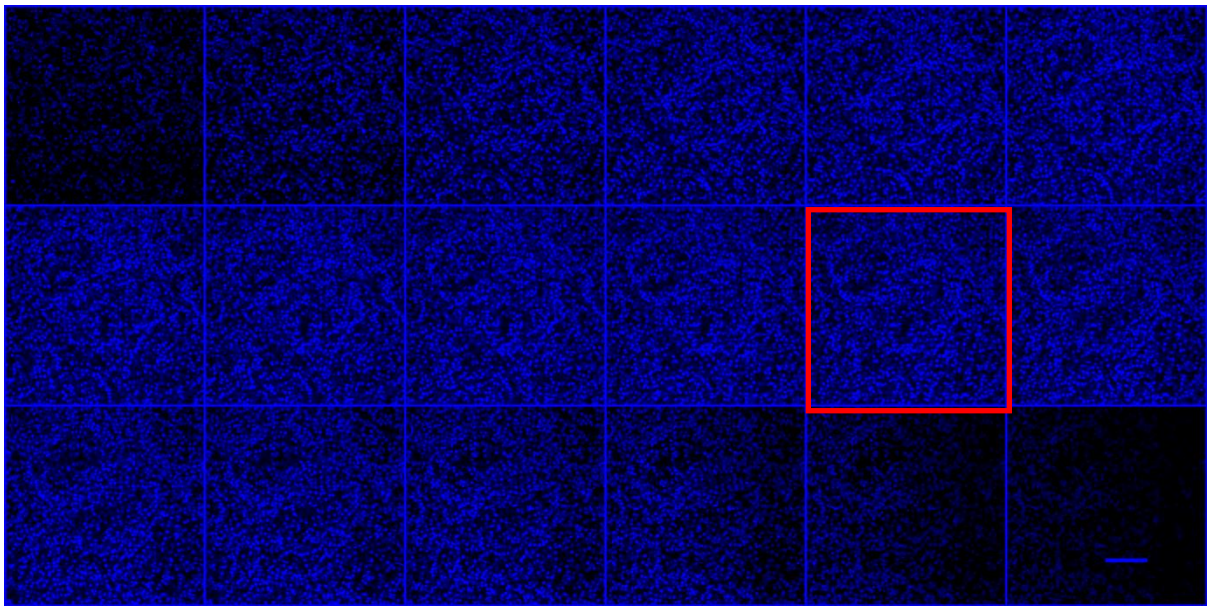

Figure 10. Montage of confocal images sampled every 3µm through a single 'barrel' at x20 magnification. In order for the segregation ratio to be quantified, the optical section with the best segregation must be identified by eye. As the figure above demonstrates it is not easy to identify which section will provide the best segregation score. In the montage presented about the optical section in red was identified as the best segregation by two observers but disputed by a third observer. Scale bar 100µm.

2.4.2. Evaluation of the current quantification method

A confocal stack of barrel C3 is taken at 3 micron intervals through layer IV. These images are then panelled together and the optical section that appears to contain the highest degree of segregation is selected by eye, (**Fig. 10**). Counting quadrates are placed around the cell dense region called the barrel *wall*, ensuring no cell nuclei will be counted twice and that the maximum number of quadrates are placed, this is to ensure there is no bias in sampling from regions that contain clusters of cells. Quadrates are then placed in the center of the barrel (called the *hollow*), again ensuring the maximum number of

quadrates are counted according to the stereological principle that objects touching two adjacent corners and sides are not counted (**Fig. 11**). The mean number of cells in the *wall* (**Fig. 11**, white rectangles) and *hollow* (**Fig.11**, red rectangles) are then calculated by dividing the total number of cells in either the 'wall' or the *hollow* by the number of quadrates. The ratio between these two means is called the segregation ratio.

This method has a number of limitations, firstly it only samples one barrel in a particular optical section and this is a very small proportion of the total barrel field. Secondly, the selection of the best optical section is subjective and as Fig 10 demonstrates this is not always clear. Thirdly, the placing of the quadrates is not random and can produce different results after a slight alteration. Finally, the greatest source of error comes from the placing of the *wall* quadrates as it is difficult to identify the *wall* at high power and minor adjustments can affect the segregation ratio.

Figure 11. Traditional method for quantifying the segregation of layer IV cells

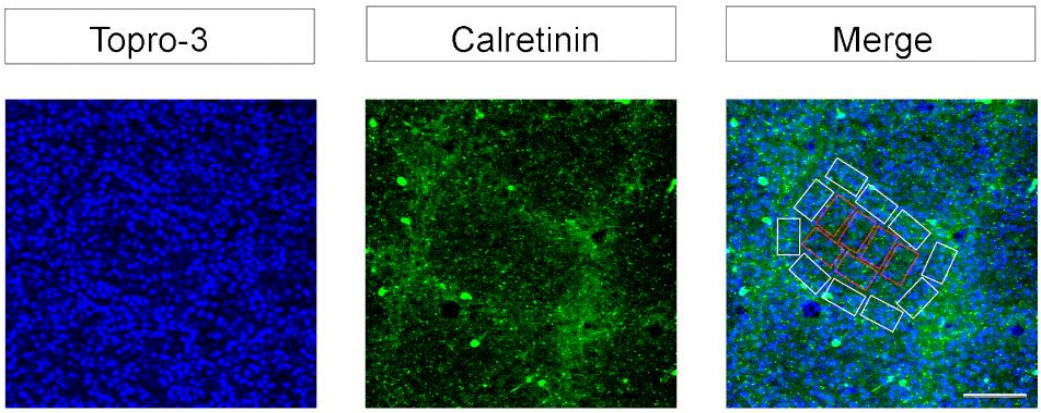

Figure 11. Traditional method for quantifying the segregation of layer IV cells. Flattened tangential sections are reacted for TO-PRO3 (**A**), calretinin (**B**). Using the septal marker calretinin as a marker counting quadrates are placed in the barrel *wall* region (white boxes) and in the barrel *hollow* (white boxes). Scale bar = 250 µm.

2.4.3. Alternatives to the traditional method

2.4.3.i Rainbow method

In order to reduce the variability from selecting the correct optical section a new method was devised. 3 adjacent optical sections are selected from a confocal stack of images sampled every 3 microns. The three different optical sections are pseudo-coloured so the depth of each section can be identified. Quadrate counts are still used to compare the proportion of cells in the wall or hollow and placed in the same manner. Cells identified in the top two sections were counted and the third section can be used to confirm the presence of a cell. The diameter of cell nuclei labelled with TO-PRO3 is approximately 8 microns therefore within a 3 micron- sampled stack cells will appear in at least 2 sections.

This technique removes the reliance on only one optical section, reducing the importance of selecting the optical section with the greatest degree of cellular segregation. The extra optical sections also aid nuclei identification. However this method still relies on the subjective placement of the counting quadrates. In order to remove the need for counting quadrates a number of methods were explored to label the boundary between the wall and the hollow.

Figure 12. The rainbow counting method

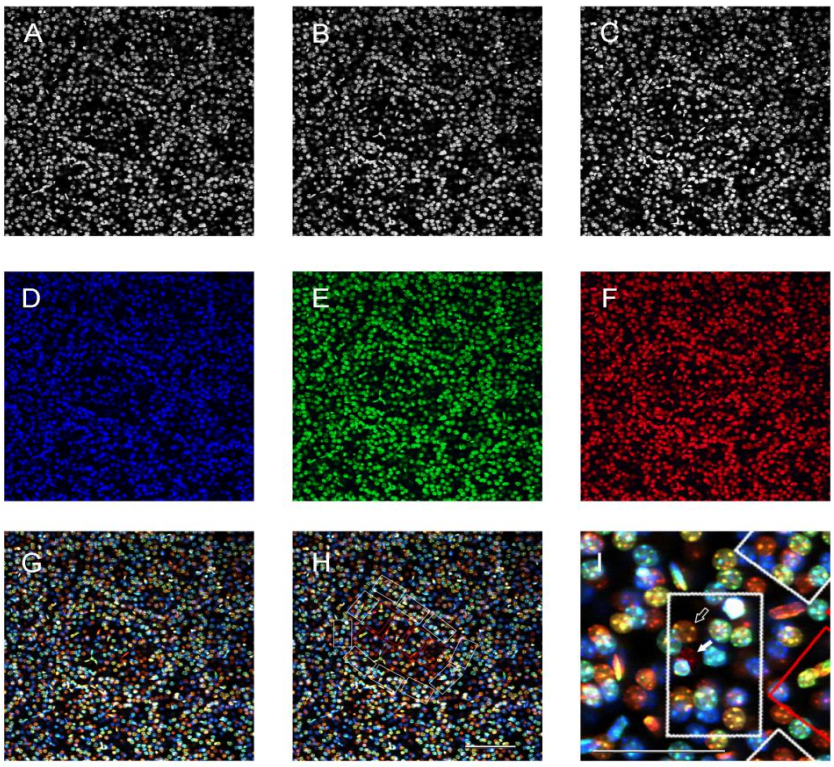

Figure 12. The Rainbow counting method. 3 adjacent confocal images which contain the highest segregation ratio are selected by eye (**A-C**), these sections are pseudo-coloured (**D-F**), these images were then combined to produce a multi-coloured image (**G**) which provided information on the z position of each confocal image. Counting quadrats were then placed in the wall and the hollow (**H**), as previously described (Figure 11). Cells were counted in the blue and green images, using the red images as a reference to confirm the presence of a cell. Cells that contained yellow spots of chromatin caused by the combination of red and green images (**I,** hollow arrow) were counted, whereas red cells void of yellow spots were not (**I**, filled arrow) as these cells are only present in the 'red' z-plane. Scale bar 100µm.

2.4.3.ii SERT model

Serotonin reuptake transporter (SERT) is expressed on TCA and restricts to a TCA *patch* pattern, SERT expression could serve as an objective delineation between the *wall* and *hollow* cells. In this technique sections were reacted for SERT and TO-PRO3. A confocal stack was taken through a single barrel and the best optical section selected from the z plane. The edge of the SERT positive area would then be traced on screen to create a mask to identify which cells belong to either the *wall* or *hollow*. The position of each cell could be mapped using a computer program and each cell could be classified as either *wall* or *hollow*. A simple computer program was designed to trace the SERT image and map the position of cells using a computer mouse. Using this method all cells in the confocal image could be mapped and classified as either *wall* or *hollow* cells. The number of *wall* or *hollow* cells could be divided by the area that was either SERT positive or SERT negative to provide a density for the *wall* and *hollow* region.

This method does not require counting quadrats and defines the shape of the barrel objectively. However processing the SERT image (by smoothing the image and converting to binary) does not always provide a perfect representation of the barrel shape, this is because smoothing an image will be affected by local regions of high or low fluorescence intensity (**Fig. 13C**). One way this problem could be resolved would be tracing the SERT region manually by hand, and this method is described in the septal model. Whilst the SERT model removes the need for counting quadrates, the SERT patch is not an accurate indicator of the *wall* boundary as many cells cluster on the edge of the SERT patch. Moreover the cell sparse septal area is included in the SERT negative region, which reduces the cell density in the *wall* region therefore the ratio in cell density between the *wall* and the *hollow* region is very low using this method.

Figure 13. The SERT model

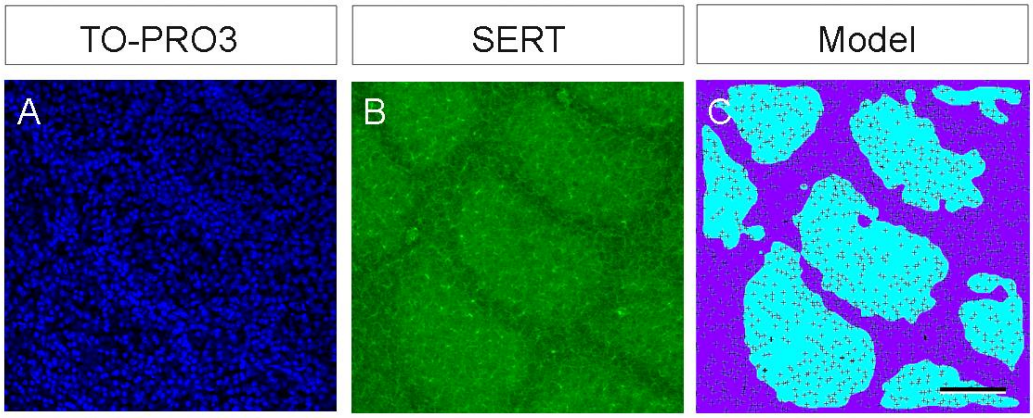

Figure 13. The SERT model uses the SERT positive area as an indicator of the cell sparse barrel *hollow* region to quantify the degree of cellular segregation in layer IV. Tangential section reacted for TO-PRO3 and SERT were imaged on a confocal microscope, the position of TO-PRO3 positive cells was mapped using a cell counter program and identified by small crosses in the model (C). The SERT image was then smoothed using a Gaussian filter and converted to a binary image, with regions defined as SERT positive (light blue area in C) or SERT negative (dark blue area in C). The segregation ratio is the ratio between cell densities in the SERT positive and SERT- negative regions. Scale bar 100µm.

2.4.3.iii Calretinin model

Using a similar method to the SERT model, markers specific to the septal region can be used to provide a boundary for the total barrel. Calretinin is a calcium binding protein that specifically labels the barrel septa and the layer IV/ V boundary. In a similar fashion to the SERT model, the septal model requires the calretinin-positive *ring* to act as a mask for the shape of a barrel. The shape of the barrel is determined by tracing around the calretinin positive septal area, and the number of cell s that lie within this area is quantified. The diameter of the calretinin mask can be reduced about the centre of the

barrel (shown as different coloured rings in **Fig. 2.14.C**) and the number of cells containing a *ring* of a given size can be recorded. The co-ordinates of both the *ring* and layer IV cells are mapped using a computer program and the size, the number or diameter of the rings can be adjusted accordingly. The density of cell within different sized *rings* can be computed to get the be computed to get the percentage change in cell density in different areas within a single barrel. Unlike other methods this makes no assumption about the width of the barrel wall making it possible to identify mutants with especially thick barrel walls provided enough control data had been collected. This could be done by recording the cell density in calretinin rings of decreasing diameter and defining the barrel wall as a percentage reduction in cell density.

Although this method makes no assertion about the thickness of the barrel wall, it does assume that barrels are the same shape as the calretinin-positive septal region, which is not usually the case. It also requires a significantly large database of wild type animals to build up a representative model of barrel dimension by which mutants could be compared. Finally, although this method is precise it is highly sensitive to the length of time in fixation each calretinin-ring provides a density of cells in a small area, the length of time in fixative affects tissue shrinkage and therefore the packing density of cells.

Figure 14. The calretinin model

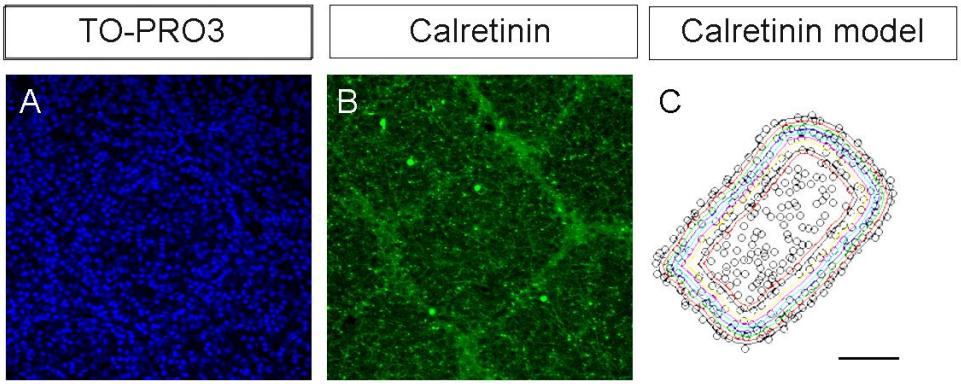

Figure 14. The calretinin model uses the calretinin positive septal region to produce an outline of the barrel shape. Tangential sections are reacted for TO-PRO3 (**A**) and calretinin (**B**). Each cell is plotted (circles in C) and the outline of the calretinin positive area is trace manually and the co-ordinates recorded using a computer program. Using the calretinin outline as a starting point (outer black line in **C**) the area of the calretinin outline is reduced about the centre point and the number of cells that fall within the reduced calretinin is recorded (shown as different coloured lines in C). The iterations and amount of by which the ring is reducted can be adjusted so that the percentage difference in cell density can be calculated. Scale bar 100µm.

2.4.4. Evaluation of alternative methods

Whilst both the SERT and calretinin model are more objective than the traditional method, and are more accurate in identifying subtle phenotypes, they both require a large amount of control data to produce a useful model of a normal barrel before their suitability of analysing mutants could be assessed. Furthermore, because both these methods rely on density measurements, they are sensitive to the length of time the tissue has spent in fixative and therefore datasets from other mutants could not be compared. This is a major problem when addressing complex genetic crosses like those described in chapter 5 (see

section 5.2.2) on SAP102/PSD95 double mutants it took 2 years to generate 6 double mutants, therefore the length of time the tissue had to be stored in fixative would

generate 6 double mutants therefore the length of time the tissue had to be stored in fixative would vary and any method sensitive to the fixation time would not be practical in analysing these mutants.

Whilst the rainbow method does reduce the variability of selecting the 'best' optical section, this did not affect the segregation ratio compared to the traditional method. When two people have independently analysed the segregation ratio in a single optical section, any variation was the result of different placement of the counting quadrats. Therefore the traditional method is judged currently as the best method for analysing the segregation of an individual barrel.

Although the traditional method has been used to analyse mutants in this thesis, a number of steps were taken to reduce the variability in the placement of the counting quadrates. Firstly the quadrate placement was independently verified with another laboratory member. Secondly all sections were reacted with calretinin which labels the septal area; this provided an objective guide for identifying the barrel edge.

Chapter 3

Characterisation of 3 neurofilament subunits in the developing S1

3.1 Introduction

Topographical and feature maps in the neocortex can be used as a model for studying the mechanisms by which the anatomical and physiological attributes of sensory systems develop. At the heart of map formation is the connectivity between and within brain areas and their development is dependent, in part, on neuronal morphology, both in terms of axon connectivity and in terms of dendritic branching. The structural specializations that create functional maps are the proteins responsible for determining neuronal shape, including those that compose the cytoskeleton. The structural stability of neurons is thought to originate from the intermediate class of cytoskeletal proteins, of which neurofilament (NF) appears to be the most abundant in adult tissue (Morris & Lasek 1982).

3.1.1. Neurofilament subunits

Neurofilaments are formed by assembly of three protein subunits that differ in their relative masses (Hoffman & Lasek 1975): neurofilament light (NFL), neurofilament medium (NFM) and neurofilament heavy (NFH). These subunits form heterodimers that form the basis of protofilaments, which intertwine to form the complete 10nm diameter NF. *In vivo* NF subunits cannot self-assemble into polymers and are obligate heteropolymers formed of NFL and either NFM or NFH (Geisler & Weber, 1981), NF subunits can also for stable filaments with intermediate filaments such as vimentin (Lee et al. 1993) and α-internexin (Ching & Liem 1993). A number of studies have demonstrated that all three NF subunits are found in cells that express neurofilaments (Sharp et al. 1982; Trojanowski et al. 1986), however in some populations of neurons, NFH is not uniformly distribution throughout the cell (Balaratnasingam et al. 2009; Sharp et al. 1982; Shaw et al.

1981; Dahl 1983; Hirokawa et al. 1984) suggesting differences in expression patterns between NF subunits. In a number of different brain regions NFH is expressed later in development compared to other subunits (Shaw & Weber 1982; Giasson & Mushynski 1997) and this has led many to suggest that NFH could be involved in the maturation of neurofilaments (Yuan et al. 2006; Fiumelli et al. 2008; Carden et al. 1987; Dahl & Bignami 1986).

3.1.2. Neurofilaments in cortical maps

A role for neurofilament in the maintenance of sensory system maps has come from the visual cortex where the pattern of neurofilament expression correlates with feature maps of the visual environment. In the supragranular layers of the monkey primary visual cortex, discrete cytochrome rich areas known as *blobs* are a feature map of colour processing. Cells within the *blob* regions selectively respond to the wavelength of light hitting the retina and receive direct thalamocortical input, NFH labels the cell bodies and dendrites of large pyramidal cells in the regions between *blobs* known as *interblobs*, a region that is void of thalamic input (Duffy & Livingstone, 2003). As NFH expression is reduced in the TCA-receiving "blob" areas this suggests that NFH is restricted to the dendrites of large pyramidal cells but not the axons. Furthermore monocular deprivation during the critical period will reduce NFH expression in the corresponding hemisphere demonstrating that expression of NFH in the primate visual cortex is dependent on sensory experience (Duffy & Livingstone, 2005).

3.1.3. Neurofilaments as axonal markers

NFs have often been used as markers of axons (Lycke, Karlsson, Andersen, & Rosengren, 1998; Petzold, 2005; Teunissen, Dijkstra, & Polman, 2005), however as

mentioned above NFH labels dendrites in the visual cortex; it is not known if any NF subunit restricts its expression solely to axons, either in adult animals or during development. The rodent S1 may provide an ideal model system to address this question. Within the rodent S1 the whisker-related pattern can be readily identified by examining staining pattern for markers of layer IV cells soma (Woolsey & Van der Loos, 1970), layer IV cell dendrites (Steffen & Van der Loos, 1980), thalamocortical axons (Agmon, Yang, O'Dowd, & Jones, 1993) or large septal interneurons (Melvin & Dyck 2003) each of which produce a unique cellular aspect of the barrels structure (see introduction 1.3.2.). Therefore evaluation of neurofilament subunits in the rodent S1 will help determine the specificity of each subunit to label subcellular structures. Furthermore, the ability to specifically label TCAs in S1 would be a valuable tool to investigate the development of sensory maps. The precise timing of TCA segregation into a whisker pattern in S1 is unclear (see introduction 1.3.3 and introduction **Fig. 3**). Some groups have reported radial bands of TCA are seen in cortical layer V at P2 before the emergence of a layer IV pattern suggesting that TCA project through layer V in an organised arrangement (Agmon et al., 1993; Catalano, Robertson, & Killackey, 1996), however single axon tracing using lipophilic dyes have shown some axons project laterally across the width of several barrels in layer V (Rebsam, Seif, & Gaspar, 2005), implying that TCA are not restricted into in a whisker-related pattern in layer V and that organisation of TCA occurs in layer IV. The ability to label TCA would help understand the role played by innervation from the thalamus in setting up sensory maps in the cortex.

This chapter aims to characterize the expression pattern of neurofilament subunits in an attempt to identify a marker for TCA. Although NF subunits have been used to label axons, evidence that some subunits may be developmentally regulated makes it important to examine the expression of all three subunits throughout S1 development. The unique

patterning of S1 makes it possible to determine if a protein restricts to axons, dendrites or soma in *ex vivo* sections.

3.1.4. Rationale and hypotheses

Some NF subunits have shown to label pyramidal cells in regions void of thalamic input (Duffy & Livingstone, 2003, 2005) yet NF are frequently been used as axonal markers (Lycke et al., 1998; Petzold, 2005; Teunissen et al., 2005). In this chapter the unique organisation of the rodent S1 is used to characterise the expression of 3 NF subunits to identify a TCA marker.

Hypothesis 1: Neurofilament subunits will restrict to different sub-cellular regions (axons, dendrites, perikarya) producing different patterns of expression in the adult S1.

NFH has been shown to be expressed at a later developmental time point compared to other NF subunits (Shaw & Weber 1982; Giasson & Mushynski 1997) and NFH is thought to be involved in maturation of stable filaments (Fiumelli et al. 2008; Carden et al. 1987; Dahl & Bignami 1986).

Hypothesis 2: There will be differential developmental expression between NF subunits.

NF expression in the visual cortex has previously been shown to be reduced by monocular deprivation (Duffy & Livingstone, 2005) and sensory deprivation may also affect NF expression in the rodent S1. Investigation into the experience dependant expression of cytoskeletal proteins would provide an insight into how cortical maps can be refined during development.

Hypothesis 3: Depriving neonatal mice of somatosensory experience by trimming whiskers will affect the expression of NF subunits.

3.2 Results

NF subunits have differential expression patterns in the adult S1 (**Fig. 1**). Coronal sections reveal NF subunits differ in their laminar expression; NFL and NFM reactivity is strongest in layers II/III and V, labelling apical dendrites from pyramidal cells coursing through layer IV (**Fig1. A,B**). NFH reactivity is strong in all layers except layer I and at the IV/V border (**Fig.1 C**). The expression of NF subunits also differs on a sub-cellular level; high power images of adult tissue reacted for NFL and NFM reveals cell bodies and apical dendrites (**Fig. 1D,E).** Although NFH also labels cell bodies in adult tissue, they are less distinct compared to labelling with other subunits and the pattern is composed of less uniform processes, possibly axons (**Fig. 1F)**. In tangential sections through layer IV, NFL and NFM are expressed in the septal region (**Fig. 1G**,**H**), whereas NFH is expressed in the region that receives thalamic input as revealed by a TCA patch pattern (**Fig. 1I**).

Figure 1. Photomicrograph of coronal and flattened tangential sections from an adult S1 reacted for each neurofilament subunit. **A-C**: Coronal sections reveal the differences in laminar expression observed between the neurofilament subunits. NFL (**A**) and NFM (**B**) show increased immunoreactivity in layers II/III and V, sections reacted for NFL reveals a decrease in layer V labelling (**A**), whereas NFM shows a dense reaction product in layer V (**B**). In contrast to the other subunits, sections reacted for NFH (**C**) display immunoreactivity in layers II/III, IV and V with a region void of reactivity at the layer IV/V boundary. **D-F:** High power images of layer IV coronal sections reveals the different subcellular expression of each NF subunit. NFL (**D**) and NFM (**E**) are localised to cell bodies and apical dendrites, whereas NFH (**F**) appears to be mostly axonal with some pyramidal cell soma. **G-I:** Flattened tangential sections through the S1 in all NF subunits reveal a distinct whisker-related patterning. NFL (**G**) and NFM (**H**) reactivity is localised to regions with reduced thalamic input (septa), whereas NFH (**I**) displays a complimentary patterning, restricting to regions rich in TCA input. Scale bar (**A-C, G-I;** 250μm) (**D-F;** 125μm).

Figure 1. Neurofilament subunit expression in adult S1

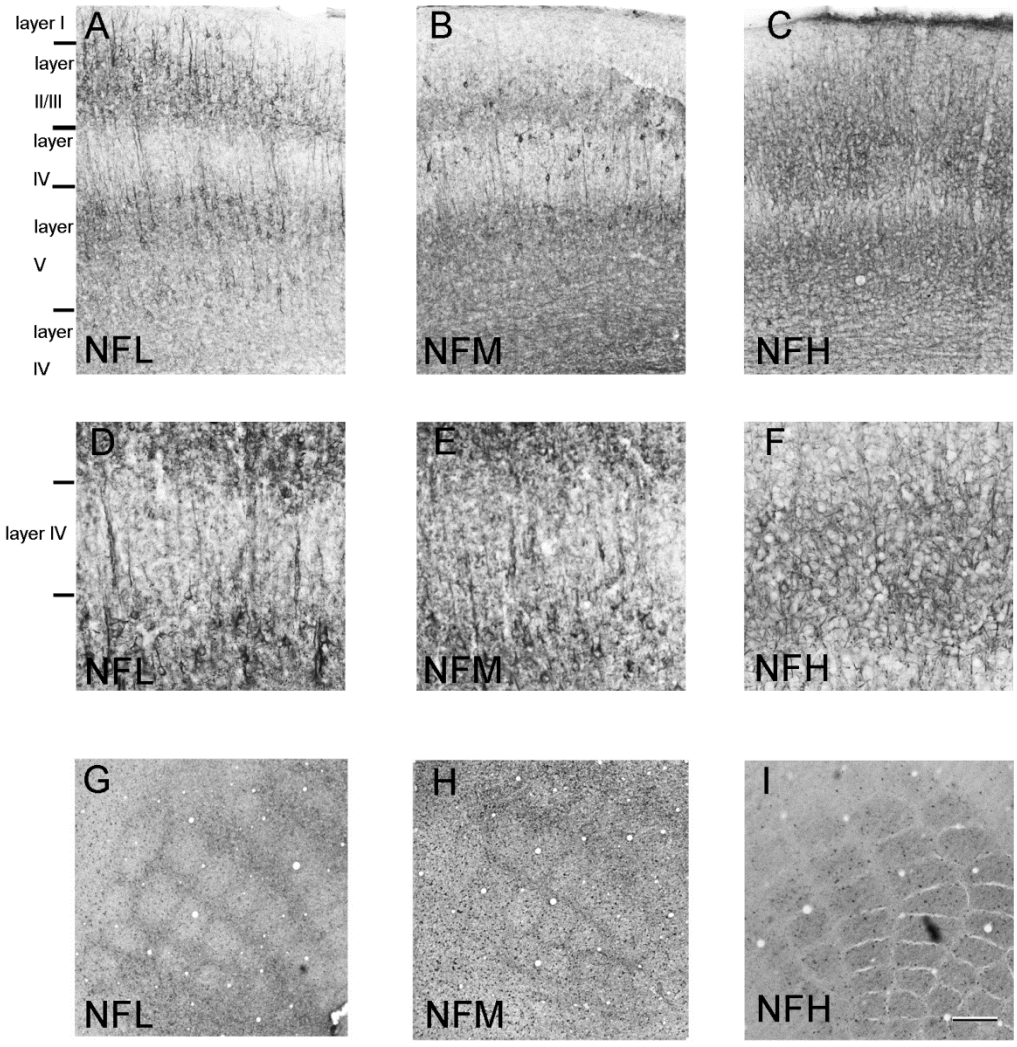

3.2.1. Laminar expression of Neurofilament subunits through development

To examine the laminar development of NF subunit expression, coronal sections were reacted at different developmental ages (**Fig. 2**). Sections reacted for NFL at P5, P7 and P14 show thin radial bands of neurites in layer IV consistent with a septal pattern (**Fig. 2A,D,G,A',D',G')**. In the first postnatal week NFL labelling is restricted to layer II/III and V, at P14 labelling is reduced in layer II/III (Fig. 2G), resembling the adult pattern of expression (**Fig. 1A**). The pattern revealed by NFM is developmentally regulated; at P5 NFM labels radial bands of neurites projecting through layers IV and V, with heavy labelling in layer VI (**Fig.2B**). At P7 this patterning has changed with a more uniform expression throughout layer V (**Fig. 2E**, **arrows**), and thin radial bands of neurites projecting through layer IV, consistent with a septal pattern is present at P14 (**Fig. 2H**, **arrows**). In the first postnatal week NFH displays a similar laminar pattern to NFM, with radial bands of axons being labelled (**Fig. 2C**), however unlike NFM, at P14 clusters of radially projecting processes are still visible in layer IV (**Fig. 2I**). NFH demonstrates an adult pattern of staining by P14 with a more uniform pattern in layer V, and a region void of reactivity at the boundary between layer IV and V (**Fig. 2I**). High magnification images through layer IV suggest that the expression of each NF subunit may be unique at a cellular level (**Fig. 2A'-I'**); NFL appears to localise to cell bodies and apical dendrites of pyramidal cells through development (**Fig. 2 A',D',G'**). NFM appears to change its cellular localisation through development, labelling what appears to be TCAs at younger ages (**Fig. 2 B',E'**) but cell bodies and apical dendrites at P14 (**Fig. 2H'**). NFH appears to label TCA at all three ages (**Fig. 2C',F',I'**), however at P14 NFH shows a more diffuse distribution in which neurites and cell bodies are far less defined (**Fig. 2I'**).

Figure 2. Photomicrograph of coronal sections through development in the S1 reveals differential laminar expression between NF subunits. High-power images of sections reacted for NFL show a consistent laminar patterning throughout development (**A, D, G**), thin radial bands of processes seen in layer IV, consistent with a septal pattern. Sections reacted for NFL reveal cell bodies at P5 (**A'**) and P7 (**D'**), with apical dendrites become visible at P14 (**G'**). Sections reacted for NFM at P5 (**B**) reveal radial columns of neurites projecting from layer VI into layer IV. At P7 the laminar patterning revealed by NFM has changed (**E**) with increased staining in Layer V compiled of cell bodies and apical dendrites. By P14 the laminar patterning revealed by NFM (**H**) closely resembles NFL, with reduced layer IV reactivity and cell bodies visible in layers II/III, V and IV (**H'**). Throughout the first postnatal week the laminar pattern as revealed by NFH is consistent, with increased reactivity in layer VI and columns of neurites in layer IV and V (**C,F**). At P14 columns of radial neurites in layer V are no longer visible and a region void of label emerges at the layer IV/V boundary (**I**). High power images of NFH at P5 (**C'**) and P7 (**F'**) shows these neurites are not apical dendrites like those seen in sections reacted for NFL and NFM. By P14 NFH labels cell bodies as well as neurites in layer IV (**I'**). Scale bar (**A-I;** 250µm) (**A'-I';** 125µm).

Figure 2. Neurofilament subunit expression in coronal sections through development

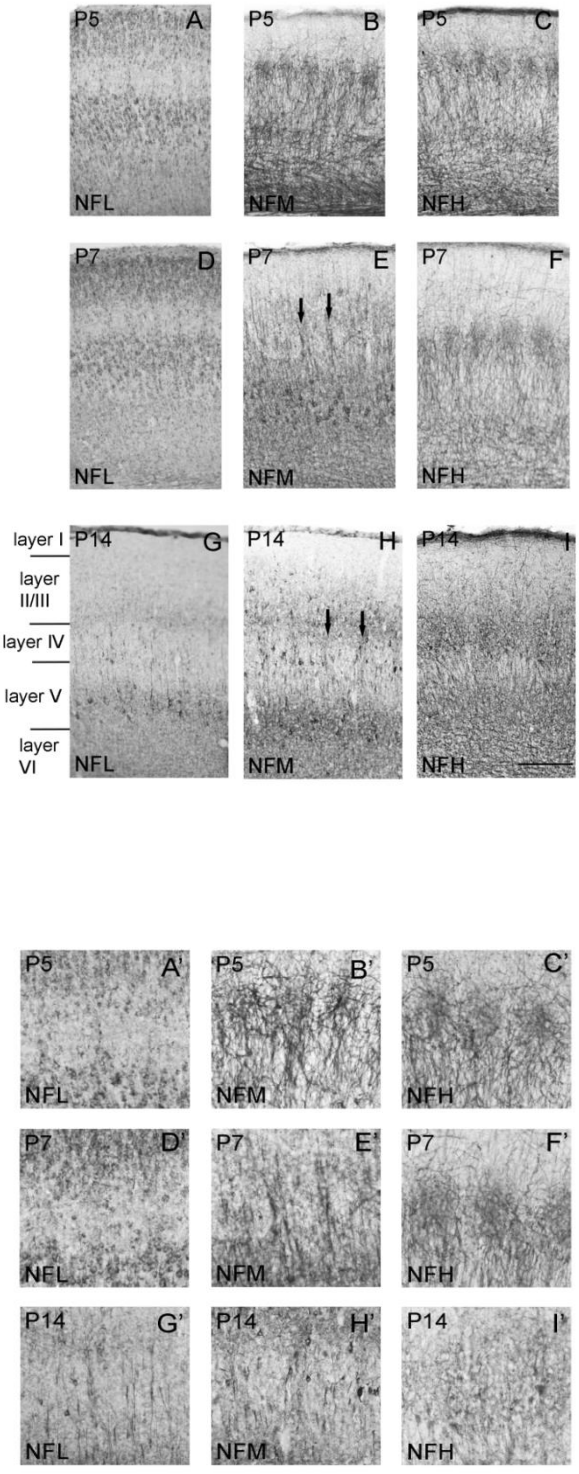

3.2.2. Layer IV patterning revealed by Neurofilament expression through development

To determine if the whisker related pattern in layer IV as revealed by NF subunits changes throughout development, tangential sections were also reacted for each NF subunit. Each NF subunit reveals a different layer IV expression pattern through development (**Fig. 3**). No whisker-related pattern could be identified in sections from all animals at P4 reacted for NFL (n=5, **Fig3. A**), however in sections reacted for NFM (**Fig. 3B**) and NFH (**Fig. 3C**) a whisker-related pattern was discernible. At P5 a septal pattern was observed in sections reacted for NFL (**Fig. 3D**), this pattern was maintained through to later ages (**Fig. 3A,D,G,J,M, Fig. 1G**). In the first postnatal week NFM labelling is restricted to a TCA patch region, however adult (**Fig. 1H**) and P14 (**Fig. 3N**) tissue reacted for NFM produces a septal pattern (**Fig. 3B,E,H,K**). Sections reacted for NFH labels TCA at P4 and throughout development (**Fig. 3C,F,I,L,O, Fig. 1I**). The transition in NFM from a TCA patch pattern to a septal pattern occurs in the second postnatal week, this is in contrast with the expression pattern of NFL and NFH, which do not show a detectable change in the pattern of staining. In 7 animals reacted for NFM at P4 only one displayed a septal-like pattern, whereas 3 out of 7 animals reacted for NFM at P7 showed a septal pattern and occasionally both patterns can be seen in the same section (**Fig. 3E**). By P14 all (n=6) animals reacted for NFM showed the mature pattern. Therefore all three NF subunits show a different spatio-temporal expression in the mouse S1.

Figure 3. NF subunits reveal differential whisker-related patterning in the S1 throughout development. NFL patterning emerges in tangential sections at P5 (**D**), and is consistent throughout development (**D,G,J,M**) . Sections reacted for NFM at P4 (**B**) reveal a pattern consistent with thalamocortical axons, between P5 and P7 (**E,H,K**) this pattern transitions to the barrel septa and occasionally both patterns can be observed in the same section (E). At P4 sections reacted for the NFH subunit also reveals a pattern consistent with thalamic input (**C**), however unlike NFM this is maintained into older ages (**F,I,L,O**). Scale bar 250µm.

Figure 3. Neurofilament subunit expression in tangential section through development

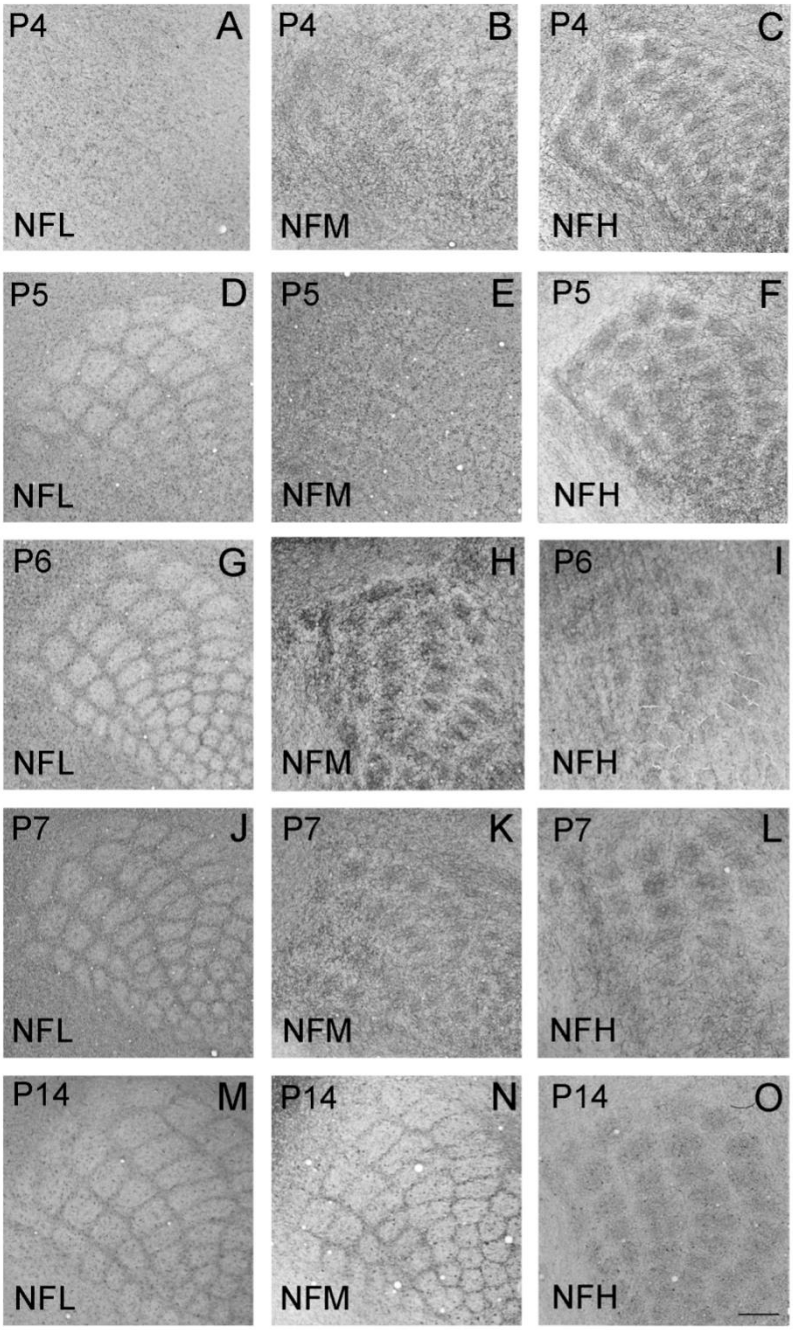

3.2.3. Neurofilament expression in the internal capsule and thalamus

To determine if NF subunits labelled TCA, neurofilament subunit expression was investigated in the thalamus and internal capsule using a TCA slice preparation (see methods **Fig.2** and 2.2.2), this maintains thalamo-coritcal and cortico-thalamic connections. All NF subunits label axon tracts in the internal capsule and the thalamus at both P6 (**Fig. 4A-C**) and P14 (**Fig. 4D-F**). In the internal capsule labelling for NFL appears to be less intense (**Fig. 4A, D**), compared to NFM (**Fig.4B, E**) and NFH (**Fig. 4C, F**).

Figure 4. Neurofilament subunit expression in the thalamus and internal capsule

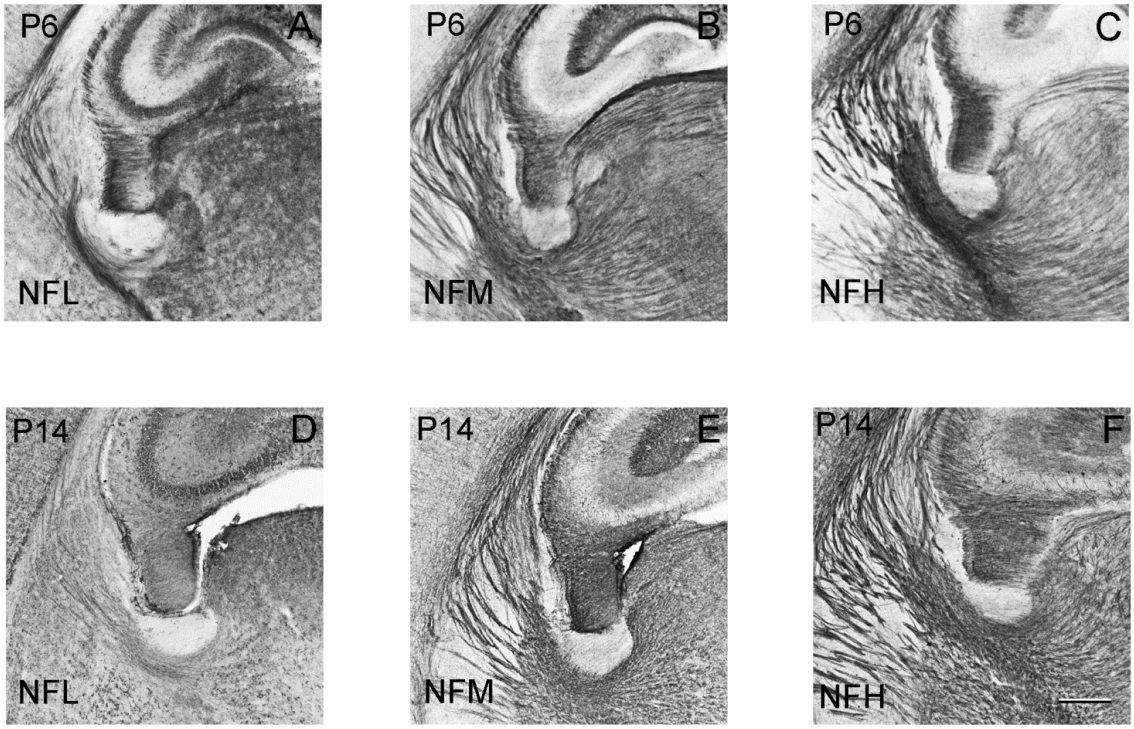

Figure 4. NF subunits label TCA tract in the internal capsule. TCA sections (See methods 2.2.2) reveal expression of NFL (**A,D**), NFM (**B,E**) and NFH (**C,F**) at P6 (**A-C**) and P14 (**D-F**) in the internal capsule. All three NF subunits label thalamocortical tract axons at both P6 and P14. TCA labelling in the internal capsule is less intense in sections reacted for NFL (**A,D**) compared to other subunits (**B,C,E,F**). Scale bar 250µm.

3.2.4. Neurofilament subunits as markers of TCA

To determine whether NFH and NFM label TCA, tangential sections through cortical layer IV were reacted for SERT; a presynaptic marker known to be expressed on TCAs in layer IV (Rebsam, Seif, & Gaspar, 2002), Topro3 to label cell nuclei and each NF subunit. Low power images confirm that NFM (**Fig. 5B,D**) and NFH (**Fig. 5F,H**) restrict the SERT-positive TCA 'patch' whereas NFL labels perikarya in the septal region between the barrels as identified by TO-PRO3 stained nuclei (**Fig. 5J,L**). High-power Nyquist-sampled confocal images reveal SERT puncta decorating both NFM and NFH positive axons (**Fig. 5D',H', arrowhead**). In the septal region there is dramatically less SERT expressed, however any visible SERT puncta were not restrict to NFL positive neurites (**Fig. 5L'**).

Figure 5. Confocal images of flattened tangential sections through layer IV of the S1 triple labelled for SERT (**A,E,I**), TO-PRO3 (**C,G,K**) and either NFL (**I-L**), NFM (**A-D**) or NFH (**E-H**). Low power images show NFM (**A-D**) and NFH (**E-H**) are localized to the SERT positive TCA patch. NFL labels cell bodies in the septal region, which is void of input received from the VpM of the thalamus (**J**). Nyquist-sampled deconvolved high-power images of NFM (**A'-D'**) and NFH (**E'-H'**) reveal SERT-positive puncta corresponding to presynaptic terminals decorating NFM and NFH positive axons (**D,H, arrowheads**) . High-power Nyquist-sampled deconvolved images of NFL (**I-L**) in the barrel septae have relatively fewer SERT positive puncta which are not restricted to NFL-positive axons (**L**). Scale bar (**A-L;** 20μm) (**A'-L';** 1μm)

Figure 5. SERT and neurofilament expression

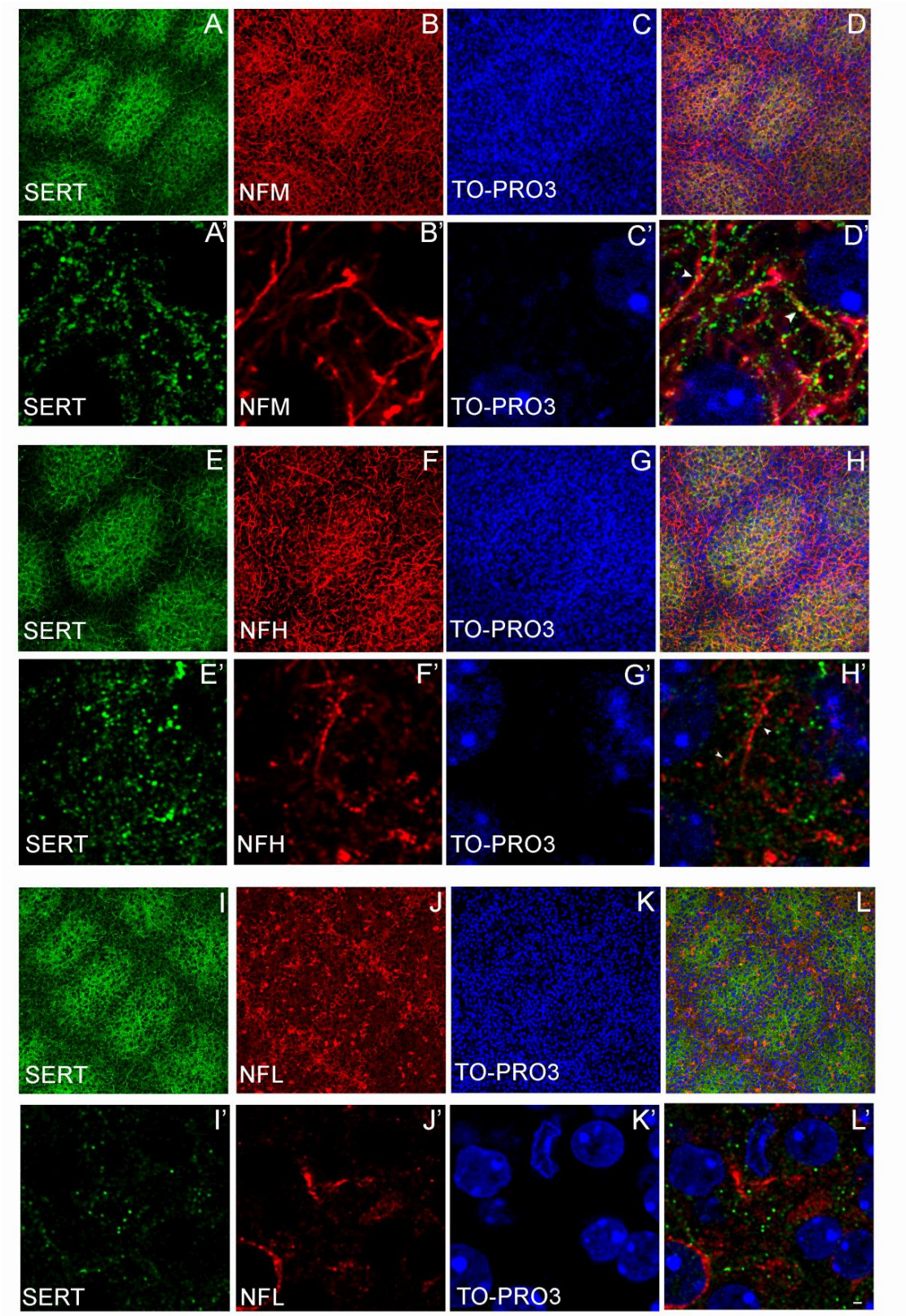

3.2.5. Development of TCA patterning in the cortex

Coronal sections reacted for NFM and NFH in the first postnatal week label radial bands of axons in layer V (**Fig. 2B,C**), and these neurites co-localise with SERT labelling in layer IV (**Fig. 5**) suggesting that NFM and NFH at young ages label TCA. These findings suggested that NF staining may be appropriate to determine whether TCA segregate prior to reaching layer 4 during the development of the murine S1. It is currently unclear when TCA segregate into a whisker-related pattern in the cortex (see introduction **Fig. 3**, 1.3.3), and some groups have seen radial bands of TCA in layer V (Agmon et al., 1993), suggesting that TCA course through layer V in a predetermined pattern. To determine whether NFM and NFH reveal whisker-related pattern in deep cortical layers, serial tangential sections and coronal section from the remaining hemisphere were reacted for NFH (**Fig. 6A,B**) and NFM (**Fig. 6C,D**). A whisker-related pattern was seen in layer IV (250 µm from the pial surface, **solid line**) and layer V (350µm from the pial surface, **dotted line**) in tangential sections reacted for NFH (**Fig. 6A**) and NFM (**Fig. 6C**). Coronal sections from P2 animals were tripled labelled for NFM or NFH, Ctip2 (which labels cortical layer V) and TO-PRO3 (to label all cell nuclei) (**Fig. 7**). At P2 layer IV cells have not segregated into 'barrel' pattern (**Fig. 7 C,G**), however TCAs have invaded the cortex and projected through layer V (Agmon et al., 1993; Rebsam et al., 2002). At this age NFH (**Fig. 7A**) and NFM (**Fig. 7E**) label radial bands of neurites in layer V suggesting that TCA cluster together as they course through layer V (**Fig. 7A,E arrowheads**).

Figure 6. NFH and NFM label TCA in cortical layer V

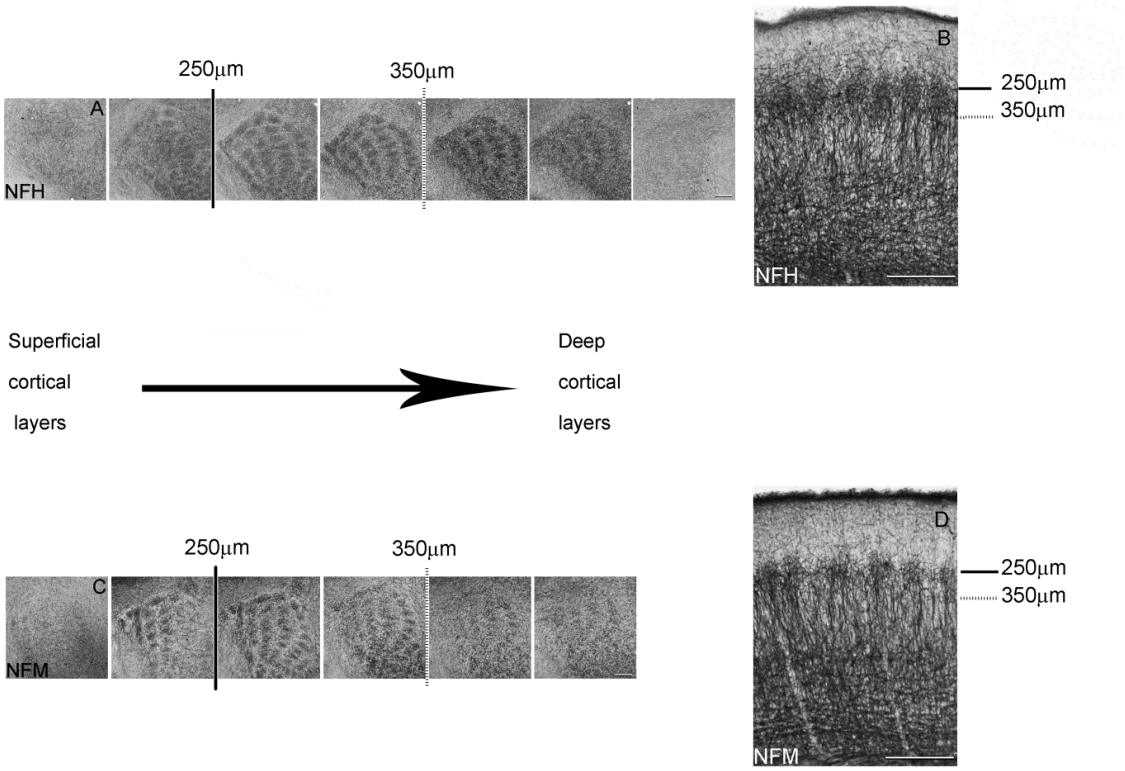

Figure 6. Sections reacted for NFM and NFH reveal a whisker-related pattern in layer V at P6. Serial tangential sections through the cortex (**A,C**) and the corresponding hemisphere sectioned coronal (**B,D**) reacted for NFH (**A,B**) and NFM (**C,D**). Solid line marking the top of layer IV approximately 250 μm from pial, dotted line layer IV/V boundary approximately 350 μm from the pial. The radial bundles of neurites seen in coronal sections reacted for NFH (**A**) and NFM (**C**) project in a barrel related pattern through layer V (**B,D**). Scale bar; 250μm.

Figure 7. NFH and NFM expression at P2

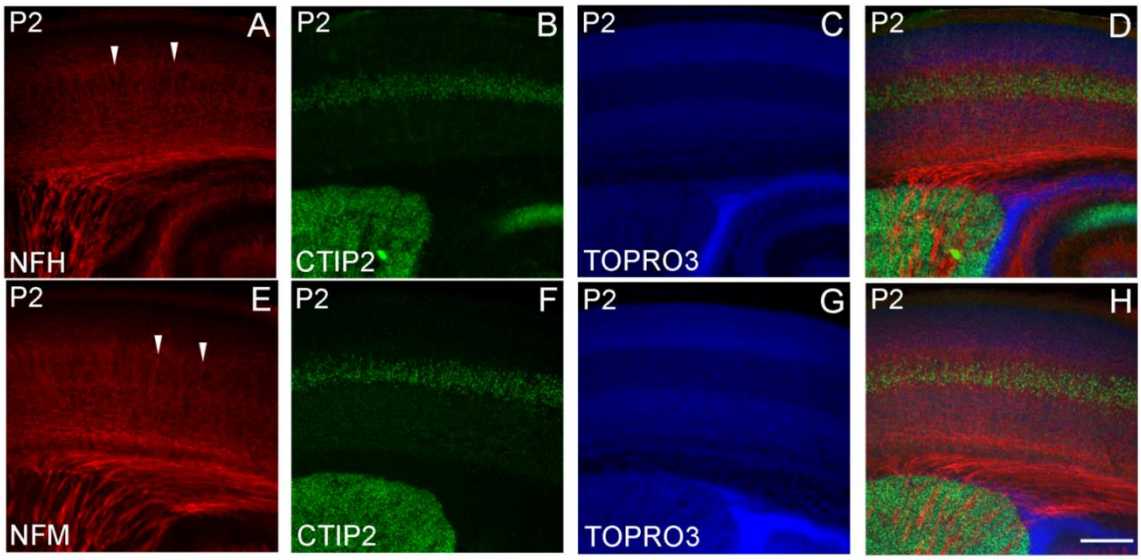

Figure 7. NFM and NFH label developing TCA in layer V revealing a radial pattern before barrels have formed. Coronal sections at P2 reacted for Ctip2, a layer V marker (**B,F**) and either NFH (**A**) or NFM (**E**). TO-PRO3, labelling cell nuclei demonstrates cells in layer IV have not segregated into whisker related 'barrel' at this age (**C,G**). Both NFH (**A**) and NFM (**E**) label bands of radial axons projecting through the cortex (**arrowheads**). Merged images demonstrate the patterning of NFH (**D**) and NFM (**H**) labelled axons in projections through layer V, as identified by Ctip2. Scale bar 250 µm.

3.2.6. Co-localisation between neurofilament subunits

To examine whether different NF subunits co-localise to the same axons, sections from a P6 animal were double labelled with NFH and either NFM (**Fig. 8A,D,C,F**) or NFL (**Fig. 8G,J,I,L**), NFM and NFL could not be examined for co-localisation as both primary antibodies were made in mouse. Sections reacted for NFM and NFH in the internal capsule demonstrated co-localisation between the subunits (**Fig. 8F, arrow**), however in the cortex some neurites were identified that expressed only NFH (**Fig. 8C, small arrowhead**) or NFM (**Fig. 8C, large arrowheads**). High power Nyquist-sampled images reveal some NFH-positive neurites lacking NFL (**Fig. 8L, arrowhead**), however double labelled neurites are also seen (**Fig. 8L, arrow**). In the centre of the TCA patch there were fewer NFL labelled processes (**Fig. 8G**) compared to other subunits (**Fig. 8A, B, H**), however both NFH positive axons lacking NFL (**Fig. 8I, arrowhead**) and double labelled neurites were identified (**Fig. 8I, arrow**).

Figure 8. High-magnification images reveal NF subunits do not always co-localise. Sections stained for NFH (**B,E,H,K**) and either NFM (**A,D**) or NFL (**G,J**) in the cortex (CTX; **A-C, G-I**) and the internal capsule (IC; **D-F, J-L**). High-power, Nyquist-sampled, deconvolved images reveal axons that contain both NFM and NFH in the cortex (**C, arrow**) and in the internal capsule (**F, arrow**), however in the cortex (**C**) axons can be seen which contain only NFH (**C, large arrowhead**) or NFM (**C, small arrowhead**). Some axons in the cortex contain both NFL and NFH (**I, arrow**), however NFH positive axons were seen in the absence of NFL in the cortex (**I, arrowhead**). In the internal capsule some axons contained both NFH and NFL co-localise (**L, arrow**), however NFH positive axons were identified that lack NFL (**arrowhead**). Scale bar; 5µm.

Figure 8. Co-localisation between Neurofilament subunits

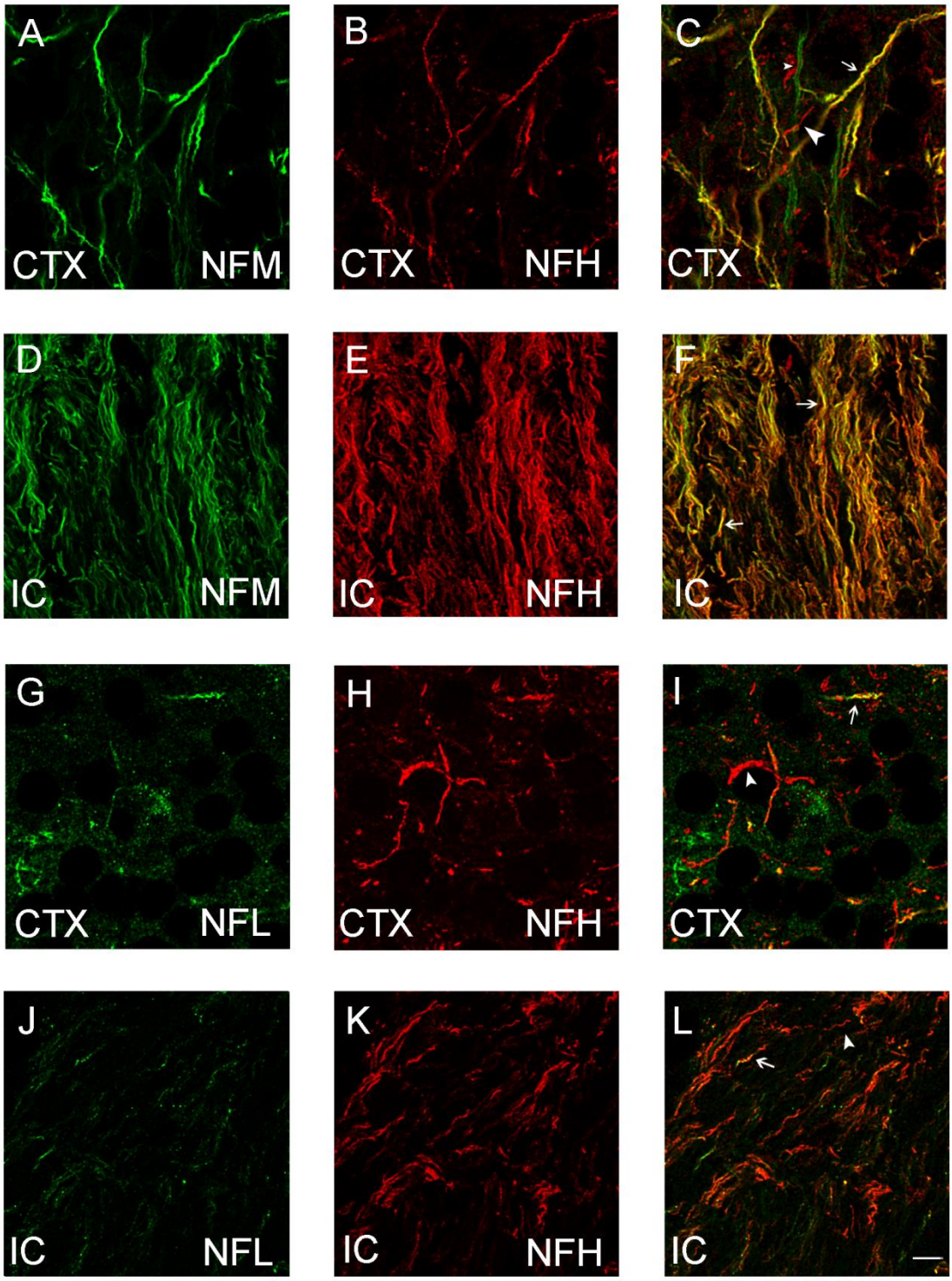

3.2.7. Neurofilament patterning is not dependent on sensory experience

Monocular deprivation in juvenile primates has been found to reduce expression of NFM and NFH in the ocular dominance columns corresponding to the deprived eye (Duffy & Livingstone, 2005). To determine if a lack of sensory experience affects neurofilament expression pattern in the rodent S1 daily whisker trims were performed on a litter of pups from P0 through to P8. The lack of sensory input did not affect layer IV patterning as all three subunits reveal mature expression in both the deprived (**Fig. 9A,C,E**) and control (**Fig. 9B,D,F)** hemispheres.

Figure 9. Trimming whiskers had no effect on NF expression pattern. Whiskers were trimmed from one side of the facepad every day from birth to P8 when mice were sacrificed. Tangential sections from both hemispheres were reacted for NFL (**A,B**), NFM (**C,D**) and NFH (**E,F**). Sections from the contralateral side (CL**; A,C,E**) to the trimmed facepad shows no difference in NF subunit expression compared to sections from the ipsilateral hemisphere (IL, **B,D,F**). Scale bar; 250µm.

Figure 9. Neurofilament patterning and sensory experience

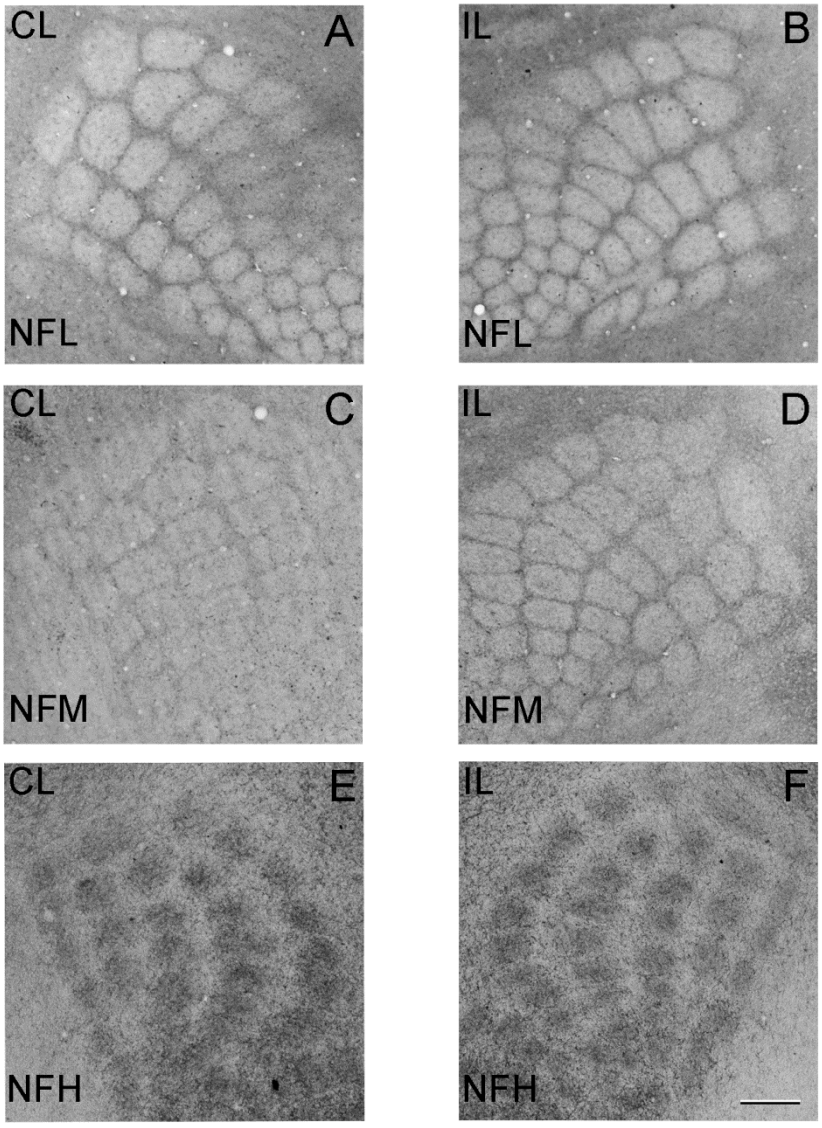

3.3. Discussion

In this chapter NF subunits were found to have differential expression patterns in the adult and developing murine S1. Further evidence of the differential expression was provided by high power confocal microscopy revealed that at P6 NF subunits do not always co-localise. NFH and at young ages NFM label TCAs and these can be seen coursing radially through layer V as early as P2. Finally unlike NF expression in the primate visual cortex, sensory deprivation paradigms during the first postnatal week did not affect the expression pattern of neurofilament subunits in the rodent S1.

3.3.1 Neurofilament subunits as TCA markers

The primary aim of this chapter was to identify a suitable immunohistochemical marker of TCA. TCA can be identified by anterograde labelling of VpM cells bodies using DiI, however the size and position of the TCA fibre tract in postnatal animals makes it difficult to ensure all axons are labelled. An immunohistochemical method for labelling TCA would have two advantages over lipophilic dyes firstly an antibody marker would ensure that all axons in a section are labelled and secondly DiI tract tracing is only possible in juvenile animals before myelination has occurred, in myelinated tissue DiI freely diffuses throughout the brain, therefore an antibody that labels TCA might also be suitable to be used at older ages. Previously other immunohistological techniques have been used to label TCA, for example SERT (Rebsam et al., 2002) or vesicular glutamate transporter (vGlut; Liguz-Lecznar & Skangiel-Kramska 2007), however these label the presynaptic active site on TCA producing a punctate pattern and therefore difficult to identify individual axons. NFM and NFH label continuous filaments which makes it possible using confocal microscopy to reconstruct the full axonal process. Furthermore NFH appears to label TCA in older ages, whereas other TCA markers such as SERT are only expressed in the first postnatal week,

although further characterisation of NFH in adult tissue is required in order for it to be used as a TCA marker, the ability to label full TCA in adults using immunohistochemistry would be beneficial. NFs are often used as axonal markers (Petzold 2005; Julien 1997; Lycke et al. 1998; Teunissen et al. 2005), and in this chapter two NF subunits at young ages were found to label TCA. Data from this chapter demonstrates that NFH and NFM label TCA at young ages however additional processes may also be labelled. Despite this caveat, the use of NF as TCA markers and would complement the precision of DiI techniques.

3.3.2. Expression pattern of NF subunits

In this chapter different expression patterns were observed with different NF subunits. In adult animals, NFM and NFL were expressed in regions void of thalamic input, whereas NFH labels mostly neurites in regions that receive thalamic input. The development of cortical maps relied on a number of different cell types, which, depending on their function and connectivity, will have different projections and morphology. Therefore neurons that share a common morphology and function in the murine S1 also share similar cytoskeletal composition. The patterning of NF in S1 reflects different structural demands of subpopulations of neurons, for example the structural demands of the apical dendrite on a layer V pyramidal cells would be different to the structural demands of a TCA. Furthermore NF subunits have previously been shown to delineate different function areas in the cortex (Paulussen, Jacobs, Van der Gucht, Hof, & Arckens, 2011) and restrict to different functional areas in other cortical maps (Duffy & Livingstone, 2003; Mellott et al., 2010).

NF subunits are subject to a significant amount of post translational modification (Yuan et al. 2012; Julien & Mushynski 1982) and phosphorylation of the C-terminal tail has been associated with subcellular localisation; with phosphorylated NF subunits are found in

axons (Nixon & Lewis 1986; Julien & Mushynski 1982) and non-phosphorylated NF mostly found in dendrites (Lee et al. 1987). In this chapter all antibodies recognise both the phosphorylated and non-phosphorylated form of NF subunits, however phosphorylation state may explain the expression patterns described in this chapter and elsewhere (Duffy & Livingstone, 2003, 2005).

In the primate visual cortex, phosphorylated NFH labels cell bodies and apical dendrites of layer V pyramidal cells in regions void of thalamic input (Duffy & Livingstone, 2003). Non phosphorylated NFH labels regions that receive thalamic input in the primate visual cortex and appears to label axons (Duffy & Livingstone, 2005). In this chapter using antibodies that identify both phosphorylated and non-phosphorylated forms of Neurofilament subunits, NFH labelled TCA throughout development (**Fig1. I, Fig. 3 C,F,I,L,O**) and in the adult also labelled cell bodies, however these are less distinct compared to other subunit (**Fig 1.**). It is possible that non-phosphorylated NFH labels TCA and is strongest in early development, whereas phosphorylated NFH labels cell bodies and appears at a later time point (around P14), this would be consistent with findings from the primate visual cortex (Duffy & Livingstone, 2005) and would fit the later developmental onset of phosphorylated NFH (Shaw & Weber 1982; Giasson & Mushynski 1997; Fiumelli et al. 2008; Carden et al. 1987; Dahl & Bignami 1986). However this hypothesis would need to be tested using antibodies specific to different phosphorylation states of NFH.

Examination of NF subunits through development reveals further differences between subunit expression. Sections reacted for NFH and NFM labelled TCA as early as P2, and a clear barrel related pattern was visible at P4 whereas no sections reacted for NFL revealed a pattern at P4 (n=5). Furthermore while the expression pattern of NFL and NFH were similar during early postnatal development, the pattern revealed by NFM changed,

initially labelling TCA then switching to a septal pattern. The phosphorylation state of NFM has been found to be developmentally regulated (Carden et al. 1987; Dahl 1988), and therefore the expression of different phospho-forms may account for the developmentally regulated change in NFM expression pattern. Different NF phosphoryation states are associated with localisation to either axons or dendrites (Dahl, Crosby, Gardner, & Bignami, 1986; V. M. Lee et al., 1987; Liu, Dyck, & Cynader, 1994) and some have suggested that neurofilament dephosphorylation stabilise the cytoskeleton and can be used as an indicator of axon maturity (Lavenex et al. 2004; Burman et al. 2007).

3.3.3. Experience and NF expression

In the visual cortex of primates, NF subunit expression is reduced by monocular deprivation (Duffy & Livingstone, 2005), therefore the effect of sensory deprivation was investigated on the expression pattern of NF subunits in the mouse S1. Whisker-trimming animals from birth did not alter the expression of neurofilament subunits in the mouse; this may be due to the difference in the deprivation paradigms or may reflect differences in the experience dependent development of the different sensory systems. Firstly the deprivation paradigms induced by removing whiskers may not be as efficient as monocular deprivation, this is because whiskers will grow back even with daily trimming and even very short whiskers will be deflected, this is likely to occur in the first postnatal week when pups will spend most of their time nested together in close proximity. Whisker plucking is a more effective method of somatosensory deprivation, but this requires daily injections of anaesthetic and dose titration is problematic in juvenile mice.

Secondly the visual and somatosensory cortices differ in the mechanism by which they develop. In the visual cortex monocular deprivation can remodel geniculocortical axons (Antonini & Stryker 1993) and reduce the area of cortex dedicated to processing

vision from that eye (Hubel et al. 1977; LeVay et al. 1980). Although trimming whiskers can decrease the selectivity of layer IV cells to respond to whisker stimulation (Fox, 1992) and reduce the branching of TCA (Wimmer, Broser, Kuner, & Bruno, 2010), it does not affect the anatomical organisation of S1 (Simons & Land, 1987; Wimmer, Broser, et al., 2010). Furthermore in the visual cortex tyrosine-related kinase B (TrkB) receptor ligands e.g. Brain derived neurotrophic factor (BDNF) and Neurotrophin-4 (NT4) are required for the segregation of eye specific ocular dominance columns (Cabelli, Hohn, & Shatz, 1995; Cabelli, Shelton, Segal, & Shatz, 1997), and monocular deprivation reduced BDNF immunoreactivity in the visual cortex (Rossi, Bozzi, Pizzorusso, & Maffei, 1999). In the rodent S1 BDNF or NT4 are not required for barrel formation (Itami, Mizuno, Kohno, & Nakamura, 2000) and genetic mutants lacking TrkB also form normal S1 patterning (Vitalis et al., 2002) demonstrating that sensory experience affects the development of the visual and somatosensory systems via different mechanisms.

3.3.4. NF subunits do not always co-localise

Given that NFL can form continuous filaments with either NFM or NFH (Geisler & Weber, 1981) it is possible that NFL would be expressed in all cells, however NFH positive neurites were found that lack NFL. NF have also been shown to form filaments with α-internexin (Yuan et al. 2006; Ching & Liem 1998) and vimentin (Lee et al. 1993). α-internexin and vimentin are expressed prior to NFs and may provide temporary support for developing filamentous networks (Giasson & Mushynski 1997; Kaplan et al. 1990; Nixon & Shea 1992). Further evidence against co-localisation of all three NF subunits comes from mutant mice lacking the NFL subunit. NFL null mutants are viable and do not demonstrate a gross phenotype; they have fewer myelinated axons and substantially reduced levels of NFM and NFH but intermediate filaments structures were seen in neonatal animals (Zhu,

Couillard-Després, & Julien, 1997), demonstrating that NFL is not necessary for intermediate filament formation.

In this chapter NF subunits were found to differ in their labelling of TCA; in young animals NFM and NFH positive neurites contained SERT positive punta, a marker for the lemniscal TCA tract originating in the VpM of the thalamus. NFL labelling was restricted to the septal region in S1 and was reduced in the internal capsule; this is consistent with the paralemniscal pathway from the POM in the thalamus to the layer IV/V boundary and barrel septal in S1. It seems unlikely that NFL labels the paralemniscal fibre tract because high-power images of NFL in the cortex suggests that the septal pattern of expression is the result of dendrites and perikarya instead of axons (**Fig 1.D, Fig2. A',D',G'**). However it would be possible to test the hypothesis that NFL labels the paralemniscal path from the thalamus using viral infection with fluorescent proteins to label each fibre tract and investigate co-localisation with NFL (Wimmer, Bruno, De Kock, Kuner, & Sakmann, 2010).

3.3.5. Development of TCA

The segregation of TCA is the first whisker-related pattern observed in the developing S1 (Erzurumlu & Gaspar 2012) and mutant analysis has demonstrated that TCA segregation is required for barrel formation (Erzurumlu & P. C. Kind 2001), therefore TCA play an instrumental role in S1 cortical map formation. Using DiI labelling of TCA, Agmon et al. 1993 suggested that TCAs have already segregated as they course through cortical layer V. However, using SERT staining of axon terminals that TCA did not form radial bands in layer V and reconstructions of DiI-labelled axons revealed that some TCA do not course directly through layer V in a radial direction (Rebsam et al., 2002). A distinction between these two mechanisms would determine to what extent cortical patterning is prescribed from the input it receives. In this chapter, radial bundles of TCA were seen in layer V at P6

and these were organised in a whisker-related pattern (**Fig. 6**), this is contrary to the findings of Rebsam et al. 2002 that identified DiI labelled TCA traversing multiple barrel areas in layer IV. However recently TCA labelled using viruses have demonstrated whisker related patterns are visible in deep cortical layers (Wimmer, Bruno, et al., 2010). It is possible that while some TCA transverse the width of multiple barrel layer V the results presented in this chapter and those of Wimmer et al. 2010 demonstrate that the majority of axons project radially through layer V within the width of a single barrel. Furthermore at P2 distinct radial bands of NFM and NFH positive neurites were seen in layer V (**Fig. 7**). This finding would appear to support the model proposed by Agmon et al. 1993, however the bands of radial axons seen at P2 many not be organised in a topographical pattern, and flattened tangential sections at P2 would be required to determine if they are organised into a whisker-related pattern. The organisation of TCA is thought to be governed by gradients of Ephs and Ephrin which are expressed in the cortex until P3 (Dufour et al. 2003; Triplett & Feldheim 2012, see introduction 1.3.3), however mutants lacking EphrinA only have slight distortions in TCA patch size (Vanderhaeghen et al. 2000) and there are likely to be other mechanisms involved. By determining the precise timing of TCA patterning in the early stages of cortical development, further insight into the development of sensory maps.

3.3.6. NF as axonal markers

NFs are often used as markers for neuropathy and axon degeneration (Petzold 2005; Julien 1999; Lycke et al. 1998; Teunissen et al. 2005). This chapter demonstrates that NF subunits do not specifically label axons, and that all three subunits are not always expressed in the same cell. NFM has frequently been used as an axonal marker (Fernyhough et al., 1999; Kennedy, Wang, Marshall, & Tessier-Lavigne, 2006; Petzold, 2005), however this chapter has shown that the expression of NFM is dynamic through

development and at some ages does not label axons in the S1. Furthermore NFH positive axons were identified that lacked NFM, demonstrating that NFM is does not label all axons in the developing murine S1. If neurofilaments are to be used as axonal markers and indicators for neuronal degeneration the expression of each neurofilament subunits through development should be first investigated.

Chapter 4

The role of SAP102 in the developing mouse S1

4.1. Introduction

SAP102 is a member of the membrane associated guanylate kinases (MAGUK), these proteins act as scaffolding molecules linking NMDA receptors to enzymes, signalling molecules and cytoskeletal proteins within the post synaptic density (PSD). There are over 1000 proteins within the PSD (Collins et al. 2006) and by organising some of these synaptic proteins MAGUKs create signalling microdomains which can mediate a neuron's response to synaptic activity (Kim & Sheng 2004). SAP102 is a typical Disc large (DLG) MAGUK with three PDZ (**P**ost synaptic density 95, **D**rosophila disc large tumor suppressor, **Z**onula occludens-1) domains, a Src Homology 3 (SH3) domain and a guanylate kinase (GK) domain (see **Fig. 6** in the introduction), it is through these binding domains that SAP102 can form multiple protein-protein interactions. SAP102 is unique among MAGUK as it contains two alternatively spliced regions that are not shared by other *DLG* MAGUKs (Müller et al., 1996).

Mutations in a number of many synaptic proteins are associated with intellectual disability in humans (Grant 2012; Valnegri et al. 2012). SAP102 is encoded by a gene on the X-chromosome, in humans this gene is called *DLG3* and mutations in the *DLG3* gene have been found in 5 families with a history of X-linked mental retardation (Tarpey et al., 2004; Zanni et al., 2010), suggesting that the loss of functional SAP102 in humans results in intellectual impairment.

Sap102 null mutant mice (*Sap102*$^{-/y}$) are slow to gain weight during development and the adults show deficits on spatial learning tasks and take longer to learn the location of a submerged platform on a watermaze (Cuthbert et al. 2007). Furthermore *Sap102*$^{-/y}$ display enhanced hippocampal long term potentiation (LTP; Cuthbert et al., 2007). *Sap102*$^{-/y}$ have a significant increase in phosphor-ERK, and the application of a mitogen-activated protein kinase (MEK) inhibitor prevents the enhanced LTP phenotype (Cuthbert et al.,

2007) implying that the increased LTP is the result of altered Extracellular signal regulated kinase/ mitogen-activated protein kinase (ERK/MAPK) signalling. These findings demonstrate that the loss of SAP102 significantly affects synaptic activity as well as learning and memory tasks in adult animals. However, SAP102 is expressed during early development (Sans et al. 2000; Sans et al. 2003; Barnett et al. 2006) and while many mechanisms of brain development are dependent on synaptic activity, very little is known about the role played by SAP102 during development or how the brain develops in the absence of SAP102.

4.1.1. SAP102 expression

In the developing mouse S1, SAP102 expression is mostly expressed in the supragranular layers and in layer IV, where SAP102 protein expression corresponds to a TCA patch pattern (Wijetunge et al. 2008). SAP102 is expressed from birth and increases postnatally reaching peak expression at the end of the first postnatal week as measured in both whole brain (Sans et al. 2000) and S1 homogenates (Barnett et al. 2006; Wijetunge et al. 2008). Whilst the majority of SAP102 is found at asymmetric synapses, it is not restricted to the PSD, SAP102 is also found in the soma, dendritic shaft and in dendritic spines (El-Husseini et al. 2000; Sans et al. 2000; Zheng et al. 2010). Immuno-labelled electron microscopy sections has revealed that SAP102 is also expressed in some axons and presynaptic terminals (El-Husseini et al., 2000). SAP102 is the main MAGUK expressed during3 the formation of S1 patterning and is one of the first proteins present in synapses during early development (Petralia et al. 2005). This makes SAP102 well-placed to play a role in synaptogenesis and activity-dependent cortical development.

4.1.2. SAP102 binding partners

Given the multiple binding domains that characterise MAGUKs, it is not surprising that SAP102 interact with a variety proteins, **Figure 1** summarises the key binding partners at the synapse. Importantly for synapse maturation (see 1.5.0 in the introduction), SAP102 is found in a complex with GluN subunits (Sans et al. 2000; Collins et al. 2006). The C-terminus of GluN2B receptors bind directly to both the PDZ domains (Müller et al. 1996; Lau et al. 1996) and to an alternative splice region in the N-terminus of SAP102 (Chen et al. 2011). Whilst SAP102 will also bind other NMDA receptor subunits, protein complex immunoprecipitation (Co-IP) experiments show a preference for GluN2B subunits over GluN2A (Sans et al. 2000). Developmental expression of the GluN2B subunit correlates with SAP102 expression providing more evidence for a preferential interaction between GluN2B and SAP102 (Sans et al. 2003; Barnett et al. 2006).

SAP102 also binds directly to SynGAP, a synaptic GTPase activating protein (Kim et al. 1998). SynGAP regulates small GTPases such as Rap, Ras and Rab (Kim et al. 1998; Krapivinsky et al. 2004; Tomoda 2004), which can mediate the trafficking of AMPA receptors at the synapse (Zhu et al. 2002). Small G proteins are also involved in the ERK/MAPK pathway which regulates a number of developmental mechanisms including axonal growth, synaptic plasticity, synaptogenesis, cytoskeletal reorganisation, local translation and spatial learning (Adams & Sweatt, 2002; Boda, Dubos, & Muller, 2010; Bozon et al., 2003; Di Cristo et al., 2001; Gu & Stornetta, 2007; Ho, Uniyal, Meakin, Morris, & Chan, 2001; Tomoda, 2004).

Figure 1. The main synaptic binding partners of SAP102

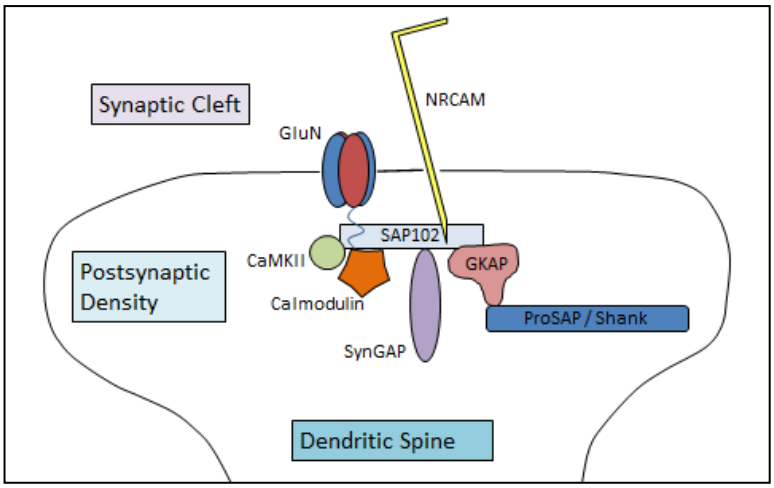

Figure 1. Schematic of a dendritic spine containing some of the main binding partners of SAP102

4.1.2. Mutants lacking SAP102 binding partners display trigeminal system defects

The development of the rodent S1 requires precise connectivity between a variety of brain regions to form a complete and accurate neuronal circuit. The patterning of the rodent S1 develops over the first postnatal week and is reliant on activity as well as a number of pre and post-synaptic proteins (see 1.3.6 introduction for review). Therefore the patterning of S1 can serve as a model of neural connectivity. Patterning of S1 is affected in a number of mutants lacking SAP102 binding partners. In mutants lacking cortex specific GluN1 subunit (the obligatory NMDA receptor subunit) TCA bundles are smaller (Datwani et al. 2002; Iwasato et al. 2000), individual TCA show exuberant axonal growth (Lee, Iwasato, Itohara, & Erzurumlu, 2005), layer IV cell do not segregate into barrels and their dendrites failing to orientate towards TCA patches (Datwani et al. 2002). Furthermore blocking NMDA receptors during the first postnatal week increases the receptive field of TCA (Fox, Schlaggar, Glazewski, & O'Leary, 1996), demonstrating that NMDA receptors are not only

responsible for S1 patterning but are key to set up the functional aspects of cortical maps. Changing the subunit composition of NMDA receptors can also affect cortical map formation. Mutants lacking the GluN2B subunit die perinatally which prevents investigation of the barrel pattern in the cortex, although they survive long enough to investigate the trigeminal patterning in the brainstem known as barrelettes. Mutants lacking the GluN2B subunit fail to form barrelettes, whereas age-match littermate display a clear barrelette pattern demonstrating that GluN2B also plays a role in the patterning of the trigeminal system. Mutants lacking SynGAP also fail to form a layer IV barrel pattern and show reduced TCA segregation (Barnett et al., 2006).

4.1.3. The role of SAP102 in synaptogenesis and synapse maturation

Synapse formation in the mouse somatosensory cortex begins perinatally, but the majority of synapses form in the second postnatal week (De Felipe, Marco, Fairén, & Jones, 1997). At P2, immune-labelled electron microscopy reveals SAP102 is located at synapses with visible PSD, in comparison other MAGUKs such as PSD93 and PSD95 are only expressed at low levels at this time point (Sans et al. 2000). The presence of SAP102 as the main MAGUK at mature synapses at such an early stage of development suggests that SAP102 plays a role in synaptogenesis. One function of SAP102 during synaptogenesis involves the trafficking of NMDA receptors SAP102 is thought to localise NMDA receptors to the synapse through its binding to Sec8, a component of the exocyst complex which transports intracellular vesicles to the membrane and live imaging of immature neurons in culture has revealed SAP102 transporting GluN1 subunits (Sans et al. 2003; Hsu et al. 1999). A dominant negative form of Sec8 which disrupts binding to SAP102 PDZ domains reduces both surface expression and miniature EPSC amplitude of NMDA receptors, therefore the

exocyst complex and Sec8 provides a mechanism for SAP102 mediated NMDA receptor trafficking (Sans et al. 2003).

In the first few postnatal weeks thalamocortical synapses in S1 undergo a series of developmental events that lead to their maturation (reviewed in Wu et al. 2011, see introduction 1.4.4). These developmental events include the unsilencing of synapses by the insertion of AMPA receptors (Isaac, 2003) and the change in NMDA receptor composition, SAP102 is thought to play a role in both of these events. SAP102 is hypothesised to aid AMPA receptor trafficking by localising SynGAP to the cell membrane, SynGAP can mediate both the insertion and removal of AMPA receptors at the surface membrane via its regulation of small G proteins (Zhu et al. 2002; Komiyama et al. 2002). In early development most NMDA receptors contain the subunit GluN2B, and during the second wave of synaptogenesis at P14 most GluN2B subunits are replaced with GluN2A (Sans et al. 2000, see introduction 1.4.4). The switch in NMDA receptor composition is mirrored by changes in MAGUK expression with Sap102 mRNA expression decreasing after the first two postnatal weeks and PSD95 increasing (Fukaya et al. 1999; Petralia et al. 2005; Porter et al. 2005), suggesting a landmark in synapse development is reached at this point. Acute knockdown of SAP102 has little effect on mature neurons in culture, but after 8 days in vitro the temporary removal of SAP102 reduces both AMPA and NMDA receptor EPSC (Elias et al. 2006; Elias et al. 2008), providing further evidence that SAP102 plays a prominent role in early synapse development.

As the main MAGUK expressed during synaptogenesis and with its potential to traffic NMDA receptors via its binding to Sec8 and the exocyst complex SAP102 is well placed to play a role in synaptogenesis. SAP102 may also play a key role in synaptic

maturation through by localising SynGAP to the synapse and trafficking of NMDA receptor subunits.

4.1.4. The role of SAP102 in forming mature dendritic spines

The formation of dendritic spines is a key component of synaptic maturity and alterations to dendritic spine density are associated with a number of different forms of intellectual impairment in humans (Fiala, Spacek, & Harris, 2002). SAP102 has been shown to affect dendritic spine morphology *in vitro* as overexpressing the full length SAP102 protein significantly increased the length of dendritic spines in a NMDA receptor dependent manner, yet overexpression of a *Sap102* splice variant lacking the N-terminus insert had no effect on spine length (Chen et al. 2011). The role of NMDA mediated activity in regulating dendritic spine morphology has been well documented (Ultanir et al. 2007; Chen et al. 2011; Harms & Dunaevsky 2007; Yuste & Bonhoeffer 2001), and cortex specific removal of functional NMDA receptors increases the density and head size of dendritic spines (Datwani et al. 2002; Ultanir et al. 2007). While the deletion of NMDA receptors increases the density of dendritic spines (Datwani et al. 2002), GluN2B subunit knockout shows a cell autonomous reduction in the density of dendritic spines (Espinosa, Wheeler, Tsien, & Luo, 2009). These findings implicate a role for NMDA receptors and SAP102 in dendritic spine formation and development with different NMDA receptor subunits and *Sap102* splice variants having differential effects on dendritic spine density.

A number of SAP102 binding partners have also been implicated in affecting dendritic spines. Neuronal cultures from embryos lacking SynGAP show an increase in mature spine morphology (Vazquez, Chen, Sokolova, Knuesel, & Kennedy, 2004) and

phosphorylated forms of CamKII can increase both dendritic spine density and volume (Pi et al., 2010). Other SAP102 binding partners have been shown to affect cytoskeletal organisation providing a mechanism by which dendritic spines could form or change morphology. Neuronal cell adhesion molecule (NR-CAM) acts as a cell adhesion molecule which can influence the cytoskeleton during synaptogenesis and directly binds to SAP102 (Backer, Sakurai, Grumet, Sotelo, & Bloch-Gallego, 2002; Davey, Hill, Falk, Sans, & Gunn-Moore, 2005). SAP102 also binds to GKAP 130 (Kim et al. 1997; van Zundert et al. 2004) which in turn binds to ProSAP/Shank; a known mediator of cytoskeletal re-organisation (Boeckers et al. 2002; Boeckers et al. 1999). Whilst there is a number of potential mechanisms by which SAP102 may affect dendritic spine density and morphology, the loss of SAP102 on dendritic spines has not been investigated *ex vivo*.

4.1.5. Summary

SAP102 is a synaptic scaffolding protein that links NMDA receptors to downstream signalling molecules within the PSD. Mutations in the gene that encodes SAP102 are associated with mental retardation in humans (Tarpey et al., 2004) and mutant mice lacking SAP102 have defects on learning tasks and have altered synaptic plasticity (Cuthbert et al. 2007). SAP102 binds to a number of post-synaptic proteins many of which play a role in dendritic spine morphology, synaptogenesis, and patterning of the trigeminal system. SAP102 is thought to play an important role in synapse maturation by trafficking NMDA receptors via Sec8 (Sans et al. 2003; Sans et al. 2005), forming complexes with GluN2 subunits, and the trafficking of AMPA receptors via its association with SynGAP (Zhu et al. 2002; Komiyama et al. 2002). Based on its expression profile and binding partners, SAP102 has the means and the opportunity to mediate a number of NMDA receptor-dependant developmental mechanisms. However, little is known about the anatomical defects caused

by the loss of SAP102. Mutants lacking SAP102 are slow to gain weight compared to wild type littermates, but gross neuroanatomy in the adult is normal (Cuthbert 2005). This chapter aims to characterise the role of SAP102 in the developing S1 using mice containing a *Sap102* null mutation. A full characterisation of the developing S1 in *Sap102* mutants will provide a model to investigate a specific form of intellectual impairment, and provide insight into NMDA receptor meditated mechanisms of postnatal development.

4.1.6. Rationale and Hypotheses

Rationale 1

Sap102$^{-/y}$ mutants maintained on a MF1 background are slow to gain weight compared to their wild type littermates yet, gross brain structures are normal in adult mutants (Cuthbert et al. 2007; Cuthbert 2005). Given the developmental delay in body mass observed by Cuthbert 2005, a more detailed examination of cortical neuroanatomy was undertaken during the first three postnatal weeks. Furthermore because the available mice were on a different background strain, body mass was also investigated to confirm the findings of Cuthbert 2005.

Hypothesis 1 *Sap102*$^{-/y}$ mutants on a C57/Bl6J/Ola background are slow to gain weight during development, have a reduced brain mass and cortical thickness.

Rationale 2

Mutants lacking the binding partners of SAP102 have defects in S1 patterning. Both SynGAP and cortex specific GluN1 mutants have defects in TCA patterning and barrel

formation (Barnett et al. 2006; Iwasato et al. 2000; Datwani 2002; Lee et al. 2005). Furthermore mutants lacking the GluN2B subunit fail to form the whisker related patterns in the brainstem (Kutsuwada et al., 1996). Given the number of SAP102 binding partners required for normal S1 patterning it is likely that the anatomical patterning of S1 is affected in *Sap102*$^{-/y}$.

Hypothesis 2 *Dlg3*$^{-/y}$ mutants have deficits in barrel formation, and the area of somatosensory regions of the neocortex will be affected by the loss of SAP102.

Rationale 3

Overexpression of *Sap102* splice variants *in vitro* has been shown to affect dendritic spine morphology (Chen et al. 2011). Furthermore mutants lacking the binding partners of SAP102 such as SynGAP and NMDA receptors have alterations in the density of in dendritic spines (Vazquez et al. 2004; Espinosa et al. 2009; Datwani et al. 2002). Therefore the density of dendritic spines was investigated in mutants lacking *Sap102*.

Hypothesis 3 the loss of SAP102 will affect the density of dendritic spines.

4.2. Results

4.2.1. *Sap102* $^{-/y}$ have reduced brain mass throughout development

Adult *Sap102*$^{-/y}$ animals have a normal body mass, although throughout development *Sap102*$^{-/y}$ are underweight compared to *Sap102*$^{+/y}$ littermates (Cuthbert 2005). To determine if this delay in body mass was still present on a C57Bl6J/ola background strain, body mass was measured at 3 developmental time points from 3 independent groups of animals (**Fig. 2A**). Genotype has a significant effect on body mass [$F_{(2,96)}$ =13.37, p>0.0005, see **Fig. 2A** for n], and no interaction was observed between genotype and age [$F_{(2,96)}$=2.56, p=0.082, see **Fig. 2A** for n], demonstrating body mass is reduced throughout the first 3 postnatal weeks.

To determine if the reduction in body mass correlated with a neuroanatomical defect, brains from these animals were removed from the skull, post-fixed overnight in 4% PFA/PB, patted dry and weighed (**Fig. 2B**). Genotype had a significant effect on brain mass [$F_{(2,102)}$ =14.77, p>0.0005, see **Fig. 2B** for n]. No interaction between genotype and age was observed [$F_{(2,102)}$ =0.12, p=0.88, see **Fig. 2B** for n] suggesting that the brain mass of *Sap102*$^{-/y}$ animals was reduced throughout development.

Figure 2. Brain and body mass of *SAP102*$^{-/y}$ and *SAP102*$^{+/y}$ animals maintained on a C57/bl6JOla background throughout development. The body mass (**A**) and brain mass (**B**) were taken at P7, P14 and P21 from three independent groups of animals. Genotype does have a significant effect on body mass and the lack of an interaction between age and genotype demonstrates that this is present throughout development (**A**). *SAP102*$^{-/y}$ also have a lower brain mass at all ages investigated (**B**). For both brain and body mass the number of replicates (animals) are given in the adjacent tables. Each circle represents a single animal and the error bars represent the standard error of the mean.

Figure 2.Body and brain mass of *Sap102*$^{-/y}$ and littermate controls

A

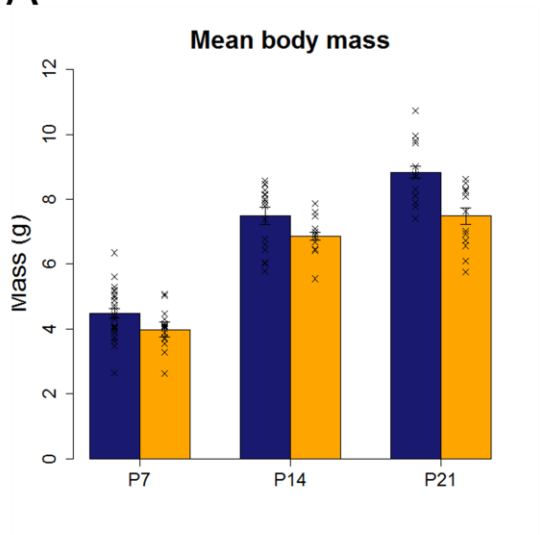

Age	Number of animals taken for body mass measurements	
	SAP102 $^{+/y}$	*SAP102* $^{-/y}$
P7	29	21
P14	18	12
P21	14	14

B

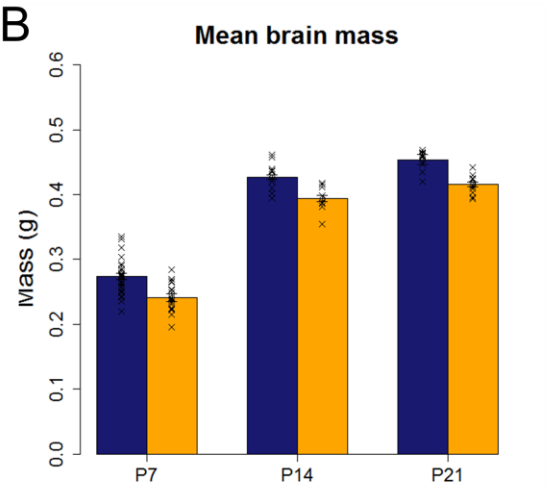

Age	Number of animals taken for brain mass measurements	
	SAP102 $^{+/y}$	*SAP102* $^{-/y}$
P7	31	18
P14	12	12
P21	13	14

4.2.2. Cortical lamination is unchanged in *Sap102*$^{-/y}$

Reduced brain mass in *SAP102* mutants might be caused by a defect in cortical lamination. To test this hypothesis coronal sections from *Sap102*$^{+/y}$ (**Fig. 3A,B**), and *Sap102*$^{-/y}$ (**Fig. 3C,D**) at P14 (**Fig. 3A,C**) and P21 (**Fig. 3B,D**) were reacted for calretinin, a calcium marker that delineates the boundary between layers IV and V. The mouse S1 occupies approximately 1mm^2 of the cortical sheet, therefore three different sections equidistant along the anterior-posterior axis were measured for cortical thickness (see methods 2.3.3.i), for each section mean measurements of the total cortical thickness (**Fig. 3E,F**), layer I-IV (**Fig. 3G,H**), or layer V-VI (**Fig. 3I,J**) were taken. These measurements of individual layers shown no clear difference between genotypes either at P14 (**Fig. 3E,G,I**) or P21 (**Fig. 3F,H,J**). In order to calculate inferential statistics on these data, cortical thickness for each section was normalised to the mean *Sap102*$^{+/y}$ measurement for that age and the mean for each genotype compared. Although animals lacking SAP102 have a reduction in brain mass throughout development, laminar measurements of the cortex taken at P14 and P21 demonstrate no significant differences between genotypes at either P14 [n_{wt}= 5,n_{ko}=5, t=1.40, df=15.19, *two-tailed p*=0.22] or P21 [n_{wt}=9 ,n_{ko}=8, t=0.27, df=13.53, *two-tailed p*=0.79].

Figure 3. Cortical thickness at P14 and P21 is unaffected by the loss of SAP102. Coronal sections from *SAP102*$^{+/y}$ (**A,B**) and *SAP102*$^{-/y}$ (**C,D**) at P14 (**A,C**) and P21 (**B,D**) reacted for calretinin were measured for cortical thickness. Three sections equidistant along the rostral-caudal plane containing S1 were selected from each animal (representative images in **A-D** show only the middle section, see methods 2.3.3.iii) in each section the thickness of layers I-IV, layers V/VI and cortex were measured (**A**). Mean measurements for each section from P14 (**E,G,I**) and P21 (**F,H,J**) shows cortical thickness (**E,F**), layer I-IV thickness (**G,H**) and layer V/VI thickness (**I,J**). To make statistical inference on these data, cortical thickness from each animal was normalised to the mean measurement for the corresponding section in *SAP102*$^{+/y}$ animals (**K**), genotype had no effect on cortical thickness. Each cross represents an individual animal and the error bars display the standard error of the mean. Scale bar = 250 μm.

Figure 3. Cortical lamination in *Sap102*$^{-/y}$ and littermate controls

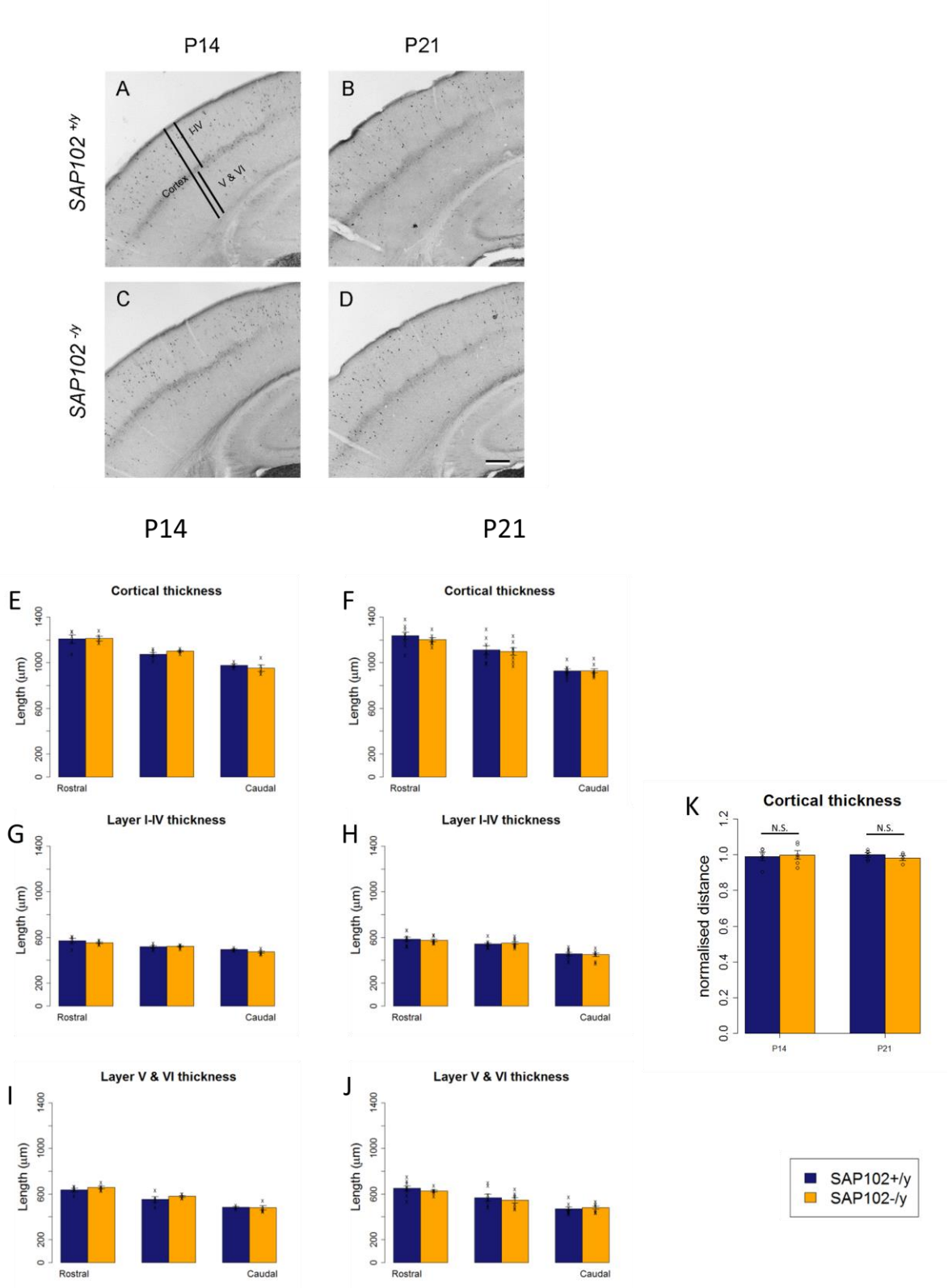

4.2.3. S1 patterning is unchanged in *Sap102*$^{-/y}$ but cortical area is reduced

Cortical lamination is unchanged in *Sap102*$^{-/y}$, therefore reduced brain mass in *Sap102*$^{-/y}$ might be the result of reduced cortical area. In order to test this hypothesis the location and size of primary sensory regions was measured in *Sap102*$^{-/y}$ by staining neocortical flattened sections with the presynaptic marker serotonin reuptake transporter (SERT). SERT labels axonal input from the thalamus and can be used to measure the position of S1 (**Fig. 4**) and the size of primary sensory areas (**Fig. 5**). Positioning of S1 was determined by taking the ratio between the rostral tip to barrel C2 distance (**R**) to the total length (**T**) [n_{wt}=15, n_{ko}= 13, t= 0.45, *two-tailed p*=0.65] (**Fig. 4D**) or the caudal tip to barrel C2 distance (**C**) to the total length (**T**) [n_{wt}= 15, n_{ko}=13, t =-1.25, *two-tailed p*=0.22] (**Fig. 4E**). The lack of a significant difference on both these measurements demonstrating that the position of the posterior medial barrel subfield (PMBSF) is unchanged, but brains from SAP102$^{-/y}$ animals are shorter along the total rostral-caudal axis [n_{wt}= 15,n_{ko}=13, t=2.38, df=21.25, *one-tailed p*=0.027] (**Fig. 4C**), consistent with the reduction in brain mass.

Area measurements were then made on the same SERT-labelled neocortical flattened sections (**Fig. 5**). The area of neocortex was significantly reduced in SAP102$^{-/y}$ animals [N_{wt}=16, N_{ko}=13, t=3.40, df= 26.88, *two-tailed p*=0.0021] (**Fig. 5E**) as was the area occupied by PMBSF [N_{wt}=16, N_{ko}=12, t=2.65, df=26.00, *two-tailed p*=0.014] (**Fig. 5F**). The total area occupied by barrels B1-3 and C1-3 was also significantly smaller in *Sap102*$^{-/y}$ animals [N_{wt}=16, N_{ko}=12, t=3.80, df =21.87, *two-tailed p*<0.001] (**Fig. 5G**). These results are consistent with the reduction in brain mass, although it is not known if the same proportions between these cortical areas are maintained between genotypes. To test this hypothesis the size of these cortical areas were normalised to each other. The ratio between the size of neocortex and PMBSF was not significantly different between

genotypes [N_{wt}=16, N_{ko}=10, t=1.53, df=24.00, t*wo-tailed p*=0.26, **Fig. 4H**], however the ratio between TCA and PMBSF area was significantly reduced in *Sap102*$^{-/y}$ (N_{wt}=16, N_{ko}=12, t=2.14, df=24.61, *two-tailed p*=0.042, **Fig. 4I**]. These ratios demonstrate that whilst the area of PMBSF is proportional to neocortical area in *Sap102*$^{-/y}$, the area of TCA patches are significantly reduced even when normalised to the size of the PMBSF, indicating a specific deficit in TCA patch size, which cannot be explained by a global reduction in brain size.

Figure 4. Positioning of S1 is unaffected by the loss of SAP102. Flatten neocortical section reacted for SERT from *SAP102*$^{+/y}$ (**A**) and *SAP102*$^{-/y}$ (**B**) were measured along three planes; the total rostral-caudal distance (**T**), from the rostral tip to barrel C2 (**R**) and from caudal tip to barrel (**C**). Whilst there is a significant reduction in the total rostral-caudal distance in *SAP102*$^{-/y}$ animals (**C**), there is no difference in the positioning of the PMBSF as defined by the normalised rostral position (**D**) or the normalised caudal position (**E**). Each cross represents an individual animal and the error bars display the standard error of the mean. Scale bar = 250 µm.

Figure 4. Positioning S1 in *Sap102*$^{-/y}$ and littermate controls

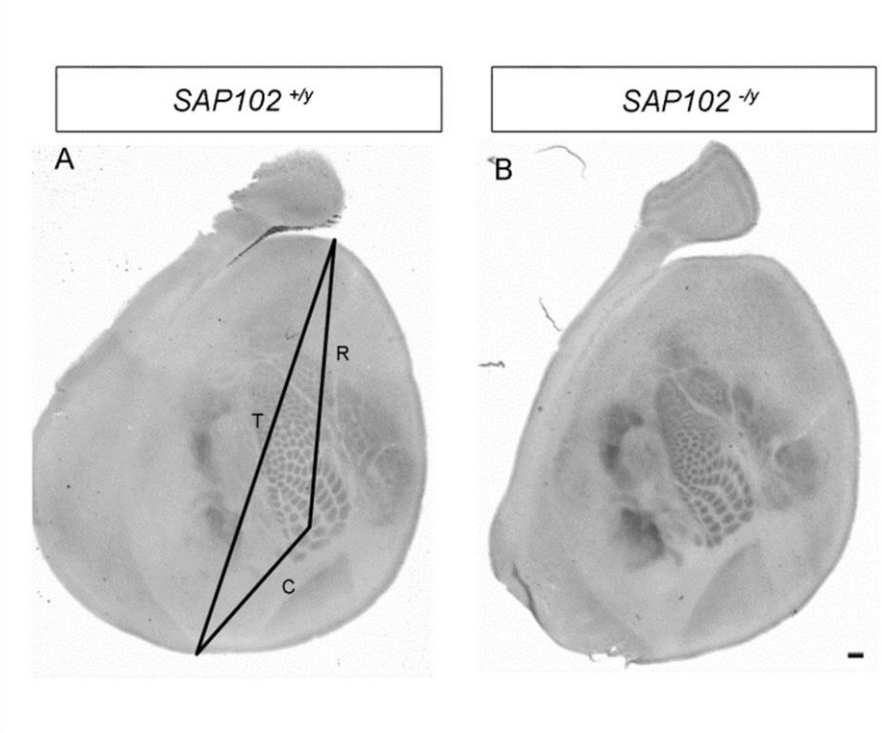

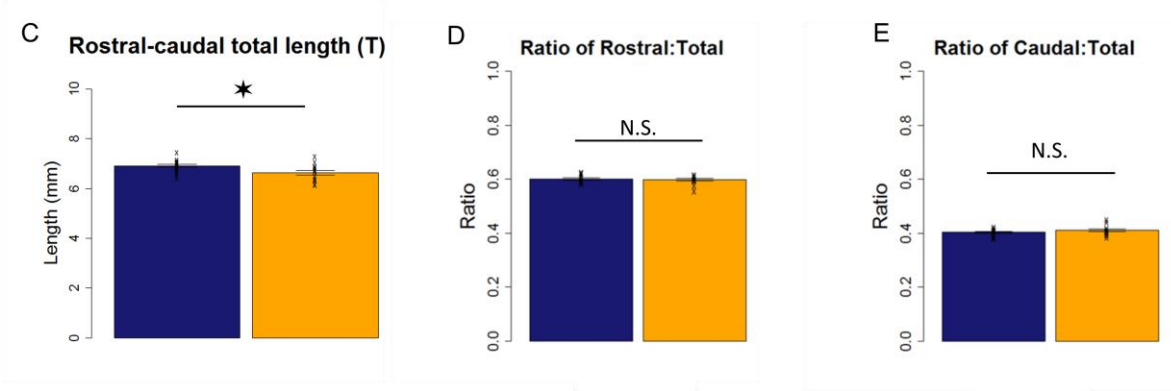

Figure 5. TCA patch size is reduced in *SAP102*$^{-/y}$ even when normalised to the area of PMBSF. Representative images from *SAP102*$^{+/y}$ (**A,C**) and *SAP102*$^{-/y}$ (**B,C**) reacted for SERT reveal sensory areas that receive thalamic input (labelling in **Fig 5A.** V; visual cortex, A; auditory cortex, LL; lower lip, FL; front limb, HL, hind limb, T; tongue, AS; anterior snout). Area measurements were taken of the neocortex , PMBSF (**A**) and the sum total of 6 barrels (barrels B1;B2;B3;C1;C2;C3, labelled in **C**). In *SAP102*$^{-/y}$ there was a significant reduction in area of neocortical sheet (**E**), PMBSF (**F**), and TCA patch (**G**). The area of PMBSF and neocortex are reduced proportionally in SAP102$^{-/y}$ (**H**), however TCA patch size is significantly reduced when normalised to PMBSF (**I**). Each cross represents an individual animal and the error bars represent the standard error of the mean. Scale bar 250 µm.

Figure 5. Area of cortical regions in SAP102$^{-/y}$ and littermate controls

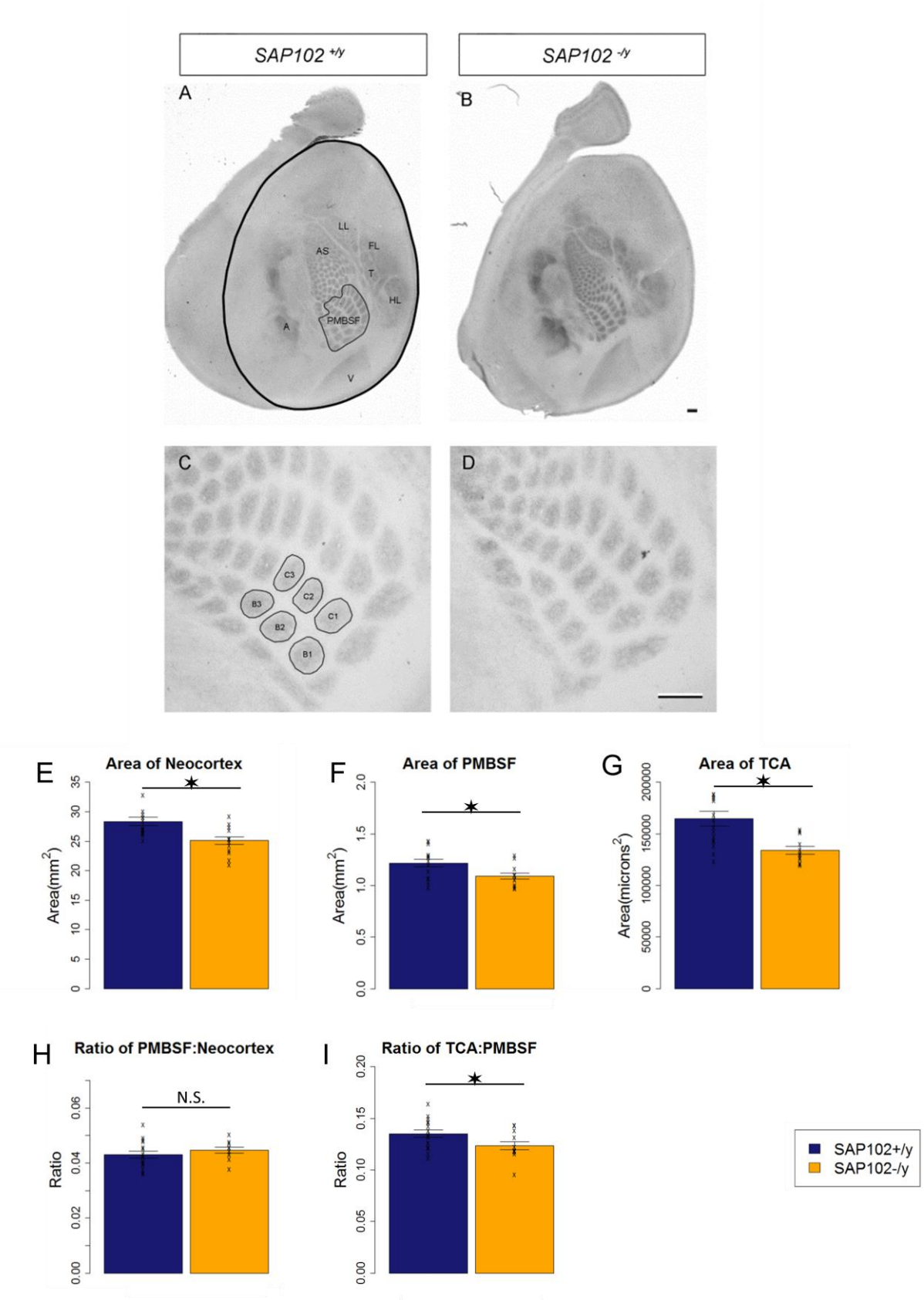

4.2.4. Barrels form normally in *SAP102*$^{-/y}$

Mutants lacking the binding partners of SAP102, e.g. SynGAP and GluN1 fail to form whisker-related cellular aggregates in layer IV called barrels (Barnett et al. 2006; Iwasato et al. 2000). In *SAP102*$^{-/y}$ mutants cells in layer IV segregate into a barrel pattern (**Fig. 6B,D**). The degree of cellular segregation in layer IV was quantified by calculating the ratio between number of cells in the cell dense barrel wall and the cell sparse barrel hollow (**Fig. 6I**, see methods 2.4 for discussion of this technique). There was no significant difference in the mean segregation ratio between *SAP102*$^{-/y}$ animals and wild type littermate controls [N_{wr}=5, N_{ko}=5, W=9, df=9, *one tail p*=0.33], demonstrating that layer IV cellular segregation is not affected by the loss of SAP102 (**Fig. 6L**).

Given the reduction in TCA patch size even when normalised to neocortical area *Sap102*$^{-/y}$ mutants, the septal area (the region between barrels) might be enlarged. Calretinin specifically labels the layer IV/V boundary and the barrel septa (**Fig. 6E-H** and see introduction 1.3.2) and the calretinin area of a single barrel was measured 54 microns from the layer IV/V boundary (see methods 2.3.3.iii). This septal area was not significantly increased in *SAP102*$^{-/y}$ animals compared to littermate controls [N_{wr}=6, N_{ko}=5, t=-1.89, df=10, two-*tailed p*=0.088] (**Fig. 6J**).

Figure 6. Layer IV cells segregate into a normal barrel pattern in SAP102$^{-/y}$ animals, however the septal area is significantly increased. Tangential sections from *SAP102*$^{+/y}$ (**A,C,E,G**) and *SAP102*$^{-/y}$ were reacted for TO-PRO3 (**A-D**) and calretinin (**E-H**) and imaged using confocal microscopy. Cellular segregation of layer IV cells was quantified by the ratio of cells in the barrel 'hollow' region (**C**, red quadrates) and the barrel 'wall' region (**C**, white quadrates, see methods 2.4.2), there was no significant difference in the segregation score between *SAP102*$^{-/y}$ and littermate controls (**I**). The septal region was defined by the area of calretinin reactivity (**G**, red ring), there was a significant increase in calretinin positive area in *SAP102*$^{-/y}$ animals (**J**). Each cross represents an individual animal and the error bars labels the standard error of the mean. Scale bar = 250 µm **C,D,G,H,** and 1mm in **A,B,E,F**.

Figure 6. Barrel formation and septal area in SAP102$^{-/y}$ and littermate controls

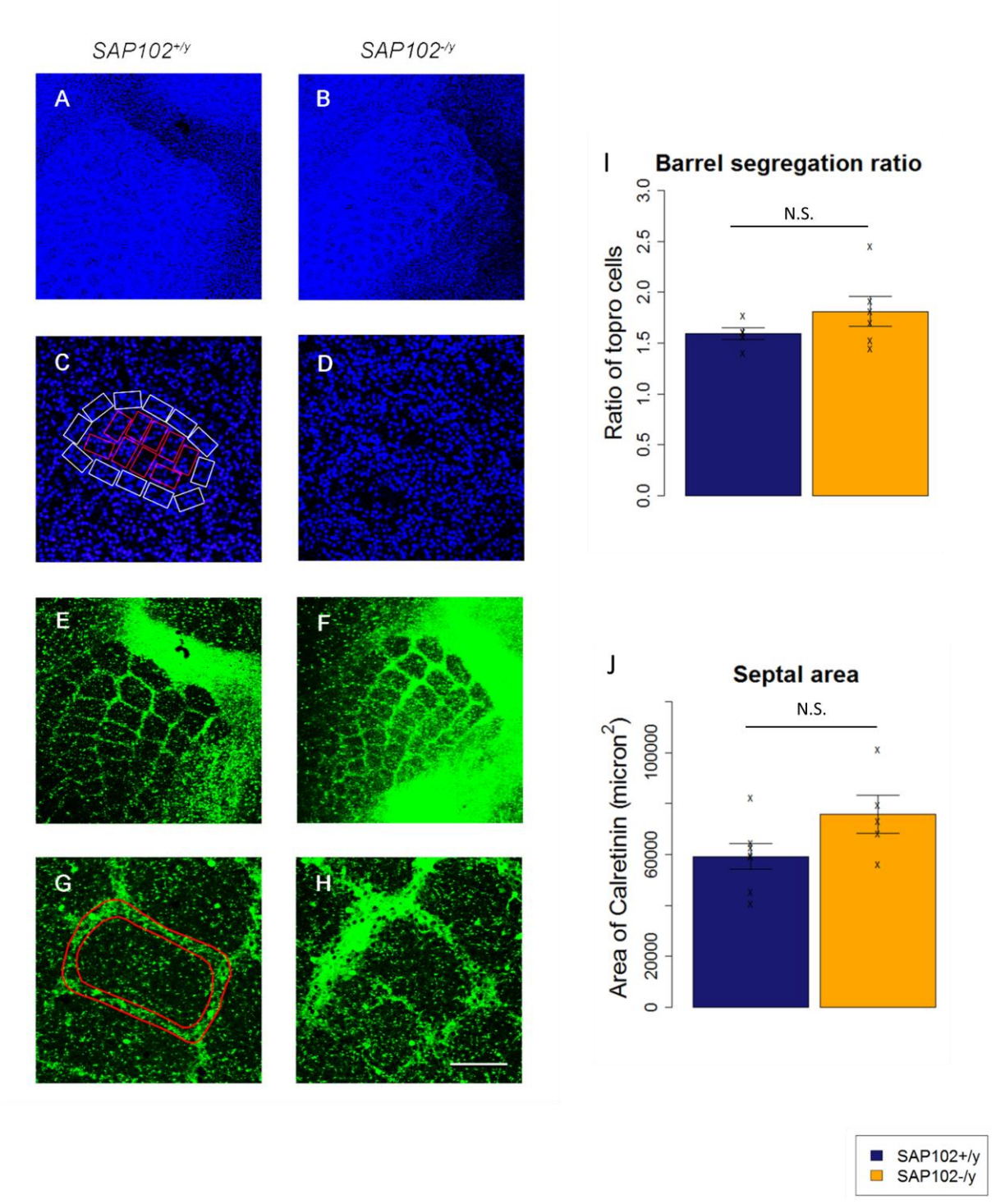

4.2.5. The morphology of individual TCA is unaffected by the loss of SAP102

The area occupied by TCA terminals at P7 in SAP102 mutants is reduced as demonstrated by the reduction in SERT-positive TCA patch size. This could be the result of fewer TCA, a restriction in TCA branching, or a reduction in SERT expression as a result of fewer synapses. In order to determine if the reduction in TCA patch size was the result of an axonal branching defect DiI was placed in the thalamus and individual TCA in the cortex were reconstructed (**Fig. 7A**). There was no significant difference in the number of branch points between *Sap102* mutants and littermate controls [N_{wt}=8, N_{ko}=4, t=-0.068, df=10, *two-tailed p*=0.31] (**Fig. 7D**). The laminar position of branch endings (**Fig. 7B**) or branch points (**Fig. 7C**) appeared not to differ across genotype (**Fig. 7C**). Although there was no difference in the number of branch points, the reduction in TCA patch size could be explained by a dramatic reduction in TCA branch length. However a non-significant trend towards an increase in axonal length was found in animals lacking SAP102 (*Sap102*$^{+/y}$; mean=1014.76, sd=172.71; *SAP102*$^{-/y}$; mean=1637.34, sd=346.04) [N_{wt}=8, N_{ko}=4, t=-1.82, df=10, *two-tailed p*=0.098] (**Fig 7F**). Furthermore there was no significant difference in the medio-lateral extent of individual TCA [N_{wt}=8, N_{ko}=4, t=-0.673, df=10, *two-tailed p*=0.5165] (**Fig. 7E**). This data demonstrates that individual axons from SAP102$^{-/y}$ animals are not restricted in their arborisation, therefore alternative explanations for the reduction in SERT-positive TCA patch size is either the result of fewer axons in layer IV or fewer synapses. To distinguish between these two outcomes, the number of TCA was investigated in *SAP102* $^{-/y}$ animals.

Figure 7. The loss of SAP102 does not affect the morphology of individual TCA. TCA sections (see methods 2.2.2) were cut and DiI was placed in the VpM of the thalamus. Individual TCA were reconstructed in layer IV of the cortex from stacks of confocal images. Representative tracings from *SAP102*$^{+/y}$ and *SAP102* $^{-/y}$ animals reveal no gross differences in the morphology of TCAs between genotypes (**A**). There was no difference in the position of either the axon endings (**B**) or branch points (**C**), and the total number of branch points was comparable between genotypes (**D**). The medio-lateral extent of TCA was equal across genotypes (**E**), and although there was a trend towards a greater branch length in *SAP102* $^{-/y}$ animals, this did not reach statistical significance [N_{wt}=8, N_{ko}=4, t=-1.82, df=10, *two-tailed* *p*=0.098]. Each cross represents an individual animal and the error bars represent the standard error of the mean.

Figure 7. TCA morphology in SAP102$^{-/y}$ and littermate controls

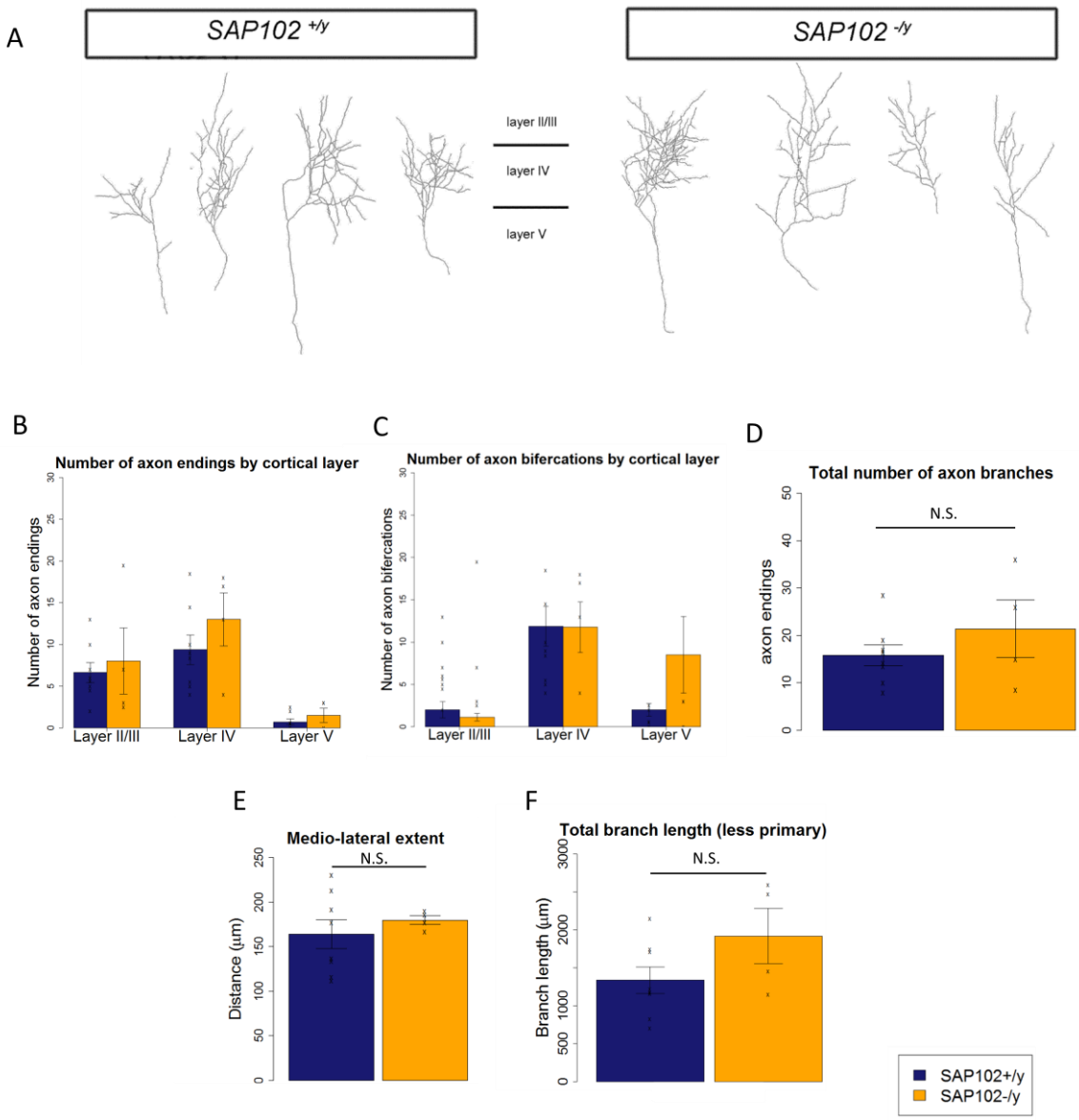

4.2.6. *Sap102*$^{-/y}$ have significantly fewer NFM-positive neurites in S1

In the previous chapter it was suggested that the medium neurofilament subunit (NFM) could be used as a marker for TCA at young ages, therefore sections from *Sap102*$^{+/y}$ and *Sap102*$^{-/y}$ were reacted for NFM at P6 and P14 (**Fig. 9**). The expression of NFM is unaffected by the loss of SAP102 as demonstrated by the developmental transition in NFM expression from a TCA patch pattern (**Fig. 8C**) to a septal pattern (**Fig. 8D**). In sections from *Sap102*$^{-/y}$ the density of NFM neurites labelled at P6 (**Fig. 8C**) appears to be visibly reduced, therefore number of NFM positive neurites was quantified (**Fig. 8**). In order to investigate the number of TCA, coronal sections from *Sap102*$^{+/y}$ (**Fig. 9A-D, A'-D'**) and *Sap102*$^{-/y}$ (**Fig. 9E-H, E'-H'**) reacted for calretinin (**Fig. 9B,B',F,F'**), TO-PRO3 (**Fig. 9C,C',G,G'**) and NFM (**Fig. 9A,A',E,E'**) were imaged on a confocal microscope and the number of NFM positive neurites crossing a region of interest was quantified. The total number of NFM-positive neurites was significantly reduced in layer IV of *Sap102*$^{-/y}$ animals [N_{wt}=5, N_{ko}=4, t=3.33, df=5.20, *two-tailed p*=0.020] (**Fig. 9I**). In order to assess the patterning of NFM-positive neurites in layer IV, the ratio between the number of neurites in the TCA patch and the septal region was calculated (**Fig. 9J**), in both genotypes there were more NFM-positive neurites in the barrel centre (as shown by a ratio greater than 1), however this ratio was not significantly reduced in *Sap102*$^{-/y}$ [N_{wt}=5, N_{ko}=4, t = 0.90, df = 6.79, *two-tailed p* = 0.32] (**Fig. 9J**). This demonstrates that although *Sap102* $^{-/y}$ animals have fewer NFM positive neurites, TCA still segregate into a normal pattern. Consistent with the reduction in the number of NFM-positive neurites in *Sap102*$^{-/y}$, fluorescence intensity of NFM appears to be reduced in *Sap102*$^{-/y}$ animals (**Fig. 9k**). This finding is consistent with the reduction in SERT positive TCA patch size and suggests that the loss of SAP102 does not affect SERT expression.

Figure 8. Normal developmentally regulated expression pattern of NFM in *SAP102*$^{-/y}$ animals. In P6 animals (**A,C**) NFM labelling in both *SAP102*$^{+/y}$ (**A**) and *SAP102*$^{-/y}$ (**C**) corresponds to whisker-related TCA patch pattern. The intensity and area of NFM labelling at P6 appears to be reduced in *SAP102*$^{-/y}$ (**C**) animals compared to *SAP102*$^{+/y}$ (**A**). At P14 (**B,C**) the expression of NFM has transitioned to a septal pattern in both *SAP102*$^{+/y}$ (**B**) and *SAP102*$^{-/y}$ (**D**). Scale bar 250µm.

Figure 8. NFM expression SAP102$^{-/y}$ and littermate controls through development

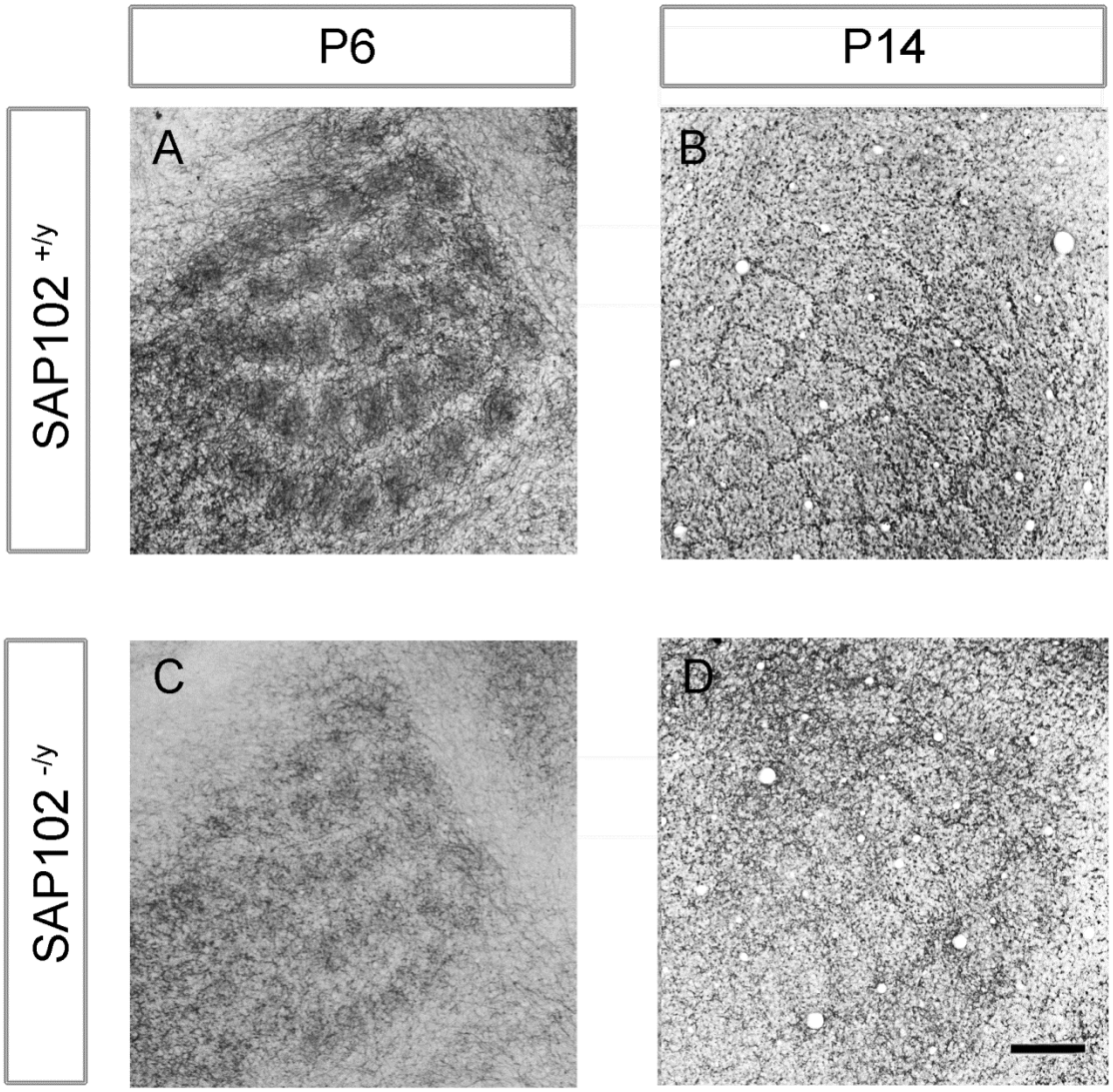

Figure 9. *SAP102*$^{-/y}$ contain fewer NFM-positive neurites in layer IV of S1. Representative images from *SAP102* $^{+/y}$ (**A-D**) and *SAP102*$^{-/y}$ (**E-H**) reacted for NFM (**A,E**), calretinin (**B,F**) and TO-PRO3 (**C-G**). Intensity measures of NFM staining at 3 different layers (white boxes; **D**) were taken at x10 magnification (**A-H**). The number of NFM-positive axons in the septal and TCA patch area (yellow boxes, **D'**) were quantified at x20 magnification (**A'-H'**). The total number of neurites in layers IV were significantly reduced in SAP102 animals compared to littermate controls (**I**). The ratio between axons in the TCA patch to the septal region was not significantly different between genotypes (**J**). Intensity measurements appear to show a reduction in NFM intensity (**K**). Scale bar = 250µm (**A-H**), 125µm (**A'-H'**). Each cross represents each individual animal and the error bars represent the standard error of the mean.

Figure 9. Number of NFM-positive axons in SAP102$^{-/y}$ and littermate controls

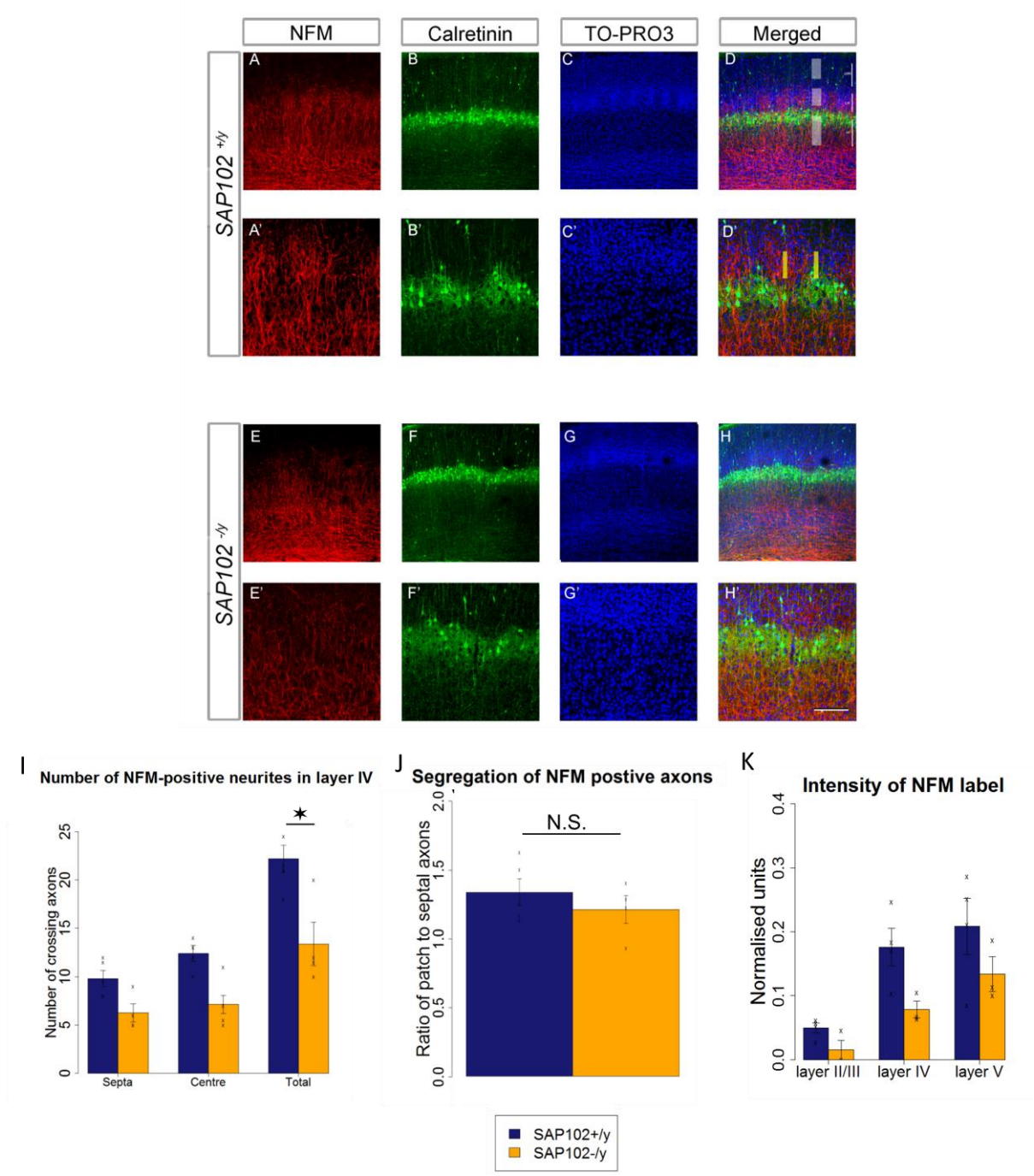

4.2.7. Intensity of MBP stain is reduced in layer IV S1 of *SAP102*$^{-/y}$

NFM is likely to label structures other than just TCA, therefore further evidence was sought to confirm the reduction in the number of TCA in *SAP102*$^{-/y}$ animals. Myelin basic protein (MBP) is specific to axons (Bjelke & Seiger, 1989) and could be used to label myelinated TCA. Myelination occurs in the 3rd postnatal week therefore sections from P21 *Sap102*$^{+/y}$ (**Fig. 10A,B,C**) and *Sap102*$^{-/y}$ (**Fig. 10D,E,F**) animals were reacted for MBP and imaged on a confocal microscope. Intensity values were obtained in different cortical layers, background intensity was subtracted and each value was normalised to a large fibre tract (fasciculus retroflexus) in that section which was positive for MBP (see methods 2.3.5.). Preliminary findings from a small number of replicates [N_{wt}=2, N_{ko}=3] would suggest that the mean intensity of MBP staining is reduced in *Sap102*$^{-/y}$ animals in layers V, IV and II/III (**Fig. 10G,H,I**), consistent with the finding of a reduction of NFM-positive neurites in layer IV.

Figure 10. Preliminary evidence for reduced MBP intensity staining *SAP102*$^{-/y}$ animals. Representative coronal sections from *SAP102* $^{+/y}$ (**A-C**) and *SAP102* $^{-/y}$ (**D-F**) reacted for MBP (**A,D**) and TO-PRO3 (**B,E**). Intensity measures were taken from layer II/III, IV and V from a single barrel (**C**; white boxes). Although the number of replicates in this experiment is insufficient to make any statistical inference [N_{wt}=2, N_{ko}=3] the mean MBP intensity was lower for SAP102$^{-/y}$ in layers V (**G**), IV (**H**) and II/III (**I**). Each cross represents each individual animal and the error bars represent the standard error of the mean. Scale bar = 250µm.

Figure 10. Intensity of MBP reactivity in SAP102$^{-/y}$ and littermate Controls

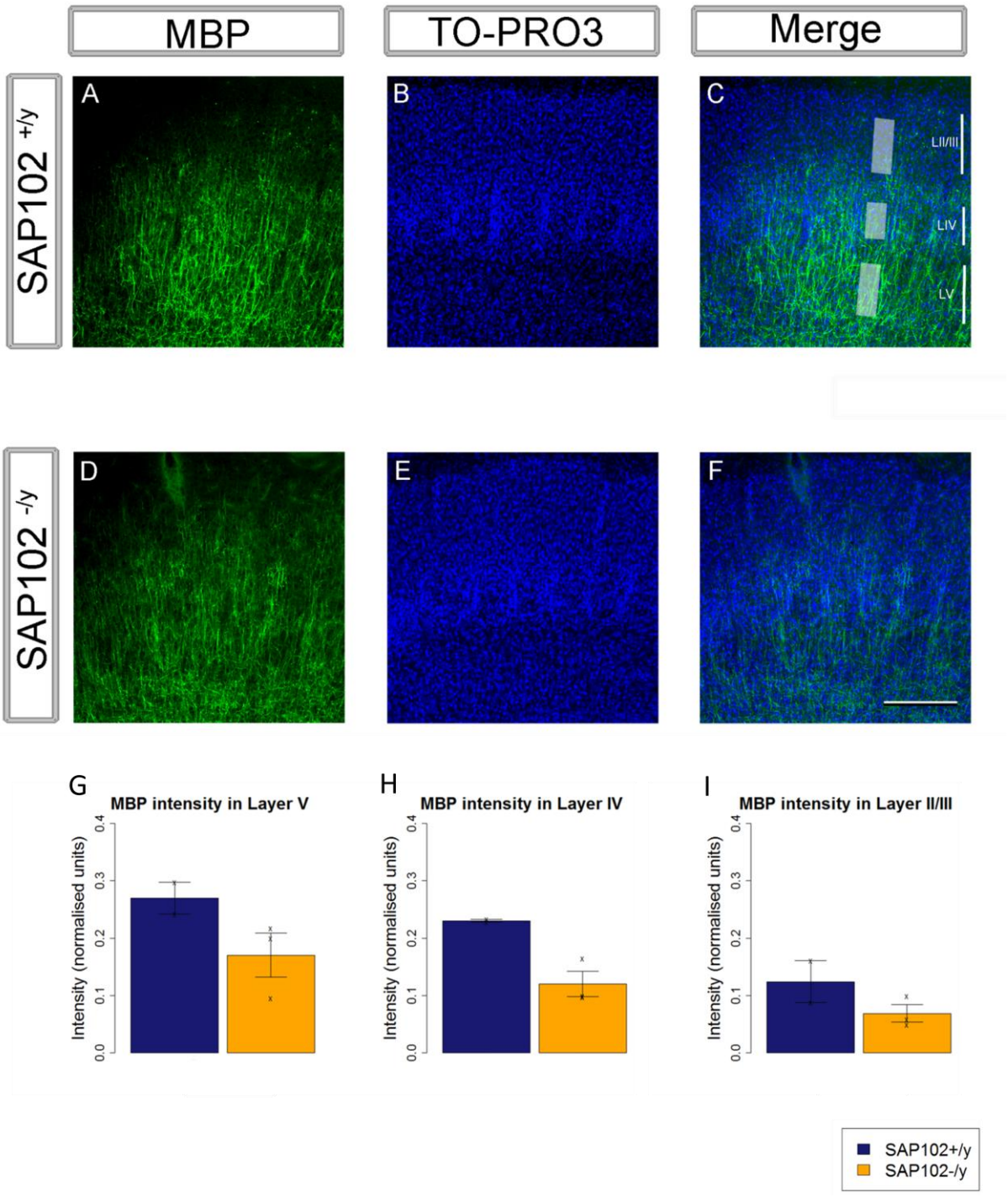

4.2.8. Fewer TCA in layer IV of S1 in *SAP102*$^{-/y}$

SERT, NFM and MBP are not specific to TCA, therefore lipophilic dyes were used to directly label axons innervating the cortex. The cortex of P7 animals was removed and DiI placed in the white matter tract and left to transport for 14 days, tangential sections were then cut and reacted for TO-PRO3 (**Fig. 11A-F**), layer IV of S1 was imaged on a confocal microscope. Confocal images were taken and the number of DiI positive axons in the TCA patch and the septal region were quantified. Consistent with the NFM and MBP immunohistochemistry, there were fewer DiI positive axons in layer IV in *Sap102*$^{-/y}$ animals [N_{wr}=4, N_{ko}=6, t=3.67, df=7.24, *two-tailed p*<0.01] (**Fig. 11G**). However the ratio between the number of axons in the TCA compared to the barrel septa was not significantly different between genotypes [N_{wr}=4, N_{ko}=6, t=0.75, df=3.57, *two-tailed p=0.50*], demonstrating that TCA still segregate into TCA patches in *Sap102*$^{-/y}$ animals (**Fig. 11H**).

Figure 11. SAP102$^{-/y}$ have fewer DiI labelled axons in layer IV. DiI was placed in the white matter and left to transport, the cortex was sectioned and reacted for TO-PRO3 (**A,D**). Representative sections from *SAP102* $^{+/y}$ (**A-C**) and *SAP102* $^{-/y}$ (**D-F**) animals, with TCA labelled with DiI (**B,E**). There were significantly fewer DiI positive axons in SAP102$^{-/y}$ (G), however there was no difference in the ratio of axons in the TCA patch to septal area (**H**). Each cross represents an individual animal and the error bars represent the standard error of the mean. Scale bar = 125µm.

Figure 11. Number of DiI-positive axons in SAP102$^{-/y}$ and littermate controls

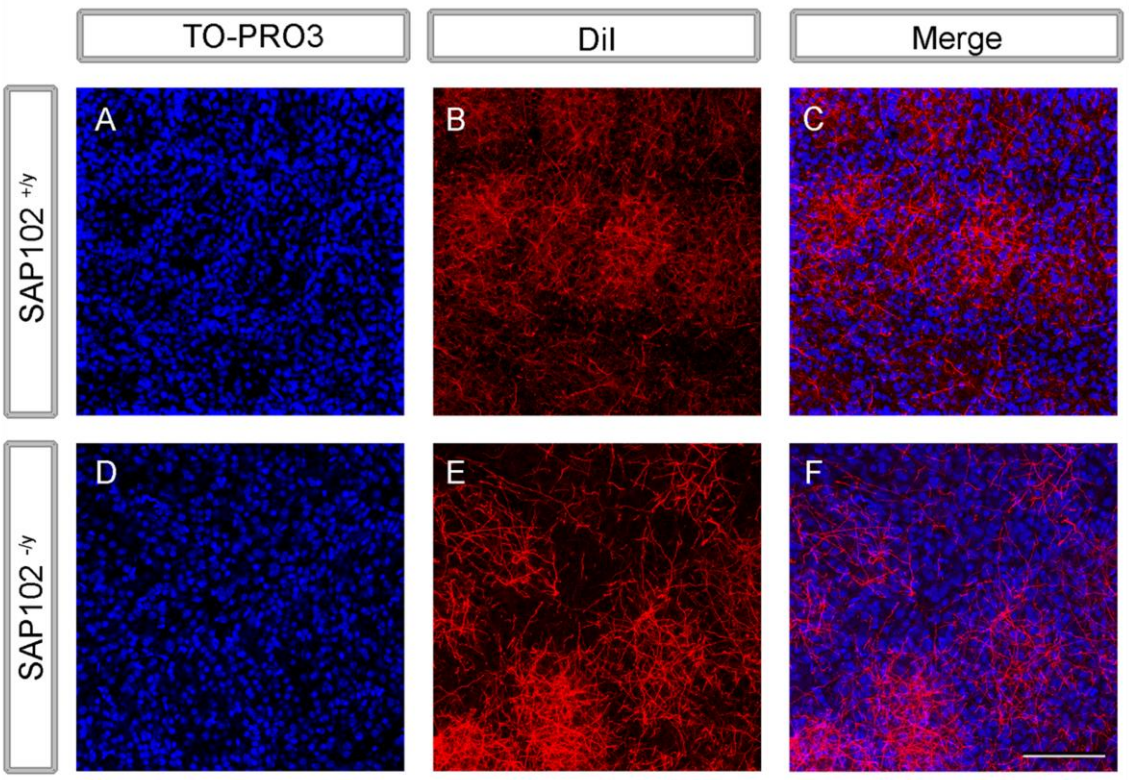

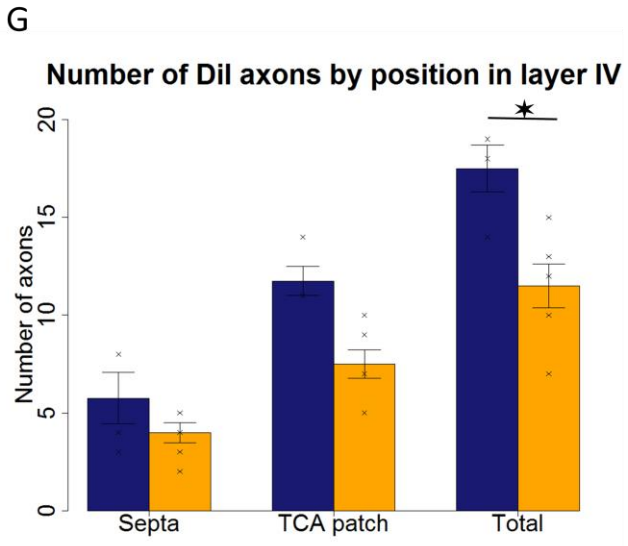

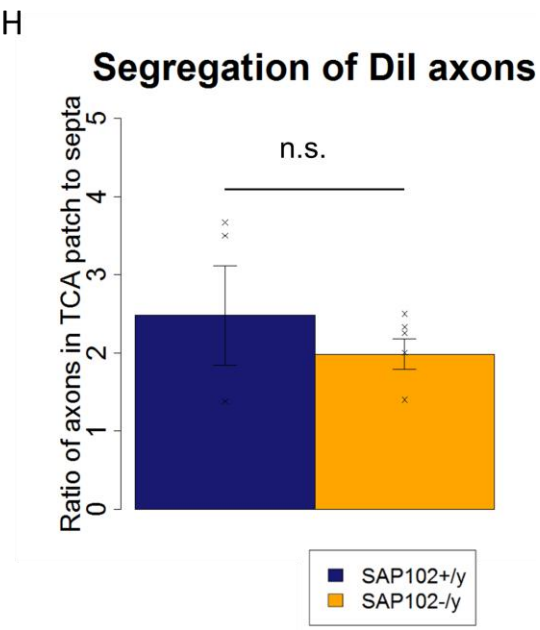

4.2.9. *SAP102*$^{-/y}$ shows layer specific defects in the density of dendritic spines

Alterations in dendritic spine density have been identified in a number of mutants lacking synaptic proteins including cortex specific-GluN1 (Datwani et al. 2002), ProSAP/Shank (Schmeisser et al., 2012), SynGAP (Vazquez et al., 2004), PSD-95 (Vickers et al., 2006), and mGluR5 (Wijetunge et al. 2008). Furthermore overexpression of *Sap102* splice variants have been shown to affect the morphology of dendritic spines and increase synapse formation *in vitro* (Chen et al. 2011), demonstrating that acute SAP102 expression can affect spine dynamics and synapse formation. In order to investigate wither the loss of SAP102 affects the number of dendritic spines, golgi impregnated layer V pyramidal cells were reconstructed and the position of dendritic spines were mapped (**Fig. 12**). There was a significant reduction in the density of dendritic spines on the apical shaft of layer V pyramidal cells [N_{wt}=10, N_{ko}=16, t=2.13, df=24, *two-tailed p*=0.043] (**Fig. 12B**). There was also a significant reduction in dendritic spine density on the portion of apical dendrite that was located in layer IV [N_{wr}=12, N_{ko}=11, t=-2.50, df=19.40, *two-tailed p*=0.022] (**Fig. 12C**), however there was no significant difference on the density of spines on the basal dendrite [N_{wt}=11, N_{ko}=15, t=0.23, df=24.00, P=0.82] (**Fig. 12E**). This demonstrates that the loss of SAP102 does not cause a universal deficit on dendritic spines density; instead the loss of SAP102 produces a layer specific deficit. The density of dendritic spines changes along the length of a dendrite, therefore dendritic spine density was plotted against dendritic position on apical layer V dendrites (**Fig. 12A**) and basal dendrites from layer V cells (**Fig. 12D**). Dendritic spine density is consistently reduced along the length of the apical dendrite (**Fig. 12A**), but plotting dendritic spine density as a function of position along the dendrite suggests that genotype has no effect at any point along the basal dendrite (**Fig. 12 E**).

Figure 12. Dendritic spine density is altered in a layer specific manner. The density of dendritic spines was calculated on the apical (**A-C**) and basal (**D,E**) dendrites of silver impregnated layer V pyramidal cells. There was a significant reduction in the density of dendritic spines along the main apical dendritic (**B**) and on the portion of the apical dendritic as it passes through layer IV (**C**), however the density of dendritic spines was comparable between genotypes on basal dendrites (**E**). Density histograms reveal the position of dendritic spines by distance from the cell soma (**A, D**), and these plots demonstrate that on apical dendrites, spine density is reduced across the complete length of the dendrite. Each cross represents an individual animal and the error bars represent the standard error of the mean.

Figure 12. Dendritic spine density on layer V pyramidal cells in SAP102$^{-/y}$ and littermate controls

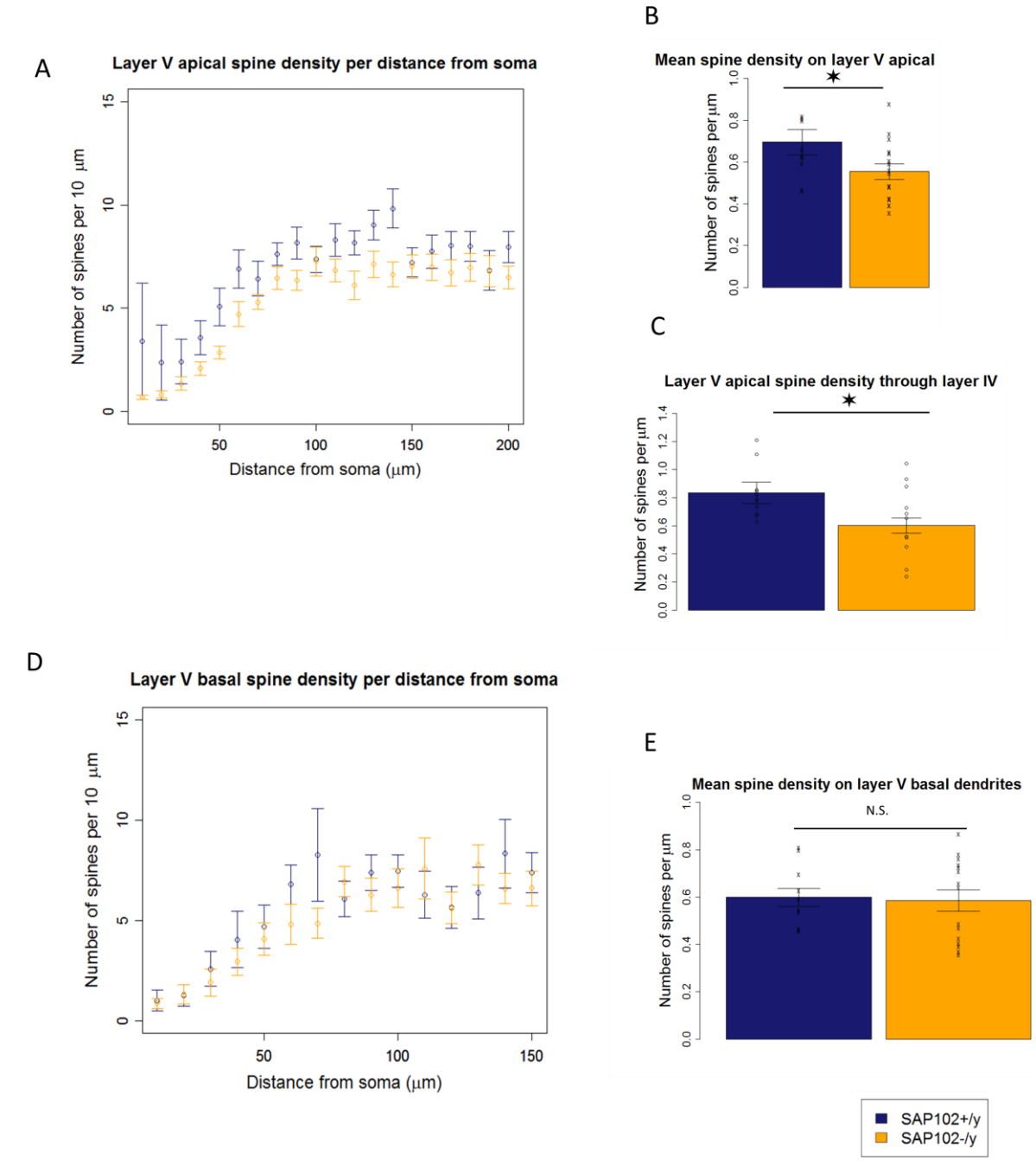

4.3. Discussion

This chapter has characterised the developing murine S1 in genetic mutants lacking the synaptic protein SAP102. Although SAP102 is a key synaptic protein present in early development, the loss of SAP102 resulted in only subtle defects to postnatal cortical development. In *Sap102*$^{-/y}$ the area of neocortex and PMBSF were significantly reduced and individual TCA patches were smaller even when normalised to the size of the PMBSF. The loss of SAP102 did not affect the morphology of individual TCA, and bulk labelling of TCA demonstrated that the reduction in TCA patch size was the result of fewer TCA reaching cortical layer IV. The loss of SAP102 had no effect on cellular segregation in layer IV but did affect the density of dendritic spines in a layer specific manner.

4.3.1. *Sap102*$^{-/y}$ have layer specific alterations in dendritic spines

SAP102 plays a fundamental role in forming some of the post-synaptic complexes required for mature synapses. These complexes are housed in dendritic spines and each dendritic spine corresponds to an excitatory synapse (Harris & Stevens 1989; Nusser et al. 1998; Hering & Sheng 2001; Harris et al. 1992). The loss of SAP102 is likely to disrupt these post-synaptic complexes and reduce the number of dendritic spines throughout the brain. However in *Sap102* mutants a global reduction in dendritic spine density was not observed; spine density was reduced on the apical shaft of layer V pyramidal cells but not on the basal dendrites suggesting that the loss of SAP102 has a layer-specific effect on dendritic spine density. The basal and apical dendrites of layer V pyramidal cells perform distinct roles; the apical shaft and apical oblique dendrites form synapses in different layers of the cortical column whereas basal dendrites form synapses only within layer V. Within S1, layer V

apical dendrites form some synapses with TCA (Benshalom & White, 1986; Hersch & White, 1981; White, 1978) therefore the reduced number of TCA in *Sap102*$^{-/y}$ may have a negative impact on the number of synapses and therefore the number of dendritic spines on layer V pyramidal cells. However this explanation seems unlikely as spine density was reduced across the total length of the apical dendrite, not just in layer IV (**Fig. 11A**).

One alternative explanation for the layer specific defects in dendritic spines density might be differential SAP102 expression in the cortex. SAP102 is mainly expressed in layers II/III and IV but is reduced in layer V (Wijetunge 2009). Decreased dendritic spine density was observed in regions where SAP102 was expressed but where SAP102 expression is reduced, no alterations in dendritic spine density was observed. However it is likely that the loss of SAP102 has a more complex effect on dendritic spine density; as recent unpublished laboratory findings demonstrated a significant increase in dendritic spine density on layer IV spiny-stellate cells from *Sap102* $^{-/y}$ also at P21._Demonstrating that at P21 the loss of SAP102 causes layer and cell type specific alterations in dendritic spine density. Layer IV cells form many more synapses with TCA than layer V pyramidal cells (Benshalom & White, 1986), demonstrating that even if alterations in dendritic spine density are the result of fewer TCA or laminar differences in SAP102 expression, the loss of SAP102 does not result in a uniform dendritic spine phenotype.

Overexpression of *Sap102* splice variants *in vitro* has been found to have differential effects on dendritic spine morphology with the full length SAP102 protein increasing dendritic spine length (Chen et al. 2011). Both the full length and the truncated form of SAP102 are expressed throughout development; however the expression pattern of these splice variants of these splice variants in the S1 is unknown. Although it is not known what effect these splice variants have in vivo, differential expression of *Sap102* splice

variants is unlikely to explain the differential effects of SAP102 on dendritic spine density because overexpression of both *SAP102* splice variants increases the number of dendritic spines (Chen et al. 2011)

4.3.2. *Sap102*$^{-/y}$ have fewer TCA in layer IV

The loss of SAP102 did not affect the position or organisation of TCAs, however SERT positive TCA patches were well defined but significantly smaller in the *Sap102*$^{-/y}$ animals. The reduced area occupied by TCAs is not the result of a global reduction in brain size as the TCA patch size was still reduced even when normalised to the size of PMBSF. The definition of SERT positive patches appears unchanged in *Sap102*$^{-/y}$ suggesting there is no differences in the density of SERT label, however this hypothesis was not explicitly tested. In sections reacted for NFM the size of TCA patches appeared to be smaller in *Sap102*$^{-/y}$; however this was not quantified (**Fig 6. A,C**). Single TCA tracings reveal that the decrease in TCA patch size is not the result of a reduction in axonal arborisation (**Fig 9. E,G**) or a decrease in lateral extent (**Fig. 7E**). Multiple methods were employed to bulk label TCA and the results of which all point towards a reduction in the number of TCA in *Sap102*$^{-/y}$. Quantification of axons labelled with NFM or DiI revealed that *Sap102*$^{-/y}$ mutants had fewer TCA compared to littermates in both the TCA patch region and the barrel septa and there was no difference in the ratio of TCA to septal axons (**Fig. 9J, Fig. 11H**). This suggests that whilst the numbers of axons reaching layer IV are reduced in *Sap102*$^{-/y}$ animals, TCA segregation is maintained.

Genetic deletion of cortical GluN1 subunit (CTX-NR1) or blocking NMDA receptors with pharmacological compounds reduces the precision of TCAs to innervate individual barrels (Fox et al., 1996; Lee, Lo, & Erzurumlu, 2005). Deletion of other post-synaptic molecules such as mGluR5 and EphrinA5 also affects the morphology of individual TCAs

(Ballester-Rosado et al., 2010; Uziel, Mühlfriedel, & Bolz, 2008). CTX-NR1 mutants have smaller, less distinct TCA patches (Lee, Iwasato, et al. 2005), and Ephrin 5A mutants have a distorted barrel field; with some TCA patches significantly larger and others smaller than corresponding wild type patches (Uziel et al., 2008). Furthermore thalamus-specific deletion of RIM 1 and RIM 2, which reduces presynaptic glutamate release from TCA by approximately 70% results in smaller TCA patches (Narboux-Nême et al., 2012). This evidence suggests that retrograde signalling from cortical cells affects both the morphology of single TCA and the size of TCA patch. It is possible that the reduction of TCA patch size in the RIM1/2 and cortex specific NR1 mutants are the result of abnormal TCA organisation as the total number of TCAs reaching the cortical layer IV was not examined in these mutants. TCA morphology was unaffected by the loss of SAP102 but fewer TCAs reached cortical layer IV and TCA patch size was reduced even when normalised to other area measurements. Compared to the deletion of CTX-NR1 the loss of SAP102 produces a more subtle TCA phenotype, therefore it is possible that the TCA morphology experiment is under-sampled to detect a small change in TCA morphology. Alternatively SAP102 affects the number of TCAs but not the morphology this would imply that there are two separate mechanisms that govern TCA developed; a SAP102 independent pathway that affects TCA morphology and a SAP102 dependant mechanism that influences the number of TCAs.

Finally a presynaptic role for SAP102 in TCA targeting cannot be ruled out. Although SAP102 is mostly found in the PSD (Petralia et al. 2005; Sans et al. 2000; Müller et al. 1996) and cytoplasm (Sans et al. 2003; Sans et al. 2005), immune-gold labelled electron microscopy has also revealed that SAP102 is present in some axons and presynaptic terminals (El-Husseini et al., 2000). However it seems unlikely that the alterations in TCA are caused by a pre-synaptic role of SAP102, given the number of binding partners that are located in the PSD that when genetically deleted also affect TCA i.e. CTX-NR1; (Lee, Lo, et

al., 2005), SynGAP; (Barnett et al., 2006). This hypothesis could be tested by immune-labelled electron microscopy to determine if SAP102 is expressed in pre-synaptic terminals at layer IV synapses.

4.3.3. Limitations of genetic deletion studies to investigate TCA patterning

While it is possible that a NMDA receptor-SAP102 pathway is involved in the organisation of TCAs, the reduction in the number of TCAs reaching the cortex may be the result of defects in other trigeminal system brain areas. Patterning of S1 is dictated by the organisation of whiskers on the facepad as well as axonal patterning in the brainstem and thalamus (Erzurumlu & Jhaveri 1990), somatotopic patterning in the thalamus and brainstem occurs earlier in development (reviewed in Erzurumlu & Gaspar 2012, see introduction 1.3.0) and if axonal patterning in the brainstem or thalamus are affected by the loss of SAP102 it may have downstream consequences in the cortex. Genetic deletion of a number of PSD proteins affect the PrV in the brainstem and VpM in the thalamus (Kutsuwada et al. 1996; Li et al. 1994; Wijetunge et al. 2008; Lee, Iwasato, et al. 2005; Barnett et al. 2006). If the deletion of a protein affects the precision of axons to innervate functional units in the brainstem fewer cells in the PrV will project to axons in the thalamus. This effect might become exaggerated in the cortex where input from the periphery has been relayed through two additional brain regions. An example of an escalating trigeminal defect can be seen in SynGAP knockout animals; in these mutants barrelette patterning in the brainstem is normal, however patterning of barreloids in the thalamus is reduced and there is no segregation of TCA in the cortex. This hypothesis does not exclude NMDA receptors and SAP102 from playing a role in TCA organisation but it does suggest that global genetic deletion studies may not be the ideal model to investigate the mechanisms that drive TCA organisation. The use of spatially restricted genetic mutants could

determine if the defects observed in the global *Sap102* $^{-/y}$ are the result of defects in other trigeminal areas, or a mechanism that is unique to cortical organisation.

4.3.4. Global delay

The loss of SAP102 has previously been reported to affect body weight during development, which has been interpreted as a developmental delay (Cuthbert 2005). *Sap102* mutants maintained on a C57/Bl6J/Ola were found to be underweight compared to wild type littermate controls (**Fig. 2A**), and brain mass of *Sap102*$^{-/y}$ was also significantly reduced (**Fig. 2B**). The loss of SAP102 may prevent weight gain as a neurological deficit on a specific brain region, for example the loss of SAP102 in cerebellum or olfactory cortical regions may affect the ability of pups to suckle and have a negative impact on weight gain (Cuthbert 2005). In human tissue SAP102 has been found to be expressed in the stomach, cardiac myocytes, islets of Langerhans and the trachea (Makino et al., 1997), however mRNA or protein has been detected in the liver, heart or muscle tissue of rats (Müller et al., 1996), therefore stunted weight gain in pups maybe the result of a defect in other organs. Although the brain mass in *Sap102*$^{-/y}$ is significantly reduced compared to littermates there is no delay in reaching developmental landmark events in S1, such as the formation of cortical layers (**Fig. 3**), the segregation of TCAs (**Fig. 5**) and the formation of a barrel pattern (**Fig. 6**). As described in the previous chapter, neurofilaments provide cytoskeletal support for axons and dendrites (Morris & Lasek 1982) and the transition in the expression pattern of neurofilament may reflect neuronal maturity (Lavenex et al. 2004; Burman et al. 2007). The normal transition of NFM expression in S1 of mutants lacking SAP102 is further evidence against a global developmental delay.

4.4.5. SAP102 in barrel formation

SAP102 is the primary MAGUK expressed during barrel formation and binds to both SynGAP and NMDA receptor subunits. Cellular segregation of layer IV cells into a barrel pattern is dependent on both SynGAP and functional NMDA receptors, therefore SAP102 was hypothesised to play a role in barrel formation possibly by localising SynGAP to the synapse. However *Sap102*$^{-/y}$ animals form a normal barrel pattern and quantification of the segregation of layer IV cells shows a non-significant trend towards a higher segregation ratio in SAP102 mutants. It is possible that in the absence of SAP102 other MAGUKs may compensate and play a more prominent role in barrel formation. There is some evidence that MAGUKs can functionally compensate for each other (Elias et al. 2008; Cuthbert et al. 2007) and the combined role of SAP102 and PSD-95, the two MAGUKs expressed in the S1 during barrel formation will be discussed in the final chapter.

4.5.6. *SAP102* null mutant as a disease model

Whilst this chapter has focused on the role played by SAP102 in neural development, these results may have implications for humans with mutation in the *DLG3* gene. As previously mentioned 5 families have been identified with a history of X-linked mental retardation that also have *DLG3* mutations (Tarpey et al., 2004; Zanni et al., 2010). The mutations in all five of these families are predicted to cause a premature stop codon in or before the third PDZ domain (**Fig. 13**), however it is not known the resulting intellectual disability is caused by the loss of functional SAP102 or if the truncated SAP102 protein disrupts a key molecular process.

A protein containing only the first 2 PDZ domains of SAP102 was still able to bind Sec8 in Glutathione S-transerase pull down assays, Sec8 is a member of the exocyst

complex which is responsible for trafficking NMDA receptors (Sans et al. 2003; Hoogenraad & Sheng 2003) and the first two PDZ domains are also responsible for binding the GluN2 subunits, therefore a truncated protein could preserve NMDA receptor binding. The truncated protein would lack the SH3 and GK domains which have been shown to be required for synaptic localisation of full length SAP102 (Zheng et al., 2010). These results demonstrate that if a truncated SAP102 protein forms in humans with *DLG3* mutants it would lack at least 3 key binding domains and would have reduced functionality.

Figure 13. Location of human *DLG3* mutations

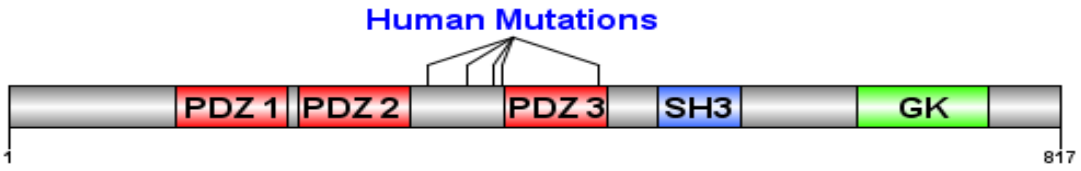

Figure 13. Location of predicted premature stop codons in the *DLG3* gene in families with X-linked mental retardation . Adapted from Tarpey et al. 2004 and Zanni et al. 2010.

4.5.7. Conclusion

In this chapter *Sap102* mutants were found to have fewer TCA in layer IV and reduced dendritic spines, these deficits would result in a connectivity defects in the trigeminal system. These defects are present in the first 3 postnatal weeks in the mouse, this corresponds to the last trimester/early postnatal development in humans. There is growing evidence that the loss of synaptic proteins which cause mental retardation in humans do so by altering connectivity within the juvenile brain (Testa-Silva et al. 2012; Grant 2012). Evidence presented in this chapter would suggest that mental retardation

caused by the loss SAP102 in humans is the result of altered connectivity during early brain development, as demonstrated by fewer axons reaching cortical targets and reduced density of dendritic spines.

Chapter 5

The combined role of SAP102 and PSD95 in S1 patterning

5.1. Introduction

The formation of barrels in the rodent S1 is an activity-dependent, postnatal event (see Introduction chapter 1.3.6. for a review). As such, the appearance of barrels has been used as an anatomical marker of normal postnatal cortical development (Iwasato et al. 2000; Wijetunge et al. 2008; Till et al. 2012; Barnet et al. 2006; Watson et al. 2006). Barrel formation in the rodent S1 is dependent on both pre-synaptic and post-synaptic signalling pathways (see Introduction chapter **1.3.6.** for review). Genetic deletion of post synaptic proteins has revealed a number of molecules required for barrel pattern formation, including glutamate receptors (Iwasato et al. 2000; Datwani et al. 2002; Wijetunge et al. 2008) and their downstream signalling enzymes (Barnett et al., 2006, Watson et al., Lu et al., 2003, Hannan et al., 2001). However, relatively little is known about the post-synaptic molecular pathways between glutamate receptors and downstream signalling enzymes (See section 1.3.6.ii and Erzurumlu & Kind 2001 for reviews).

5.1.1. MASC in barrel formation

To form a barrel pattern, cortical cells must contain functional NMDA receptors. This was demonstrated by the absence of a barrel pattern in mutants lacking the obligatory GluN1 subunit of NMDA receptor in excitatory cortical neurons (Iwasato et al. 2000). NMDA receptors are part of the MAGUK-associated signalling complex (MASC), one of a number of synaptic protein complexes (see introduction **1.4.1**). The backbone of the MASC is a group of scaffolding molecules called membrane-associated guanylate kinases (MAGUKs). Another MASC component, SynGAP (Synaptic GTPase Activating Protein, Krapivisky et al. 2004; see Introduction chapter **1.5.7**) can regulate synaptic strength via its effects on the ERK/MAPK pathway which ultimately regulates AMPA receptor trafficking (Kim, Liao, Lau, & Huganir, 1998). SynGAP can be activated by calcium influx through the NMDA receptor, and

interacts with two MAGUKs; PSD95 and SAP102 (Chen et al. 1998; Kim et al. 1998). In this way the MASC serves to link NMDA receptors to downstream signalling enzymes such as SynGAP. Although deletion of either SynGAP or GluN1 prevents barrel formation (Barnett et al., 2006) it is unclear whether all components of the MASC are required for barrel formation.

5.1.2. MAGUKs and barrel pattern formation

The barrel pattern forms in the first postnatal week, a period of development when SAP102 is the principle MAGUK expressed in layer IV. PSD95 is also present during barrel formation, but levels of PSD95 are significantly lower at this age relative to adult expression levels (Barnett et al., 2006; Petralia, Sans, Wang, & Wenthold, 2005). As we saw in the previous chapter, the loss of SAP102 causes some specific defects in S1, but the overall barrel pattern is unaffected (**Fig. 4.6**). In *Psd95* null mutants (*Psd95*$^{-/-}$) barrel formation appears to be unaffected (Barnett et al., 2006). However, it is possible that functional compensation between MAGUKs in mutants lacking either *Sap102* or *Psd95,* occludes a barrel pattern defect. This chapter aims to further examine the role of the MASC in cortical development by examining barrel formation in the absence of both SAP102 and PSD95, to overcome issues of functional compensation between these proteins in single mutants.

5.1.3. Evidence for compensation between MAGUKs

Although SAP102 and PSD95 have different expression profiles and binding partners (see introduction **1.5**) they may play similar roles at the synapse as genetic deletion of one MAGUK can affect the expression of other MAGUKs and their binding partners (Elias & Nicoll, 2007). In adult animals lacking PSD95, levels of SAP102 are increased, suggesting that the expression of SAP102 may compensate for the absence of

PSD95. In addition, more PSD95 immunoprecipitates with GluN1 subunits in *Sap102*$^{-/y}$ animals compared to wildtype controls (Cuthbert et al 2007) demonstrating that MAGUKs may compete for NMDA receptor binding at the synapse. MAGUKs have also been shown to functionally compensate for each other *in vitro*; acute knockdown of SAP102 has no effect on synaptic transmission in wild type cells, although, in cells lacking both *Psd95/Psd93*, acute knockdown of *Sap102* reduces AMPA receptor EPSCs (Elias et al 2006). Therefore the MAGUKs SAP102, PSD95 and PSD93 may all play overlapping roles at the synapse.

Interestingly, while single mutations of either *Sap102* or *Psd95* show no gross anatomical abnormalities (Migaud et al. 1998; Cuthbert et al. 2007, see **Fig. 4.6.**), animals lacking both *Sap102* and *Psd95* are under-represented at birth compared to expected mendelian ratios and do not survive beyond P3 (Cuthbert et al. 2007, Petrie 2008). Although double knockout animals die perinatally, all other genotypes survive (Cuthbert et al. 2007, Petrie 2008), demonstrating that only one copy of either *Sap102* or *Psd95* is required to produce viable offspring and that these MAGUKs perform a vital role in an animal's survival. In order to examine the combined role of SAP102 and PSD95 an alternative strategy was adopted to examine double knockout cells by utilising X-inactivation to create mosaic animals.

5.1.4. SAP102 and X-inactivation

Females have 2 X-chromosomes whereas males only have 1, therefore during early development a female embryo will undergo a dosage compensation mechanism called X-inactivation that randomly silences or inactivates the vast majority of genes on a single X-chromosome in every cell. In an adult female, all cells will express genes from only one X-

chromosome, approximately half of the cells will express genes located on the maternal X-chromosome and the other half will express from the paternal X-chromosome. A significant deviation from this 50:50 ratio (usually agreed to be greater than 80:20, Plenge et al. 2002) is termed skewed X-inactivation. *Sap102* is located on the X-chromosome, therefore as a result of X-inactivation, females heterozygous for the null *Sap102* allele will be mosaic with approximately 50% of cells being $Sap102^{-}$ and the remaining cells being $Sap102^{+}$.

During X-inactivation each cell must undertake two processes; *counting* which acts to determine the number of X-chromosomes to inactivate, and *choice* which randomly determines which X-chromosome will become inactivated. These processes were identified by studying mutants with defects in the *X-inactivation centre*, a region of the X-chromosome which contains the functional elements required to initiate X-inactivation and control *counting* and *choice*. The molecular mechanism behind these two processes is not completely understood and a number of models have sought to explain them (reviewed in Starmer & Magnuson 2009). X-inactivation is under the control of two complimentary genes, *Xist* and *Tsix*, *Xist* is expressed on the X-chromosome that will become inactivated (Brown et al., 1991) and *Tsix* which suppresses the action of *Xist* on the chromosome that will remain active (Lee, Davidow, & Warshawsky, 1999). Following *choice Xist* RNA coats the inactivated X-chromosome and silences transcription by DNA methylation, histone modification and asynchronous replication (Heard & Disteche, 2006; Heard, 2004; Wutz, Rasmussen, & Jaenisch, 2002). The whole inactivated X-chromosome undergoes heterochromatization and is coated in *Xist* RNA, forming a dense bundle that can be seen in female somatic cells known as a Barr body (Barr & Bertram 1949). X-inactivation occurs late in the blastocyst stage of development and once an X-chromosome has become inactivated, the same X-chromosome will be inactivated throughout the linage of that cell.

5.1.5. Strategy

As mentioned above double *Sap102/Psd95* null mutants are not viable, so an alternative strategy was sought to investigate barrel formation in the absence of both SAP102 and PSD95. In this chapter, I exploit the random nature of X-inactivation to create animals which are mosaic for SAP102 expression on a background that lacks PSD95 ($Sap102^{+/-}$ /$Psd95^{-/-}$). Previous reports suggest that this genotype is viable although it is underrepresented at birth, 2% of all offspring generated from a breeding pair were $Sap102^{+/-}$/$Psd95^{-/-}$ whereas normal mendelian ratio would have predicted 12.5% (Cuthbert et al '07). Furthermore, it is not known if double knockout cells survive and if they do, whether they are represented in normal X-inactivation ratios.

If double knockout cells are viable and normally represented, a $Sap102^{+/-}$ /$Psd95^{-/-}$ animal will contain approximately 50% of cells that lack only PSD95 and the remaining cells will lack both SAP102 and PSD95. To identify cells expressing SAP102, animals were bred onto a line containing an X-linked *LacZ* transgene containing a nuclear localisation sequence, making it possible to identify whether a cell has inactivated the maternal or paternal X-chromosome by staining for β-galactosidase. This strategy allowed the genotype of individual cells to be identified making it possible to determine if double knockout cells are viable and normally represented in the cortex.

5.1.6. Cell autonomous or cell non-autonomous

Assuming SAP102 and PSD95 play no role in barrel development, none of the mice would be expected to show altered barrel development, irrespective of the contribution of double mutant cells. In contrast, if PSD95 and SAP102 do regulate barrel formation, this strategy makes it possible to determine if the mechanism by which MAGUKs affect barrel

formation is cell autonomous or cell non-autonomous. For a cell autonomous defect, only the genotype of a cell determines its phenotype, whereas in a cell non-autonomous mechanism the phenotype is determined, in whole or in part, by the genotype of the surrounding cells. If the loss of SAP102 and PSD95 results in a cell autonomous defect, cells lacking both SAP102 and PSD95 would fail to segregate into a barrel pattern. Conversely if a defect in barrel pattern formation is cell non-autonomous, the proportion of double knockout cells would be expected to determine the phenotype, with barrels containing more double knockout cells would have a lower segregation score. This next section outlines all possible outcomes and identifies what each outcome will mean in terms of MAGUK function. Each figure represents a single barrel with a normal barrel pattern represented by a ring of high cell density.

5.1.7. Potential outcomes

Figure 5.1. Outcome 1 Normal barrel formation but double knockout cells do not survive.

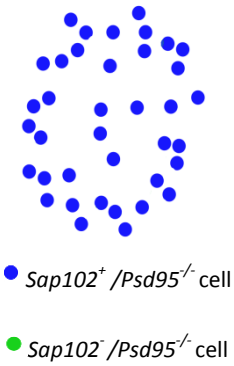

Figure 5.1. Double knockout cells are not viable in this outcome and therefore not shown in this figure. If this outcome is observed the absence of double knockout cells would demonstrate that the loss of SAP102 and PSD95 results in a cell autonomous defect that prevents double knockout cells survival. In this scenario it is not possible to determine if SAP102 and PSD95 are required for barrel formation.

Figure 5.2. Outcome 2 Only *Psd95*$^{-/-}$ cells form a barrel pattern.

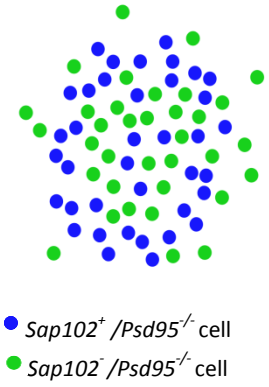

Figure 5.2. Double knockout cells survive, but do not segregate into a barrel pattern. *Psd95*$^{-/-}$ cells form a normal barrel pattern, however double knockout cells fail to segregate. If this outcome was observed it would demonstrate the need for at least 1 copy of either MAGUK to form a normal barrel pattern. The defect resulting from the loss of both SAP102 and PSD95 in this outcome is cell autonomous.

Figure 5.3. Outcome 3 Both *Sap102*$^{+}$ */Psd95*$^{-/-}$ and *Sap102*$^{-}$ */Psd95*$^{-/-}$ cells contribute towards the barrel pattern.

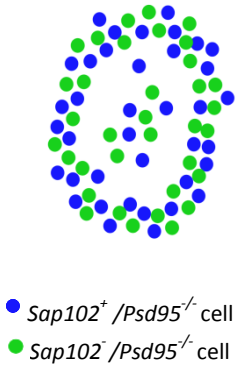

Figure 5.3. Double knockout cells survive and contribute to normal layer IV patterning. There are two possible explanations for this outcome; either SAP102 and PSD95 are not required for barrel formation or the presence of *Sap102*$^{+}$ cells is sufficient to 'rescue' cells lacking both MAGUKs (i.e. the defect is cell non-autonomous). In order to address this issue the number of *Sap102*$^{+}$ *Psd95*$^{-/-}$ cells would need to be considered.

Figure 5.4. Outcome 3a A normal barrel pattern irrespective of the percentage of double Knockout cells.

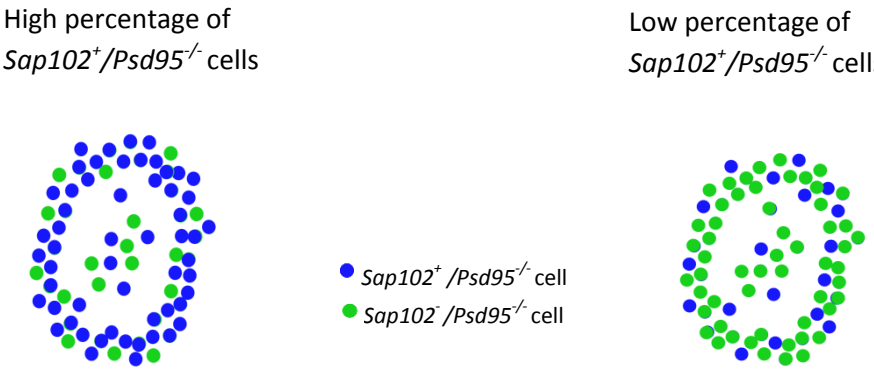

Figure 5.4. Double knockout cells contribute to barrel formation and the proportion of double knockout cells does not affect the segregation of layer IV cells. Both *Sap102*$^{+}$*/Psd95*$^{-/-}$ and double knockout cells contribute to barrel formation regardless of the percentage of X-inactivation. The ability for double knockout cells to segregate into a barrel pattern even when skewed X-inactivation results in a low percentage of *Sap102*$^{+}$*/Psd95*$^{-/-}$ cells would demonstrate that MAGUKs are not required for barrel formation.

Figure 5.5. Outcome 3b Barrel pattern formation is dependent on the percentage of double knockout cells.

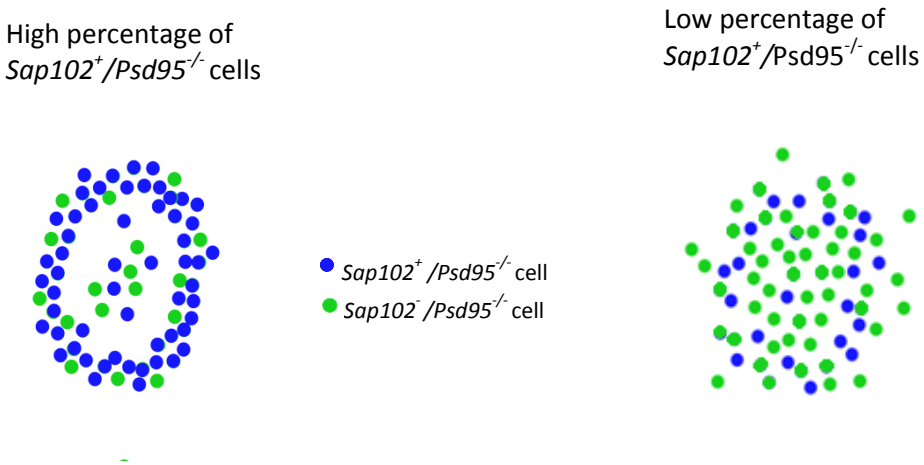

Figure 5.5. Double knockout cells survive, and the segregation of layer IV cells is proportional to the percentage of *Psd95*$^{-/-}$ cells. When fewer *Sap102*$^{+}$*/Psd95*$^{-/-}$ are present the overall cellular segregation is reduced. This outcome would demonstrate that the presence of *Sap102*$^{+}$*/Psd*$^{-/-}$ cells is required to rescue the phenotype of double knockout cells, in a cell non autonomous manner.

Figure 5.6. Outcome 4 Neither *Sap102*$^{-}$ */Psd95*$^{-/-}$ cell nor *Sap10*$^{+}$ */Psd95*$^{-/-}$ cells form a barrel pattern.

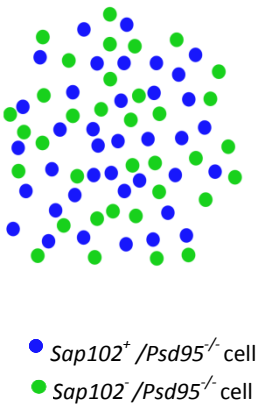

Figure 5.6. Double knockout cells survive but no barrel pattern forms. Neither the *Psd95*$^{-/-}$ nor the double knockout cells form a barrel pattern. In this scenario the presence of double knockout cells prevents the formation of a barrel pattern and the effect of the *Sap102*$^{+}$ */Psd95*$^{-/-}$ cells would be classed as cell non-autonomous.

5.2. Results

5.2.1. *Sap102*$^{+/-}$/*Psd95*$^{-/-}$ animals are viable and form barrels

S1 patterning was investigated in 3 MAGUK mutants; *Sap102*$^{-/y}$, *Psd95*$^{-/-}$ and *Sap102*$^{+/-}$/*Psd95*$^{-/-}$ mutants (**Fig. 5.7**). *Sap102*$^{+/-}$/*Psd95*$^{-/-}$ mutants were generated by crossing *Sap102*$^{-/y}$/*Psd95*$^{+/-}$ males with *Psd95*$^{+/-}$ females (see **Fig. 5.9A**), the genotyping for all animals in this chapter are described in methods 2.1.1. Sections from these mutants were reacted for TO-PRO3 to visualise the segregation of layer IV cells (**Fig. 5.7A-D**) and SERT (serotonin reuptake transporter) to visualise the pattern of thalamocortical axon terminals (**Fig. 5.7E-H**). SAP102 and PSD95 are the two MAGUKs expressed in layer IV of the S1 during barrel formation, single mutation of either *Sap102* (**Fig. 5.7B,G**) or *Psd95* (**Fig. 5.7C,F**) does not affect either barrel pattern formation (**Fig. 5.7B,C**) or thalamocortical axon segregation (**Fig. 5.7G,F**). In *Sap102*$^{+/-}$/*Psd95*$^{-/-}$ animals thalamocortical axons segregate into whisker-related patches (**Fig. 5.7H**) and layer IV cells form a normal barrel pattern (**Fig. 5.7D).** Although a barrel pattern forms normally in *Sap102*$^{+/-}$ *Psd95*$^{-/-}$ animals, it is not known if double mutant cells survive and, if they do, whether they contribute to the barrel pattern.

Figure 5.7. S1 patterning in MAGUK mutants

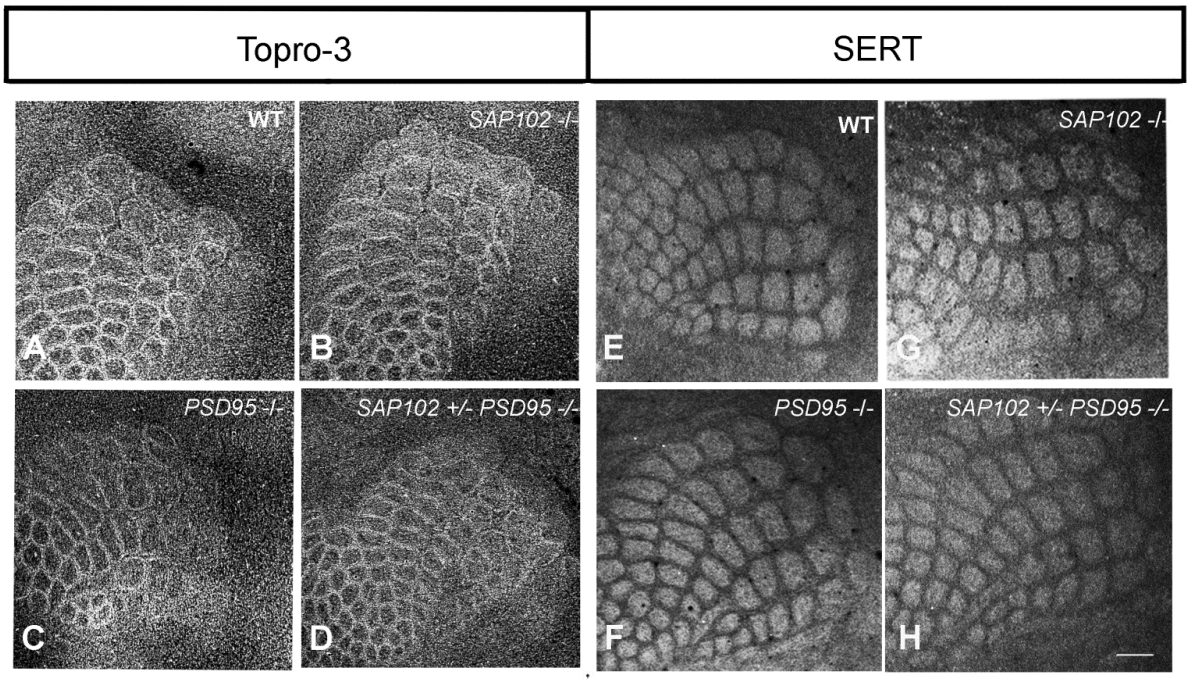

Figure 5.7. Normal S1 patterning in animals lacking MAGUKs. Flattened tangential sections through S1 reacted for TO-PRO3 (**A-D**), and serotonin re-uptake transporter (SERT; **E-H**). TO-PRO3 which labels cell nuclei reveals the segregation of layer IV cells, SERT labels TCA terminals and reveals the TCA patch pattern. Sections reacted from SAP102$^{-/-}$ (**B,G**), Psd95$^{-/-}$ (**C,F**), Sap102$^{+/-}$/Psd95$^{-/-}$, or wild type (WT) (**A,E**), all reveal normal barrel formation and TCA segregation. SAP102 resides on the X-chromosome therefore in a *Sap102*$^{+/-}$/*Psd95*$^{-/-}$ animal (**D,H**) approximately 50% of cells should lack both SAP102 and PSD95. However, it is not known if these double knockout cells are viable. Scale bar = 250 um

5.2.2. Cells containing either X chromosome are evenly distributed throughout the cortex in X^{LacZ} X females

It has previously been reported that cells with the same activated X-chromosome cluster together in radial stripes through the cortex (Tan & Breen 1993). In order to evaluate the distribution of cells expressing different activated X-chromosomes, the distribution of cells that express β-galactosidase was first investigated in females heterozygous for X-linked LacZ transgene ($X^{LacZ}X$). Coronal (**Fig. 5.8i**) and parasagittal (**Fig. 5.8ii**) sections from $X^{lacZ}X$ mutants were reacted for β-galactosidase at different postnatal time points, and sections were counterstained for TO-PRO3 to identify cortical layers (**Fig. 5.8**). None of the sections reacted showed the clear columns of alternating high and low percentages of β-galactosidase positive cells that have been previously published (Tan et al. 1995, Tan and Breen 1993). Faint stripes of alternative high and low percentages of β-galactosidase positive cells were seen in some animals at young ages (P2;**Fig. 5.8iA**, P4;**Fig. 5.8iiH arrows**). These occasional faint stripes of β-galactosidase positive cells were seen in both coronal and parasagittal sections.

Figure 5.8. Patterning of X-inactivation in coronal cortical sections throughout postnatal development. Representative images of coronal sections from animals heterozygous for the X-linked *LacZ* transgene reacted at P2 (**A**), P4 (**B**), P8 (**C**), P11 (**D**), P14 (**E**), P21 (**F**). Sections were reacted for β-galactosidase (green) to label one X-chromosome and TO-PRO3 (Blue) to label all cells. Faint radial bands containing higher percentages of β-galactosidase positive (**A**, **arrowhead**) and β-galactosidase negative (**A**, **arrow**) cells were seen in some sections at young ages (**A**). Scale bar = 250 microns.

Figure 5.8. Patterning of X-inactivation through postnatal development in coronal sections

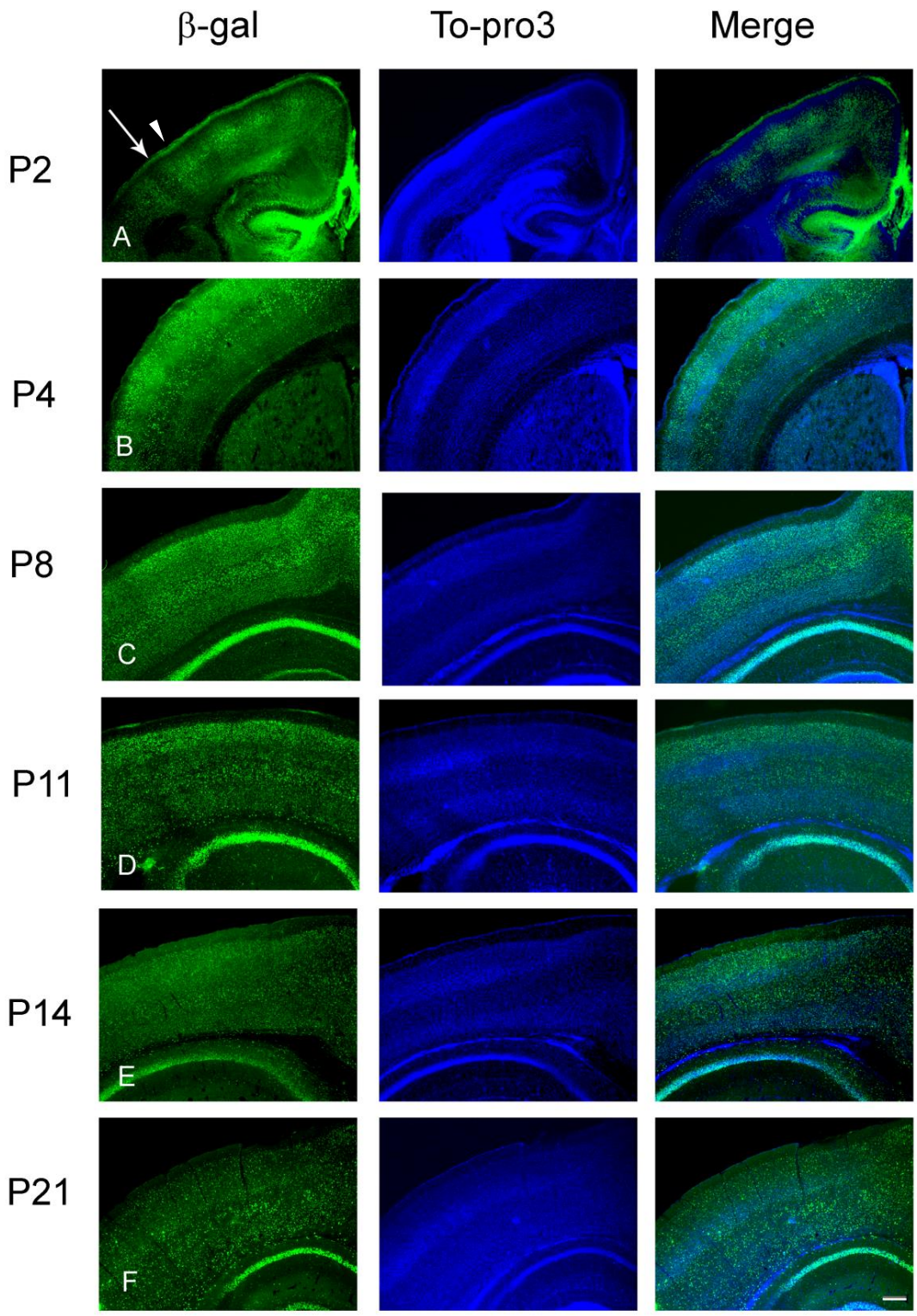

Figure 5.8cont. Patterning of X-inactivation in the cortex through postnatal development. Representative images of parasagittal (**G-L**) sections from animals heterozygous for the X-linked *LacZ* transgene reacted at P2 (**G**), P4 (**H**), P8 (**I**), P11 (**J**), P14 (**K**), P21 (**L**). Sections were reacted for β-galactosidase (green) to label one X-chromosome and TO-PRO3 (Blue) to label all cells. Faint radial bands containing higher percentages of β-galactosidase positive (**H**, **arrowhead**) or negative (**H**, **arrow**) cells were seen in some parasagittal sections at young ages (**H**). Scale bar = 250 microns.

Figure 5.8 cont. Patterning of X-inactivation through postnatal development in parasagittal sections

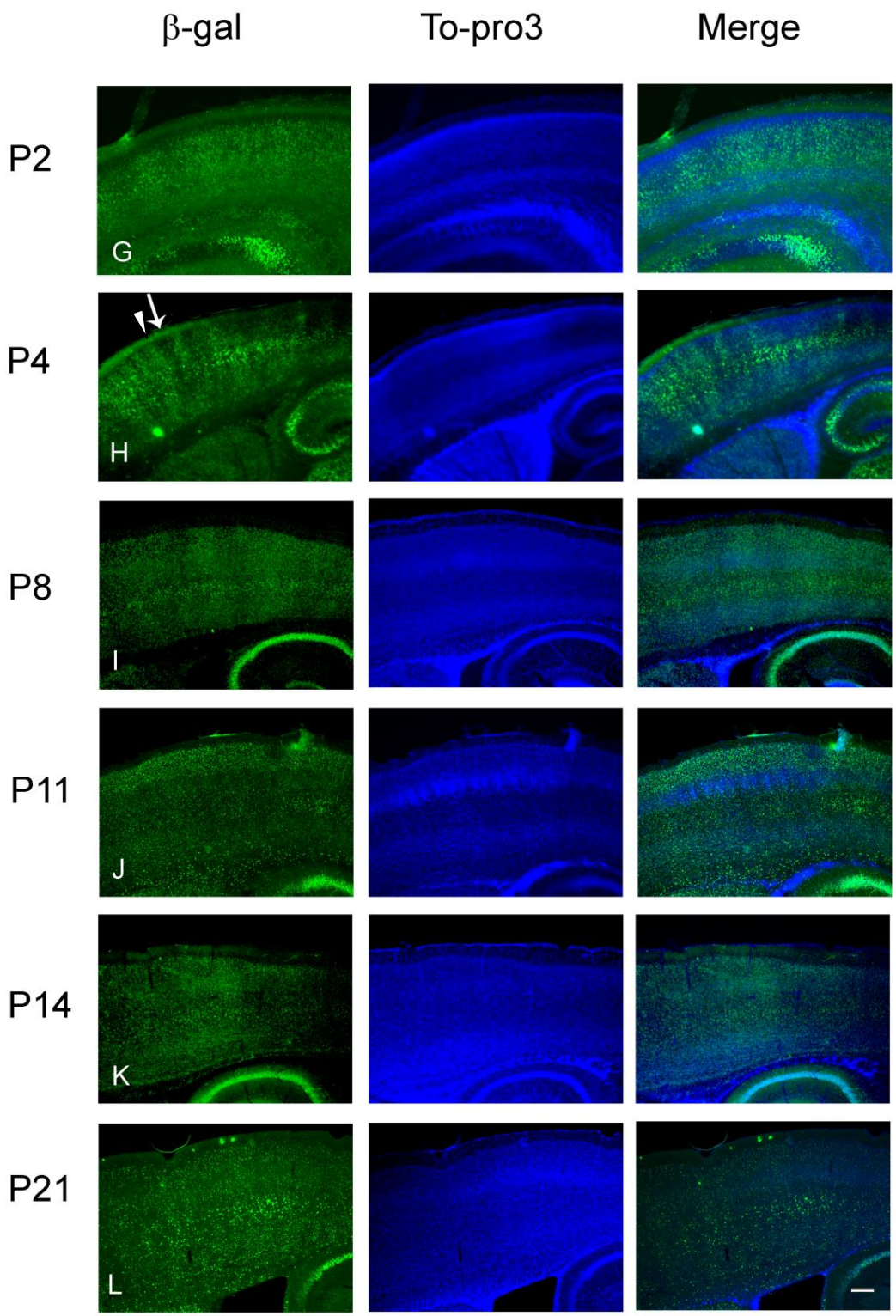

5.2.3 Breeding Strategy

In order to determine if cells lacking both SAP102 and PSD95 are viable, the genotype of each cell was identified using an X-linked LacZ transgene, which, depending on the breeding strategy will identify either *Sap102*$^{+}$ or *Sap102*$^{-}$ cells (**Fig. 5.9B,C**). This strategy was restricted by a number of complications; firstly female animals lacking both copies of *PSD95* often failed to nurse pups, therefore homozygous *Psd95*$^{-/-}$ mutants were not used as breeders. Secondly, compared to expected mendelian ratio *Sap102*$^{+/-}$/*Psd95*$^{-/-}$ mutants are underrepresented at birth (Cuthbert et al. 2007), making it likely that only a small number of *Sap102*$^{+/-}$/*Psd95*$^{-/-}$ animals would be generated. Two separate breeding strategies were designed whereby the *LacZ* transgene would be labelling either *Sap102* $^{-}$ (**Fig. 5.9B**) or *Sap102*$^{+}$ (**Fig. 5.9C**) allele.

Figure 5.9. Three different breeding strategies were employed to produce *SAP102*$^{+/-}$ /*PSD95*$^{-/-}$ animals. Only the female offspring were analysed, therefore male offspring are not included in these diagrams. Circles represent an X-chromosome, a black semi-circle refers to an X-chromosome expressing the *Sap102* mutant allele, blue semi circles correspond to an X-chromosome containing the *LacZ* transgene, and a red square represents the *Psd95* genotype, with a filled red square representing a null allele. One breeding strategy was designed to produce *Sap102*$^{+/-}$/*Psd95*$^{-/-}$ without the LacZ transgene (**A**) to investigate barrel formation in all layer IV cells (**Fig. 5.7D,H**). An X-linked LacZ transgene was introduced to identify the genotype of individual cells (**B,C**). Breeding strategies were designed where the *LacZ* transgene labelled the X-chromosome that expresses either the *Sap102* mutant (**B**) or wild type (**C**) allele.

Figure 5.9. Breeding strategy to produce *SAP102*$^{+/-}$/*PSD95*$^{-/-}$

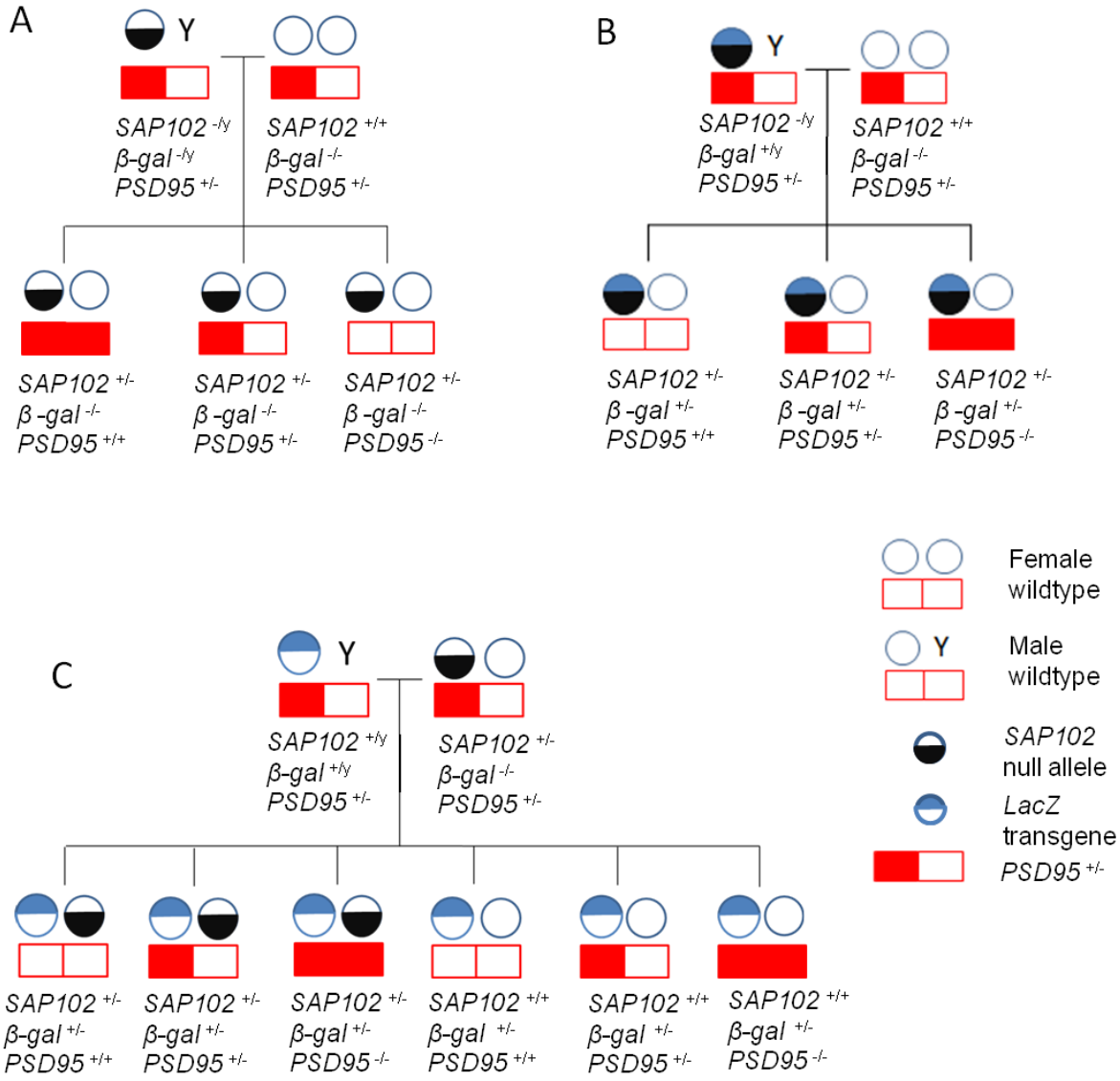

5.2.4. X-linked *LacZ* transgene as a marker of the one X-chromosome

In order to evaluate the reliability of the *LacZ* transgene as a reporter, sections from homozygous ($X^{LacZ}X^{LacZ}$) and heterozygous ($X^{LacZ}X$) females carrying the *LacZ* transgene were compared (**Fig. 5.10**). Sections from these animals were reacted with an antibody raised against β-galactosidase to identify *LacZ* positive cells (**Fig. 5.10A,D**) and TO-PRO3 to identify all cells (**Fig. 5.10B,E**). For each section a stack of confocal sections was taken and the number of cells in each channel counted separately. Up to 3% of cells were identified in the $X^{LacZ}X^{LacZ}$ animals that were TO-PRO3 positive but lacked β-galactosidase (**Fig. 5.10C**, **arrows**). After cell counts were conducted these TO-PRO3 positive, β-galactosidase negative cells were re-examined; cells that lacked β-galactosidase in the $X^{LacZ}X^{LacZ}$ animals were irregular in shape and fainter compared to other TO-PRO3 positive cells. Furthermore, when these cells were examined in adjacent optical sections from the confocal stack it was found that they did contain β-galactosidase. This demonstrates that when only a small portion of the nucleus was visible in one optical section, a cell may appear to be β-galactosidase negative, when it does in fact express β-galactosidase. To account for this limitation the criteria for identifying cells was adjusted; only TO-PRO3 nuclei that were uniform in shape with a clear edge were counted.

In $X^{LacZ}X$ animals the number of β-galactosidase positive cells was normally distributed (Shapiro-Wilk test w=0.94, N=17, *p*=0.32) around a mean of 50% (mean=50.29, sd=15.47) (**Fig. 5.10H**) furthermore, the mean percentage of β-galactosidase positive cells was approximately half that of homozygous animals (**Fig. 5.10G**). Therefore the presence of X-linked LacZ transgene did not affect the distribution of X-inactivation.

Figure 5.10. X-linked *LacZ* transgene used to label one X-chromosome. High power images of sections through the S1 reacted for β-galactosidase (**A,D**) and TO-PRO3 (**B,E**) in a $X^{LacZ}X^{LacZ}$ (**A-C**) and a $X^{LacZ}X$ (**D-F**) animal. Sections from $X^{LacZ}X^{LacZ}$ animals were used to develop an accurate counting criteria for β-galactosidase positive cells, in animals homozygous for *LacZ* , some TO-PRO3 positive cells were identified that did not contain β-galactosidase (**arrows**), these were usually not uniform in shape and when compared to the adjacent optical section did contain β-galactosidase. The percentage of β-galactosidase positive cells in a $X^{LacZ}X^{LacZ}$ female are twice as many as in a $X^{LacZ}X$ female (**G**), the percentage of X-inactivation is normally distributed in $X^{LacZ}X$ females with a mean of 50.30% (sd 15.47, **H**). Scale bar = 20um

Figure 5.10. X-Linked *LacZ* transgene as a reporter of X-inactivation

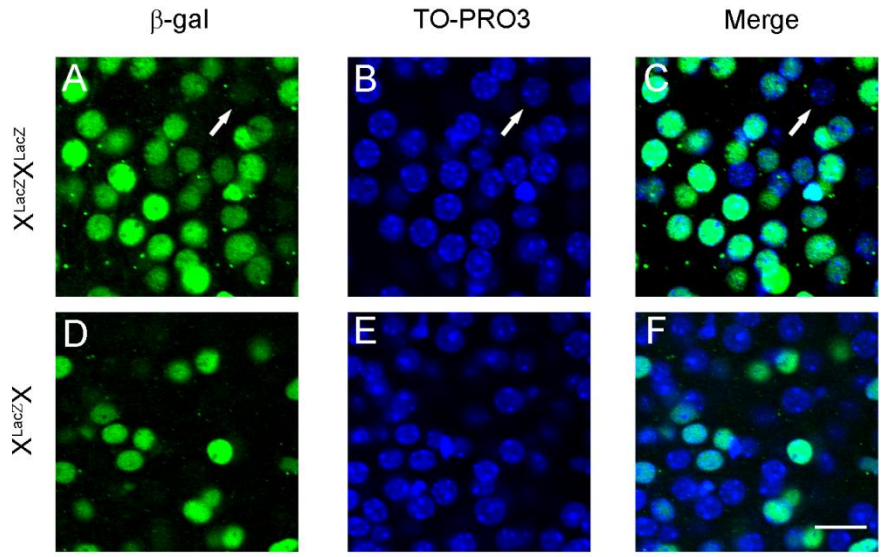

G

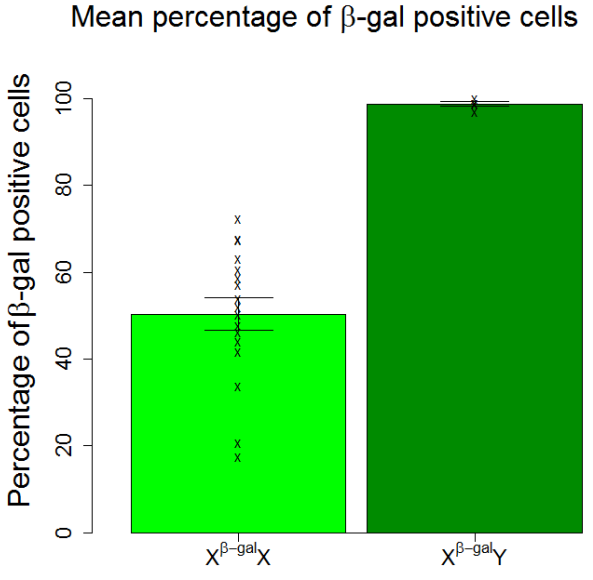

N=17 N=5

H

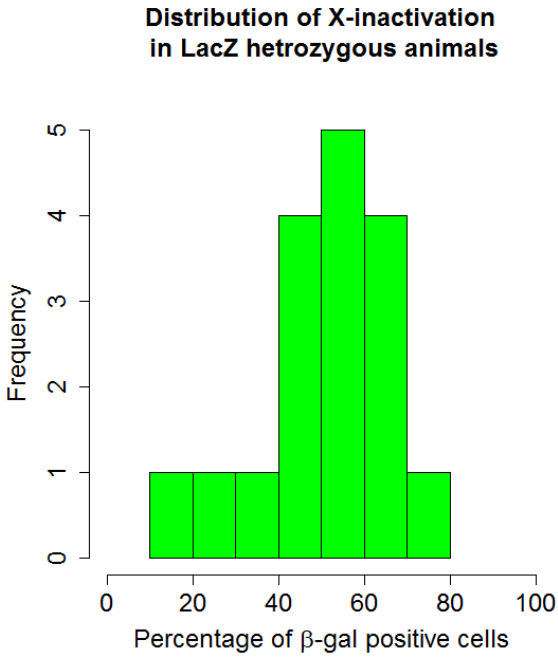

Mean = 50.3

SD = 15.47

N = 17

5.2.5. Double knockout cells are viable

To determine if double knockout cells were viable, the presence of β-galactosidase was used as a marker to identify which X-chromosome had been inactivated and therefore which cells expressed the *Sap102* mutant allele. Tangential sections were reacted for β-galactosidase (**Fig. 5.11A,D,G**) and TO-PRO3 (**Fig. 5.11B,E,H**), and a confocal stack of optical sections through a single barrel was taken. The number of TO-PRO3 and double labelled cells in the barrel wall and the barrel hollow was quantified (Methods Chapter 2.4.2). **Fig. 5.11** shows *Sap102*$^{+/-}$ animals with different gene dosages of *Psd95*, each animal expresses the *LacZ* transgene on the same X-chromosome as the *Sap102* mutant allele. Therefore in these animals β-galactosidase identifies cells where the activated X-chromosome contains both the LacZ transgene and the *Sap102* mutant allele. Sections from these animals were reacted for TO-PRO3 (**Fig. 5.11B,E,H**), and β-galactosidase (**Fig. 5.11A,D,G**). The presence of β-galactosidase positive cells in a *Sap102*$^{+/-}$/*Psd95*$^{-/-}$ animal reveals that double knockout cells are viable (**Fig. 5.11G**). The mean percentage of double knockout cells in five *Sap102*$^{+/-}$/*Psd95*$^{-/-}$ animals was 48.63 (sd= 10.50), which is not statistically significant from the expected 50% mean X-inactivation [*two tailed*, t-test, t=2.03, df=4, *p*=0.11]. Percentages of X-inactivation from other genotypes were not significantly different [$F_{(1,12)}$ =3.43, *p*=0.089]; *SAP102*$^{+/-}$/*PSD95*$^{+/+}$ (mean= 59.32, sd=17.29) and *Sap102*$^{+/-}$/*Psd95*$^{+/-}$ (mean= 56.66, sd=15.20) (**Fig. 5.11J**).

Figure 5.11. In *Sap102*$^{+/-}$ /*Psd95*$^{-/-}$ animals double knockout cells are viable and are proportionally represented compared to normal X-inactivation ratios. Representative confocal images through a single barrel from *Sap102* $^{+/-}$ /*Psd95* $^{+/+}$ (**A-C**), *Sap102* $^{+/-}$ /*Psd95* $^{+/-}$ (**D-F**) and *Sap102*$^{+/-}$ /*Psd95*$^{-/-}$ (**G-L**), reacted for β-galactosidase (**A,D,G**) and TO-PRO3 (**B,E,H**). This figure shows sections from animals where the *LacZ* transgene is located on the same X-chromosome as the SAP102 mutant allele, therefore in the *Sap102*$^{+/-}$/*Psd95*$^{-/-}$ animal (**G-L**), β-galactosidase (**G**) is labelling double knockout cells. Quantification of *Sap102* knockout cells reveals a normal percentage of X-inactivation across all genotypes (**J**). Scale bar =125 microns.

Figure 5.11. X-inactivation in MAGUK mutants

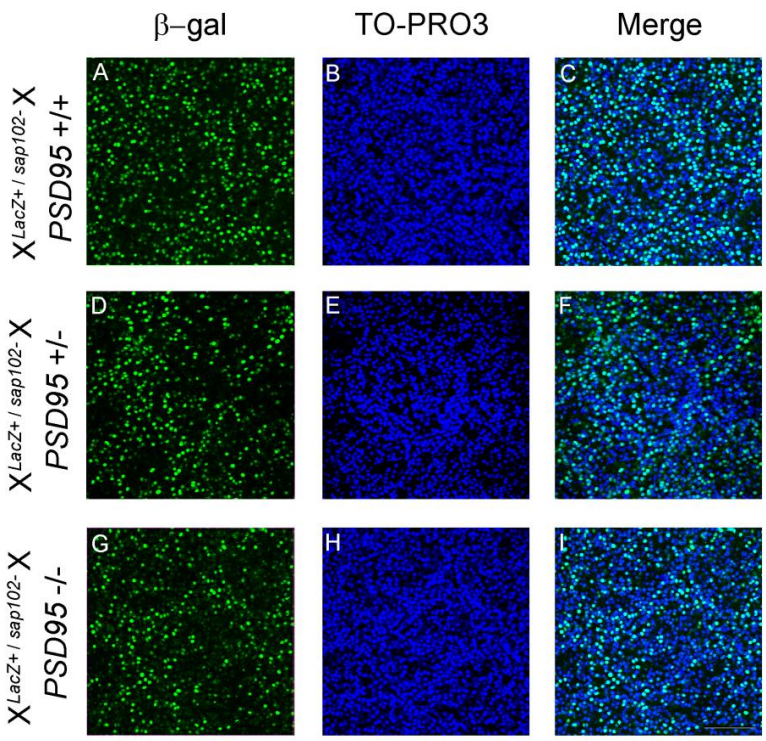

J

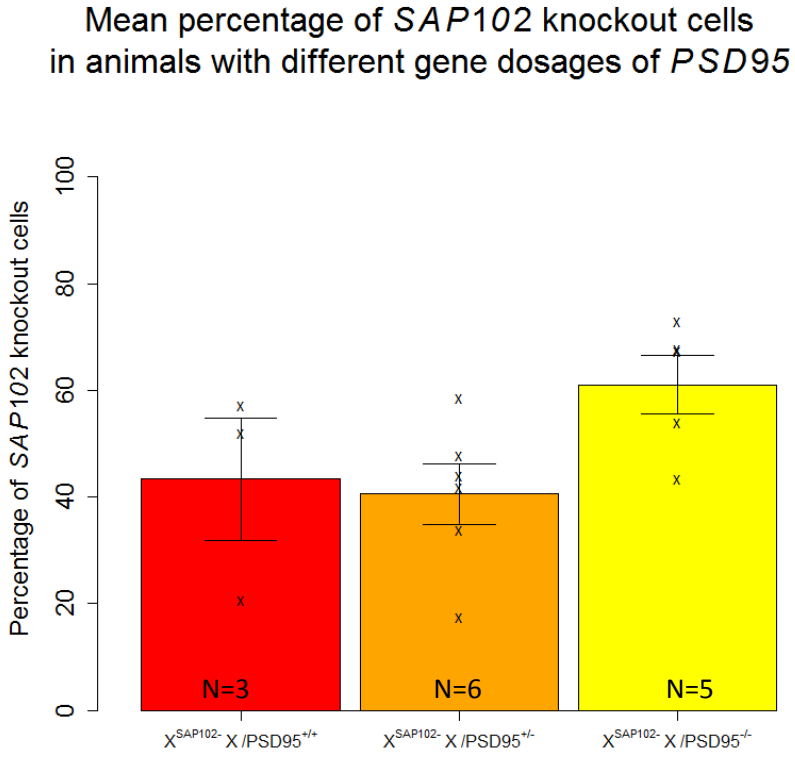

5.2.6. Double knockout cells contribute to barrel formation

To determine if cells lacking both SAP102 and PSD95 can contribute towards a barrel pattern, tangential flats were reacted for β-galactosidase, TO-PRO3 and calretinin from *Sap102*$^{+/-}$/*Psd95*$^{-/-}$ mutants, with a LacZ transgene marking the paternal X-chromosome. **Figure 5.12** shows representative images from a *Sap102*$^{+/+}$/*Psd95*$^{-/-}$ (**Fig. 5.12A-D**), a *Sap102*$^{+/-}$/*Psd95*$^{+/+}$ (**Fig. 5.12E-F**) and a *Sap102*$^{+/-}$/*Psd95*$^{-/-}$ (**Fig. 5.12I-L**) animals. In sections from both *Sap102*$^{+/-}$ animals (**Fig. 5.12 E-L**), β-galactosidase is labelling the *SAP102* knockout cells. These sections were reacted for calretinin; a calcium binding protein to delineates barrel septae (**Fig. 5.12A,E,I**, red channel in **Fig. 5.12D,H,L**) , TO-PRO3 to identify all cells (**Fig. 5.12B,F,J**, blue channel in **Fig. 5.12D,H,L**) and β-galactosidase to identify the genotype of each cell (**Fig. 5.12C,G,K**, green channel in **Fig. 5.12D,H,L**). The barrel pattern is less distinct when only a subpopulation of cells are labelled (β-galactosidase label **Fig. 5.12C,G,K**), although a barrel pattern is visible when only the double knockout cells are shown (**Fig. 5.12K**), demonstrating that double knockout cells contribute to barrel formation. This result excludes the possibility that genetic deletion of *Sap102* and *Psd95* causes a cell autonomous defect (**Figure 5.2.**Outcome 2).

Figure 5.12. Cells lacking both SAP102 and PSD95 contribute to normal barrel formation. Representative images of tangential sections through layer IV reveal the barrel pattern in *Psd95*$^{-/-}$ (**A-D**), *Sap102* $^{+/-}$ (**E-H**) and *Sap102* $^{+/-}$ /*Psd-95*$^{-/-}$ animals. In both *Sap102* $^{+/-}$ animals (**E-L**) the *LacZ* transgene is labelling the *Sap102*$^{-}$ chromosome. TO-PRO3 labelling all cells (**B,F,J**), β-galactosidase labelling *Sap102*$^{-}$ cells (**C,G,K**) and calretinin to aid barrel identification (**A,E,I**). Merged images (**D,H,L**) with β-galactosidase cells in green, TO-PRO3 in blue and calretinin in red, show all channels overlaid. Whilst the barrel pattern is difficult to visualise when only approximately half the cells are labelled (**C,G,K**), a faint barrel pattern can be seen in double knockout cells (**K**). Scale bar = 250 microns.

Figure 5.12. Contribution of *Sap102*$^{-}$ /*Psd95*$^{-/-}$ cells to barrel patterning

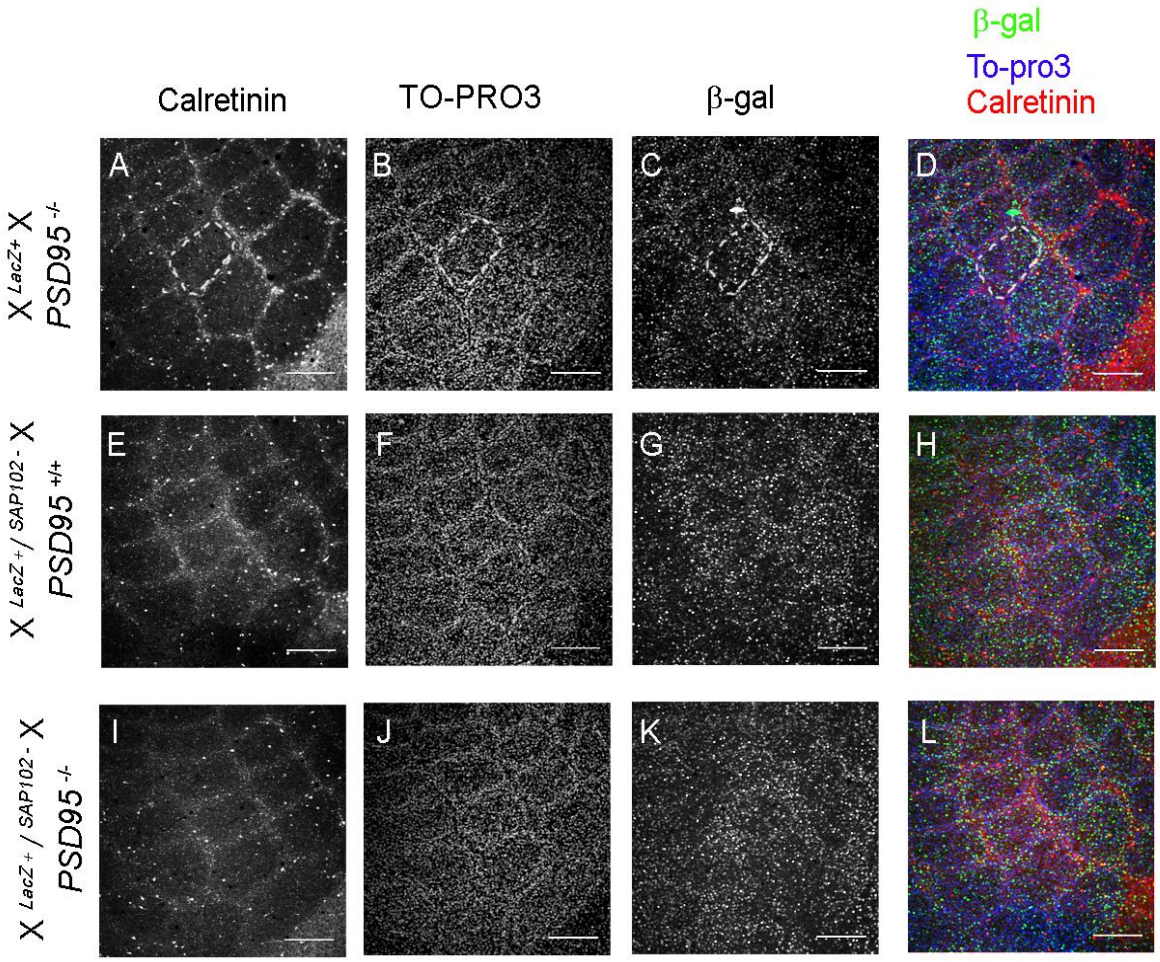

5.2.7. Barrel quantification in *Sap102*$^{+/-}$ with three different gene dosages of *Psd95*

The degree of cellular segregation in a barrel was quantified for *Sap102*$^{+}$ and *Sap102*$^{-}$ cells in animals with 3 different gene dosages of *Psd95*. The segregation score was calculated by comparing the number of cells located in the barrel *wall* to the barrel *hollow* (see Methods Chapter **2.4.2**). The results of this quantification are shown in **Fig. 5.13**; each line represents a barrel from a single animal, and the segregation of both *Sap102*$^{+}$ cells (**Fig. 5.13**, triangles) and *Sap102*$^{-}$ cells (**Fig. 5.13**, circles) are plotted. A segregation score greater than 1 identifies a barrel pattern (as demonstrated by higher cell density in the barrel wall compared to the hollow, see Methods Chapter **2.4.2**). The percentage of *Sap102*$^{-}$ cells is identified for each animal above the plotted line. Although this figure displays the *Sap102*$^{-}$ cells, these were identified by the presence or absence of β-galactosidase depending on the breeding strategy (**Fig. 5.9**). All double knockout cells had a segregation score greater than 1 (triangles in yellow section), demonstrating that there were more cells in the barrel *wall* than the barrel *hollow*. The degree of cellular segregation for *Sap102*$^{-}$ cells is variable across all genotypes, with no clear trend (**Fig. 5.13**), suggesting that it is unlikely that double knockout cells affect the segregation score. The mean cellular segregation for double knockout cells compared to *Psd95* knockout cells was analysed in 5 *Sap102*$^{+/-}$ *Psd95*$^{-/-}$ animals (**Fig. 5.13**, animals 11-15); there was no significant difference in the mean cellular segregation score between cells of different genotypes [*two way*, paired t-test, t = 1.49, df=4, p= 0.21]. Indeed a trend towards a higher segregation score was observed in double knockout cells; *Sap102*$^{+}$*/Psd95*$^{-/-}$ cells (mean 1.65, se 0.23) and *Sap102*$^{-}$*/Psd95*$^{-/-}$ cells (mean 2.92, se 0 .72).

As previously mentioned if double knockout cells contribute to barrel formation there are 2 possible interpretations of this result (see outcome 3 in **5.1.4**); either SAP102

and PSD95 are not required for barrel formation (**Figure 5.4.** Outcome 3A), or the presence of *Sap102*$^{+}$ cells rescues double knockout cells in a cell non-autonomous mechanism (**Figure 5.5.** Outcome 3B). As explained in outcome 3b, if PSD95 and SAP102 are required for barrel formation, the degree of X-inactivation would affect the cellular segregation score. This is unlikely because in the animal with the highest percentage of double knockout cells (67%, animal 13), double knockout cells had a higher segregation score than *Psd95*$^{-/-}$ cells (3.60 compared to 1.79 respectively). Furthermore there was no correlation between the percentage of double knockout cells and the overall segregation score for all cells in *Sap102*$^{+/-}$*/Psd95*$^{-/-}$ animals (PMCC= -0.087, t = -0.15, df = 3, p = 0.89). While I cannot rule out that a low percentage of *Sap102*$^{+}$ cells are sufficient to rescue double knockout cells, this data suggests that SAP102 and PSD95 are not required for barrel formation.

Figure 5.13. Quantification of layer IV cellular segregation in different MAGUK genotypes. Segregation ratio (y-axis) for each animal analysed (x axis) is calculated for *Sap102*$^{-}$ cells (blue triangles) and *Sap102*$^{+}$ cells (green circles), with the percentage of X-inactivation given above each line. Animals are grouped according to genotype; those in the red section are *SapP102* $^{+/-}$ *Psd95* $^{+/+}$, orange section; *Sap102*$^{+/-}$*/Psd95*$^{+/-}$, and yellow section; *Sap102*$^{+/-}$ *Psd95*$^{-/-}$. A segregation ratio greater than 1 indicates a barrel pattern, all *Sap102*$^{-}$ cells in *Sap102*$^{+/-}$ *Psd95*$^{-/-}$ (yellow sections) show a segregation ratio above 1, demonstrating that double knockout cells contribute towards the barrel pattern.

Figure 5.13. Segregation ratio for SAP102- and SAP102+ cells with different gene dosages of PSD95

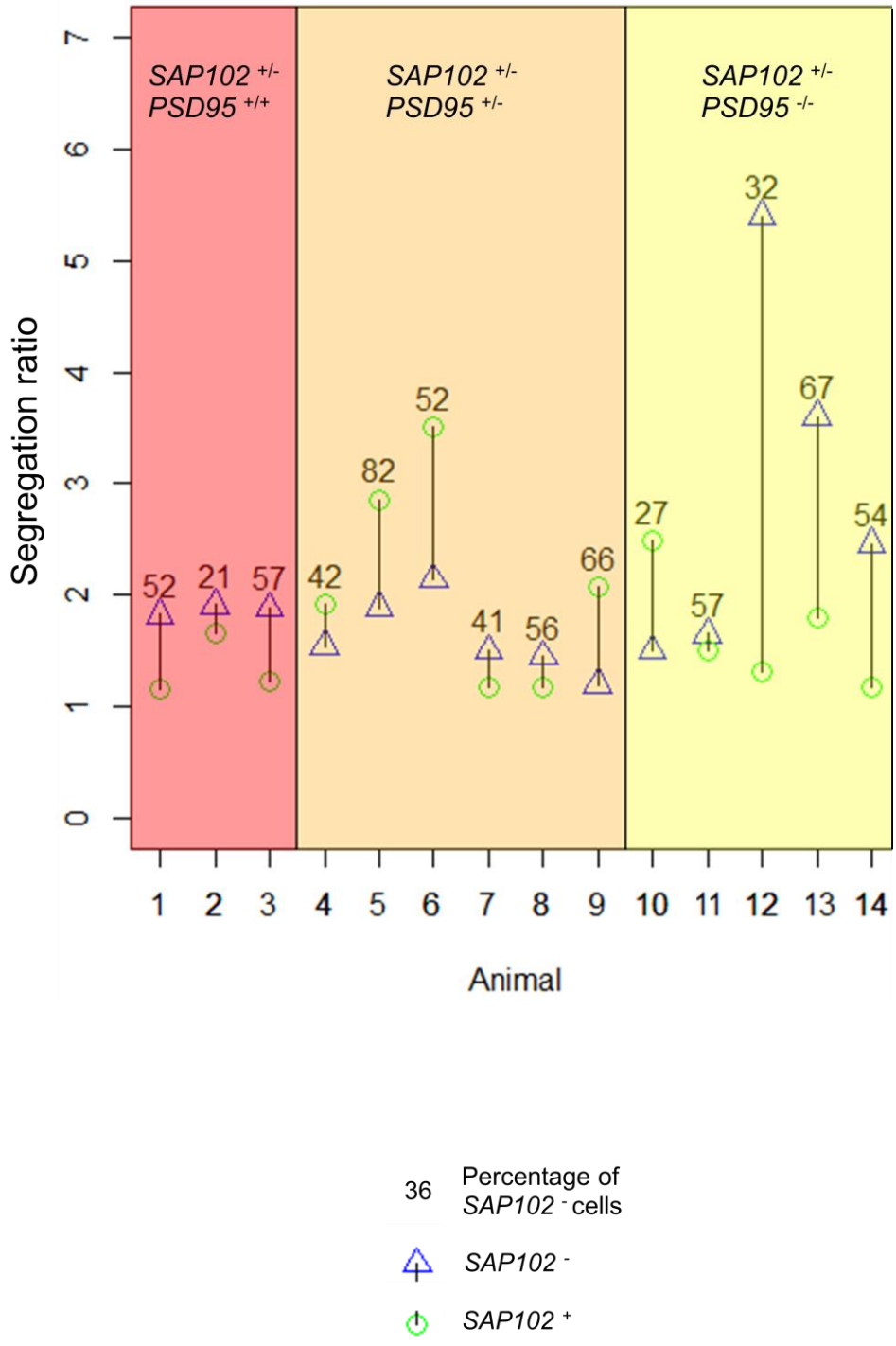

5.3. Discussion

This chapter has attempted to genetically dissect the intracellular pathways involved in barrel formation. Several genetic mutants lacking glutamate receptors (Iwasato et al. 2000; Datwani et al. 2002; Wijetunge et al. 2008) and downstream signalling enzymes show disrupted barrel formation (Barnett et al., 2006; Watson et al., 2006). MAGUKs link NMDA receptors to downstream signalling proteins in the PSD, therefore it was hypothesised that the deletion of MAGUKs would disrupt this pathway and affect barrel formation. Mutants lacking either SAP102 or PSD95 form barrels normally, even though mutants that lack both SAP102 and PSD95 die before barrels form. Given that *Sap102* is X-linked, in this chapter X-inactivation was used to investigate cells lacking both SAP102 and PSD95 in a mosaic environment where approximately 50% of cells lacked only PSD95. The genotype of individual cortical cells was identified by the presence or absence of an X-linked *LacZ* transgene. Double knockout cells were found to be viable in $Sap102^{+/-}/Psd95^{-/-}$ animals and represented at a level that was expected with normal X-inactivation, furthermore these double knockout cells contribute towards a normal barrel pattern.

5.3.1. The role of MAGUKs in cortical development

The findings presented in this chapter demonstrate that double knockout cells survive and contribute to normal barrel formation (**Figure 5.3.** Outcome 3). There are two potential interpretations for this result; either the presence of cells lacking only PSD95 is sufficient to rescue the phenotype in a cell non-autonomous manner (**Figure 5.4.** Outcome 3a, see introduction **5.1.4**), or SAP102 and PSD95 are not required for barrel formation (**Figure 5.5.** Outcome 3b, see introduction **5.1.4**). In order to distinguish between these explanations, the number of double knockout cells has to be considered. If the presence of $Psd95^{-/-}$ single mutant cells 'rescues' a barrel pattern defect, a correlation between the

percentage of double knockout cells and the segregation ratio would be expected, whereby animals with more double mutant (*Sap102*$^{-}$*/Psd95*$^{-/-}$) cells would have a lower segregation ratio.

No such correlation was found: the animal with the highest percentage of double knockout cells (67% of all cells in animal 13 lacked SAP102 and PSD95), gave a segregation ratio that was considerably higher for double knockout cells than for cells only lacking PSD95 and an overall segregation ratio in the normal range. These findings suggest that the ability of double knockout cells to contribute to a barrel pattern is not the result of a cell non-autonomous 'rescue' by *Sap102*$^{+}$*/Psd95*$^{-/-}$ cells.

The work presented in this chapter would suggest that MAGUKs are not require for barrel formation, although further work would be required to conclusively rule out a cell non-autonomous rescue effect (**Figure 5.4.** Outcome 3a). This explanation could be excluded by analysing a mosaic mutant containing a high proportion of double knockout cells. Such a mutant would require further breeding or could be achieved with more sophisticated genetic techniques, for example it may be possible to use Cre-Lox techniques to delete *Psd95* in all excitatory cortical cells by using expression of *EMX1* to drive the expression of Cre recombinase. This would require generating triple transgenic animals with LoxP sites flanking *Psd95* alleles, expressing Cre recombinase from the endogenous *Emx1* locus, on a background that lack *Sap102*. If barrels were to form in this conditional mutant, it would clearly demonstrate that SAP102 and PSD95 are not required for barrel formation.

5.3.2. Role of MAGUKs I. MAGUKs not required for barrel formation.

In the introduction to this chapter a simple molecular pathway was suggested for barrel formation; NMDA receptor activation triggered a signalling cascade of PSD molecules

such as SynGAP, which are recruited to the synapse by the MAGUK scaffolding molecules. SynGAP, NMDA receptors and a number of other PSD proteins are required for barrel formation, therefore it was hypothesized that by deleting MAGUKs the organisation of the PSD would be disrupted and barrel pattern formation would be arrested; i.e. that an organised MASC was necessary for barrel formation. The findings of this chapter suggest that the MASC is not required for barrel formation indicating that alternative pathways from NMDA receptors to SynGAP signalling are required, or that these two proteins act independently of one another to regulate barrel formation.

In this context it is important to note that SynGAP can localise to the synapse via a MAGUK-independent mechanisms. A number of SynGAP splice variants have been identified, and while only splice variants containing the SynGAP α1 C-terminal contain the PDZ binding domain that allows them to associate with SAP102 and PSD95 (Kim et al '98), all SynGAP isoforms have been shown to associate with the PSD and dendritic spines (Mahon et al. 2012). It is possible that other splice variants bind to MAGUKs but this seems unlikely as no other C-terminal splice variant identified contains the QTRV sequence required for binding to the PDZ domain of MAGUKs (Barnett et al. 2008, Li et al. 2001). Although the expression pattern in S1 of each SynGAP isoform are not known, SynGAP α1 is expressed in low concentrations compared to adult levels during the barrel development (Barnett et al. 2008) and therefore it is unlikely to be the principle splice variant required for barrel formation. In addition to the PDZ binding domains SynGAP also has C2, PH and CamKII binding domains, and is likely to regulate a number of NMDAr-independant pathways. It is therefore possible that the loss of SynGAP prevents barrel formation via a NMDAr independant mechanism.

5.3.3. Role of MAGUKs II. potential rescue mechanism (Outcome 3a)

Should further work reveal that MAGUKs are required for barrel formation, the results of this chapter demonstrates a cell non-autonomous effect of *Sap102*$^{+}$*/Psd95*$^{-/-}$ cells enabling double knockout cells to contribute towards the barrel pattern. The results of animal 13 implies that only 33% of cells need to be *Sap102*$^{+}$*/Psd95*$^{-/-}$ to facilitate double knockout cells contributing towards a normal barrel pattern, this has therapeutic implications as it suggests that a defect caused by the absence of MAGUKs can be alleviated by a small population of *Sap102*$^{+}$ cells.

If *Sap102*$^{+}$*/Psd95*$^{-/-}$ cells were enabling double knockout cells to contribute towards a barrel pattern, it would provide some insight into the mechanism of barrel pattern formation. A cell non-autonomous effect would suggest that *Sap102*$^{+}$*/Psd95*$^{-/-}$ cells can trigger a mechanism that affects all cells regardless of MAGUK genotype, for example a diffusible factor that is released via a MAGUK dependent pathway which would affect the segregation of both *Sap102*$^{-}$ and double knockout cells.

5.3.4. Technical considerations

Patterning of X-inactivation in the cortex

It has previously been reported that cells containing the same X-chromosome cluster together in radial stripes throughout the cortex (Tan & Breen 1993). This patterning could have been exploited in this chapter as radial bands containing a high proportion of cells with the same inactivated X-chromosome would result in barrels with different percentages of double knockout cells. This would allow the patterning of double knockout cells to be investigated in barrels that contain only a very low percentage of *Sap102*$^{+}$*/Psd95*$^{-/-}$ cells.

X-inactivation is completed by embryonic day 8.5 (Tan and Breen 1993), at this developmental age the cortical plate has not formed, therefore only progenitor cells in the subventricular zone undergo random X-inactivation. As the cortical plate develops the clonal progeny of these progenitor cell (with the same inactivated X-chromosome) will migrate radially to reach their final position in the cortex, therefore a small cluster of progenitors with the same inactivated X-chromosome will produce a column containing a large number of cells with the same inactivated X-chromosome.

Whilst previous reports have documented images of X^{LacZ} X animals displaying a clear striped pattern (Tan & Breen 1993), this was not observed in this chapter (**Figure 5.8** and **Figure 5.12**). Quantifying the ratio of β-galactosidase positive to negative cells in a single stripe from multiple animals reveals a mean ratio of approximately 2:1 (Tan et al. 1995), suggesting that most 'stripes'

contain a mix of cells which have inactivated different X-chromosomes. This demonstrates that the published images which display a very distinctive pattern (Tan and Breen 1993) are likely to be rare examples.

Why are X-inactivation stripes not always observed?

Not all cortical cells reach their final positions by radial migration, for example GABAergic interneurons originate in the lateral ganglionic eminence and migrate tangentially across the cortex (Anderson et al. 1997; Hevner et al., 2004; Stühmer et al. 2002). The number of tangentially migrating cells that express the X-linked LacZ transgene may affect the clarity of the striped pattern. However, the number of tangentially migrating cells will only constitute a small proportion of all cortical cells and therefore this may not be sufficient to disrupt the striped pattern that arises from radial migration. It is also likely that there is some lateral movement of neurons during postnatal development as axons

and dendrites elaborate. This is supported by the observation that a faint striped pattern was observed in young ages before neuropil elaboration and when the packing density of cells is greater.

Skewed X-inactivation

It was important to confirm that all mutants analysed expressed normal X-inactivation ratios for two reasons. Firstly the precise locus of the LacZ mutant allele was not known and it is possible that the transgene would either be spared from X-inactivation or its insertion would affect X-inactivation. Secondly skewed X-inactivation has been found in some forms of X-linked mental retardation (Plenge et al., 2002) and it was not known if this occurred in SAP102 heterozygous animals. There was no difference in the X-inactivation ratios in different MAGUK mutants therefore skewed X-inactivation did not affect this analysis.

Use of LacZ transgene as a reporter

The number of β-galactosidase positive cells was quantified in heterozygous females to evaluate the distribution of X-inactivation (**5.2.3., Figure 5.10**), and homozygous animals to determine the efficacy of the LacZ transgene as a reporter for the paternal X-chromosome. In sections from homozygous LacZ animals, the number of β-galactosidase and TO-PRO3 positive cells was quantified separately to evaluate the criteria for identifying labelled neuclei. In these animals all cells should be β-galactosidase positive, and because the proportion of β-galactosidase positive cells was not always 100%, this reflects the difficulty in identifying cells labelled by different methods; TO-PRO3 is a histochemical stain which binds directly to double stranded DNA whereas β-galactosidase was revealed by immunohistochemistry. This experiment provides the percentage error to compare the

two techniques, in $X^{lacz}X^{lacz}$ animals the mean percentage of double labelled cells was 97% which suggests that the number of β-galactosidase positive cells was slightly underreported. When TO-PRO3 positive cells were investigated in adjacent z planes these cells were found to be β-galactosidase positive, demonstrating that this was not the result of poor antibody penetration. Although this small percentage difference is unlikely to change the result, it was accounted for by designing two alternate breeding strategies where the *LacZ* transgene could be used to identify either *Sap102* $^{+}$ or *Sap102*$^{-}$ cells in different animals.

Chapter 6

Implications and final thoughts

6. Implications and final thoughts

The topics covered in this thesis have implications for a variety of areas. This final chapter will bring together these findings in the wider context of neuroscientific research and discuss the implication of some of the main findings. First the use of the rodent S1 as a model for cortical development will be evaluated, then a brief discussion on co-localisation between NF subunits, followed by a discussion on TCA labelling and development. The final three sections will focus on the MAGUKs and discuss the further work required to test connectivity in the *SAP102*$^{-/y}$, then the implications of the *SAP102*$^{-/y}$ as a disease model and finally the combined role of SAP102 and PSD95.

6.1. The rodent S1 as a model of cortical development

In the introductory chapter we saw how some of the mechanisms of brain development interact to form cortical maps, these include spontaneous activity, chemical gradients and experience dependent activity. The precise mechanism involved in organising and positioning of S1 is not known however both spontaneous activity and gradients of cell surface molecules such as Ephs and Ephrins are likely to play a role (introduction section 1.3.3). Other sensory areas have different mechanisms of creating fine maps, for example in the olfactory bulb a complex interplay between activity and attractant cues work together to create a functional network (Cho et al. 2007; Imai et al. 2006; Serizawa et al. 2006; reviewed in Sakano 2010). Therefore it is important to recognise the limitation of S1 as a model for global brain development. Cortical maps can be easily distinguished by their precise organisation however other brain areas involved in

the integration of stimulus or higher processing cannot be so easily identified. Whilst it may be easy to infer principles of cortical development from the formation of cortical maps, this extrapolation may not be valid. Even If we were to assume that the rest of the brain develops using the same principles of S1 formation, it is unclear how a specific defect in S1 patterning relates to global neural development. The underlying assumption is that the mechanisms responsible for S1 patterning are also required in other brain areas. Contrary to this assumption, SynGAP mutants have severe disruption in S1 patterning however the trigeminal regions of the brainstem and thalamus are largely unaffected, therefore the same principles of pattern formation are not consistent across brain areas. Furthermore, while the layer IV cellular segregation in S1 provides a useful model of cellular patterning, the process by which the barrel pattern forms is not fully understood which makes it difficult to infer what the loss of barrel segregation would mean in terms of global cortical development.

In the first data chapter the developing rodent S1 was also used to identify the locations of proteins *ex vivo*. The distinct patterns produced by labelling cell bodies, axons or extracellular matrix makes the rodent S1 a useful model to determine if a protein restricts to a particular sub-cellular structure. This was used to identify a marker for TCA and other TCA markers could be found using similar methods, however it is important to note that the topographical organisation of the rodent S1 might make it a unique example of protein expression. For example some extracellular matrix molecules such as tenascin and lectins are uniformly expressed throughout the cortex, except in the S1 where they restrict to the septal region (Cooper & Steindler, 1986; Mitrovic, Dörries, & Schachner, 1994; Steindler et al., 1995; Watanabe et al., 1995). Therefore using the rodent S1 to determine if a protein restricts to axons or dendrites may not extrapolate to other brain areas.

6.2. Co-localisation between neurofilament subunits

In chapter 3 differential expression between NF subunits was observed (Chapter 3, **Fig. 1,2,3**), and processes were identified that contained NFH but not NFL (Chapter 3, **Fig. 8**). Previous cell culture studies have shown that NFL is able to form filaments with both NFM and NFH (Geisler & Weber, 1981). Individual NF subunits have been found to form filaments in the presence of other intermediate filaments such as α-internexin and vimentin (Yuan et al. 2006; Ching & Liem 1998) and these may provide temporary support for some NF subunits during development before the full complement of NF subunits are expressed (Giasson & Mushynski 1997; Kaplan et al. 1990; Nixon & Shea 1992). These data would suggest that NFL is sufficient but not necessary to form filamentous chains with other NF subunits. Further investigation is warranted to more closely examine co-localisation between intermediate filaments and NF subunits through development.

Neurofilaments have been used as biomarkers for a number of neurodegenerative disorders including Huntington's disease (Constantinescu, Romer, Oakes, Rosengren, & Kieburtz, 2009), Parkinson's disease (Abdo, Bloem, Van Geel, Esselink, & Verbeek, 2007), diabetic neuropathy (Fernyhough et al., 1999), Alzheimer's disease (Zhang et al., 1989), multiple sclerosis (Gresle, Butzkueven, & Shaw, 2011; Trapp et al., 1998) and amyloid lateral sclerosis (Rouleau et al., 1996). Many of these diseases are associated with aberrant NF phosphorylation (reviewed in Dale & Garcia 2012) and can result in the distinct neuropathology such as the tangles and plaques seen in Alzheimer's disease (Deng et al., 2008; Su, Cummings, & Cotman, 1996), or the Lewy bodies associated with Parkinson's diseases (Goldman, Yen, Chiu, & Peress, 1983). Overexpression of NFH not only causes defects in axonal transport of actin, tubulin and other neurofilaments but also results in the accumulation of NF in the perikaryon which is associated with many neurological disorders

(Côté, Collard, & Julien, 1993). Furthermore genetic manipulation of neurofilament expression can slow the progression of neuropathy and increase survival in the superoxide dismutase (SOD1) mutant, which is a model of amyloid lateral sclerosis (Couillard-Després et al., 1998; Williamson et al., 1998). Although aberrant NF expression may not be the primary cause of these neurodegenerative disorders, it might result in the neuronal death and axonal degeneration that is responsible for the neurological symptoms. In addition a number of NF mutations have been identified that result in neurological disorders. Genetic mutations of the NFL subunits are associated with Charot-Marie-Tooth disease (Mersiyanova et al., 2000) and mutations in the NFM are associated with early onset Parkinson's disease (Lavedan, Buchholtz, Nussbaum, Albin, & Polymeropoulos, 2002). By understanding intermediate filament composition and phosphorylation through development an insight might be gained into diseases that are associated with either the loss of neurofilament subunits or their aberrant expression. Furthermore the patterning of the rodent S1 may be useful to study neurofilament aberrant expression in neurodegenerative disease models *ex vivo*.

6.3. Methods of labelling TCA

In chapter 3 the characterisation of 3 NF subunits provided a new method for labelling TCA. As previously mentioned using NF as a marker of TCA has important advantages over both DiI and other current TCA labels (Chapter 3; discussion 3.3.1). Although NF may label additional structures other than TCA, the combined use of both DiI and NF immunohistochemistry would provide complimentary evidence. In chapter 4 the use of DiI and Neurofilament was used to investigate TCA in mutants lacking SAP102, which allowed the two techniques to be compared. Using both NFM and DiI SAP102 mutants

were found to have had fewer TCA reaching cortical layer IV despite TCA still segregating into whisker-related patches. Analysis conducted using NFM as a TCA marker identified more axons in the septal region of wild type tissue than analysis conducted with DiI (NFM mean=9.800, sd=1.891, DiI mean=5.500, sd=2.6299). This was not the result of NFM labelling more axons from the paralemniscal pathway, because in this analysis DiI was placed in the cortical white matter tract and therefore would label axons from the VpM, PoM and corticothalamic processes. The difference in the two techniques is likely to be the result of NFM labelling other cortical processes which are present in the septal region. It is also important to note the variability in the ratio of TCA to septal axons in both techniques for WT animals; the standard deviation was lower using NFM (0.0698) compared to DiI (1.277) this may reflect the difficulty in correctly placing DiI to label all TCA. It may not be fair to directly compare the NFM and DiI techniques used in chapter 4 as they were conducted using different planes of section; NFM was conducted on coronal sections whereas DiI was placed in tissue section in the tangential plane. Whilst this may not be a fair comparison of each technique it does demonstrate the advantages and disadvantages of both methods; NFM is not specific to TCA and DiI may not label all axons. The different limitations of each technique mean that NF analysis compliments the use of lipophilic dyes when investigating axonal projections.

6.4. TCA development

The ability to bulk label TCA with NF subunits has provided some insight into the mechanisms of S1 pattern development. The presence of radial neurites in layer V at P2, and whisker-related patterns observed at P6 would suggest that TCA project to layer IV in a pre-determined pattern. Whilst further evidence is required to determine if the radial

bands observed at P2 correspond to a whisker-related pattern (see chapter3 discussion 3.3.5), the layer V pattern observed at P6 demonstrates that the majority of TCA project straight through layer V and do not transverse multiple barrels. This suggests that most TCA are organised into a rough whisker-related pattern before reaching layer IV, and imply that TCA receive a form of guidance cue before reaching layer IV.

Given the reduced size of TCA patches in SAP102 mutants, CTX-NR1 knockouts, and RIM1/2 mutants (Narboux-Nême et al. 2012), it is likely that SAP102 and NMDA receptors play a role in TCA organisation. As discussed in Chapter 3, it is possible that smaller TCA patches are not the result of fewer TCA in CTX-NR1 mutants and this could be tested by using NF to label TCA. TCA rely on retrograde signalling via Ephs/Ephrins neurons to located layer IV targets (see introduction 1.3.3). Ephrin A5-EhA interaction has been shown to induce expression of MASC components such as PSD95, GluN2A, GluN2B and GluN1 (Akaneya et al., 2010), and whilst the PDZ binding domain on the C-terminal of Ephrins is thought to interact with intracellular proteins no association has been found with MAGUK proteins (Pitulescu & Adams, 2010; Torres et al., 1998). Alternatively the loss of SAP102 may prevent TCA reaching cortical layer IV by affecting electrophysiological properties of subplate neurons. Cells in the subplate form transient connections between TCA and layer IV cells during early cortical development and play a role in setting up thalamocortical synapses (reviewed in Kanold & Luhmann 2010). Furthermore, ablation of subplate neurons affects both spontaneous and sensory evoked activity in the developing S1, and prevents S1 patterning (Tolner, Sheikh, Yukin, & Kanold, 2012). Subplate neurons express NR2B subunits as Ifenprodil reduces amplitude of NMDA receptor currents evoked by thalamic stimulation (Hanganu, Kilb, & Luhmann, 2002), therefore the loss of SAP102 may affect the electrophysiological properties of subplate neurons and therefore perturb the formation of layer IV thalamocortical synapses.

6.5. Connectivity deficits in SAP102 mutants

Layer specific alterations in the density of dendritic spines were found in mutants lacking SAP102. As discussed in chapter 4 it is unclear what causes the layer specific alterations in dendritic spines, however a reduction in dendritic spine density implies fewer stable synapses which would affect neural connectivity and may explain the intellectual impairments seen in humans with *DLG3* mutations.

Given that the loss of SAP102 has been shown to affect spine morphology *in vitro* (Chen et al. 2011) and the alteration in dendritic spine density *ex vivo* presented in chapter 4, it would be interesting to investigate spine morphology *ex vivo* in sections from mutants lacking SAP102. Dendritic spine head size correlates with the size of PSD (Harris, Jensen, & Tsao, 1992), and the size of the presynaptic pool of vesicles (Schikorski & Stevens, 1997) and therefore spine morphology is linked more closely to synaptic function than density of dendritic spines. Overexpression of *SAP102* splice variants have been shown to have differential effects on spine morphology (Chen et al. 2011) , however it not known when these splice variants are expressed. Understanding the developmental expression of *SAP102* splice variants and how they influence spine morphology *ex vivo* would provide further insight into the role of SAP102, and as mentioned in chapter 4, this may explain the layer specific alterations in dendritic spine density.

The other main finding of chapter 4 was that *SAP102* mutants had smaller TCA patches which were a result of fewer TCA reaching cortical layer IV. If S1 is seen as a model for normal cortical development, it is likely that in other brains regions of mutants lacking *SAP102* fewer axons reach their required targets. Furthermore reduced connectivity between brain regions (as the result of fewer axons reaching their targets) may explain why *DLG3* mutations are associated with X-linked intellectual disability in humans (Tarpey et al.,

2004; Zanni et al., 2010). With the techniques developed in chapter 3 it might be possible to label thalamic axons in other brain areas using NF. Preliminary data presented in chapter 4 suggests that MBP expression may be reduced in the cortex of P21 *SAP102*$^{-/y}$ animals and myelinated axon tracts could be investigated in *SAP102*$^{-/y}$ mutants using diffusion tensor magnetic resonance imaging, this would identify all axonal tracts in the brain and could be used to access connectivity in other brain areas.

6.6. SAP102$^{-/y}$ as a disease model

As previously discussed, *Sap102*$^{-/y}$ mice may not be an ideal disease model to investigate human intellectual disability caused by *DLG3* mutations (Chapter 4, discussion 4.5.6). If the human *DLG3* mutations results in a non-functioning protein, the results of this thesis will have a number of implications. Adult *SAP102*$^{-/y}$ mice demonstrate deficits in synaptic plasticity and specific behavioural learning tasks (Cuthbert et al., 2007), however results of this thesis demonstrate that the loss of SAP102 causes specific anatomical deficits in early development and can have differential effects on cells depending on the cortical layer they are in. Given that SAP102 is the main MAGUK expressed during development, it is likely that the phenotype described in adult animals is the result of alterations in synaptic signalling during development. Recently mutant mice lacking different MAGUK have been found to display different behavioural phenotypes, furthermore the same behavioural phenotypes have been observed in humans carrying mutations in the same MAGUK gene (Nithianantharajah et al., 2012) suggesting that the null mutation mouse model replicates learning deficits seen in humans with *DLG* mutations. The results presented in this thesis may therefore have implications for humans with *DLG3* mutations; importantly it provides some insight into when and how the loss of SAP102 affects early brain development. In

SAP102$^{-/y}$ two key phenotypes were observed at different developmental ages; the reduction in TCA number was identified at P6, and the defects in dendritic spine density were observed at P21. In murine development P6 in the mouse corresponds to the last trimester of human embryonic development whereas P21 corresponds to approximately 24 months in humans (Clancy et al., 2007). An understanding of the temporal and spatial affects caused by the loss of SAP102 will provide an insight into the onset, symptoms and potential treatment of intellectual impairment.

6.7. The combined role of SAP102 and PSD95

Chapter 5 used the formation of the barrel pattern to assess the role of MAGUKs in cortical development. This chapter can serve as a proof of principal for using X-inactivation to develop further question about the combined role of SAP102 and PSD95. Morphological analysis of double knockout cells could be achieved by filling β-galactosidase expressing cells with an intracellular fluorescent protein and confocal microscopy imaging. This could be combined with physiological recordings to determine if double knockout cells can form functional synapses. MAGUKs are hypothesised to play a key role in NMDA receptor trafficking, synapse formation and synaptic plasticity therefore MAGUKs are likely to play a key role in the formation of synapses or dendritic spines. Although various lines of evidence suggest MAGUKs play a role in synaptogenesis (Montgomery et al. 2004; Chih et al. 2005; Elias & Nicoll 2007, see introduction 1.5.4), and recent research suggests that the loss of different MAGUKs play distinct but overlapping roles at the synapse (Elias, Elias, Apostolides, Kriegstein, & Nicoll, 2008; Grant, 2012; Nithianantharajah et al., 2012). By investigating mutants lacking multiple MAGUKs, we can discover which functions are

mediated by specific MAGUKs and which defects can be alleviated by compensation between MAGUKs.

Understanding which neuronal processes are mediated by MAGUK may impact a variety of human disorders. PSD95 also has the ability to modulate excitotoxicity via its binding to NMDA receptors and neuronal nitric oxide synthase (nNOS), PSD95 binds to nNOS via its second PDZ domain and suppression of PSD95 have been found to protects against excitotoxic vulnerability (Cui et al., 2007). This has led to the use of PSD95 inhibitors for the treatment of stroke in animal models (Cook, Teves, & Tymianski, 2012; Sun et al., 2008). Altered levels of MAGUK have been identified in autopsies from patients with a number of neuroaffective disorders, including Bipolar disorder (Beneyto & Meador-Woodruff, 2008; McCullumsmith et al., 2007), Epilepsy (Qu et al., 2009), Alzheimer's disease (Gylys et al., 2004; Proctor, Coulson, & Dodd, 2010) and Schizophrenia (Kristiansen & Meador-Woodruff 2005; Clinton & Meador-Woodruff 2004; Toro & Deakin 2005). MAGUK are also hypothesised to play a role in neurodegenerative disorders such as Alzheimer's and Parkinson's disease due to their ability to modulate synaptic function and excitotoxicity via NMDA receptors (reviewed in Gardoni et al. 2009). This demonstrates that understanding the different roles played by MAGUK and compensation between them may provide insight into other human diseases beyond intellectual disability.

6.8. Implications for other allosomal disorders

Using X-inactivation to create mosaic animals could also be used to investigate other allosomal genes, however the complex breeding strategies requires a large number of animals and therefore modern genetic techniques such as *in utero* electroporation or conditional gene deletion experiments might be more practical.

Most research on allosomal genes focuses on characterising hemizygous mutants as this most accurately replicates the disease model. However, analysis of heterozygous females will provide insight into protein function and can determine how the loss of the protein affects the system, for example whether the defects are cell autonomous or cell non-autonomous. The distinction between cell autonomous and cell non autonomous has implications for developing potential therapeutics, for example a cell non-autonomous defect can be alleviated by re-introducing the protein. Furthermore, investigating heterozygous females would help understand the phenotype of female carriers of X-linked mutations, for example females heterozygous for Fragile X syndrome have cognitive impairments (Hagerman & Connor, 2012). Allosomal disorders may affect female carriers because of skewed X-inactivation or because the hemizygous mutation is lethal, as in the case of Rett syndrome (Sirianni, Naidu, Pereira, Pillotto, & Hoffman, 1998). By studying heterozygous mutation of allosomal genes further insight can also be provided into female carriers, which has implications on screening, and identifying subtle phenotypes in a population that is as large as those carrying hemizygous mutations.

References

Abdo, W. F., Bloem, B. R., Van Geel, W. J., Esselink, R. a J., & Verbeek, M. M. (2007). CSF neurofilament light chain and tau differentiate multiple system atrophy from Parkinson's disease. *Neurobiology of aging*, *28*(5), 742–7.

Ackman, J. B., Burbridge, T. J., & Crair, M. C. (2012). Retinal waves coordinate patterned activity throughout the developing visual system. *Nature*, *490*(7419), 219–25.

Adams, J. P., & Sweatt, J. D. (2002). Molecular psychology: roles for the ERK MAP kinase cascade in memory. *Annual review of pharmacology and toxicology*, *42*(1), 135–63.

Agmon, A., Yang, L. T., O'Dowd, D. K., & Jones, E. G. (1993). Organized growth of thalamocortical axons from the deep tier of terminations into layer IV of developing mouse barrel cortex. *The Journal of neuroscience*, *13*(12), 5365–82.

Agmon, A., Yang, L. T., Jones, G., & O'Dowd, D. K. (1995). Topological precision in the thalamic projection to neonatal mouse barrel cortex. *The Journal of Neuroscience*, *15(1)*(January), 549–561.

Ahmari, S. E., Buchanan, J., & Smith, S. J. (2000). Assembly of presynaptic active zones from cytoplasmic transport packets. *Nature neuroscience*, *3*(5), 445–51.

Akaneya, Y., Sohya, K., Kitamura, A., Kimura, F., Washburn, C., Zhou, R., Ninan, I., et al. (2010). Ephrin-A5 and EphA5 interaction induces synaptogenesis during early hippocampal development. *PloS one*, *5*(8).

Al-Hallaq, R. a, Conrads, T. P., Veenstra, T. D., & Wenthold, R. J. (2007). NMDA di-heteromeric receptor populations and associated proteins in rat hippocampus. *The Journal of neuroscience*, *27*(31), 8334–43.

Anderson, S. A., Eisenstat, D. D., Shi, L., & Rubenstein, J. L. R. (1997). Interneuron Migration from Basal Forebrain to Neocortex: Dependence on Dlx Genes. *Science*, *278*(5337), 474–476.

Backer, S., Sakurai, T., Grumet, M., Sotelo, C., & Bloch-Gallego, E. (2002). NR-CAM and TAG-1 are expressed in distinct populations of developing precerebellar and cerebellar neurons. *Neuroscience*, *113*(4), 743–748.

Balaratnasingam, C., Morgan, W. H., Johnstone, V., Cringle, S. J., & Yu, D.-Y. (2009). Heterogeneous distribution of axonal cytoskeleton proteins in the human optic nerve. *Investigative ophthalmology & visual science*, *50*(6), 2824–38.

Baldi, a, Calia, E., Ciampini, a, Riccio, M., Vetuschi, a, Persico, a M., & Keller, F. (2000). Deafferentation-induced apoptosis of neurons in thalamic somatosensory nuclei of the newborn rat: critical period and rescue from cell death by peripherally applied neurotrophins. *The European journal of neuroscience*, *12*(7), 2281–90.

Ballester-Rosado, C. J., Albright, M. J., Wu, C.-S., Liao, C.-C., Zhu, J., Xu, J., Lee, L.-J., et al. (2010). mGluR5 in cortical excitatory neurons exerts both cell-autonomous and -nonautonomous influences on cortical somatosensory circuit formation. *The Journal of neuroscience, 30*(50), 16896–909.

Barr, M, L., & Bertram, E. . (1949). A morphological distinction between neurones of the male sna females and the behaviour of the nucleoprotein synthesis. *Nature*.

Barnett, M. W., Watson, R. F., & Kind, P. C. (2006). Pathways to Barrel Development. *Development and plasticity in ssensory thalamus and cortex* (pp. 138–157).

Barnett, M. W., Watson, R. F., Vitalis, T., Porter, K., Komiyama, N. H., Stoney, P. N., Gillingwater, T. H., et al. (2006). Synaptic Ras GTPase activating protein regulates pattern formation in the trigeminal system of mice. *The Journal of neuroscience*, *26*(5), 1355–65.

Barth, a L., & Malenka, R. C. (2001). NMDAR EPSC kinetics do not regulate the critical period for LTP at thalamocortical synapses. *Nature neuroscience*, *4*(3), 235–6.

Béïque, J.-C., Lin, D., Kang, M., Aizawa, H., Takamiya, K., Huganir, R. L., & Be, J. (2006). Synapse-specific regulation of AMPA receptor function by PSD-95. *PNAS*, *103*(51), 19535–19540.

Bjelke, B., & Seiger, A. (1989). Morphological distribution of MBP-like immunoreactivity in the brain during development. *International journal of developmental neuroscience*, *7*(2), 145–64.

Belmont, J. W. (1996). Genetic Control of X Inactivation and Processes Leading to X-Inactivation Skewing. *American journal of human genetics*, *58*, 1101–1108.

Benshalom, G., & White, E. L. (1986). Quantification of thalamocortical synapses with spiny stellate neurons in layer IV of mouse somatosensory cortex. *The Journal of comparative neurology*, *253*(3), 303–14.

Benson, D. L., Colman, D. R., & Huntley, G. W. (2001). Molecules, maps and synapse specificity. *Nature reviews. Neuroscience*, *2*(12), 899–909.

Bernardo, K. L., & Woolsey, T. A. (1987). Axonal trajectories between mouse somatosensory thalamus and cortex. *The Journal of comparative neurology*, *258*(4), 542–64.

Beneyto, M., & Meador-Woodruff, J. H. (2008). Lamina-specific abnormalities of NMDA receptor-associated postsynaptic protein transcripts in the prefrontal cortex in schizophrenia and bipolar disorder. *Neuropsychopharmacology, 33*(9), 2175–86.

Boeckers, T M, Kreutz, M. R., Winter, C., Zuschratter, W., Smalla, K. H., Sanmarti-Vila, L., Wex, H., et al. (1999). Proline-rich synapse-associated protein-1/cortactin binding protein 1 (ProSAP1/CortBP1) is a PDZ-domain protein highly enriched in the postsynaptic density. *The Journal of Neuroscience*, *19*(15), 6506.

Boeckers, Tobias M, Bockmann, J., Kreutz, M. R., & Gundelfinger, E. D. (2002). ProSAP/Shank proteins - a family of higher order organizing molecules of the postsynaptic density with an emerging role in human neurological disease. *Journal of neurochemistry*, *81*(5), 903–10.

Boda, B., Dubos, A., & Muller, D. (2010). Signaling mechanisms regulating synapse formation and function in mental retardation. *Current opinion in neurobiology*, *20*(4), 519–27.

Bozon, B., Kelly, A., Josselyn, S. a, Silva, A. J., Davis, S., & Laroche, S. (2003). MAPK, CREB and zif268 are all required for the consolidation of recognition memory. *Philosophical transactions of the Royal Society of London. Series B, Biological sciences*, *358*(1432), 805–14.

Brown, C. J., Ballaabio, A., Rupert, J. L., Lafreniere, R. G., Grompe, M., Tonlorenzi, R., & Willard, H. F. (1991). A gene from the region of the human X inactivation centre is expressed exclusively from the inactive X chromosome. *Nature*, *349*, 38–44.

Burman, K. J., Lui, L. L., Rosa, M. G. P., & Bourne, J. A. (2007). Development of non-phosphorylated neurofilament protein expression in neurones of the New World monkey dorsolateral frontal cortex. *The European journal of neuroscience*, *25*(6), 1767–79.

Cancedda, L., Putignano, E., Impey, S., Maffei, L., Ratto, G. M., & Pizzorusso, T. (2003). Patterned vision causes CRE-mediated gene expression in the visual cortex through PKA and ERK. *The Journal of neuroscience*, *23*(18), 7012–20.

Cabelli, R. J., Hohn, a, & Shatz, C. J. (1995). Inhibition of ocular dominance column formation by infusion of NT-4/5 or BDNF. *Science*, *267*(5204), 1662–6.

Cabelli, R. J., Shelton, D. L., Segal, R. a, & Shatz, C. J. (1997). Blockade of endogenous ligands of trkB inhibits formation of ocular dominance columns. *Neuron*, *19*(1), 63–76.

Carden, M. J., Trojanowski, J. Q., & Lee, M. (1987). Two-Stage Expression of Neurofilament Neurogenesis with Early Establishment Patterns Polypeptides During Rat of Adult Phosphorylation. *Neuroscience*.

Carlisle, H. J., Fink, A. E., Grant, S. G. N., & O'Dell, T. J. (2008). Opposing effects of PSD-93 and PSD-95 on long-term potentiation and spike timing-dependent plasticity. *The Journal of physiology*, *586*(Pt 24), 5885–900.

Caruana, G., & Bernstein, A. (2001). Craniofacial Dysmorphogenesis Including Cleft Palate in Mice with an Insertional Mutation in the discs large Gene Craniofacial Dysmorphogenesis Including Cleft Palate in Mice with an Insertional Mutation in the discs large Gene, *21*(5).

Cases, O., Vitalis, T., Seif, I., De Maeyer, E., Sotelo, C., & Gaspar, P. (1996). Lack of barrels in the somatosensory cortex of monoamine oxidase A-deficient mice: role of a serotonin excess during the critical period. *Neuron*, *16*(2), 297–307.

Catalano, S. M., Robertson, R. T., & Killackey, H. P. (1996). Individual axon morphology and thalamocortical topography in developing rat somatosensory cortex. *The Journal of comparative neurology*, *367*(1), 36–53.

Chalupa, L. M. (2009). Retinal waves are unlikely to instruct the formation of eye-specific retinogeniculate projections. *Neural development*, *4*, 25.

Chen, B.-S., Thomas, E. V, Sanz-Clemente, A., & Roche, K. W. (2011). NMDA receptor-dependent regulation of dendritic spine morphology by SAP102 splice variants. *The Journal of neuroscience : the official journal of the Society for Neuroscience*, *31*(1), 89–96.

Chen, H.-J., Rojas-Soto, M., Oguni, A., & Kennedy, M. B. (1998). A Synaptic Ras-GTPase Activating Protein (p135 SynGAP) Inhibited by CaM Kinase II. *Neuron*, *20*(5), 895–904.

Chen, L., Chetkovich, D. M., Petralia, R. S., Sweeney, N. T., Kawasaki, Y., Wenthold, R. J., Bredt, D. S., et al. (2000). Stargazin regulates synaptic targeting of AMPA receptors by two distinct mechanisms. *Nature*, *408*(6815), 936–43.

Cheng, H. J., Nakamoto, M., Bergemann, a D., & Flanagan, J. G. (1995). Complementary gradients in expression and binding of ELF-1 and Mek4 in development of the topographic retinotectal projection map. *Cell*, *82*(3), 371–81.

Chiaia, N. L., Fish, S. E., Bauer, W. R., Bennett-Clarke, C. a, & Rhoades, R. W. (1992). Postnatal blockade of cortical activity by tetrodotoxin does not disrupt the formation of vibrissa-related patterns in the rat's somatosensory cortex. *Brain research. Developmental brain research*, *66*(2), 244–50.

Chih, B., Engelman, H., & Scheiffele, P. (2005). Control of excitatory and inhibitory synapse formation by neuroligins. *Science*, *307*(5713), 1324–8.

Ching, G. Y., & Liem, R. K. (1993). Assembly of type IV neuronal intermediate filaments in nonneuronal cells in the absence of preexisting cytoplasmic intermediate filaments. *The Journal of cell biology*, *122*(6), 1323–35.

Ching, G. Y., & Liem, R. K. (1998). Roles of head and tail domains in alpha-internexin's self-assembly and coassembly with the neurofilament triplet proteins. *Journal of cell science*, *111 (Pt 3*, 321–33.

Cho, J. H., Lépine, M., Andrews, W., Parnavelas, J., & Cloutier, J.-F. (2007). Requirement for Slit-1 and Robo-2 in zonal segregation of olfactory sensory neuron axons in the main olfactory bulb. *The Journal of neuroscience*, *27*(34), 9094–104.

Clancy, B., Kersh, B., Hyde, J., Darlington, R. B., Anand, K. J. S., & Finlay, B. L. (2007). Web-Based Method for Translating Neurodevelopment From Laboratory Species to Humans, *00*.

Cline, H. (2005). Synaptogenesis: A Balancing Act between excitation and inhibition. *Current biology*, *15*(6), 203–205.

Clinton, S. M., & Meador-Woodruff, J. H. (2004). Abnormalities of the NMDA Receptor and Associated Intracellular Molecules in the Thalamus in Schizophrenia and Bipolar Disorder. *Neuropsychopharmacology : official publication of the American College of Neuropsychopharmacology*, *29*(7), 1353–62.

Colledge, M., Dean, R. a, Scott, G. K., Langeberg, L. K., Huganir, R. L., & Scott, J. D. (2000). Targeting of PKA to glutamate receptors through a MAGUK-AKAP complex. *Neuron*, *27*(1), 107–19.

Collins, M. O., Husi, H., Yu, L., Brandon, J. M., Anderson, C. N. G., Blackstock, W. P., Choudhary, J. S., et al. (2006). Molecular characterization and comparison of the components and multiprotein complexes in the postsynaptic proteome. *Journal of neurochemistry*, *97*(Suppl 1), 16–23.

Constantinescu, R., Romer, M., Oakes, D., Rosengren, L., & Kieburtz, K. (2009). Levels of the light subunit of neurofilament triplet protein in cerebrospinal fluid in Huntington's disease. *Parkinsonism & related disorders*, *15*(3), 245–8.

Cook, D. J., Teves, L., & Tymianski, M. (2012). Treatment of stroke with a PSD-95 inhibitor in the gyrencephalic primate brain. *Nature*, *483*(7388), 213–7.

Cooper, N. G., & Steindler, D. a. (1986). Lectins demarcate the barrel subfield in the somatosensory cortex of the early postnatal mouse. *The Journal of comparative neurology*, *249*(2), 157–69.

Couillard-Després, S., Zhu, Q., Wong, P. C., Price, D. L., Cleveland, D. W., & Julien, J. P. (1998). Protective effect of neurofilament heavy gene overexpression in motor neuron disease induced by mutant superoxide dismutase. *Proceedings of the National Academy of Sciences of the United States of America*, *95*(16), 9626–30.

Côté, F., Collard, J. F., & Julien, J. P. (1993). Progressive neuronopathy in transgenic mice expressing the human neurofilament heavy gene: a mouse model of amyotrophic lateral sclerosis. *Cell*, *73*(1), 35–46.

Crair, M. C., Gillespie, D.C., & Stryker, M.P. (1998). The Role of Visual Experience in the Development of Columns in Cat Visual Cortex. *Science*, *279*(5350), 566–570.

Crair, Michael C, & Malenka, R. C. (1995). A critical period for long-term potentiation at thalamocortical synapses.

Cui, H., Hayashi, A., Sun, H.-S., Belmares, M. P., Cobey, C., Phan, T., Schweizer, J., et al. (2007). PDZ protein interactions underlying NMDA receptor-mediated excitotoxicity and neuroprotection by PSD-95 inhibitors. *The Journal of neuroscience : the official journal of the Society for Neuroscience*, *27*(37), 9901–15.

Cuthbert, P. (2005). *The role of synapse-associated protein 102 in postsynaptic signalling , synaptic plasticity and learning*. *Philosophy*. University of Cambridge.

Cuthbert, P. C., Stanford, L. E., Coba, M. P., Ainge, J. a, Fink, A. E., Opazo, P., Delgado, J. Y., et al. (2007). Synapse-associated protein 102/dlgh3 couples the NMDA receptor to specific plasticity pathways and learning strategies. *The Journal of neuroscience : the official journal of the Society for Neuroscience*, *27*(10), 2673–82.

Dahl, D. (1983). Immunohistochemical differences between neurofilaments in perikarya, dendrites and axons. Immunofluorescence study with antisera raised to neurofilament polypeptides (200K, 150K, 70K) isolated by anion exchange chromatography. *Experimental cell research*, *149*(2), 397–408.

Dahl, D. (1988). Early and late appearance of neurofilament phosphorylated epitopes in rat nervous system development: in vivo and in vitro study with monoclonal antibodies. *Journal of neuroscience research*, *20*(4), 431–41.

Dahl, D., & Bignami, A. (1986). Neurofilament Phosphorylation. *Experimental Cell Research*, *162*(1), 220–230.

Dahl, D., Crosby, C. J., Gardner, E. E., & Bignami, a. (1986). Delayed phosphorylation of the largest neurofilament protein in rat optic nerve development. *Journal of neuroscience research*, *15*(4), 513–9.

Dale, J. M., & Garcia, M. L. (2012). Neurofilament Phosphorylation during Development and Disease: Which Came First, the Phosphorylation or the Accumulation? *Journal of amino acids*, *2012*, 382107.

Dailey, E., & Smith, S. J. (1996). The Dynamics of Dendritic Hippocampal Slices Structure in Developing hippocampal slices. *The journal of Neuroscience*, *76*(9), 2983–2994.

Dakoji, S., Tomita, S., Karimzadegan, S., Nicoll, R. a., & Bredt, D. S. (2003). Interaction of transmembrane AMPA receptor regulatory proteins with multiple membrane associated guanylate kinases. *Neuropharmacology*, *45*(6), 849–856.

Dalva, M. B., Takasu, M. a, Lin, M. Z., Shamah, S. M., Hu, L., Gale, N. W., & Greenberg, M. E. (2000). EphB receptors interact with NMDA receptors and regulate excitatory synapse formation. *Cell*, *103*(6), 945–56.

Datwani, A., Iwasto, T., Itohara, S., & Erzurumlu, R. (2002). NMDA Receptor-Dependent Pattern Transfer from Afferents to Postsynaptic Cells and Dendritic Differentiation in the Barrel Cortex. *Molecular and Cellular Neuroscience*, *21*(3), 477–492.

Davey, F., Hill, M., Falk, J., Sans, N., & Gunn-Moore, F. J. (2005). Synapse associated protein 102 is a novel binding partner to the cytoplasmic terminus of neurone-glial related cell adhesion molecule. *Journal of neurochemistry*, *94*(5), 1243–53.

Daw, M. I., Bannister, N. V, & Isaac, J. T. R. (2006). Rapid, activity-dependent plasticity in timing precision in neonatal barrel cortex. *The Journal of neuroscience*, *26*(16), 4178–87.

Daw, M. I., Scott, H. L., & Isaac, J. T. R. (2007). Developmental synaptic plasticity at the thalamocortical input to barrel cortex: mechanisms and roles. *Molecular and cellular neurosciences*, *34*(4), 493–502.

De Felipe, J., Marco, P., Fairén, a, & Jones, E. G. (1997). Inhibitory synaptogenesis in mouse somatosensory cortex. *Cerebral cortex*, *7*(7), 619–34.

Deng, Y., Li, B., Liu, F., Iqbal, K., Grundke-Iqbal, I., Brandt, R., & Gong, C.-X. (2008). Regulation between O-GlcNAcylation and phosphorylation of neurofilament-M and their dysregulation in Alzheimer disease. *FASEB journal*, *22*(1), 138–45.

Di Cristo, G., Berardi, N., Cancedda, L., Pizzorusso, T., Putignano, E., Ratto, G. M., & Maffei, L. (2001). Requirement of ERK activation for visual cortical plasticity. *Science*, *292*(5525), 2337–40.

Diamond, M. E., Armstrong-James, M., & Ebner, F. F. (1992). Somatic sensory responses in the rostral sector of the posterior group (POm) and in the ventral posterior medial nucleus (VPM) of the rat thalamus. *The Journal of comparative neurology*, *318*(4), 462–76.

Doetsch, F., & Alvarez-Buylla, a. (1996). Network of tangential pathways for neuronal migration in adult mammalian brain. *Proceedings of the National Academy of Sciences of the United States of America*, *93*(25), 14895–900.

Duffy, K. R., & Livingstone, M. S. (2003). Distribution of non-phosphorylated neurofilament in squirrel monkey V1 is complementary to the pattern of cytochrome-oxidase blobs. *Cerebral cortex*, *13*(7), 722–7.

Duffy, K. R., & Livingstone, M. S. (2005). Loss of neurofilament labeling in the primary visual cortex of monocularly deprived monkeys. *Cerebral cortex*, *15*(8), 1146–54.

Dufour, A., Seibt, J., Passante, L., Depaepe, V., Ciossek, T., Frisén, J., Kullander, K., et al. (2003). Area specificity and topography of thalamocortical projections are controlled by ephrin/Eph genes. *Neuron*, *39*(3), 453–65.

El-Husseini, a E., Topinka, J. R., Lehrer-Graiwer, J. E., Firestein, B. L., Craven, S. E., Aoki, C., & Bredt, D. S. (2000). Ion channel clustering by membrane-associated guanylate kinases. Differential regulation by N-terminal lipid and metal binding motifs. *The Journal of biological chemistry*, *275*(31), 23904–10.

Elias, G M, Elias, L. A. B., Apostolides, P. F., Kriegstein, A. R., & Nicoll, R. A. (2008). Differential trafficking of AMPA and NMDA receptors by SAP102 and PSD-95 underlies, *105*(52), 20953–20958.

Elias, Guillermo M, Funke, L., Stein, V., Grant, S. G., Bredt, D. S., & Nicoll, R. A. (2006). Synapse-specific and developmentally regulated targeting of AMPA receptors by a family of MAGUK scaffolding proteins. *Neuron*, *52*(2), 307–20.

Elias, Guillermo M, & Nicoll, R. a. (2007). Synaptic trafficking of glutamate receptors by MAGUK scaffolding proteins. *Trends in cell biology*, *17*(7), 343–52.

Emes, R. D., Pocklington, A. J., Anderson, C. N. G., Bayes, A., Collins, M. O., Vickers, C. a, Croning, M. D. R., et al. (2008). Evolutionary expansion and anatomical specialization of synapse proteome complexity. *Nature neuroscience*, *11*(7), 799–806.

Erzurumlu, R S, & Jhaveri, S. (1990). Thalamic axons confer a blueprint of the sensory periphery onto the developing rat somatosensory cortex. *Brain research. Developmental brain research*, *56*(2), 229–34.

Erzurumlu, R S, & Kind, P. C. (2001). Neural activity: sculptor of “barrels” in the neocortex. *Trends in neurosciences*, *24*(10), 589–95.

Erzurumlu, Reha S, & Gaspar, P. (2012). Development and critical period plasticity of the barrel cortex. *The European journal of neuroscience*, *35*(10), 1540–53.

Espinosa, J. S., & Stryker, M. P. (2012). Development and plasticity of the primary visual cortex. *Neuron*, *75*(2), 230–49.

Espinosa, J. S., Wheeler, D. G., Tsien, R. W., & Luo, L. (2009). Uncoupling dendrite growth and patterning: single-cell knockout analysis of NMDA receptor 2B. *Neuron*, *62*(2), 205–17.

Ethell, I. M., & Pasquale, E. B. (2005). Molecular mechanisms of dendritic spine development and remodeling. *Progress in neurobiology*, *75*(3), 161–205.

Farr, C. D., Gafken, P. R., Norbeck, A. D., Doneanu, C. E., Stapels, M. D., Barofsky, D. F., Minami, M., et al. (2004). Proteomic analysis of native metabotropic glutamate receptor 5 protein complexes reveals novel molecular constituents. *Journal of neurochemistry*, *91*(2), 438–50.

Feldman, D E, Nicoll, R. a, Malenka, R. C., & Isaac, J. T. (1998). Long-term depression at thalamocortical synapses in developing rat somatosensory cortex. *Neuron*, *21*(2), 347–57.

Feldman, Daniel E. (2009). Synaptic mechanisms for plasticity in neocortex. *Annual review of neuroscience*, *32*, 33–55.

Feller, M. (2012). Cortical development: the sources of spontaneous patterned activity. *Current biology : CB*, *22*(3), R89–91.

Feller, M. B. (2009). Retinal waves are likely to instruct the formation of eye-specific retinogeniculate projections. *Neural development*, *4*, 24.

Fernyhough, P., Gallagher, a, Averill, S. a, Priestley, J. V, Hounsom, L., Patel, J., & Tomlinson, D. R. (1999). Aberrant neurofilament phosphorylation in sensory neurons of rats with diabetic neuropathy. *Diabetes*, *48*(4), 881–9.

Fiala, J C, Feinberg, M., Popov, V., & Harris, K. M. (1998). Synaptogenesis via dendritic filopodia in developing hippocampal area CA1. *The Journal of neuroscience : the official journal of the Society for Neuroscience*, *18*(21), 8900–11.

Fiala, John C, Spacek, J., & Harris, K. M. (2002). Dendritic spine pathology: cause or consequence of neurological disorders? *Brain research. Brain research reviews*, *39*(1), 29–54.

Fischer, M., Kaech, S., Knutti, D., & Matus, a. (1998). Rapid actin-based plasticity in dendritic spines. *Neuron*, *20*(5), 847–54.

Fiumelli, H., Riederer, I. M., Martin, J.-L., & Riederer, B. M. (2008). Phosphorylation of neurofilament subunit NF-M is regulated by activation of NMDA receptors and modulates cytoskeleton stability and neuronal shape. *Cell motility and the cytoskeleton*, *65*(6), 495–504.

Fox, K. (2008). *Barrel Cortex*. Cambridge: Cambridge University Press.

Fox, Kevin. (1992). A Critical Period for Experience-dependent Barrel Cortex Synaptic Plasticity in Rat. *Science*, *12*(5), 1626–1636.

Fox, K., Schlaggar, B. L., Glazewski, S., & O'Leary, D. D. (1996). Glutamate receptor blockade at cortical synapses disrupts development of thalamocortical and columnar organization in somatosensory cortex. *Proceedings of the National Academy of Sciences of the United States of America*, *93*(11), 5584–9.

Fukaya, M., Ueda, H., Yamauchi, K., Inoue, Y., & Watanabe, M. (1999). Distinct spatiotemporal expression of mRNAs for the PSD-95/SAP90 protein family in the mouse brain. *Neuroscience research*, *33*(2), 111–8.

Fukuchi-Shimogori, T., & Grove, E. a. (2001). Neocortex patterning by the secreted signaling molecule FGF8. *Science*, *294* (5544), 1071–4.

Gallagher, S. M., Daly, C. a, Bear, M. F., & Huber, K. M. (2004). Extracellular signal-regulated protein kinase activation is required for metabotropic glutamate receptor-dependent long-term depression in hippocampal area CA1. *The Journal of neuroscience*, *24*(20), 4859–64.

Galvez, R., & Greenough, W. T. (2005). Sequence of abnormal dendritic spine development in primary somatosensory cortex of a mouse model of the fragile X mental retardation syndrome. *American journal of medical genetics. Part A*, *135*(2), 155–60.

Gardoni, F., Marcello, E., & Di Luca, M. (2009). Postsynaptic density-membrane associated guanylate kinase proteins (PSD-MAGUKs) and their role in CNS disorders. *Neuroscience*, *158*(1), 324–33.

Gerrow, K., Romorini, S., Nabi, S. M., Colicos, M. a, Sala, C., & El-Husseini, A. (2006). A preformed complex of postsynaptic proteins is involved in excitatory synapse development. *Neuron*, *49*(4), 547–62.

Geisler, N., & Weber, K. (1981). Self-assembly of the 68,000 molecular weight component of the mammalian neurofilament triplet proteins into intermediate-sized filaments. *Journal of Molecular Biology*, *151*(3), 565–571.

Giasson, B. I., & Mushynski, W. E. (1997). Developmentally regulated stabilization of neuronal intermediate filaments in rat cerebral cortex. *Neuroscience letters*, *229*(2), 77–80.

Goldman, J. E. ., Yen, S.-H., Chiu, F.-C., & Peress, N. S. (1983). Lewy Bodies of Parkinson's Disease Contain Neurofilament Antigens, *221*(4615), 1082–1084.

Grant, S. G. N. (2012). Synaptopathies: diseases of the synaptome. *Current opinion in neurobiology*, *22*(3), 522–9.

Grant, S. G. N., Marshall, M. C., Page, K.-L., Cumiskey, M. A, & Armstrong, J. D. (2005). Synapse proteomics of multiprotein complexes: en route from genes to nervous system diseases. *Human molecular genetics*, *14 Spec No*(2), R225–34.

Gresle, M. M., Butzkueven, H., & Shaw, G. (2011). Neurofilament proteins as body fluid biomarkers of neurodegeneration in multiple sclerosis. *Multiple sclerosis international*, *2011*, 315406.

Grossman, A. W., Elisseou, N. M., McKinney, B. C., & Greenough, W. T. (2006). Hippocampal pyramidal cells in adult Fmr1 knockout mice exhibit an immature-appearing profile of dendritic spines. *Brain research*, *1084*(1), 158–64.

Gu, J., Firestein, B. L., & Zheng, J. Q. (2008). Microtubules in dendritic spine development. *The Journal of neuroscience*, *28*(46), 12120–4.

Gu, Y., & Stornetta, R. L. (2007). Synaptic plasticity, AMPA-R trafficking, and Ras-MAPK signaling. *Acta pharmacologica Sinica*, *28*(7), 928–36.

Gylys, K. H., Fein, J. a., Yang, F., Wiley, D. J., Miller, C. a., & Cole, G. M. (2004). Synaptic Changes in Alzheimer's Disease. *The American Journal of Pathology*, *165*(5), 1809–1817.

Hagerman, J., & Connor, O. (2012). Girls With Fragile X Syndrome : Physical and Neurocognitive Status and Outcome Randi J . Hagerman , Carey Jackson , Khaled Amiri , Rebecca O' Connor, William Sobesky and Amy Cronister Silverman

Hamasaki, T., Leingärtner, A., Ringstedt, T., & O'Leary, D. D. M. (2004). EMX2 regulates sizes and positioning of the primary sensory and motor areas in neocortex by direct specification of cortical progenitors. *Neuron*, *43*(3), 359–72.

Hamdan, F. F., Daoud, H., Piton, A., Gauthier, J., Dobrzeniecka, S., Krebs, M.-O., Joober, R., et al. (2011). De novo SYNGAP1 mutations in nonsyndromic intellectual disability and autism. *Biological psychiatry*, *69*(9), 898–901.

Hannan, A. J., Blakemore, C., Katsnelson, A., Vitalis, T., Huber, K. M., Bear, M., Roder, J., et al. (2001). PLC-beta1, activated via mGluRs, mediates activity-dependent differentiation in cerebral cortex. *Nature neuroscience*, *4*(3), 282–288.

Hanganu, I. L., Kilb, W., & Luhmann, H. J. (2002). Functional synaptic projections onto subplate neurons in neonatal rat somatosensory cortex. *The Journal of neuroscience*, *22*(16), 7165–76.

Harlow, E. G., Till, S. M., Russell, T. a, Wijetunge, L. S., Kind, P., & Contractor, A. (2010). Critical period plasticity is disrupted in the barrel cortex of FMR1 knockout mice. *Neuron*, *65*(3), 385–98.

Harms, K. J., & Dunaevsky, A. (2007). Dendritic spine plasticity: looking beyond development. *Brain research*, *1184*, 65–71.

Harris, K. M., Jensen, F. E., & Tsao, B. (1992). Three-dimensional structure of dendritic spines and synapses in rat hippocampus (CA1) at postnatal day 15 and adult ages: implications for the maturation of synaptic physiology and long-term potentiation. *The Journal of neuroscience*, *12*(7), 2685–705.

Harris, K. M., & Stevens, J. K. (1989). Dendritic spines of CA 1 pyramidal cells in the rat hippocampus: serial electron microscopy with reference to their biophysical characteristics. *The Journal of neuroscience*, *9*(8), 2982–97.

Harris, R. M., & Woolsey, T. A. (1979). Morphology of Golgi-impregnated neurons in mouse cortical barrels following vibrissae damage at different post-natal ages. *Brain research*, *161*, 143–149.

Heard, E. (2004). Recent advances in X-chromosome inactivation. *Current opinion in cell biology*, *16*(3), 247–55.

Heard, E., & Disteche, C. M. (2006). Dosage compensation in mammals: fine-tuning the expression of the X chromosome. *Genes & development*, *20*(14), 1848–67.

Hebb, D. (1949). *The organisation of Behaviour*. New York: John Wiley and Sons.

Hensch, T. K. (2004). Critical period regulation. *Annual review of neuroscience*, *27*, 549–79. d

Hering, H., & Sheng, M. (2001). Dendritic spines: structure, dynamics and regulation. *Nature reviews. Neuroscience*, *2*(12), 880–8.

Hersch, S. M., & White, E. L. (1981). Thalamocortical synapses involving identified neurons in mouse primary somatosensory cortex: a terminal degeneration and golgi/EM study. *The Journal of comparative neurology*, *195*(2), 253–63.

Hevner, R. F., Daza, R. a M., Englund, C., Kohtz, J., & Fink, a. (2004). Postnatal shifts of interneuron position in the neocortex of normal and reeler mice: evidence for inward radial migration. *Neuroscience*, *124*(3), 605–18.

Hindges, R., McLaughlin, T., Genoud, N., Henkemeyer, M., & O'Leary, D. D. M. (2002). EphB forward signaling controls directional branch extension and arborization required for dorsal-ventral retinotopic mapping. *Neuron*, *35*(3), 475–87.

Hirokawa, N., Glicksman, M. A., & Willard, M. B. (1984). Organization of mammalian neurofilament polypeptides within the neuronal cytoskeleton. *The Journal of cell biology*, *98*(4), 1523–36.

Ho, W., Uniyal, S., Meakin, S. O., Morris, V. L., & Chan, B. M. (2001). A differential role of extracellular signal-regulated kinase in stimulated PC12 pheochromocytoma cell movement. *Experimental cell research*, *263*(2), 254–64.

Hoffman, P. N., & Lasek, R. (1975). THE SLOW COMPONENT OF AXONAL TRANSPORT: Identification of Major Structural Polypeptides of the Axon and Their Generality among Mammalian Neurons. *Journal of Cell Biology*, *66*, 351–366.

Hoogenraad, C. C., & Sheng, M. (2003). The return of the exocyst. *Nature cell biology*, *5*(6), 493–5.

Horton, J. C., & Hocking, D. R. (1996). An adult-like pattern of ocular dominance columns in striate cortex of newborn monkeys prior to visual experience. *The Journal of neuroscience : the official journal of the Society for Neuroscience*, *16*(5), 1791–807.

Howard, M. a, Elias, G. M., Elias, L. a B., Swat, W., & Nicoll, R. a. (2010). The role of SAP97 in synaptic glutamate receptor dynamics. *Proceedings of the National Academy of Sciences of the United States of America*, *107*(8), 3805–10.

Hubel, D. H., Wiesel, T. N., & LeVay, S. (1977). Plasticity of ocular dominance columns in the monkey stirate cortex. *Philosophical transactions of the Royal Society of London. Series B, Biological sciences*, *278*, 377–409.

Husi, H., Ward, M. a, Choudhary, J. S., Blackstock, W. P., & Grant, S. G. (2000). Proteomic analysis of NMDA receptor-adhesion protein signaling complexes. *Nature neuroscience*, *3*(7), 661–9.

Hsu, S. C., Hazuka, C. D., Foletti, D. L., & Scheller, R. H. (1999). Targeting vesicles to specific sites on the plasma membrane: the role of the sec6/8 complex. *Trends in cell biology*, *9*(4), 150–3.

Imai, T., Suzuki, M., & Sakano, H. (2006). Odorant receptor-derived cAMP signals direct axonal targeting. *Science*, *314*(5799), 657–61.

Isaac, J. (2003). Postsynaptic silent synapses: evidence and mechanisms. *Neuropharmacology*, *45*(4), 450–460.

Isaac, J. T., Crair, M. C., Nicoll, R. a, & Malenka, R. C. (1997). Silent synapses during development of thalamocortical inputs. *Neuron*, *18*(2), 269–80.

Itami, C., Mizuno, K., Kohno, T., & Nakamura, S. (2000). Brain-derived neurotrophic factor requirement for activity-dependent maturation of glutamatergic synapse in developing mouse somatosensory cortex. *Brain research*, *857*(1-2), 141–50.

Iwasato, T, Datwani, a, Wolf, a M., Nishiyama, H., Taguchi, Y., Tonegawa, S., Knöpfel, T., et al. (2000). Cortex-restricted disruption of NMDAR1 impairs neuronal patterns in the barrel cortex. *Nature*, *406*(6797), 726–31.

Iwasato, Takuji, Inan, M., Kanki, H., Erzurumlu, R. S., Itohara, S., & Crair, M. C. (2008). Cortical adenylyl cyclase 1 is required for thalamocortical synapse maturation and aspects of layer IV barrel development. *The Journal of neuroscience*, *28*(23), 5931–43.

Jaworski, J., Kapitein, L. C., Gouveia, S. M., Dortland, B. R., Wulf, P. S., Grigoriev, I., Camera, P., et al. (2009). Dynamic microtubules regulate dendritic spine morphology and synaptic plasticity. *Neuron*, *61*(1), 85–100.

Julien, J. P. (1997). Neurofilaments and motor neuron disease. *Trends in cell biology*, *7*(6), 243–9.

Julien, J. P. (1999). Neurofilament functions in health and disease. *Current opinion in neurobiology*, *9*(5), 554–60.

Julien, J. P., & Mushynski, W. E. (1982). Multiple phosphorylation sites in mammalian neurofilament polypeptides. *The Journal of biological chemistry*, *257*(17), 10467–70.

Kaeser, P. S., Deng, L., Wang, Y., Dulubova, I., Liu, X., Rizo, J., & Südhof, T. C. (2011). RIM proteins tether Ca2+ channels to presynaptic active zones via a direct PDZ-domain interaction. *Cell*, *144*(2), 282–95.

Kanold, P. O., & Luhmann, H. J. (2010). The subplate and early cortical circuits. *Annual review of neuroscience*, *33*, 23–48.

Kaplan, M. P., Chin, S. S., Fliegner, K. H., & Liem, R. K. (1990). Alpha-internexin, a novel neuronal intermediate filament protein, precedes the low molecular weight neurofilament protein (NF-L) in the developing rat brain. *The Journal of neuroscience*, *10*(8), 2735–48.

Kennedy, T. E., Wang, H., Marshall, W., & Tessier-Lavigne, M. (2006). Axon guidance by diffusible chemoattractants: a gradient of netrin protein in the developing spinal cord. *The Journal of neuroscience : the official journal of the Society for Neuroscience*, *26*(34), 8866–74.

Kidd, F. L., & Isaac, J. T. (1999). Developmental and activity-dependent regulation of kainate receptors at thalamocortical synapses. *Nature*, *400*(6744), 569–73.

Kim, E., & Sheng, M. (2004). PDZ domain proteins of synapses. *Nature reviews. Neuroscience*, *5*(10), 771–81.

Kim, J. H., Lee, H.-K., Takamiya, K., & Huganir, R. L. (2003). The role of synaptic GTPase-activating protein in neuronal development and synaptic plasticity. *The Journal of neuroscience*, *23*(4), 1119–24.

Kim, J. H., Liao, D., Lau, L., & Huganir, R. L. (1998). SynGAP: a Synaptic RasGAP that Associates with the PSD-95 / SAP90 Protein Family. *Cell*, *20*, 683–691.

Kim, E, Naisbitt, S., Hsueh, Y. P., Rao, a, Rothschild, a, Craig, a M., & Sheng, M. (1997). GKAP, a novel synaptic protein that interacts with the guanylate kinase-like domain of the PSD-95/SAP90 family of channel clustering molecules. *The Journal of cell biology*, *136*(3), 669–78.

Kind, P. C., & Neumann, P. E. (2001). Plasticity: downstream of glutamate. *Trends in neurosciences*, *24*(10), 553–5.

Kleinfeld, D., & Deschênes, M. (2011). Neuronal basis for object location in the vibrissa scanning sensorimotor system. *Neuron*, *72*(3), 455–68.

Knott, G. W., Holtmaat, A., Wilbrecht, L., Welker, E., & Svoboda, K. (2006). Spine growth precedes synapse formation in the adult neocortex in vivo. *Nature neuroscience*, *9*(9), 1117–24.

Komiyama, N. H., Watabe, A. M., Carlisle, H. J., Porter, K., Charlesworth, P., Monti, J., Strathdee, D. J. C., et al. (2002). SynGAP Regulates ERK / MAPK Signaling , Synaptic Plasticity , and Learning in the Complex with Postsynaptic Density 95 and NMDA Receptor. *Currents*, *22*(22), 9721–9732.

Koralek, K. a, Jensen, K. F., & Killackey, H. P. (1988). Evidence for two complementary patterns of thalamic input to the rat somatosensory cortex. *Brain research*, *463*(2), 346–51.

Korkotian, E., & Segal, M. (2000). Structure-function relations in dendritic spines: is size important? *Hippocampus*, *10*(5), 587–95.

Krapivinsky, G., Medina, I., Krapivinsky, L., Gapon, S., & Clapham, D. E. (2004). SynGAP-MUPP1-CaMKII Synaptic Complexes Regulate p38 MAP Kinase Activity and NMDA Receptor- Dependent Synaptic AMPA Receptor Potentiation. *Neuron*, *43*, 563–574.

Kristiansen, L. V, & Meador-Woodruff, J. H. (2005). Abnormal striatal expression of transcripts encoding NMDA interacting PSD proteins in schizophrenia, bipolar disorder and major depression. *Schizophrenia research*, *78*(1), 87–93.

Kutsuwada, T., Sakimura, K., Manabe, T., Takayama, C., Katakura, N., Kushiya, E., Natsume, R., et al. (1996). Impairment of suckling response, trigeminal neuronal pattern formation, and hippocampal LTD in NMDA receptor epsilon 2 subunit mutant mice. *Neuron*, *16*(2), 333–44.

Lau, L. F., Mammen, a, Ehlers, M. D., Kindler, S., Chung, W. J., Garner, C. C., & Huganir, R. L. (1996). Interaction of the N-methyl-D-aspartate receptor complex with a novel synapse-associated protein, SAP102. *The Journal of biological chemistry*, *271*(35), 21622–8.

Lavedan, C., Buchholtz, S., Nussbaum, R. L., Albin, R. L., & Polymeropoulos, M. H. (2002). A mutation in the human neurofilament M gene in Parkinson's disease that suggests a role for the cytoskeleton in neuronal degeneration. *Neuroscience Letters*, *322*(1), 57–61.

Lavenex, P., Lavenex, P. B., & Amaral, D. G. (2004). Nonphosphorylated high-molecular-weight neurofilament expression suggests early maturation of the monkey subiculum. *Hippocampus*, *14*(7), 797–801.

Lee, L.-J., Chen, W.-J., Chuang, Y.-W., & Wang, Y.-C. (2009). Neonatal whisker trimming causes long-lasting changes in structure and function of the somatosensory system. *Experimental neurology*, *219*(2), 524–32.

Lee, J. T., Davidow, L. S., & Warshawsky, D. (1999). Tsix, a gene antisense to Xist at the X-inactivation centre. *Nature genetics*, *21*(4), 400–4.

Lee, L.-J., Iwasato, T., Itohara, S., & Erzurumlu, R. S. (2005). Exuberant thalamocortical axon arborization in cortex-specific NMDAR1 knockout mice. *The Journal of comparative neurology*, *485*(4), 280–92.

Lee, L.-J., & Erzurumlu, R. S. (2005). Altered parcellation of neocortical somatosensory maps in N-methyl-D-aspartate receptor-deficient mice. *The Journal of comparative neurology*, *485*(1), 57–63.

Lee, L.-J., Iwasato, T., Itohara, S., & Erzurumlu, R. S. (2005). Exuberant thalamocortical axon arborization in cortex-specific NMDAR1 knockout mice. *The Journal of comparative neurology*, *485*(4), 280–92.

Lee, M. K., Xu, Z., Wong, P. C., & Cleveland, D. W. (1993). Neurofilaments are obligate heteropolymers in vivo. *The Journal of Cell Biology*, *122*(6), 1337–1350.

Lee, V. M., Carden, M. J., Schlaepfer, W. W., & Trojanowski, J. Q. (1987). Monoclonal antibodies distinguish several differentially phosphorylated states of the two largest rat neurofilament subunits (NF-H and NF-M) and demonstrate their existence in the normal nervous system of adult rats. *The Journal of neuroscience*, *7*(11), 3474–88.

Leonard, A. S., Davare, M. A., Horne, M. C., Garner, C. C., & Hell, J. W. (1998). SAP97 Is Associated with the alpha-Amino-3-hydroxy-5-methylisoxazole- 4-propionic Acid Receptor GluR1 Subunit. *The Journal of biological chemistry*, *273*(31), 19518–19524.

LeVay, S., Wiesel, T. N., & Hubel, D. H. (1980). The development of ocular dominance columns in normal and visually deprived monkeys. *The Journal of comparative neurology*, *191*(1), 1–51. 2

Levelt, C. N., & Hübener, M. (2012). Critical-period plasticity in the visual cortex. *Annual review of neuroscience*, *35*, 309–30.

Li, Y., Erzurumlu, R. S., Chen, C., Jhaveri, S., & Tonegawa, S. (1994). Whisker-related neuronal patterns fail to develop in the trigeminal brainstem nuclei of NMDAR1 knockout mice. *Cell*, *76*(3), 427–37.

Li, W., Okano, A., Tian, Q. B., Nakayama, K., Furihata, T., Nawa, H., & Suzuki, T. (2001). Characterization of a novel synGAP isoform, synGAP-beta. *The Journal of biological chemistry*, *276*(24), 21417–24.

Liguz-Lecznar, M., & Skangiel-Kramska, J. (2007). Vesicular glutamate transporters VGLUT1 and VGLUT2 in the developing mouse barrel cortex. *International journal of developmental neuroscience*, *25*(2), 107–14.

Linke, R., Soriano, E., & Frotscher, M. (1994). Transient dendritic appendages on differentiating septohippocampal neurons are not the sites of synaptogenesis. *Brain research. Developmental brain research*, *83*(1), 67–78.

Liu, Y., Dyck, R., & Cynader, M. (1994). The correlation between cortical neuron maturation and neurofilament phosphorylation: a developmental study of phosphorylated 200 kDa neurofilament protein in cat visual cortex. *Brain research. Developmental brain research*, *81*(2), 151–61.

Lu, H. C., Gonzalez, E., & Crair, M. C. (2001). Barrel cortex critical period plasticity is independent of changes in NMDA receptor subunit composition. *Neuron*, *32*(4), 619–34.

Lush, M. E., Ma, L., & Parada, L. F. (2005). TrkB signaling regulates the developmental maturation of the somatosensory cortex. *International journal of developmental neuroscience : the official journal of the International Society for Developmental Neuroscience*, *23*(6), 523–36.

Lycke, J. N., Karlsson, J. E., Andersen, O., & Rosengren, L. E. (1998). Neurofilament protein in cerebrospinal fluid: a potential marker of activity in multiple sclerosis. *Journal of neurology, neurosurgery, and psychiatry*, *64*(3), 402–4.

Ma, P. M. (1991). The barrelettes--architectonic vibrissal representations in the brainstem trigeminal complex of the mouse. I. Normal structural organization. *The Journal of comparative neurology*, *309*(2), 161–99.

Makino, K., Kuwahara, H., Masuko, N., Nishiyama, Y., Morisaki, T., Sasaki, J., Nakao, M., et al. (1997). Cloning and characterization of NE-dlg: a novel human homolog of the Drosophila discs large (dlg) tumor suppressor protein interacts with the APC protein. *Oncogene*, *14*(20), 2425–33.

Malinow, R. (2003). AMPA receptor trafficking and long-term potentiation. *Philosophical transactions of the Royal Society of London. Series B, Biological sciences*, *358*(1432), 707–14.

Marín, O., & Rubenstein, J. L. (2001). A long, remarkable journey: tangential migration in the telencephalon. *Nature reviews. Neuroscience*, *2*(11), 780–90.

McCullumsmith, R. E., Kristiansen, L. V, Beneyto, M., Scarr, E., Dean, B., & Meador-Woodruff, J. H. (2007). Decreased NR1, NR2A, and SAP102 transcript expression in the hippocampus in bipolar disorder. *Brain research*, *1127*(1), 108–18.

McMahon, a C., Barnett, M. W., O'Leary, T. S., Stoney, P. N., Collins, M. O., Papadia, S., Choudhary, J. S., et al. (2012). SynGAP isoforms exert opposing effects on synaptic strength. *Nature communications*, *3*(may), 900.

Mersiyanova, I. V, Perepelov, a V, Polyakov, a V, Sitnikov, V. F., Dadali, E. L., Oparin, R. B., Petrin, a N., et al. (2000). A new variant of Charcot-Marie-Tooth disease

type 2 is probably the result of a mutation in the neurofilament-light gene. *American journal of human genetics*, *67*(1), 37–46.

Meister, M., Wong, R. O., Baylor, D. a, & Shatz, C. J. (1991). Synchronous bursts of action potentials in ganglion cells of the developing mammalian retina. *Science (New York, N.Y.)*, *252*(5008), 939–43.

Mellott, J. G., Van der Gucht, E., Lee, C. C., Carrasco, A., Winer, J. a, & Lomber, S. G. (2010). Areas of cat auditory cortex as defined by neurofilament proteins expressing SMI-32. *Hearing research*, *267*(1-2), 119–36.

Melvin, N. R., & Dyck, R. H. (2003). Short communication D evelopmental distribution of calretinin in mouse barrel cortex. *Developmental Brain Research*, *143*, 111–114.

Migaud, M., Charlesworth, P., Dempster, M., Webster, L. C., Watabe, a M., Makhinson, M., He, Y., et al. (1998). Enhanced long-term potentiation and impaired learning in mice with mutant postsynaptic density-95 protein. *Nature*, *396*(6710), 433–9.

Mitrovic, N., Dörries, U., & Schachner, M. (1994). Expression of the extracellular matrix glycoprotein tenascin in the somatosensory cortex of the mouse during postnatal development: an immunocytochemical and in situ hybridization analysis. *Journal of neurocytology*, *23*(6), 364–78.

Mitrovic, N., Mohajeri, H., & Schachner, M. (1996). Effects of NMDA receptor blockade in the developing rat somatosensory cortex on the expression of the glia-derived extracellular matrix glycoprotein tenascin-C. *The European journal of neuroscience*, *8*(9), 1793–802.

Molnár, Z., Garel, S., López-Bendito, G., Maness, P., & Price, D. J. (2012). Mechanisms controlling the guidance of thalamocortical axons through the embryonic forebrain. *The European journal of neuroscience*, *35*(10), 1573–85.

Montgomery, J. M., Zamorano, P. L., & Garner, C. C. (2004). MAGUKs in synapse assembly and function: an emerging view. *Cellular and molecular life sciences : CMLS*, *61*(7-8), 911–29.

Morris, J. R., & Lasek, R. J. (1982). Stable polymers of the axonal cytoskeleton: the axoplasmic ghost. *The Journal of cell biology*, *92*(1), 192–8.

Müller, B. M., Kistner, U., Kindler, S., Chung, W. J., Kuhlendahl, S., Fenster, S. D., Lau, L. F., et al. (1996). SAP102, a novel postsynaptic protein that interacts with NMDA receptor complexes in vivo. *Neuron*, *17*(2), 255–65.

Narboux-Nême, N., Evrard, A., Ferezou, I., Erzurumlu, R. S., Kaeser, P. S., Lainé, J., Rossier, J., et al. (2012). Neurotransmitter release at the thalamocortical synapse instructs barrel formation but not axon patterning in the somatosensory cortex. *The Journal of neuroscience*, *32*(18), 6183–96.

Nimchinsky, E a, Oberlander, a M., & Svoboda, K. (2001). Abnormal development of dendritic spines in FMR1 knock-out mice. *The Journal of neuroscience*, *21*(14), 5139–46.

Nimchinsky, Esther a, Sabatini, B. L., & Svoboda, K. (2002). Structure and function of dendritic spines. *Annual review of physiology*, *64*, 313–53.

Nithianantharajah, J., Komiyama, N. H., McKechanie, A., Johnstone, M., Blackwood, D. H., Clair, D. S., Emes, R. D., et al. (2012). Synaptic scaffold evolution generated components of vertebrate cognitive complexity. *Nature Neuroscience*, (December), 1–11.

Nixon, R. A., & Lewis, S. E. (1986). Differential Turnover of Phosphate Groups on Neurofilament Subunits in, 16298–16301.

Nixon, R. A., & Shea, T. B. (1992). Views and Reviews Dynamics of Neuronal Intermediate Filaments : A Developmental Perspective. *Cell*, *91*, 81–91.

Nusser, Z., Lujan, R., Laube, G., Roberts, J. D., Molnar, E., & Somogyi, P. (1998). Cell type and pathway dependence of synaptic AMPA receptor number and variability in the hippocampus. *Neuron*, *21*(3), 545–59.

Nägerl, U. V., Köstinger, G., Anderson, J. C., Martin, K. a C., & Bonhoeffer, T. (2007). Protracted synaptogenesis after activity-dependent spinogenesis in hippocampal neurons. *The Journal of neuroscience*, *27*(30), 8149–56.

Okabe, S. (2007). Molecular anatomy of the postsynaptic density. *Molecular and cellular neurosciences*, *34*(4), 503–18.

Opazo, P., Watabe, A. M., Grant, S. G. N., & O'Dell, T. J. (2003). Phosphatidylinositol 3-kinase regulates the induction of long-term potentiation through extracellular signal-related kinase-independent mechanisms. *The Journal of neuroscience*, *23*(9), 3679–88.

O'Brien, J., & Unwin, N. (2006). Organization of spines on the dendrites of Purkinje cells. *Proceedings of the National Academy of Sciences of the United States of America*, *103*(5), 1575–80.

Papa, M., Bundman, M. C., Greenberger, V., & Segal, M. (1995). Morphological analysis of dendritic spine development in primary cultures of hippocampal neurons. *The Journal of neuroscience*, *15*(1 Pt 1), 1–11.

Paulussen, M., Jacobs, S., Van der Gucht, E., Hof, P. R., & Arckens, L. (2011). Cytoarchitecture of the mouse neocortex revealed by the low-molecular-weight neurofilament protein subunit. *Brain structure & function*, *216*(3), 183–99.

Penn, a. a. (1998). Competition in Retinogeniculate Patterning Driven by Spontaneous Activity. *Science*, *279*(5359), 2108–2112.

Peters, a, & Kaiserman-Abramof, I. R. (1970). The small pyramidal neuron of the rat cerebral cortex. The perikaryon, dendrites and spines. *The American journal of anatomy*, *127*(4), 321–55.

Petralia, R. S., Sans, N., Wang, Y., & Wenthold, R. J. (2005). Ontogeny of postsynaptic density proteins at glutamatergic synapses. *Molecular and cellular neurosciences*, *29*(3), 436–52.

Petzold, A. (2005). Neurofilament phosphoforms: surrogate markers for axonal injury, degeneration and loss. *Journal of the neurological sciences*, *233*(1-2), 183–98.

Pi, H. J., Otmakhov, N., El Gaamouch, F., Lemelin, D., De Koninck, P., & Lisman, J. (2010). CaMKII control of spine size and synaptic strength: role of phosphorylation states and nonenzymatic action. *Proceedings of the National Academy of Sciences of the United States of America*, *107*(32), 14437–42.

Pitulescu, M. E., & Adams, R. H. (2010). Eph / ephrin molecules — a hub for signaling and endocytosis. *Genes & Development*, *24*, 2480–2492.

Plenge, R. M., Stevenson, R. a, Lubs, H. a, Schwartz, C. E., & Willard, H. F. (2002). Skewed X-chromosome inactivation is a common feature of X-linked mental retardation disorders. *American journal of human genetics*, *71*(1), 168–73.

Pocklington, A. J., Cumiskey, M., Armstrong, J. D., & Grant, S. G. N. (2006). The proteomes of neurotransmitter receptor complexes form modular networks with distributed functionality underlying plasticity and behaviour. *Molecular systems biology*, *2*, 2006.0023.

Porter, K., Komiyama, N. H., Vitalis, T., Kind, P. C., & Grant, S. G. N. (2005). Differential expression of two NMDA receptor interacting proteins, PSD-95 and SynGAP during mouse development. *The European journal of neuroscience*, *21*(2), 351–62.

Probstmeier, R., & Pesheva, P. (1999). Tenascin-C inhibits beta1 integrin-dependent cell adhesion and neurite outgrowth on fibronectin by a disialoganglioside-mediated signaling mechanism. *Glycobiology*, *9*(2), 101–14.

Proctor, D. T., Coulson, E. J., & Dodd, P. R. (2010). Reduction in post-synaptic scaffolding PSD-95 and SAP-102 protein levels in the Alzheimer inferior temporal cortex is correlated with disease pathology. *Journal of Alzheimer's disease*, *21*(3), 795–811.

Prokop, a, Landgraf, M., Rushton, E., Broadie, K., & Bate, M. (1996). Presynaptic development at the Drosophila neuromuscular junction: assembly and localization of presynaptic active zones. *Neuron*, *17*(4), 617–26.

Qu, M., Aronica, E., Boer, K., Fällmar, D., Kumlien, E., Nistér, M., Wester, K., et al. (2009). DLG3/SAP102 protein expression in malformations of cortical development: a study of human epileptic cortex by tissue microarray. *Epilepsy research*, *84*(1), 33–41.

Rakic, P., Ayoub, A. E., Breunig, J. J., & Dominguez, M. H. (2009). Decision by division: making cortical maps. *Trends in neurosciences*, *32*(5), 291–301.

Rebsam, A., Seif, I., & Gaspar, P. (2002). Refinement of thalamocortical arbors and emergence of barrel domains in the primary somatosensory cortex: a study of normal and monoamine oxidase a knock-out mice. *The Journal of neuroscience*, *22*(19), 8541–52. 8

Rebsam, A., Seif, I., & Gaspar, P. (2005). Dissociating barrel development and lesion-induced plasticity in the mouse somatosensory cortex. *The Journal of neuroscience*, *25*(3), 706–10.

Rochefort, N. L., Narushima, M., Grienberger, C., Marandi, N., Hill, D. N., & Konnerth, A. (2011). Development of direction selectivity in mouse cortical neurons. *Neuron*, *71*(3), 425–32.

Rossi, F. M., Bozzi, Y., Pizzorusso, T., & Maffei, L. (1999). Monocular deprivation decreases brain-derived neurotrophic factor immunoreactivity in the rat visual cortex. *Neuroscience*, *90*(2), 363–8.

Rouleau, G. ., Clark, A. ., Rooke, K., Pramatrarova, A., Krizus, A., Suchowersky, O., Julien, S. J., et al. (1996). SOD1 mutation is associated with accumulation of neurofilaments in Amyotrophic lateral sclerosis. *Annals of Neurology*, *39*(1), 128–131.

Ryan, T. J., & Grant, S. G. N. (2009). The origin and evolution of synapses. *Nature reviews. Neuroscience*, *10*(10), 701–12.

Sakano, H. (2010). Neural map formation in the mouse olfactory system. *Neuron*, *67*(4), 530–42.

Sala, C., Piëch, V., Wilson, N. R., Passafaro, M., Liu, G., & Sheng, M. (2001). Regulation of dendritic spine morphology and synaptic function by Shank and Homer. *Neuron*, *31*(1), 115–30.

Salichon, N., Gaspar, P., Upton, a L., Picaud, S., Hanoun, N., Hamon, M., De Maeyer, E., et al. (2001). Excessive activation of serotonin (5-HT) 1B receptors disrupts

the formation of sensory maps in monoamine oxidase a and 5-ht transporter knock-out mice. *The Journal of neuroscience*, *21*(3), 884–96.

Sans, N, Petralia, R. S., Wang, Y. X., Blahos, J., Hell, J. W., & Wenthold, R. J. (2000). A developmental change in NMDA receptor-associated proteins at hippocampal synapses. *The Journal of neuroscience*, *20*(3), 1260–71.

Sans, Nathalie, Prybylowski, K., Petralia, R. S., Chang, K., Wang, Y.-X., Racca, C., Vicini, S., et al. (2003). NMDA receptor trafficking through an interaction between PDZ proteins and the exocyst complex. *Nature cell biology*, *5*(6), 520–30.

Sans, Nathalie, Wang, P. Y., Du, Q., Petralia, R. S., Wang, Y.-X., Nakka, S., Blumer, J. B., et al. (2005). mPins modulates PSD-95 and SAP102 trafficking and influences NMDA receptor surface expression. *Nature cell biology*, *7*(12), 1179–90.

Scheiffele, P., Fan, J., Choih, J., Fetter, R., & Serafini, T. (2000). Neuroligin expressed in nonneuronal cells triggers presynaptic development in contacting axons. *Cell*, *101*(6), 657–69.

Schikorski, T., & Stevens, C. F. (1997). Quantitative ultrastructural analysis of hippocampal excitatory synapses. *The Journal of neuroscience*, *17*(15), 5858–67.

Schlagger, B., Fox, K., & O'Leary, D. D. (1993). Postsynaptic control of plasticity in developing somatosensory cortex. *Nature*.

Schmeisser, M. J., Ey, E., Wegener, S., Bockmann, J., Stempel, a. V., Kuebler, A., Janssen, A.-L., et al. (2012). Autistic-like behaviours and hyperactivity in mice lacking ProSAP1/Shank2. *Nature*.

Schnell, E., Sizemore, M., Karimzadegan, S., Chen, L., Bredt, D. S., & Nicoll, R. a. (2002). Direct interactions between PSD-95 and stargazin control synaptic AMPA receptor number. *Proceedings of the National Academy of Sciences of the United States of America*, *99*(21), 13902–7.

Serizawa, S., Miyamichi, K., Takeuchi, H., Yamagishi, Y., Suzuki, M., & Sakano, H. (2006). A neuronal identity code for the odorant receptor-specific and activity-dependent axon sorting. *Cell*, *127*(5), 1057–69.

Senft, S. L., & Woolsey, T. a. (1991). Growth of thalamic afferents into mouse barrel cortex. *Cerebral cortex*, *1*(4), 308–35.

Sengpiel, F., Stawinski, P., & Bonhoeffer, T. (1999). Influence of experience on orientation maps in cat visual cortex. *Nature neuroscience*, *2*(8), 727–32.

Shatz, C. J. (1996). Emergence of order in visual system development. *Proceedings of the National Academy of Sciences of the United States of America*, *93*(2), 602–8.

Shatz, & Stryker, M. P. (1988). Prenatal Tetrodotoxin Infusion Blocks Segregation of. *Science*, *242*(4875), 87–89.

Sharp, G. A., Shaw, G., & Weber, K. (1982). Immunoelectronmicroscopical localization of the three neurofilament triplet proteins along neurofilaments of cultured dorsal root ganglion neurones. *Experimental Cell Research*, *137*(2), 403–413.

Shaw, G, Osborn, M., & Weber, K. (1981). An immunofluorescence microscopical study of the neurofilament triplet proteins, vimentin and glial fibrillary acidic protein within the adult rat brain. *European journal of cell biology*, *26*(1), 68–82.

Shaw, Gerry, & Weber, K. (1982). Differential expression of neurofilament triplet proteins in brain development. *Nature*, *298* (July), 277–279.

Sheng, M. H., Cummings, J., Roldan, L. A., Jan, Y. N., & Jan, Y. J. (1994). Changing subunit composition of heteromeric NMDA receptors during development of rat cortex. *Nature*, *368*, 144–147.

Shepherd, J. D., & Huganir, R. L. (2007). The cell biology of synaptic plasticity: AMPA receptor trafficking. *Annual review of cell and developmental biology*, *23*, 613–43.

Shi, J., Aamodt, S. M., & Constantine-Paton, M. (1997). Temporal correlations between functional and molecular changes in NMDA receptors and GABA neurotransmission in the superior colliculus. *The Journal of neuroscience*, *17*(16), 6264–76.

Siegel, F., Heimel, J. A., Peters, J., & Lohmann, C. (2012). Peripheral and central inputs shape network dynamics in the developing visual cortex in vivo. *Current biology*, *22*(3), 253–8.

Simons, D., & Land, P. (1987). Early experience of tactile stimulation influences organization of somatic sensory cortex.

Sirianni, N., Naidu, S., Pereira, J., Pillotto, R., & Hoffman, E. (1998). Rett Syndrome: Confirmation of X-linked dominant inheritnace, and localization of the gene to Xq28. *American journal of human genetics*, *63*, 1552.

Sotelo, C. (1990). Cerebellar synaptogenesis: what we can learn from mutant mice. *The Journal of experimental biology*, *153*, 225–49.

Star, E. N., Kwiatkowski, D. J., & Murthy, V. N. (2002). Rapid turnover of actin in dendritic spines and its regulation by activity. *Nature neuroscience*, *5*(3), 239–46.

Starmer, J., & Magnuson, T. (2009). A new model for random X chromosome inactivation. *Development (Cambridge, England)*, *136*(1), 1–10.

Steindler, D. a, Settles, D., Erickson, H. P., Laywell, E. D., Yoshiki, a, Faissner, a, & Kusakabe, M. (1995). Tenascin knockout mice: barrels, boundary molecules, and glial scars. *The Journal of neuroscience*, *15* (3 Pt 1), 1971–83.

Steffen, H., & Van der Loos, H. (1980). Early lesions of mouse vibrissal follicles: Their influence on dendrite orientation in the cortical barrelfield. *Experimental Brain Research*, *431*, 419–431.

Stühmer, T., Puelles, L., Ekker, M., & Rubenstein, J. L. R. (2002). Expression from a Dlx gene enhancer marks adult mouse cortical GABAergic neurons. *Cerebral cortex*, *12*(1), 75–85.

Sweatt, J. D. (2001). The neuronal MAP kinase cascade: a biochemical signal integration system subserving synaptic plasticity and memory. *Journal of neurochemistry*, *76*(1), 1–10.

Su, J. H., Cummings, B. J., & Cotman, C. W. (1996). Plaque biogenesis in brain aging and Alzheimer's disease. Progressive changes in phosphorylation states of paired helical filaments and neurofilaments, *739*, 79–87.

Sun, H.-S., Doucette, T. a, Liu, Y., Fang, Y., Teves, L., Aarts, M., Ryan, C. L., et al. (2008). Effectiveness of PSD95 inhibitors in permanent and transient focal ischemia in the rat. *Stroke; a journal of cerebral circulation*, *39*(9), 2544–53.

Suzuki, S. O., & Goldman, J. E. (2003). Multiple cell populations in the early postnatal subventricular zone take distinct migratory pathways: a dynamic study of glial and neuronal progenitor migration. *The Journal of neuroscience*, *23*(10), 4240–50.

Tan, S. S., & Breen. (1993). Radial mosaicism and tangential cell dispersion both contribute to mouse neocortical development. *nature*, *362*, 638–640.

Tan, S. S., Faulkner-Jones, B., Breen, S. J., Walsh, M., Bertram, J. F., & Reese, B. E. (1995). Cell dispersion patterns in different cortical regions studied with an X-inactivated transgenic marker. *Development (Cambridge, England)*, *121*(4), 1029–39.

Tarpey, P., Parnau, J., Blow, M., Woffendin, H., Bignell, G., Cox, C., Cox, J., et al. (2004). Mutations in the DLG3 gene cause nonsyndromic X-linked mental retardation. *American journal of human genetics*, *75*(2), 318–24.

Testa-Silva, G., Loebel, A., Giugliano, M., De Kock, C. P. J., Mansvelder, H. D., & Meredith, R. M. (2012). Hyperconnectivity and slow synapses during early development of medial prefrontal cortex in a mouse model for mental retardation and autism. *Cerebral cortex*, *22*(6), 1333–42.

Tekki-Kessaris, N., Woodruff, R., Hall, a C., Gaffield, W., Kimura, S., Stiles, C. D., Rowitch, D. H., et al. (2001). Hedgehog-dependent oligodendrocyte lineage specification in the telencephalon. *Development*, *128*(13), 2545–54.

Teunissen, C. E., Dijkstra, C., & Polman, C. (2005). Biological markers in CSF and blood for axonal degeneration, *4*, 32–41.

Thomas, G. M., & Huganir, R. L. (2004). MAPK cascade signalling and synaptic plasticity. *Nature reviews. Neuroscience*, *5*(3), 173–83.

Till, S. M., Wijetunge, L. S., Seidel, V. G., Harlow, E., Wright, A. K., Bagni, C., Contractor, A., et al. (2012). Altered maturation of the primary somatosensory cortex in a mouse model of fragile X syndrome. *Human molecular genetics*, *21*(10), 2143–56.

Tolner, E., Sheikh, A., Yukin, K., & Kanold, P. (2012). Subplate neurons promote spindle bursts and thalamocortical patterning in the neonatal rat somatosensory corrtex. *Journal of Neuroscience*, *32*(2), 692–702.

Tomoda, T. (2004). Role of Unc51.1 and its binding partners in CNS axon outgrowth. *Genes & Development*, *18*(5), 541–558. doi:10.1101/gad.1151204

Toro, C., & Deakin, J. F. W. (2005). NMDA receptor subunit NRI and postsynaptic protein PSD-95 in hippocampus and orbitofrontal cortex in schizophrenia and mood disorder. *Schizophrenia research*, *80*(2-3), 323–30.

Torres, R., Firestein, B. L., Dong, H., Staudinger, J., Olson, E. N., Huganir, R. L., Bredt, D. S., et al. (1998). PDZ proteins bind, cluster, and synaptically colocalize with Eph receptors and their ephrin ligands. *Neuron*, *21*(6), 1453–63.

Trapp, B. D., Peterson, J., Ransohoff, R. M., Rudick, R., Mörk, S., & Bö, L. (1998). Axonal transection in the lesions of multiple sclerosis. *The New England journal of medicine*, *338*(5), 278–85.

Trachtenberg, J. T., Chen, B. E., Knott, G. W., Feng, G., Sanes, J. R., Welker, E., & Svoboda, K. (2002). Long-term in vivo imaging of experience-dependent synaptic plasticity in adult cortex. *Nature*, *420*(6917), 788–94.

Triplett, J. W., & Feldheim, D. a. (2012). Eph and ephrin signaling in the formation of topographic maps. *Seminars in cell & developmental biology*, *23*(1), 7–15.

Trojanowski, J. Q., Walkenstein, N., & Lee, V. M. (1986). Expression of neurofilament subunits in neurons of the central and peripheral nervous system: an immunohistochemical study with monoclonal antibodies. *The Journal of neuroscience*, *6*(3), 650–60.

Ultanir, S. K., Kim, J.-E., Hall, B. J., Deerinck, T., Ellisman, M., & Ghosh, A. (2007). Regulation of spine morphology and spine density by NMDA receptor signaling in vivo. *Proceedings of the National Academy of Sciences of the United States of America*, *104*(49), 19553–8.

Uziel, D., Mühlfriedel, S., & Bolz, J. (2008). Ephrin-A5 promotes the formation of terminal thalamocortical arbors. *Neuroreport*, *19*(8), 877–81.

Valnegri, P., Sala, C., & Passafaro, M. (2012). Synaptic Dysfunction and Intellectual disability. In M. R. Kreutz & C. Sala (Eds.), *Synaptic Plasticity: Dynamics, Development and Disease* (Vol. 970, pp. 433–449). Vienna: Springer Vienna.

Van der Loos, H., & Woolsey, T. A. (1973). Somatosensory Cortex: Structural Alterations following Early Injury to Sense Organs. *Science*, *179*(4071), 395–398.

Vanderhaeghen, P., Lu, Q., Prakash, N., Frisén, J., Walsh, C. a, Frostig, R. D., & Flanagan, J. G. (2000). A mapping label required for normal scale of body representation in the cortex. *Nature neuroscience*, *3*(4), 358–65.

Van Zundert, B., Yoshii, A., & Constantine-Paton, M. (2004). Receptor compartmentalization and trafficking at glutamate synapses: a developmental proposal. *Trends in Neurosciences*, *27*(7), 428–437.

Vazquez, L., Chen, H., Sokolova, I., Knuesel, I., & Kennedy, M. B. (2004). SynGAP regulates spine formation. *The Journal of neuroscience*, *24*(40), 8862–72.

Vickers, C. a, Stephens, B., Bowen, J., Arbuthnott, G. W., Grant, S. G. N., & Ingham, C. a. (2006). Neurone specific regulation of dendritic spines in vivo by post synaptic density 95 protein (PSD-95). *Brain research*, *1090*(1), 89–98.

Vitalis, T., Cases, O., Gillies, K., Hanoun, N., Hamon, M., Seif, I., Gaspar, P., et al. (2002). Interactions between TrkB signaling and serotonin excess in the developing murine somatosensory cortex: a role in tangential and radial organization of thalamocortical axons. *The Journal of neuroscience*, *22*(12), 4987–5000.

Waites, C. L., Specht, C. G., Härtel, K., Leal-Ortiz, S., Genoux, D., Li, D., Drisdel, R. C., (2009). Synaptic SAP97 isoforms regulate AMPA receptor dynamics and access to presynaptic glutamate. *The Journal of neuroscience*, *29*(14), 4332–45.

Watanabe, E., Aono, S., Matsui, F., Yamada, Y., Naruse, I., & Oohira, A. (1995). Distribution of a brain-specific proteoglycan, neurocan, and the corresponding mRNA during the formation of barrels in the rat somatosensory cortex. *The European journal of neuroscience*, *7*(4), 547–54.

Watson, R. F., Abdel-Majid, R. M., Barnett, M. W., Willis, B. S., Katsnelson, A., Gillingwater, T. H., McKnight, G. S., et al. (2006). Involvement of protein kinase A in patterning of the mouse somatosensory cortex. *The Journal of neuroscience*, *26*(20), 5393–401.

White, E. L. (1978). Identified neurons in mouse Sml cortex which are postsynaptic to thalamocortical axon terminals: a combined Golgi-electron microscopic and degeneration study. *The Journal of comparative neurology*, *181*(3), 627–61.

Welker, E., & Van der Loos, H. (1986). Quantitative correlation between barrel-field size and the sensory innervation of the whiskerpad: a comparative study in six strains of mice bred for different patterns of mystacial vibrissae. *The Journal of neuroscience*, *6*(11), 3355–73.

Wijetunge, L. (2009). *Role of mGluR5 and FMRP in Mouse Primary Somatosensory Cortex*. *Thesis*.

Wijetunge, L. S., Till, S. M., Gillingwater, T. H., Ingham, C. a, & Kind, P. C. (2008). mGluR5 regulates glutamate-dependent development of the mouse somatosensory cortex. *The Journal of neuroscience*, *28*(49), 13028–37.

Williamson, T. L., Bruijn, L. I., Zhu, Q., Anderson, K. L., Anderson, S. D., Julien, J. P., & Cleveland, D. W. (1998). Absence of neurofilaments reduces the selective vulnerability of motor neurons and slows disease caused by a familial amyotrophic lateral sclerosis-linked superoxide dismutase 1 mutant. *Proceedings of the National Academy of Sciences of the United States of America*, *95*(16), 9631–6.

Wimmer, V. C., Broser, P. J., Kuner, T., & Bruno, R. M. (2010). Experience-induced plasticity of thalamocortical axons in both juveniles and adults. *The Journal of comparative neurology*, *518*(22), 4629–48.

Wimmer, V. C., Bruno, R. M., De Kock, C. P. J., Kuner, T., & Sakmann, B. (2010). Dimensions of a projection column and architecture of VPM and POm axons in rat vibrissal cortex. *Cerebral cortex*, *20*(10), 2265–76.

Wong, R. O. L., Yamawaki, R. M., & Shatz, C. J. (1992). Synaptic Contacts and the Transient Dendritic Spines of Developing Retinal Ganglion Cells. *The European journal of neuroscience*, *4*(12), 1387–1397.

Wong, Rachel O. L. (1999). Retinal waves and visual system development. *Annual review of neuroscience*, *22*, 29–47.

Woolsey, T. A., & Van der Loos, H. (1970). The structural organization of layer IV in the somatosensory region (S1) of mouse cerebral cortex. *Brain research*, *17*, 205–242.

Woolsey, T. a, & Wann, J. R. (1976). Areal changes in mouse cortical barrels following vibrissal damage at different postnatal ages. *The Journal of comparative neurology*, *170*(1), 53–66.

Wu, C.-S., Ballester Rosado, C. J., & Lu, H.-C. (2011). What can we get from "barrels": the rodent barrel cortex as a model for studying the establishment of neural circuits. *The European journal of neuroscience*, *34*(10), 1663–76.

Wutz, A., Rasmussen, T. P., & Jaenisch, R. (2002). Chromosomal silencing and localization are mediated by different domains of Xist RNA. *Nature genetics*, *30*(2), 167–74.

Xu, N.-J., & Henkemeyer, M. (2012). Ephrin reverse signaling in axon guidance and synaptogenesis. *Seminars in cell & developmental biology*, *23*(1), 58–64.

Yuan, A., Rao, M. V, Sasaki, T., Chen, Y., Kumar, A., Veeranna, Liem, R. K. H., et al. (2006). Alpha-internexin is structurally and functionally associated with the neurofilament triplet proteins in the mature CNS. *The Journal of neuroscience*, *26*(39), 10006–19.

Yuan, A., Rao, M. V, Veeranna, & Nixon, R. a. (2012). Neurofilaments at a glance. *Journal of cell science*, *125*(Pt 14), 3257–63.

Yoshii, A., Sheng, M. H., & Constantine-paton, M. (2003). Eye opening induces a rapid dendritic localization of PSD-95 in central visual neurons. *PNAS*, *100*(3), 1334–1339.

Yuste, R., & Bonhoeffer, T. (2001). Morphological changes in dendritic spines associated with long-term synaptic plasticity. *Annual review of neuroscience*, *24*, 1071–1089.

Zanni, G., Van Esch, H., Bensalem, A., Saillour, Y., Poirier, K., Castelnau, L., Ropers, H. H., et al. (2010). A novel mutation in the DLG3 gene encoding the synapse-associated protein 102 (SAP102) causes non-syndromic mental retardation. *Neurogenetics*, *11*(2), 251–5.

Zhang, H., Sternberger, N. H., Rubinstein, L. J., Herman, M. M., Binder, L. I., & Sternberger, L. a. (1989). Abnormal processing of multiple proteins in Alzheimer disease. *Proceedings of the National Academy of Sciences of the United States of America*, *86*(20), 8045–9.

Zheng, C.-Y., Petralia, R. S., Wang, Y.-X., Kachar, B., & Wenthold, R. J. (2010). SAP102 is a highly mobile MAGUK in spines. *The Journal of neuroscience*, *30*(13), 4757–66.

Zhu, Q., Couillard-Després, S., & Julien, J. P. (1997). Delayed maturation of regenerating myelinated axons in mice lacking neurofilaments. *Experimental neurology*, *148*(1), 299–316.

Zhu, J. J., Qin, Y., Zhao, M., Van Aelst, L., & Malinow, R. (2002). Ras and Rap control AMPA receptor trafficking during synaptic plasticity. *Cell*, *110*(4), 443–55.

Ziv, N. E., & Smith, S. J. (1996). Evidence for a role of dendritic filopodia in synaptogenesis and spine formation. *Neuron*, *17*(1), 91–102.